MODELING OF ELECTRONICALLY COMMUTATED MOTOR CONTROLLED FAN-POWERED TERMINAL UNITS

A Thesis

by

JACOB LEE EDMONDSON

Submitted to the Office of Graduate Studies of
Texas A&M University
in partial fulfillment of the requirements for the degree of

MASTER OF SCIENCE

December 2009

Major Subject: Mechanical Engineering

MODELING OF ELECTRONICALLY COMMUTATED MOTOR CONTROLLED FAN-POWERED TERMINAL UNITS

A Thesis

by

JACOB LEE EDMONDSON

Submitted to the Office of Graduate Studies of
Texas A&M University
in partial fulfillment of the requirements for the degree of

MASTER OF SCIENCE

Approved by:

Chair of Committee,	Dennis O'Neal
Committee Members,	Warren Heffington
	Calvin Parnell
Head of Department,	Dennis O'Neal

December 2009

Major Subject: Mechanical Engineering

ABSTRACT

Modeling of Electronically Commutated Motor Controlled Fan Powered Terminal Units.

(December 2009)

Jacob Lee Edmondson, B.S., Brigham Young University

Chair of Advisory Committee: Dr. Dennis O'Neal

Empirical models of airflow and power consumption were developed for series and parallel variable air volume fan powered terminal units (FPTUs). An experimental setup and test procedure were developed to test the terminal units over typical operating ranges. The terminal units in this study used either an 8 in. (20.32 cm) or a 12 in. (30.48 cm) primary air inlet. All terminal units utilized electronically commutated motor (ECM) controllers. Data collected were compared against previous data collected for silicon controlled rectifier (SCR) units. Generalized models were developed for both series and parallel units, and compared against models developed for SCR units.

In addition to the performance modeling, power factor and power quality data were also collected for each terminal unit. The power quality analysis included recording and analyzing harmonic distortion for current, voltage, and power up to the 25^{th} harmonic. The total harmonic distortion (THD) was also recorded and presented.

For the series terminal units, models were developed for fan airflow, fan power, and primary airflow. The models for fan airflow all had R^2 values above 0.987. The

models for fan power all had R^2 values above 0.968. The models for primary airflow all had R^2 values above 0.895.

For the parallel terminal units, models were developed for leakage, fan airflow, fan power, and primary airflow. All of the leakage models had R^2 values above 0.826. All of the fan airflow models had R^2 values above 0.955. All of the fan power models had R^2 values above 0.922. All of the primary airflow models had R^2 values above 0.872.

The real power THD was below 1.5% for both series and parallel FPTUs. The current THD ranged from 84% to 172% for series FPTUs and from 83% to 183% for parallel FPTUs. The voltage THD was below 1.4% for both series and parallel FPTUs.

The performance models developed will help improve the accuracy of building energy simulation programs for heating, ventilation, and air conditioning (HVAC) systems utilizing ECM controlled FPTUs. Increasing the accuracy of these simulations will allow HVAC system designers to better optimize their designs for specific building types in a wide variety of climates.

DEDICATION

To Lizel and Auzten

ACKNOWLEDGEMENTS

I would like to thank Kelly Milligan and other staff at the Energy Systems Laboratory facility at the Riverside Campus of Texas A&M University. Their assistance in setting up and troubleshooting equipment was very valuable. I would also like to thank Andrew Cramlet who helped me understand the equipment and testing procedure when I first started working on this project. I'd also like to thank Sterling Debner and Peng Yin for their help in running tests, which helped me finish the project much sooner than I would have otherwise.

I'd like to thank Dr. O'Neal for giving me the opportunity to work on this project, as well as his help and insight in getting the testing done well. I'd like to thank all of my other teachers and professors who encouraged me to continue on to graduate school, and helped me reach that goal. I'd like to thank my parents for giving me a love of learning, and helping me to achieve as much as I can.

Lastly, I'd like to thank my wife for her encouragement and patience while finishing my thesis, as well as my little boy for being such an inspiration when it felt like the project would never end.

NOMENCLATURE

CFM	Cubic Feet Per Minute
ECM	Electronically Commutated Motor
FPTU	Fan Powered Terminal Unit
P_{down}	Downstream Static Pressure
PF	Power Factor
P_{up}	Upstream Static Pressure
SCR	Silicon Controlled Rectifier
THD	Total Harmonic Distortion
VAV	Variable Air Volume
Triplen	Odd Multiple of Three Harmonic Frequency
CAV	Constant Air Volume
P_{iav}	Inlet Air Velocity Pressure
D, or S	Primary Air Inlet Damper Setting
AMCA	Air Movement and Control Association
RC	Passive Filter Using Resistors and Capacitors
$Q_{primary}$	Upstream Airflow
RH	Relative Humidity
Q_{fan}	Airflow Produced by Terminal Unit Fan
EIA	Energy Information Administration
BTU	British Thermal Unit

kWh	Kilowatt Hour
HVAC	Heating, Ventilation, and Air Conditioning
IAQ	Indoor Air Quality
AC	Alternating Current
DC	Direct Current
VAC	Alternating Current Voltage
VDC	Direct Current Voltage
DOE	Department of Energy
VSD	Variable Speed Drive
VFD	Variable Frequency Drive
$Q_{leakage}$	Airflow Leaking from the FPTU
Q_{out}	Airflow Downstream of the FPTU
$Q_{induced}$	Airflow Induced by Terminal Unit Fan
DAQ	Data Acquisition
Q_{supply}	Upstream Airflow

TABLE OF CONTENTS

CHAPTER Page

LIST OF FIGURES

Page

Page

Page

Page

Page

LIST OF TABLES

Page

Page

CHAPTER I

INTRODUCTION

Recent fluctuations in the price of energy and concern for the environment have renewed interest in reducing energy use. Much of the focus has been on reducing fossil fuel use to both decrease the environmental impact of producing and using fossil fuels, and to reduce the impact of instability in fossil fuel rich regions. One way to reduce the amount of fossil fuels we consume is to transition to alternative sources of energy, but this is costly and time consuming. Another way, which is both less expensive and quicker, is to increase the efficiency of the energy we use. One way to increase this efficiency is to optimize current technologies.

In the United States, data from the Energy Information Administration (EIA) indicates commercial buildings used approximately 3.559 quadrillion BTUs (1043 billion kWh) of electricity in 2003. Of this, about 30%, 1.084 quadrillion BTUs (317.7 billion kWh), was used for heating, ventilating, and air conditioning (HVAC) (EIA 2008). Variable air volume (VAV) systems allow greater HVAC system efficiency without sacrificing occupant comfort (Ardehali and Smith 1996). In VAV systems (Figure 1-1), a terminal unit is used to adjust the amount of primary air delivered to a zone to maintain the temperature of the zone. Some terminal units are also designed to facilitate the induction of recycled zone air to provide better temperature control while

---

This thesis follows the style of *HVAC&R Research*.

maintaining a minimum flow of primary air to maintain Indoor Air Quality (IAQ). In fan powered terminal units (FPTUs), the ratio of conditioned primary air and recycled zone air is a function of mechanical damper settings and the speed of the fan in the FPTU.

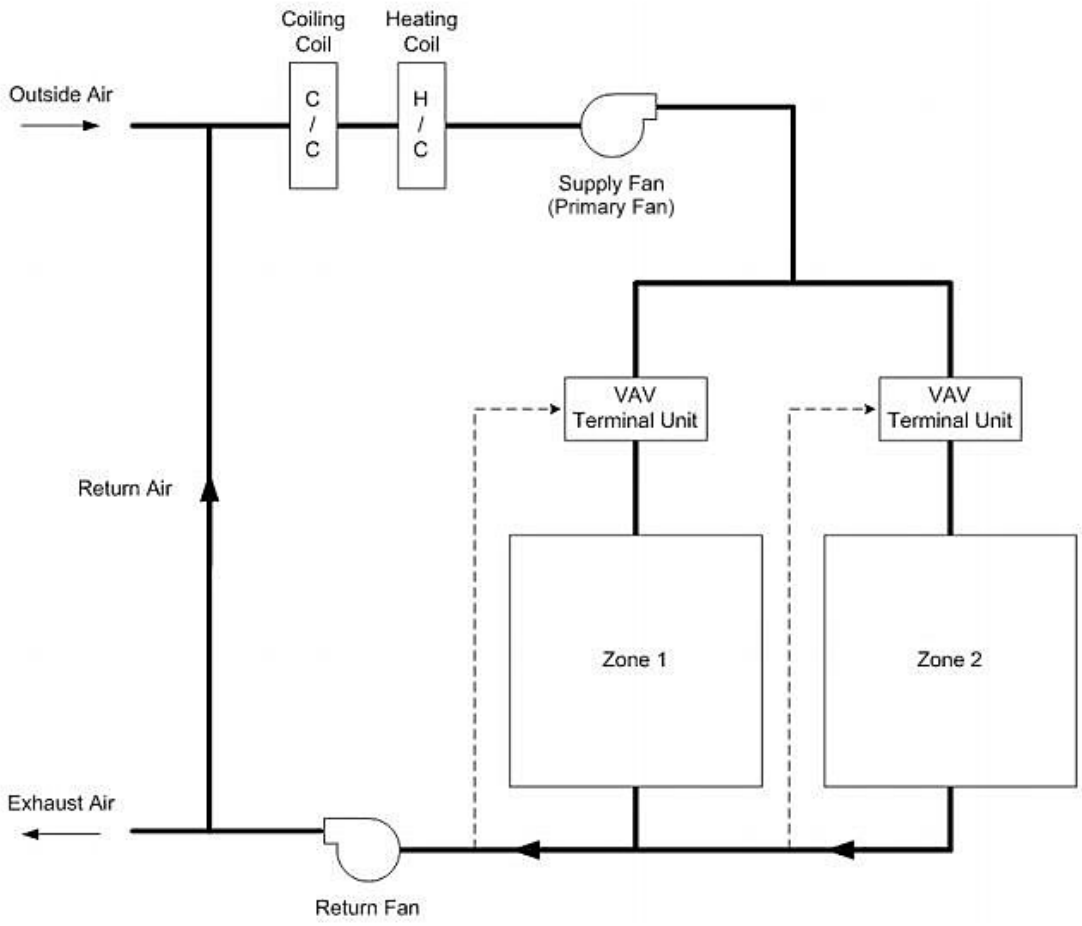

Figure 1-1: Typical VAV System Configuration (Cramlet 2008)

There are two basic configurations of FPTUs: series and parallel. In a series FPTU (Figure 1-2a), the internal fan is in series with the primary air, meaning the fan

must be on in series with the primary fan to supply air to the zone. In a parallel FPTU (Figure 1-2b), the internal fan is in parallel with the primary fan, meaning fan operation is not mandatory for the FPTU. Another difference between the two types of FPTUs is that the fan in a series FPTU can create a slight vacuum inside the unit which draws air into it. The fan in a parallel unit pressurizes the FPTU causing some of the primary air to leak out of the unit. Another difference between them is that series terminal units allow the primary air system to operate at a lower static pressure because the terminal unit fan adds static pressure to the system.

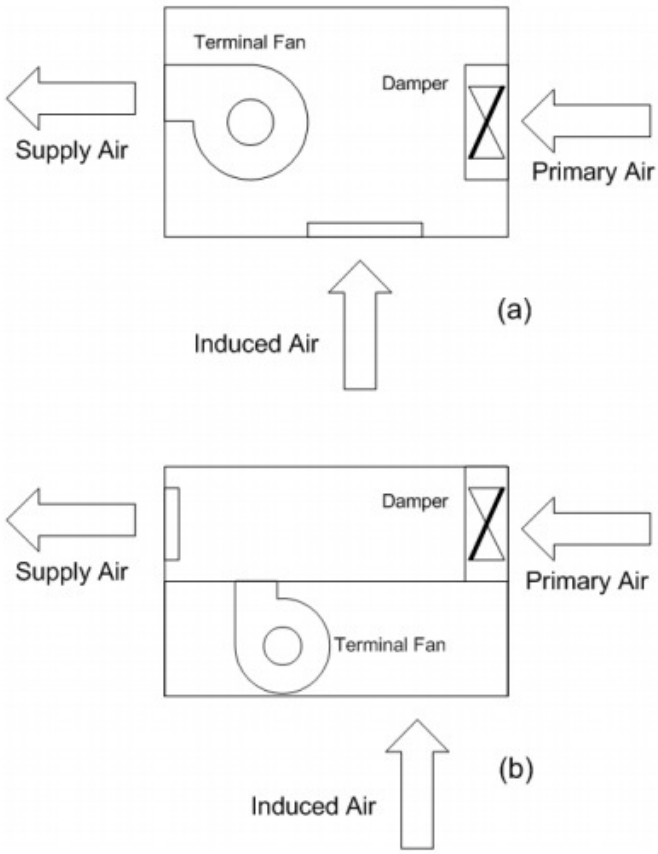

Figure 1-2: Generic Sketches of a) Series FPTU, and b) Parallel FPTU (Cramlet 2008)

Because parallel units do not require the internal fan to operate continuously, many authors have concluded that parallel terminal units use less energy than series units (Wendes 1994, Chen and Demster 1996, Elleson 1993). This perception has led ASHRAE (2004) in Standard 90.1 and the California Energy Commission (Hydeman et al. 2003) to prescribe the use of parallel FPTUs in VAV systems. This conclusion is accurate if based only on the energy use of the FPTU. However, with a series unit, it is possible to operate the primary fan at a lower static pressure because the FPTU fan adds static pressure to the system. This creates a potential for energy savings in the overall system with the lower static pressure of the primary air system. In addition, leakage in a parallel terminal unit increases primary air energy use because the fan has to make up for the leakage.

Computer simulations by Elleson (1993) and Kolderup et al. (2003) indicated that systems utilizing parallel terminal units use less energy overall than systems using series units. These studies did not account for all the variables affecting terminal unit performance. To more accurately account for these variables, Furr (2006) developed semi-empirical models of FPTU airflow and power performance on terminal units using silicon controlled rectifier (SCR) controlled AC induction fan motors. Newer FPTUs are controlled by using electronically commutated motor (ECM) variable speed fan motors. Cramlet (2008) began developing empirically derived models for these ECM controlled units, and this thesis is a direct continuation of his work.

One objective of this study was developing semi-empirical models of airflow performance of the FPTUs over a wide variety of operating conditions. Characteristic

equations were developed using variables such as inlet air velocity pressure, upstream and downstream static pressures, damper setting, and fan speed. These models can be used by building energy simulation programs to better predict the airflow performance of FPTUs for different operating conditions. This will allow VAV systems to be tuned for stability and performance (Khoo et al. 1998).

A second objective of this study was characterizing the energy performance of ECM controlled FPTUs. Semi-empirical models of the power consumption of these units over a wide variety of operating conditions were developed. These models can be used in conjunction with the airflow models mentioned above to allow simulation software to more accurately predict the power consumption of the FPTU.

A third objective of this study was to characterize the power factor and power quality of the ECM controlled fans. The power factor is important for several reasons. One reason is that a low power factor increases the losses in the electrical distribution system and limits the capacity for expansion. It also results in increased voltage drop at the point of use, which can cause loss of efficiency and reduced load capacity of motors (EnergyIdeas Clearinghouse 2002). Some utilities also asses a surcharge for power factors below a certain level. To avoid these problems, low power factors must be corrected.

The power quality analysis included harmonics of voltage, current, and real power. Specific attention was paid to triplen harmonics, which are odd harmonics that are also multiples of three. These harmonics are in phase with the fundamental current, and they add together increasing heat generation and voltage drop along the neutral

conductor. They can also induce noise into nearby circuits (Kennedy 2000). The total harmonic distortion (THD) was also analyzed. THD is the sum of all harmonic values of current, voltage, or real power. High THD can cause overheating in electrical equipment and overloading of neutrals (Gosbell 2000).

This thesis has seven chapters. Chapter II is a review of applicable research concerning VAV systems and FPTUs especially with regards to energy performance. Chapter III details the experimental apparatus and setup. Chapter IV describes the procedures used to perform the experiments and analyze the data to develop the semi-empirical models. Chapter V presents the results for series terminal units. Chapter VI presents the results for the parallel units. Chapter VII discusses the results and presents conclusion. A complete set of data is presented in the appendices.

CHAPTER II

LITERATURE REVIEW

The HVAC industry has largely adopted VAV systems because they consume less energy than Constant Air Volume (CAV) systems. Both systems can provide similar levels of occupant comfort. Studies have been conducted on improving and optimizing the performance of VAV systems for both thermal comfort and IAQ. One of the first studies to verify the energy savings of VAV systems was a study conducted by Inoue and Matsumoto (1979) in Japan. They used HASP/ACLD 7101 (1971) simulation software to compare building energy use for several CAV and VAV systems, and then verified their conclusions with field measurements at a building in Tokyo. They concluded that a VAV system could save 30% to 50% of fan energy over a CAV system, either dual duct or terminal reheat. They also concluded that VAV systems could save up to 40% in cooling costs.

Sekhar (1997) used DOE2.2 (LBNL 1998) energy simulation software to conduct a similar simulation study on buildings in hot humid climates, particularly those found in Southeast Asia. He found that using a VAV system could save 50% to 70% on fan energy compared to a CAV system. Utilizing a VAV system also reduced space cooling from 10.9% to 18.5%, and total HVAC energy use 11.5% to 25.7% depending on the specific building being simulated. One common limitation of these studies is that they both used damper only terminals with no fan.

One study that included FPTUs in its analysis concluded that a VAV system utilizing FPTUs could save 40% on utility costs compared to a CAV system (Ardehali and Smith 1996). They utilized the TRACE (1993) program to model a "typical" existing office building in Des Moines, IA, but did not differentiate between series and parallel units. As these studies show, VAV systems are more energy efficient than CAV systems, including fan powered terminal systems. It is important to determine the differences between series and parallel units, so they can be applied properly to maximize energy savings and occupant comfort.

One study (Elleson 1993) that did differentiate between series and parallel units was performed on a cold air system. These systems supply conditioned air at 45°F (7.2°C) instead of the 55°F (12.8°C) in traditional systems. The study simulated a 12 story office building in Southern California, and a 21 story office building in Seattle, WA. The computer models were verified by field measurements at both of these buildings. Although focused on showing the benefits of a cold air distribution system, the system also showed the relative energy consumption of the different types of FPTUs. Elleson concluded that parallel units can save between 24% and 47% on fan energy compared to series units in a traditional system, and between 30% and 54% in a cold-air system. The study included a supply duct static pressure 0.25 in. w.g. (62.3 Pa) lower for series units than for parallel units.

A study commissioned by the California Energy Commission (Kolderup et al. 2003) compared series and parallel fan powered terminal units with unpowered VAV terminal units. The study utilized the built in terminal unit types in DOE2.2 (LBNL

1998) simulation software, with the FPTUs serving the perimeter zones. The use of series terminal units in this simulation allowed for a reduction in the supply fan static pressure from 4.0 in w.g. (996 Pa) for parallel and unpowered terminal units to 3.67 in w.g. (914 pa) for the series FPTUs. Despite the lower supply static pressure, the series terminal units were found to have an overall fan energy use 94% higher than parallel units. This result was partially due to the assumed lower efficiency of the small terminal unit fan compared the main supply fan. They also found a slight reduction in fan energy use with the parallel FPTUs compared to unpowered terminal units. Comparing overall HVAC system utility costs resulted in parallel units performing nearly identical to unpowered units, and series units increasing utility costs about 10% (Kolderup et al. 2003).

Though both of these studies (Elleson 1993 and Kolderup et al. 2003) indicate a significant reduction in utility costs for parallel units compared to series units, they were focused on specific buildings in specific locations, and may not apply to different climates. In the California Energy Commission Study, it was noted that one reason the small effect of parallel units on fan energy may be due to the low reheat requirements in California (Kolderup et al. 2003). In climates where more reheat is required, the terminal unit fan may be in operation more often, resulting in higher energy costs. Both of these studies used the built in functions in their HVAC simulation software.

There is little experimental evidence to support the simulations of fan powered terminal units, especially terminal units utilizing ECM controlled fans. Khoo et al. (1998) developed non-linear models of unpowered VAV terminal units, and found that

they were significantly more accurate than the damper only models traditionally used. Because many software packages utilize damper only models, the results of simulations may not be accurate. Furr (2006) provided the first work on developing models of fan powered units that accurately reflect real world performance. His work focused on FPTUs utilizing SCR controlled fans. Cramlet (2008) began work on modeling FPTUs with ECM controlled fans. He also compared performance of nearly identical terminal units, the only difference being the use of SCR or ECM controlled fans. He found that the energy savings realized by using ECM control instead of SCR control may be dependent on the usage characteristics of the FPTU, especially for parallel units.

Cramlet (2008) also investigated the power quality performance of FPTUs. He found that the ECM controlled fans had lower power factor (PF), and increased harmonic distortion compared to SCR controlled units. The magnitude of this impact is important for two reasons. First, equipment damage from excessive harmonic distortion may go unnoticed for many years, especially if the distortion is unknown (Gosbell 2000). Second, low PF may incur increased utility costs from utility company fees and increased losses in the distribution system (EnergyIdeas Clearinghouse 2002). If the magnitude of power factor and harmonic distortion problems is known, corrective equipment can be installed in the facility.

Developing better models of terminal units using ECM controlled fans will allow building simulation programs to more accurately simulate energy use in HVAC systems. Better performance data and models will allow designers to make better decisions of which type of FPTU to install based on overall system costs. By determining the

magnitude of possible problems resulting from low PF and high harmonic distortion, HVAC system designers will be better able to determine if PF and THD corrective equipment needs to be installed, or if the impact is small enough to the whole system that corrective equipment would be an unwise investment.

CHAPTER III

EXPERIMENTAL APPARATUS

This research contained two main phases: data acquisition and data analysis. This chapter focuses on the equipment used for data acquisition, including the equipment used to run the tests, as well as the data acquisition equipment. Different data acquisition systems were used for airflow and power measurements.

3.1. Airflow Equipment

Figure 3-1 shows a general overview of the airflow test setup. The equipment consisted of a VAV FPTU, two airflow test chambers, and primary and assist blowers. The upstream airflow chamber (AMCA Figure 15) was used to measure the primary air supplied to the VAV terminal unit. The primary blower attached to this chamber was used to control the amount of air and the upstream static pressure. The downstream airflow chamber (AMCA Figure 12) was used to measure the airflow provided by the FPTU to the zone. The assist blower on this chamber was used to control the downstream static pressure. The equipment shown in Figure 3-1 is explained in more detail in the following sections of this chapter.

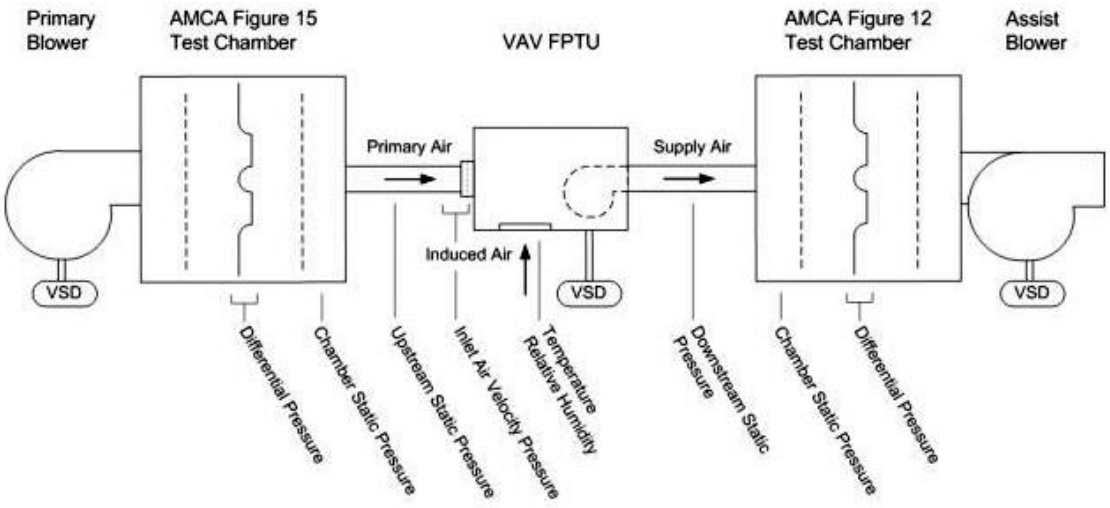

Figure 3-1: Experimental Apparatus (Cramlet 2008)

3.1.1. Variable Air Volume Fan Powered Terminal Units. The purpose of this study was to evaluate and model the airflow and power performance of the fan powered terminal units. These units came in both series (Figure 3-2a), and parallel (Figure 3-2b) configurations. Both configurations allow the terminal unit to induce air from the return plenum space and mix it with the conditioned primary air to maintain thermal comfort. The terminal units used in this study came in two sizes, 8 in. (20.32 cm) and 12 in. (30.48 cm) primary air inlets, from three different manufacturers. One manufacturer supplied terminal units using motors from two different manufacturers. Since Cramlet (2008) tested two of the FPTUs provided by one manufacturer, 14 different terminal units were tested in this study. The different manufactures are named using A, B, and C, with -M1 and -M2 being used to denote the different brand of motors provided by manufacturer C. All terminal units were also categorized by size (8 in. (20.32 cm) and

12 in. (30.48 cm)), type (parallel or series), and ECM controlled FPTUs. This led to the following naming convention. ECM_P12C-M1 is the name for a 12 in. (30.48 cm) parallel FPTU from manufacturer C using brand 1 of the fan motor. For manufacturers A and B, a 12 in. (30.48 cm) parallel FPTU would be EMC_P12A and ECM_P12B respectively.

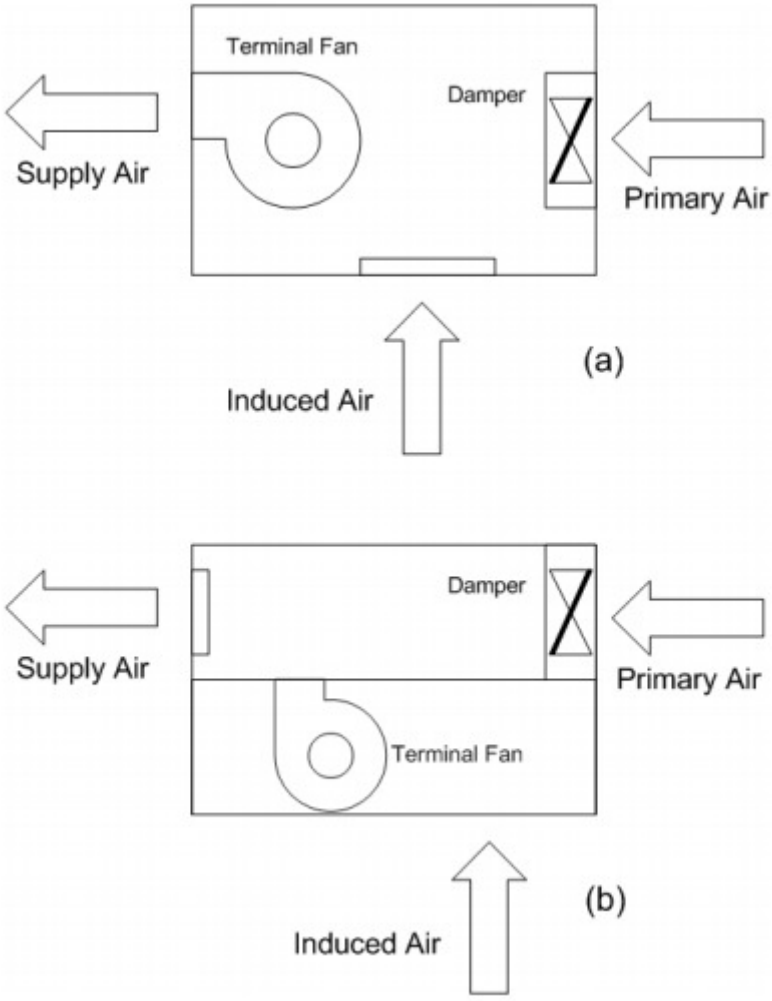

Figure 3-2: (a) Generic Series Terminal Unit, (b) Generic Parallel Terminal Unit (Cramlet 2008)

While the manufacturers differed in their specific designs, they all followed the general design elements shown in Figure 3-2, and thus contain similar elements. The internal components of the VAV FPTUs are now discussed.

All terminal units have a primary air inlet to which the primary air ducts are connected. The inlet duct was circular, and contained a differential pressure sensor to measure the airflow into the FPTU. The sensor was designed to take a multi-point average pressure reading of the air entering the FPTU through the primary air inlet. Specifically, it took the velocity pressure at four points to gain a better representation of the average velocity pressure across the duct to gain a more accurate representation of the airflow in case of uneven flow. The outlet taps were then connected to a pressure transducer which read the differential pressure at the primary air inlet. Figure 3-3 shows a representation of this device.

Immediately after the inlet velocity pressure sensor was a mechanical damper used to regulate the amount of primary air delivered to the terminal unit. The terminal units tested in this study used one of two primary air dampers. The first was a butterfly

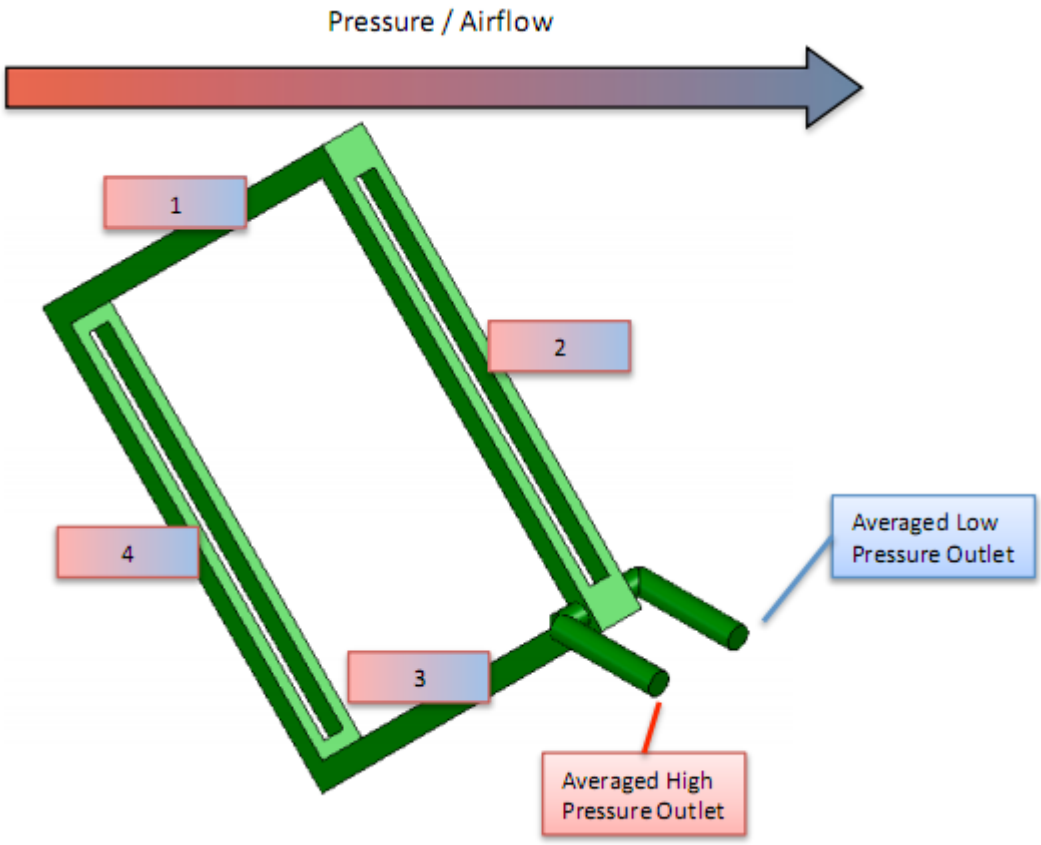

Figure 3-3: Inlet Air Velocity Pressure Sensor (Cramlet 2008)

type damper, shown in Figure 3-4a, which had an operating range from 0°, fully open, to 90°, fully closed. This design was used in the parallel terminal units. The second type of primary damper was an opposing blade damper, shown in Figure 3-4b, which had an operating range from 0°, fully open, to 45°, fully closed. This design was used in the series terminal units.

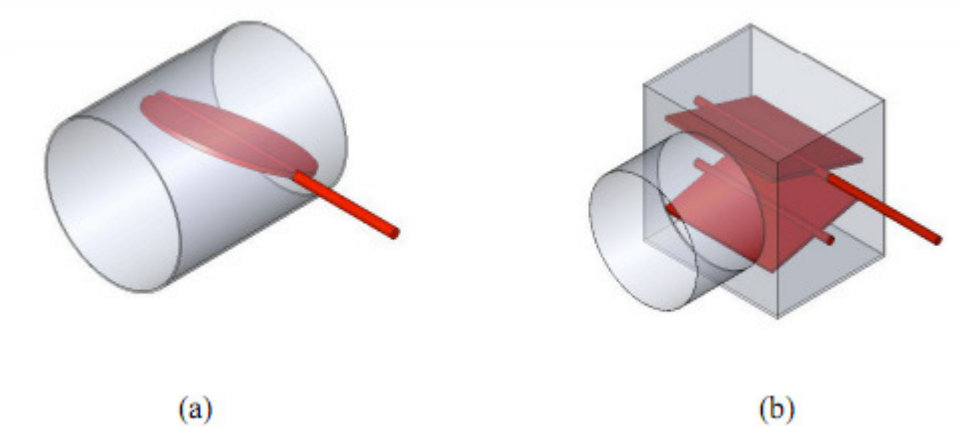

Figure 3-4: (a) Butterfly Damper, (b) Opposing Blade Damper (Cramlet 2008)

Both damper designs allowed the dampers to be operated by rotating a single shaft. The dampers were operated by using an actuator with a 0-10 VDC input control voltage. By using an electronically controlled actuator, damper angles were able to be accurately and precisely controlled for all terminal units. Figure 3-5 illustrates the damper actuator and control of a butterfly damper, which is similar to an opposing blade damper except for angle of shaft rotation.

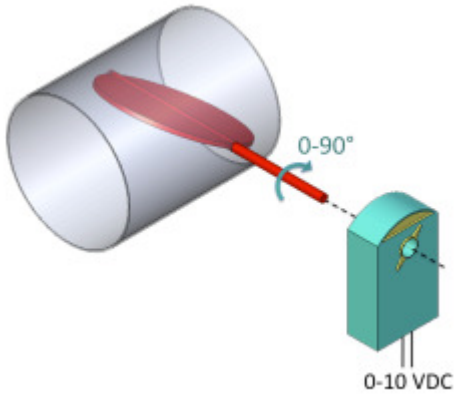

Figure 3-5: Electronic Damper Actuator (Cramlet 2008)

After the damper actuator, some designs incorporated a diffuser to smooth the airflow into the terminal unit. The diffuser type implemented in this study was a piece of perforated sheet metal placed orthogonal to the primary inlet. Figure 3-6 shows the basic design and location of this diffuser.

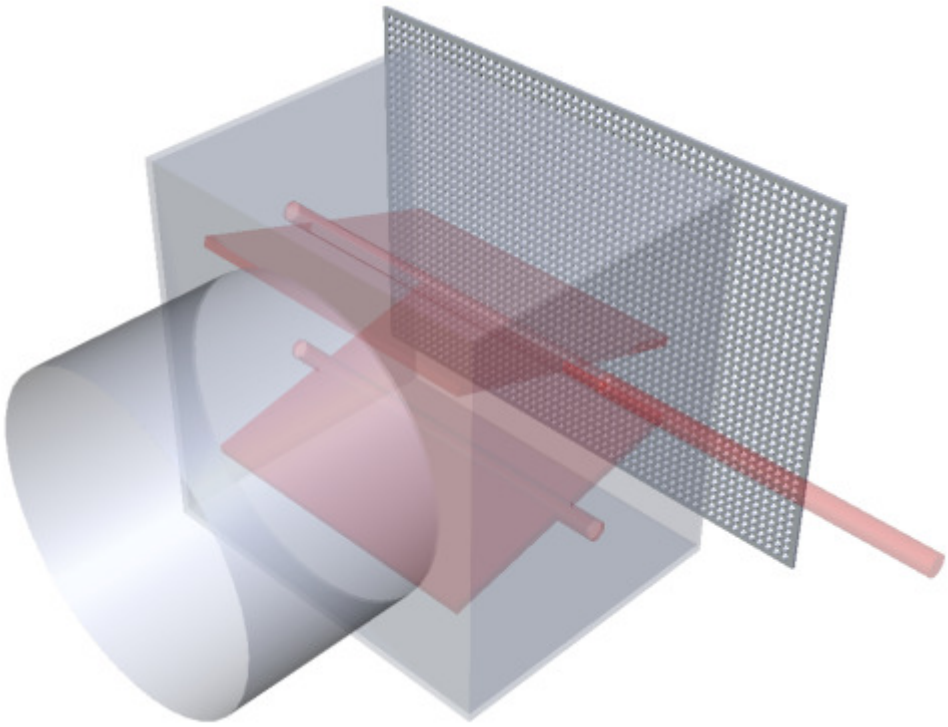

Figure 3-6: Primary Air Inlet Diffuser (Cramlet 2008)

The main feature of a FPTU is the small fan located inside the terminal unit. Although these fans are typically single width centrifugal fans using a forward curve blade, shown in Figure 3-7, they do come in a variety of sizes and voltages. All of the fans in this study were supplied with single phase 277 VAC power. Depending on the size and airflow needs of the FPTU, several different capacities were used. Table 3-1 shows the fan capacities used in the different terminal units.

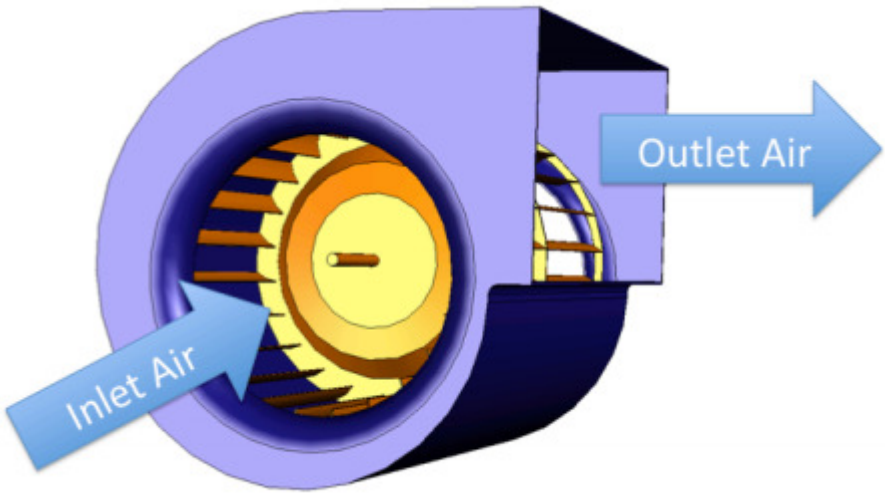

Figure 3-7: Single Width, Forward Curve Centrifugal Fan (Cramlet 2008)

Table 3-1: Terminal Unit Fan Capacities

FPTU	Rated Fan Power
S8A	½ hp (373 W)
S8B	½ hp (373 W)
S8C-M2	½ hp (373 W)
S12A	1 hp (746 W)
S12B	½ hp (373 W)
S12C-M1	¾ hp (559 W)
S12C-M2	¾ hp (559 W)
P8A	½ hp (373 W)
P8B	½ hp (373 W)
P8C-M2	½ hp (373 W)
P12A	1 hp (746 W)
P12B	½ hp (373 W)
P12C-M1	¾ hp (559 W)
P12C-M2	¾ hp (559 W)

All terminal unit fans in this study utilized electronically commutated motors (ECM). These consist of a brushless DC motor containing an internal inverter and microprocessor based motor controller. Figure 3-8 shows a typical ECM motor. The controller and motor were matched to the terminal unit fan, and then programmed by the manufacturer depending on the specific needs of the FPTU. The ECM controller can dynamically adjust fan torque and speed to provide a specific airflow through the fan.

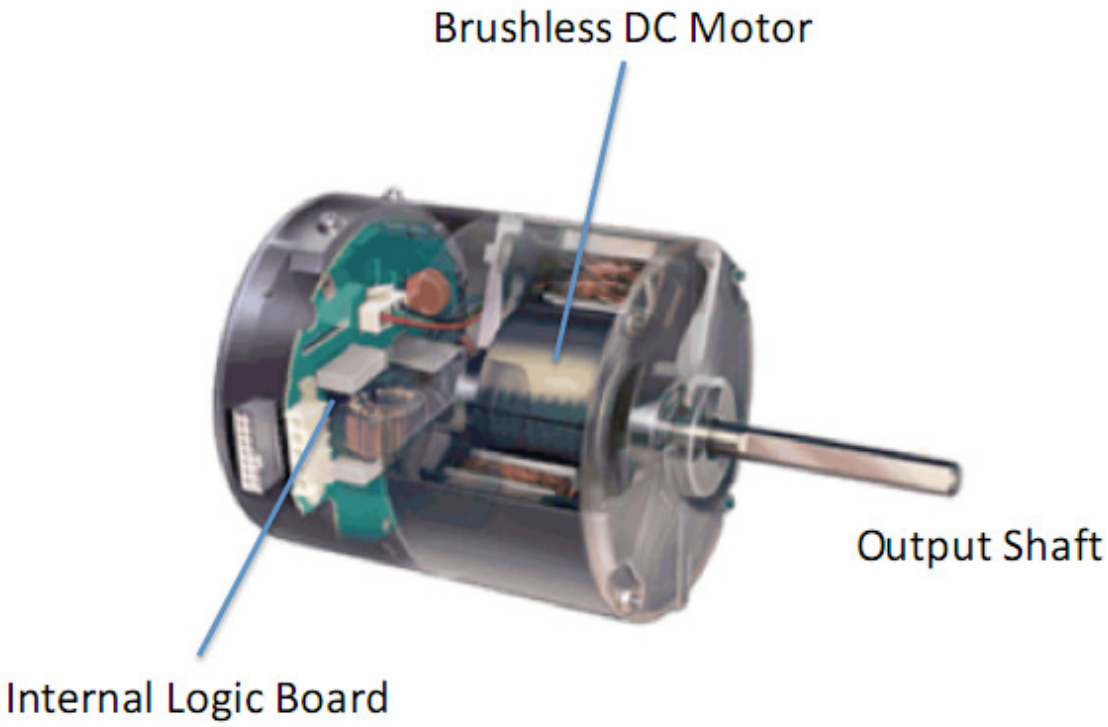

Figure 3-8: Typical ECM Motor (Cramlet 2008)

The final feature of the terminal units is this study is the back draft damper, which is only found on parallel units. The purpose of this damper is to prevent

conditioned primary air from flowing back through the terminal unit fan during times that the fan is not operating. By limiting the amount of leakage through the fan, overall terminal unit efficiency is improved. Although some parallel FPTUs have utilized a back draft damper operated by the primary air stream (Furr 2006), illustrated in Figure 3-9, all terminal units in this study used a gravity operated design Figure 3-10. The air operated damper was hinged along the upstream edge, and was closed by the force of the primary air striking the damper arm. The gravity operated damper was hinged along the upper edge of the fan outlet, and closed due to the weight of the damper itself. The internal pressure of the FPTU also assisted the seal of the back draft damper once it was closed. Both types were meant to remain closed except when the terminal unit fan is in operation, in which case the pressure at the fan outlet would overcome the pressure on the damper and open it up.

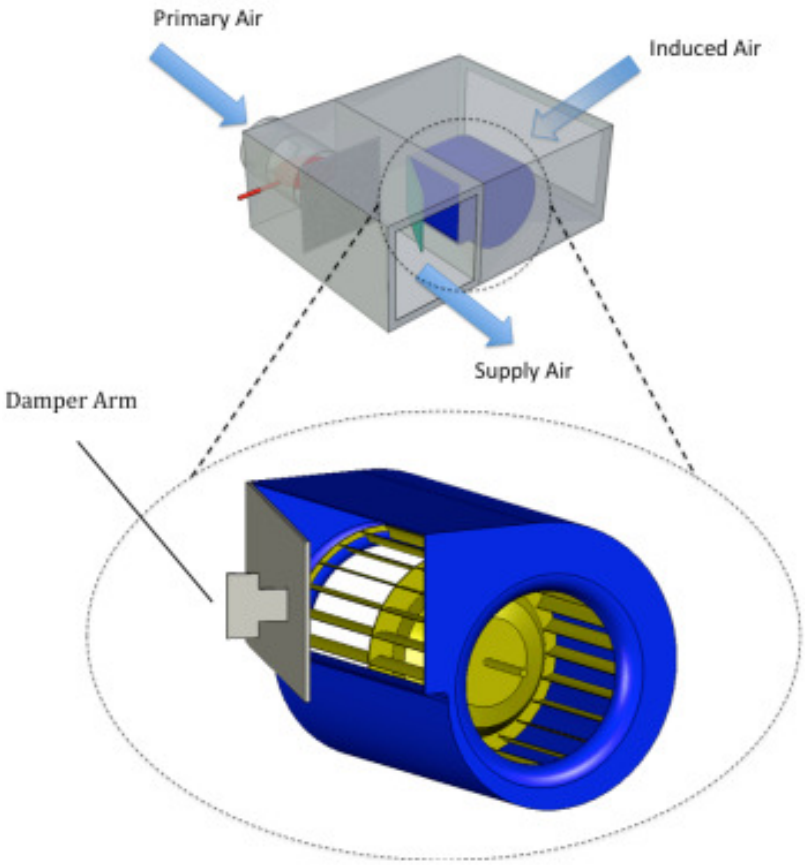

Figure 3-9: Air Operated Back Draft Damper (Cramlet 2008)

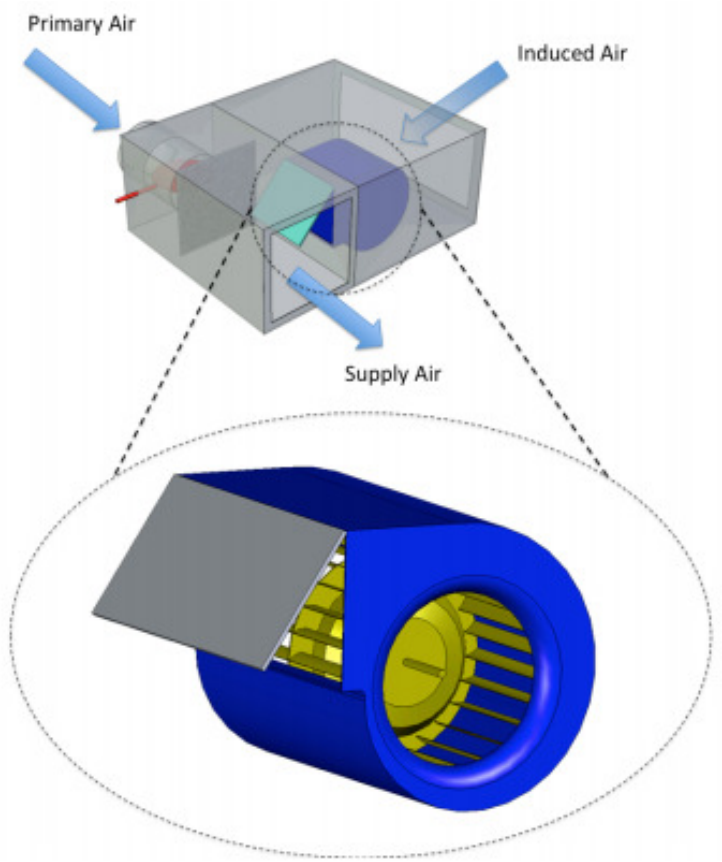

Figure 3-10: Gravity Operated Damper (Cramlet 2008)

3.1.2. Primary and Assist Fans. All airflow quantities were calculated using the procedures outlined in ANSI/ASHRAE Standard 120 (1999). The overall airflow equipment configuration setup is shown in Figure 3-1, while the configuration and features of the upstream and downstream airflow chambers are detailed in Figure 3-11 and Figure 3-12 respectively. Both the AMCA Figure 15 and AMCA Figure 12 airflow chambers were built to the specifications in Air Movement & Control Association International, Inc. (AMCA) Standard 210 (1999).

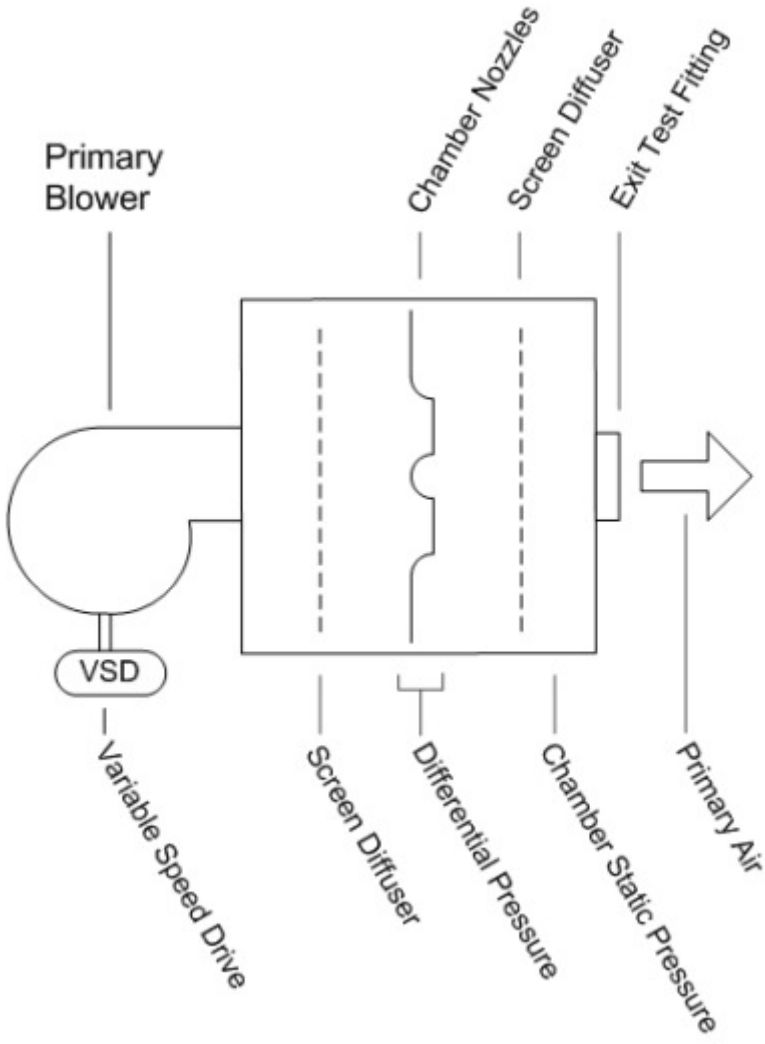

Figure 3-11: AMCA Figure 15 Flow Metering Nozzle Chamber (Cramlet 2008)

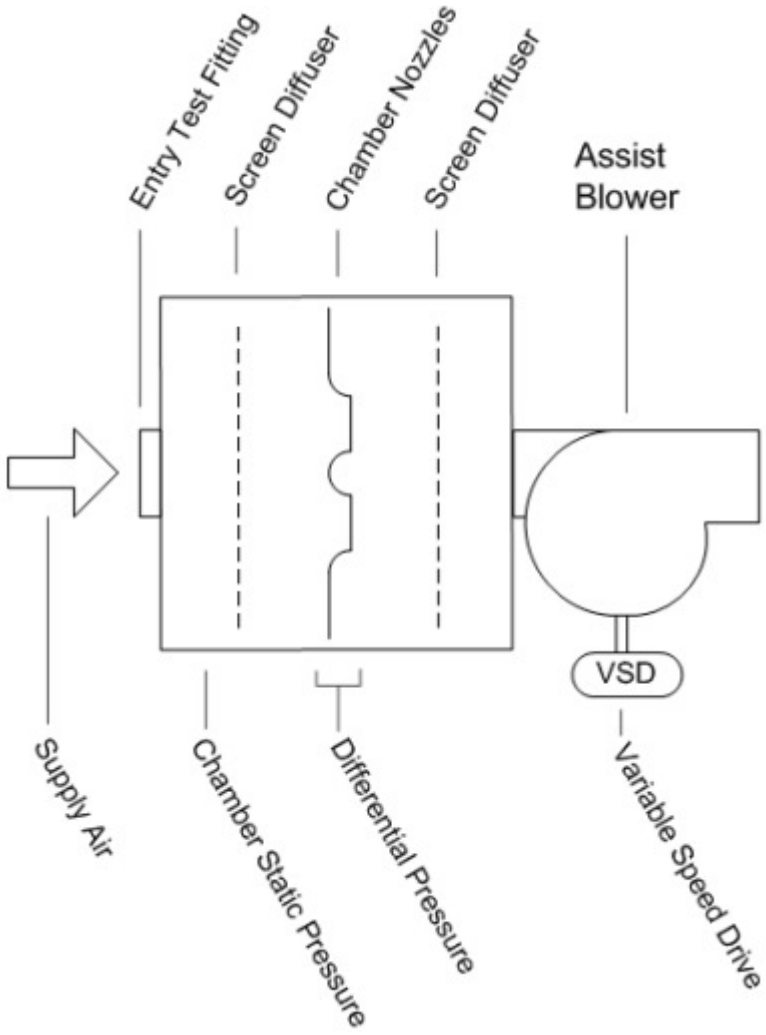

Figure 3-12: AMCA Figure 12 Flow Metering Chamber (Cramlet 2008)

A large capacity primary blower supplied air to the AMCA Figure 15 chamber. The blower was dynamically controlled using a variable speed drive (VSD) controller. Two diffuser screens were used to smooth air entering and exiting a nozzle bank. Nozzles were selected by covering or uncovering the outlet of the nozzle. Airflow was determined from the cumulative cross-sectional area of the nozzles, the pressure

differential across the nozzles, and the static pressure inside the chamber. Airflow was adjusted to standard temperature and pressure to compensate for variations in the environmental conditions inside the lab during testing. At the exit of the chamber was a fitting built to specifications in ANSI/ASHRAE Standard 120 (1999).

The AMCA Figure 12 chamber was similar to the AMCA Figure 15 chamber, except that the fitting was on the entrance and the fan at the exit. The assist blower was used to decrease the pressure immediately upstream of the chamber downstream static pressure in Figure 3-1. The nozzles in this chamber allowed for the measurement of the airflow downstream of the FPTU, which included air induced by the terminal unit fan as well as leakage from the VAV FPTU.

Figure 3-13 shows the different air streams for an FPTU. Several assumptions were used to simplify the conservation of mass equations (Equation 3-1). All airflow measurements were assumed to be taken at steady state, which leads to Equation 3-2. The mass flow is equal to volumetric flow multiplied by density (Equation 3-3). Since uniform unconditioned laboratory air was used for both primary and induced air, and the temperature rise across the fan was assumed to be negligible, the density of the air was assumed to be constant. This results in the airflow in being equal to the airflow out (Equation 3-4).

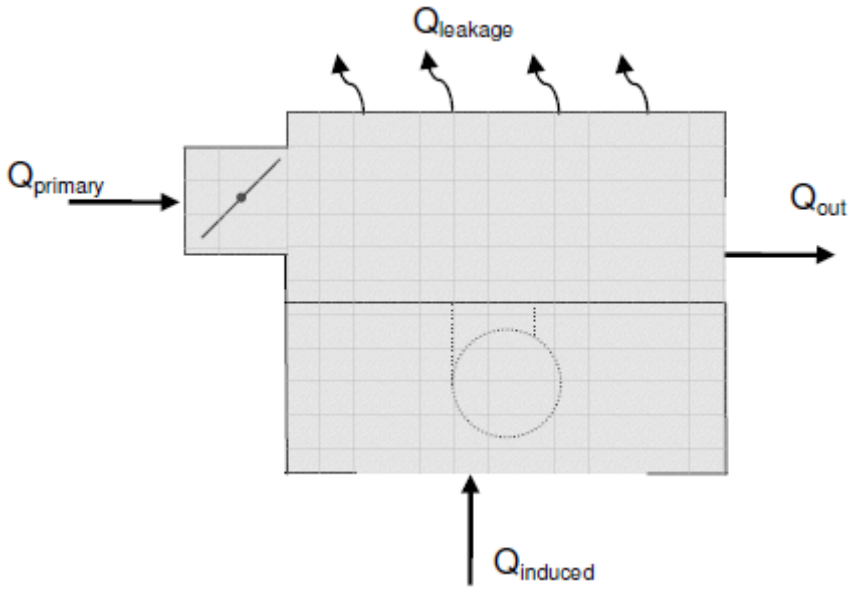

Figure 3-13: Volumetric Balance of FPTU (Furr 2006)

$$\frac{dm}{dt} = \sum \dot{m}_{in} - \sum \dot{m}_{out} \tag{3-1}$$

$$\dot{m}_{out} = \dot{m}_{in} \tag{3-2}$$

$$\dot{m} = \dot{Q}\rho \tag{3-3}$$

$$\sum_{out} airflow = \sum_{in} airflow \tag{3-4}$$

The airflow induced by the terminal unit fan in a parallel FPTU is calculated as the difference between the airflow through the AMCA Figure 15, $Q_{primary}$, and AMCA Figure 12, Q_{out}, chambers (Equation 3-5). It must be noted that this includes leakage

from the terminal unit. In a series FPTU, the flow rate of the terminal unit fan is simply the airflow through the AMCA Figure 12 chamber.

$$Q_{induced} = Q_{out} - Q_{primary} \quad (3\text{-}5)$$

Table 3-2 shows the different characteristics of the two airflow chambers used in the test. As shown, nozzle combinations differed between the chambers, and were operator selectable depending on the specific needs of the test. As the cumulative nozzle area was increased, less static pressure was required to generate the same amount of airflow. The complete procedures used to calculate airflow were in ANSI/ASHRAE Standard 120 (1999). Table 3-3 shows the power, controller, and motor characteristics of the two chambers.

Table 3-2: Chamber Airflow Characteristics

AMCA Chamber	**Maximum Flow** CFM (m^3/s)	**Available Nozzles' Diameters** Inches (cm)					
Figure 15	4000 (1.89)	1.5 (3.8)	3 (7.6)	5 (12.7)	5 (12.7)	5 (12.7)	5 (12.7)
Figure 12	5000 (2.36	1.5 (3.8)	5 (12.7)	5 (12.7)	8 (20.3)		

Table 3-3: Chamber Power Characteristics

AMCA Chamber	**Fan Power** Hp (kW)	Controller	Motor
Figure 15	10 (7.5)	VSD	AC Induction
Figure 12	7.5 (5.8)	VSD	AC Induction

Sheet metal ductwork was used to connect the airflow chambers to the terminal unit being tested, see Figure 3-14. The length of this ductwork, as well as the location of the static pressure points, was dictated by ANSI/ASHRAE Standard 130 (2006). The duct upstream of the terminal unit was circular duct of the same diameter as the air inlet port on the terminal unit. The downstream duct was a rectangular duct 16 in (40.6cm) x 15 in. (38.1 cm) with an equivalent diameter of 17 in. (43.2 cm). At the location of the static pressure measurements, holes were drilled into the metal, and covered with copper pressure taps of the same diameter. The copper taps were then sealed with adhesive tape. To measure the average static pressure inside the duct, four holes were used, 90° apart, with the taps connected in such a way that the length of tubing to the pressure transducer was the same for all of the taps. Figure 3-15 shows an illustration of the copper pressure taps and how they were applied to the sheet metal ducting. Figure 3-16 illustrates how the taps were connected with tubing to measure the average static pressure.

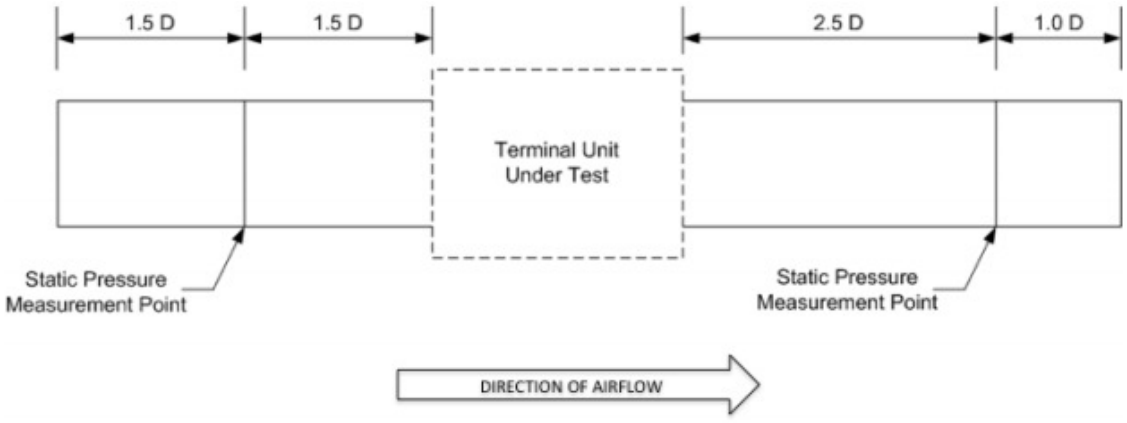

Figure 3-14: Experimental Ductwork (Cramlet 2008)

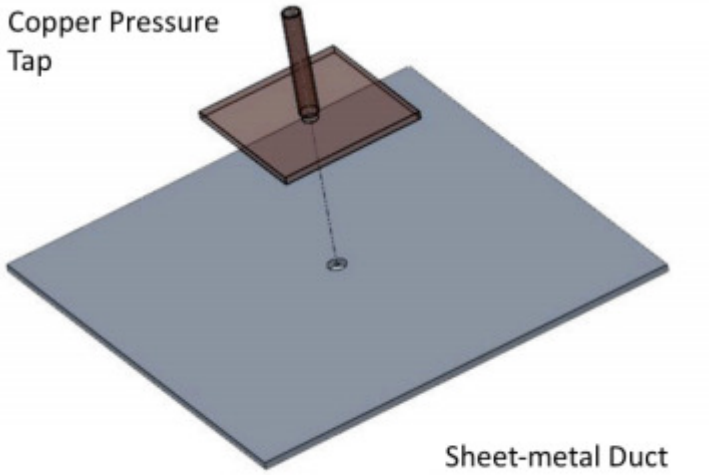

Figure 3-15: Pressure Tap (Cramlet 2008)

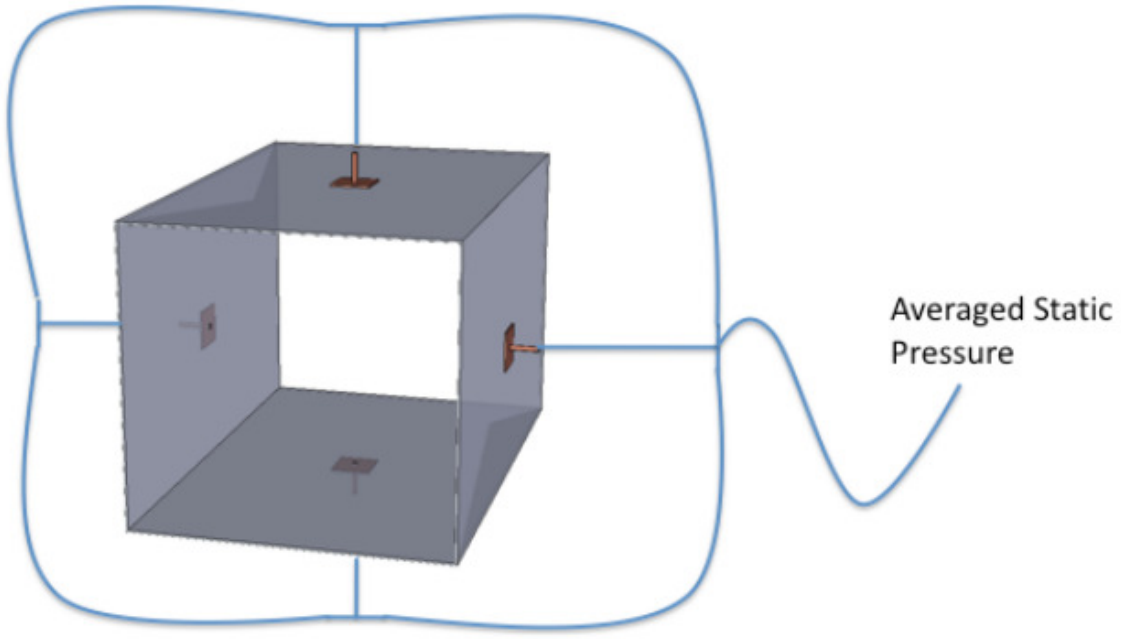

Figure 3-16: Pressure Taps and Connecting Tubing (Cramlet 2008)

3.1.3. Data Acquisition. This study required the measurement of several different pressures, both static and differential, as well as temperature and relative humidity (RH) to accurately measure the airflow. All pressure measurements were made using Dwyer Series 616C pressure transducers connected to pressure taps with flexible tubing. Since the different pressure measurements were in different pressure ranges, several sizes of pressure transducers were used, a complete listing can be found in Table 3-4. All transducers were calibrated with a water manometer to within 0.01 in. w.g. (2.49 Pa), and had an accuracy of 0.25% of full-scale output.

Table 3-4: Sizing of Pressure Transducers

Pressure Location	Transducer size in. w.g. (kPa)
Figure 15 differential pressure	0-6 (0-1.5)
Figure 15 static pressure	0-10 (0-2.5)
Upstream static pressure	0-2 (0-0.5)
Inlet air velocity pressure	0-2 (0-0.5)
Downstream static pressure	0-2 (0-0.5)
Figure 12 static pressure	0-10 (0-2.5)
Figure 12 differential pressure	0-6 (0-1.5)

All pressure transducers utilized an output signal of 4-20 mA, so terminating resistors were used to convert the current into a voltage for the data acquisition system to measure. During testing, the output signal of the pressure transducers was found to contain significant noise, sometimes of a much greater magnitude than the real signal. Some of this came from pressure pulsations of the fans, and some appeared to be due to dirty system power. For this reason, low-pass RC filters were constructed for each of the

pressure transducers; see Figure 3-17 for design of a low-pass RC filter. These filters used a 330 Ω resistor and a 1000 μF capacitor, which when used in Equation (3-6) indicate a cutoff frequency of 0.5 Hz. Using this cutoff frequency in Equation (3-7) means that noise from dirty power, which was the largest source, at 60 Hz will be reduced by over 99%. To further reduce the impact of noise, pressure measurements were made at 1000Hz and averaged over 10 seconds.

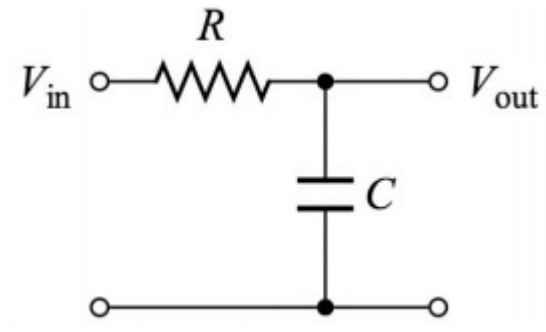

Figure 3-17: RC Filter (Cramlet 2008)

$$f_b = \frac{1}{2\pi RC} \tag{3-6}$$

$$|H(f)| = \frac{1}{\sqrt{1+(\frac{f}{f_b})^2}} \tag{3-7}$$

Temperature and RH measurements were also taken with transducers with a linear output, though in this case it was a voltage output rather than a current output, so

no terminating resistors were needed. These measurements were taken using a dual purpose probe (Rotronic L-Series) placed near the induced air inlet on the FPTU, though care was taken to insure it did not interfere with airflow into the FPTU. The output signal from this probe did not seem to be as affected by noise, so no RC filters were needed. The probe had an accuracy of ±0.9°F (±0.5°C) for temperature and ±0.3% for RH. A mercury thermometer was also placed near this probe to allow for quick verification of temperature. Periodically, the RH reading was verified using the wet bulb temperature in the lab.

The computer data acquisition system consisted of two internal and two external DAQ boards from national instruments. All pressure measurements were recorded using a 16-bit, 8-channel differential input NI-SC2040 external board connected to an NI-6034 internal PCI board. Temperature and RH were recorded using an NI-6024E internal PCI board used in conjunction with a CB-68LP external terminal block. This allowed for 12-bit resolution on inputs, and also provided two 0-10 VDC analog outputs. These outputs were used to control the primary and assist blowers on the airflow chambers. A custom Visual Basic (Microsoft 1998) program was the user interface for the National Instruments DAQ equipment. The 0-10 VDC control signals for the damper actuator and ECM control were provided by manual external power supplies. A custom program was written using VB.net (Microsoft 2007) to automatically collect the data from all of the tests for a FPTU into a single spreadsheet, and also sorted the data into another spreadsheet for ease of analysis.

3.2. Power Equipment

All electrical power measurements were made in accordance with ASHRAE Standard-130 (2006). A Fluke 435 power quality analyzer was used to measure the FPTU power characteristics. The measurements were made exterior to any internal components of the ECM motor setup, including the ECM controller which was powered via the main supply line using a transformer to convert the 277 VAC to 24 VAC. For most of the FPTUs, the total current draw was less than 5A, so Fluke i5s current probes with a 0-5A range were used. These probes had a basic accuracy of 1% of reading, plus 5mA for readings below 1A (Fluke 2005). On some of the larger FPTUs, the current draw exceeded 5A at higher ECM settings, but remained below 10A. For these cases, Fluke i1000s selectable range current probes were used. For the 0-10A range, these probes had a basic accuracy of 3% of reading plus 0.1A (Fluke 2000). Table 3-5 lists which tests used the different current probes with 5A representing the i5s probes and 10A representing the i1000s probes set to the 10A range.

Table 3-5: List of Current Probes Used

FPTU	ECM Setting			
	25%	50%	75%	100%
ECM_S8A	5A	5A	5A	5A
ECM_S8B	5A	5A	10A	10A
ECM_S8C-M2	5A	5A	5A	5A
ECM_S12A	5A	5A	5A	10A
ECM_S12B	5A	5A	5A	10A
ECM_S12C-M1	5A	5A	10A	10A
ECM_S12C-M2	5A	5A	5A	10A
ECM_P8A	5A	5A	5A	5A
ECM_P8B	5A	5A	5A	5A
ECM_P8C-M2	5A	5A	5A	5A
ECM_P12A	5A	5A	5A	10A
ECM_P12B	5A	5A	5A	5A
ECM_P12C-M1	5A	5A	5A	5A
ECM_P12C-M2	5A	5A	5A	5A

The simultaneously measured and recorded electrical data included, but was not limited to, voltage, current, real power, apparent power, power factor, THD, and up to the 25th harmonic of voltage, current, and power. Current probes were placed on the main power and neutral lines, while voltage probes were placed on the main, neutral, and ground lines, see Figure 3-18. The data from several tests were stored in the analyzer's internal flash memory, and then downloaded all at once to the pc via a proprietary usb interface. Fluke Power Log (2008) software was used to operate the usb interface. After the files were downloaded and saved on the pc, the Power Log (2008) software was used to export most of the electrical data into text files. These text files were then converted into Excel files prior to the data being collected by the previously mentioned vb.net (Microsoft 2007) program.

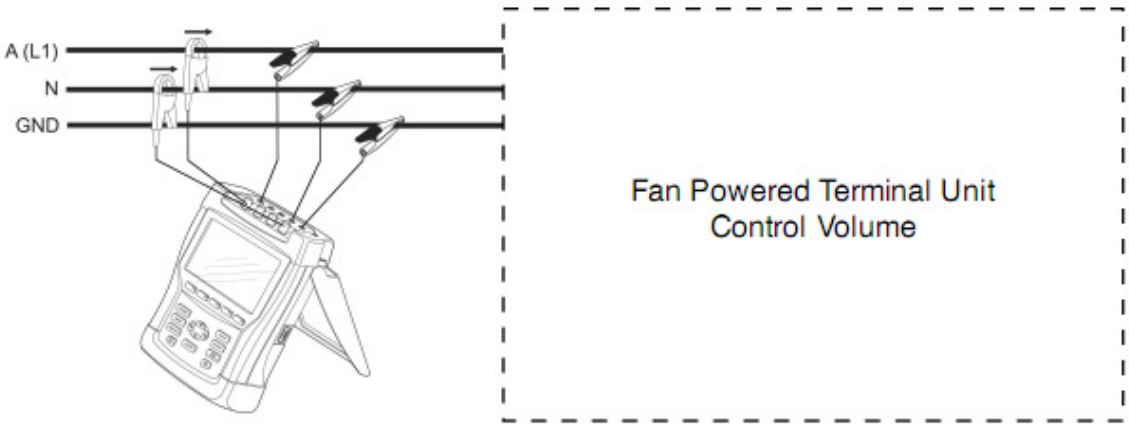

Figure 3-18: Setup of Electrical Measurements (Cramlet 2008)

CHAPTER IV

EXPERIMENTAL PROCEDURE

Experimental data were collected on 14 VAV fan powered terminal units from three different manufacturers. The previous chapter explains the equipment used to perform the tests and measure the different variables. This chapter explains the procedures used to conduct the tests, the process used to acquire the data, and the statistical analysis applied to the raw data to develop the semi-empirical models of terminal unit performance.

4.1. Method of Experimentation

This study used the same basic factorial test matrix developed by Cramlet (2008). Several independent test variables were chosen for both their representative nature of terminal unit performance, as well as availability for measurement in the field. The range and levels used for the variables was chosen to obtain an accurate representation of performance for typical operating conditions found in the field. Some tests were also performed at more extreme operating conditions to determine their effect on FPTU performance. Table 4-1 and Table 4-2 list the independent variables chosen, as well as the levels used for testing the series and parallel FPTUs respectively. For parallel units, a level of 0.0 in. w.g. (0 Pa) of upstream static pressure represented the minimum upstream static pressure required for positive air flow through the terminal unit, and was higher than the downstream static pressure. Test levels were adjusted based on each

unit's specific characteristic performance limits, due to differences in size and terminal unit design from manufacturer to manufacturer.

Table 4-1: Series Test Matrix

Independent Variable	Number of Test Points	Value Range
D, damper position	4	100%, 75%, 50%, 25% open
$\dot{V}$, ECM setting	4	100%, 75%, 50%, 25% full scale
P_{up}, upstream static pressure	6	0.0 – 2.0 in. w.g. (0 – 498 Pa)
P_{down}, downstream static pressure	1	0.25 in. w.g. (62 Pa)

Table 4-2: Parallel Test Matrix

Independent Variable	Number of Test Points	Value Range
D, damper position	4	100%, 75%, 50%, 25% open
$\dot{V}$, ECM setting	5	100%, 75%, 50%, 25%, 0% full scale
P_{up}, upstream static pressure	5	0.0 – 2.0 in. w.g. (0 – 498 Pa)
P_{down}, downstream static pressure	3	0.1 – 0.5 in. w.g. (25 – 125 Pa)

The position of the damper, D, varied for different FPTU configurations. Common to all was the use of a damper actuator operated by a 0-10 VDC control signal, generated by a regulated DC power supply. This actuator varied linearly from 0° (fully open) to fully closed as a function of control voltage. For units with a butterfly damper, the range of motion was from 0° to 90°. The test positions used were 0°, 22.5°, 45°, and

67.5°. For units with opposing blade dampers, the range of motion was only 0° to 45°, so the tests were performed at 0°, 11.25°, 22.5°, and 33.75°. The fully closed position was not included in the factorial matrix because it eliminated the effect of upstream static pressure on the terminal unit performance. It also eliminated any primary supply air flow into the FPTU.

Each manufacturer used a different method to operate the ECM controller, which controlled the speed and torque of the fan motor. Each motor controller was uniquely programmed, so motor speed did not correlate precisely to input voltage. ECM input setting was used as the independent variable. Three types of controllers were provided, and each controller was set to airflows of 100%, 75%, 50%, and 25%. Manufacturer A provided a controller that was set to a value between 0 and 100, so settings of 100, 75, 50, and 25 were used. Manufacturer B provided a controller that was set using a 2 – 10 VDC signal, so settings of 4 VDC, 6 VDC, 8 VDC, and 10 VDC were used. Manufacturer C provided a controller that was set with a 0 – 10 VDC signal, so settings of 2.5 VDC, 5 VDC, 7.5 VDC, and 10 VDC were used. On series units, testing with the terminal unit fan off was impractical because the fan had to be running for air to be supplied to the zone. For parallel units, however, turning the terminal fan off put the FPTU into full cooling mode. This allowed the performance to be measured for times when the terminal fan would not required to operate, and also helped quantify FPTU leakage since there would be no induced air in this case.

Both upstream and downstream static pressures depend on the conditions inside a building. They were both included in the data collection due to their significant effect

on VAV FPTU performance. These pressures were adjusted by varying the speed of the primary and assist blowers, which was facilitated by a Visual Basic (Microsoft 1998) data acquisition program. Upstream static pressures were varied from 0 in. w.g. (0 Pa) to 2.0 in. w.g.(498 Pa) for both series and parallel terminal units. The downstream static pressure affected each configuration differently. In parallel terminal units, the upstream pressure must be greater than the downstream pressure to prevent air from flowing backwards through the terminal unit. The test matrix for parallel units ensured that upstream static pressure would always be greater than the downstream pressure. Because series units do not have this same limitation, a different test matrix was used which did not vary downstream static pressure.

4.2. Environmental Considerations

All testing was performed at the Energy Systems Laboratory facility at the Riverside Campus of Texas A&M University. The test setup was located in an open, high-bay lab. Depending on the local environmental conditions, the lab had the capability to operate without external cooling. Some tests were run during these time periods, while others were run during times when space heating or cooling was required. Because of this variation in laboratory operation, the air temperature for testing ranged from 67.0°F (19.4°C) to 81.6°F (27.6°C). The relative humidity (RH) ranged from 22.5% to 79%.

Though typical HVAC systems supply cooled air at 55°F (12.8°C), this study used unconditioned laboratory air since it was primarily concerned with the performance of the terminal unit itself. Temperature and humidity were recorded as outlined in the

previous chapter, and were assumed to be uniform throughout the test setup, though there could be a temperature rise of as much as 2°F (1.2°C) across the fans. For example, the density of air at 70°F (21°C) and 60% RH is 0.0738 lb/ft^3 (1.18 kg/m^3). The density of air at 75°F (24°C) and 50% RH is 0.0731 lb/ft^3 (1.17 kg/m^3). Note, both of these conditions have approximately the same specific humidity. This 5°F (2.8°C) temperature difference results in a density difference of less than 1%. This shows that the effect of temperature rise due to fans can be ignored.

The procedures used to calculate air flow can be found in ANSI/ASHRAE Standard 120-99 (1999). This standard specifies a procedure to calculate airflow utilizing temperature, RH, and pressure measurements. All air flow calculations were adjusted to a standard air flow based on a reference air density of 0.075 lb/ft^3 (1.20 kg/m^3). This was done for two main reasons. First, all test results, regardless of actual conditions at time of testing, needed to be directly comparable. Second, it allowed results to be applicable across different climate and altitude conditions.

4.3. Statistical Analysis

The statistical analysis was performed using SPSS (2008) software. The goal of the analysis was to generate simple, intuitive, and, most importantly, accurate models of FPTU performance. Models were generated for primary airflow, fan airflow, terminal unit power consumption, and leakage (for parallel units).

Models were developed using similar techniques as used in previous VAV FPTU research performed by Furr (2006) and Cramlet (2008). The linear and non-linear regressions performed on airflow and power data included temperature, upstream and

downstream static pressures, inlet air velocity pressure, damper position, and ECM input voltage. Interdependent variables were carefully excluded as they would generate unnecessary redundancy. The assumptions used for the regression analysis were: an appropriate linear relationship between the response variable and predictors, independent and random errors, and constant variance of the errors (Montgomery et al. 2001).

The R^2 statistic was used to quantify the accuracy with which the statistical model correlated with the test data. The R^2 statistic varies between 0 and 1, and gives a measure of how well the statistical model represents the variance in the real data. As the value of R^2 rises, the model correlates better with the data. An R^2 value equal to one means the statistical model correlates with the data perfectly (Montgomery et al. 2001).

Since series and parallel terminal have fundamentally different performance characteristics, different statistical analyses were required for each type of FPTU. The main difference in the two analyses was in the specific variables used, though the general form was consistent. For example, in modeling the airflow of the terminal fan in series units, inlet air velocity pressure was used. In parallel units, the inlet air velocity pressure was replaced by the downstream static pressure. This pressure could not be used for series units because it was constant for all tests. When possible, while maintaining sufficiently high R^2 values, the same form of equations was used for both series and parallel units. Since the same form of expressions were used as in previous research (Furr 2006 and Cramlet 2008), it was possible to compare results from both ECM and SCR controlled FPTUs. It should be noted that due to the difference of type

and magnitude of the voltages used, 160 VAC to 280 VAC on SCR units and 0 VDC to 10 VDC on ECM units, the coefficients between the two had different meanings.

CHAPTER V

SERIES TERMINAL UNITS RESULTS AND MODELS

Experimental data were collected on seven ECM controlled fan powered terminal units. This section discusses those results, and compares them to results from previous studies by Cramlet (2008) and Furr (2006). Models were developed for both the airflow and power performance of the units. The goal was to develop simple models similar to previous models by Cramlet and Furr that would provide sufficient characterization of the FPTUs for use in building simulation models. The airflow and power results and models are discussed in separate sections. Each section contains a brief summary of the method used, the results of this study, a comparison to previous results, and a discussion.

During testing, it was observed that some conditions caused the terminal unit fan to run backwards. These conditions were usually well beyond the normal operating conditions of the terminal units, and were not used for the data analysis.

It was also observed, that when the ECM controller was turned to its highest setting, the fan sometimes pulsed or even cycled on and off. While this is a normal result of operating the motor at or exceeding its designed range, it caused several difficulties in testing. First, it was difficult to achieve equilibrium to run some tests. A second difficulty arose from using the PC to measure airflow and the Fluke 435 to measure power, since they were not synchronous. At these conditions, it was possible that the airflow was measured during a spike in airflow, while the power was measured

in a dip, or vice versa. This meant that the recorded power could vary from the power being consumed at the moment the airflow was measured.

5.1. Series Terminal Unit Airflow

Series terminal units are characterized by a centrifugal fan in line with the primary airstream. These units require that the fan be operated continuously to supply air to the conditioned space. If the primary airflow is lower than the air being supplied by the terminal unit fan, additional air can be drawn in from the plenum. Both the primary airflow delivered to the FPTU and the air delivered by the FPTU fan need to be quantified.

In a series terminal unit, the internal pressure is affected by variations in upstream duct static pressure, damper position, and primary airflow. Even with these variations, a series terminal unit will typically provide fairly constant airflow at a given fan setting (Alexander and Int-Hout 1998). This result has been confirmed by this study, as well as by Cramlet (2008) and Furr (2006). The exception would be at extreme conditions which caused the fan to rotate backward or pulse on and off. Absent these extreme conditions, the variable with the largest impact was the ECM fan setting.

5.1.1. Primary Airflow Analysis and Model. The primary air supplied to the FPTU was modeled as a function of the pressure differential across the FPTU and the air inlet damper position. In this study, the downstream static pressure was used in conjunction with the upstream static pressure to calculate this differential pressure, DP. If the internal pressure of the terminal unit were typically measured in series units, it would

probably provide a better variable for the unit's performance rather than the downstream static pressure. However, no FPTUs provide static pressure taps at this location.

Different manufactures used either butterfly or opposing blade designs for the primary air inlet damper. During testing, both types of dampers were set at 100% open, 75% open, 50% open, and 25% open. Manufacturer C used an opposing blade type damper for both brands of motors. In this case, 0° indicated a fully open damper, while 45° represents a fully closed damper. Both Manufacturers A and B used a butterfly damper. In this case, 0° indicates a fully open damper, while 90° represents a fully closed damper.

Figure 5-1 shows the primary air plotted against DP for the 8" series FPTU from Manufacturer C, using motor M2. Figure 5-2 shows this same plot for the 12" series FPTU from Manufacturer A. The curves are generated using the models presented later in this section. A full set of results were included in Appendix A.

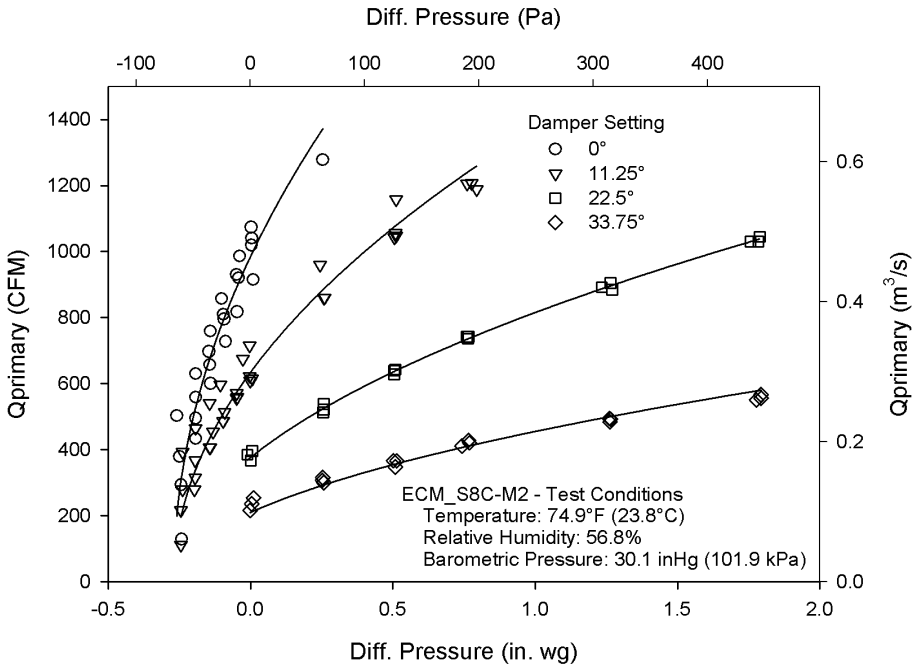

Figure 5-1: $Q_{primary}$ vs. DP for ECM_S8C-M2

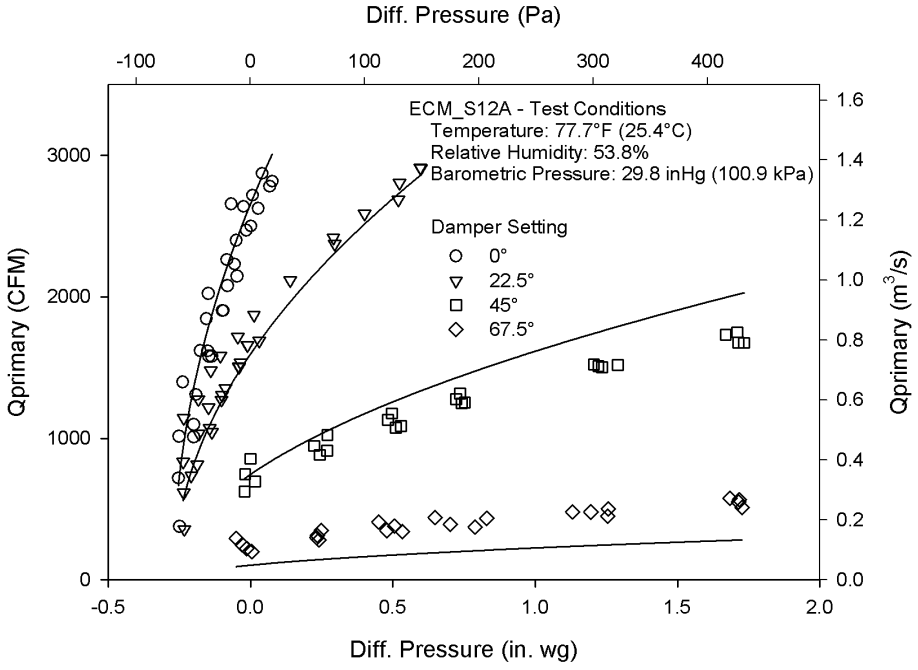

Figure 5-2: $Q_{primary}$ vs. DP for ECM_S12A

The form of the equation of these curves was originally developed by Furr et al. (2008), and presented in Equation (5-1). The primary airflow delivered to the FPTU was proportional to the square root of the differential pressure across the terminal unit at a given damper setting. Because the downstream static pressure was maintained at 0.25 in w.g. for all of the tests, the DP required an offset to keep the value inside the square root positive. Furr et al. (2008) determined that an offset of 0.27 in. w.g. best fit the empirical data, and the same offset was used in this study to maintain model consistency. If the static pressure internal to the FPTU were measured and used in the model, it is likely no offset would be needed. It would also likely improve the model, since the pressure rise across the fan would be eliminated.

$$Q_{primary} = C_1 * (1 + C_2 * S + C_3 * S^2) * \sqrt{DP + 0.27} \qquad (5\text{-}1)$$

The coefficients of the model for the different terminal units tested, as well as the R^2 values are presented in Table 5-1. The results for FPTU ECM_S8C-M1 were measured by Cramlet (2008). The results for the SCR FPTUs were determined by Furr et al. (2008), and presented in Table 5-2. When comparing FPTUs from Manufacturer C, the M1 terminal units were identical in design to the SCR controlled FPTUs, while the M2 terminal units had a slightly different design. None of the ECM controlled FPTUs were the same units used in the SCR controlled FPTU study (Furr 2006).

In general, this model correlated well with the measured performance. The R^2 values for the ECM controlled FPTUs ranged from 0.895 to 0.977. The R^2 values for the

SCR controlled FPTUs were slightly higher, with the lowest value being 0.920 and the highest reaching 0.987.

Table 5-1: Model Coefficients for ECM Controlled FPTU

FPTU	C1	C2	C3	R^2
ECM_S8A	1637	-1.95E-02	7.80E-05	0.955
ECM_S12A	5109	-2.15E-02	1.14E-04	0.946
ECM_S8B	2094	-2.83E-02	2.06E-04	0.962
ECM_S12B	5886	-3.17E-02	2.54E-04	0.895
ECM_S8C-M1	2344	-3.84E-02	4.15E-04	0.977
ECM_S8C-M2	1895	-3.58E-02	3.70E-04	0.951
ECM_S12C-M1	5125	-3.09E-02	1.28E-04	0.927
ECM_S12C-M2	4561	-1.86E-02	-1.71E-04	0.909

Table 5-2: Model Coefficients for SCR Terminal Units

FPTU	C1	C2	C3	R^2
SCR_S8A	1644	-1.94E-02	8.46E-05	0.970
SCR_S12A	4350	-2.24E-02	1.29E-04	0.963
SCR_S8B	2127	-2.53E-02	1.78E-04	0.987
SCR_S12B	5903	-3.11E-02	2.67E-04	0.934
SCR_S8C	2137	-3.17E-02	2.82E-04	0.920
SCR_S12C	4022	-1.85E-02	-9.5E-.05	0.964

5.1.2. Fan Airflow Analysis and Model. The airflow provided by the fan in an ECM Controlled series FPTU is mainly a function of the ECM input setting. Some of the FPTUs also showed a slight dependence on inlet air velocity pressure, Piav. These results were similar to those obtained by Cramlet (2008) and Furr et al. (2008). One reason for the similar results was the design of the series terminal units. Because

upstream airflow and pressure have little effect on the internal static pressure, the fan sees approximately the same pressure differential over a wide range of operating conditions. Another reason the results were similar was the ECM Controller, which was designed to maintain constant airflow for a given ECM input setting despite changes in operating conditions. Figure 5-3 and Figure 5-4 show fan airflow versus inlet velocity pressure for FPTUs ECM_S8B and ECM_S12C-M2 respectively.

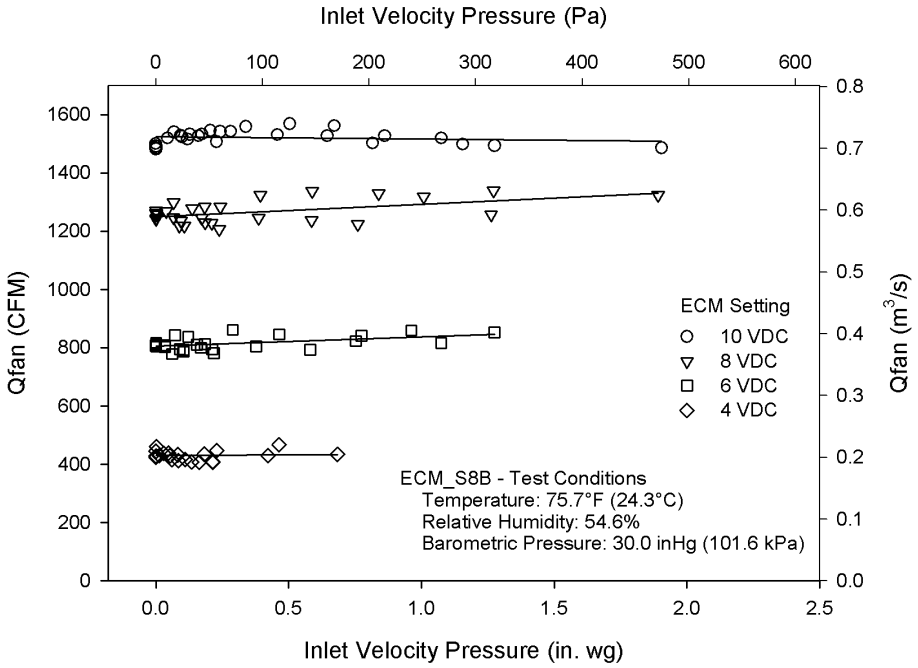

Figure 5-3: Q_{fan} vs. P_{iav} for ECM_S8B

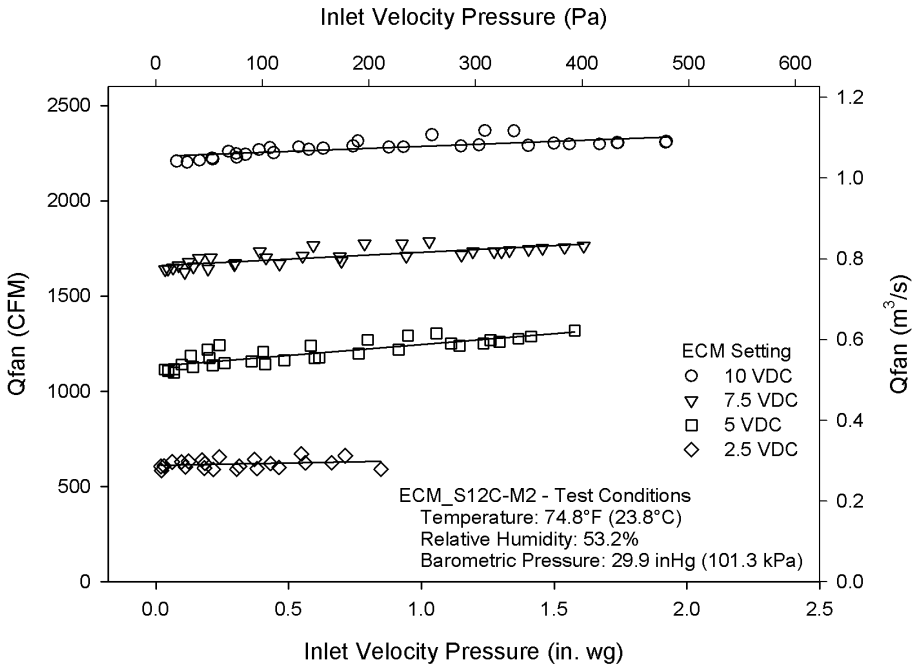

Figure 5-4: Q_{fan} vs. P_{iav} for ECM_S12C-M2

The main difference between these results and those obtained by Furr (2006) for the SCR controlled units, was the dependence of fan airflow on the fan setting. Due to the design of the ECM controller, the fan airflow varied approximately linearly with the change in ECM input setting. For example, if the ECM setting was doubled, the airflow approximately doubled. On the SCR models, changing the voltage by the same percentage did not change the airflow the same amount depending on what the starting voltage is. Starting at the minimum voltage, and increasing the SCR voltage by 30VAC did not result in the same airflow change as going from 30VAC below max voltage to the maximum SCR voltage.

The model used to fit the data is shown in Equation (5-2), and was similar to that used by Furr (2006). The ECM results are shown in Table 5-3, and the SCR results from Furr (2006) are shown in Table 5-4. It must be noted that V did not mean the same thing for the ECM and SCR models. In the ECM models, it was a percentage of the voltage between minimum and maximum ECM setting. The reason for using percentage instead of a straight DC voltage as used by Cramlet (2008) was that the ECM controllers were controlled by the three manufacturers in different ways, Table 5-5 provides a summary of the ECM settings used.

$$Q_{fan} = C_1 + C_2 * V^2 + C_3 * V + C_4 * P_{iav} \quad (5\text{-}2)$$

Manufacturer A provided a controller that was adjusted by turning a set screw to change the setting from 0 to 100, so settings of 25, 50, 75, and 100 were used. FPTUs from Manufacturer B were controlled with a 2-10 VDC input, so settings of 4, 6, 8, and 10 VDC were used. Manufacturer C provided a controller that was adjusted using a 0 – 10 VDC signal, so settings of 2.5, 5, 7.5, and 10 VDC were used. For the SCR units, V represents the AC voltage measured after the SCR controller. The SCR controller was set at several different voltages ranging from the minimum to the maximum voltage (Furr 2006).

This model correlated well with the data. The lowest R^2 value was 0.987 for ECM_S8A. For the SCR controlled FPTUs, the lowest R^2 was 0.989 for SCR_S8A. No results are included for SCR_S12B here because it required a different model due to a

malfunctioning SCR controller (Furr 2006). The coefficients for ECM_S8C-M1 were converted from VDC to % to match the other ECM controlled FPTU coefficients.

Table 5-3: ECM Coefficients for Fan Airflow Model

FPTU	C1	C2	C3	C4	R^2
ECM_S8A	58.918	0.016	8.502	6.602	0.987
ECM_S12A	148.921	0.025	20.236	43.5	0.996
ECM_S8B	-90.795	-0.052	21.411	20.123	0.991
ECM_S12B	375.117	0.015	11.587	-32.312	0.993
ECM_S8C-M1	108.301	0.0113	12.2977	12.441	0.997
ECM_S8C-M2	-82.18	-0.043	18.18	34.252	0.992
ECM_S12C-M1	467.397	0.025	15.48	26.097	0.995
ECM_S12C-M2	67.426	-.000787	21.47	75.604	0.997

Table 5-4: SCR Coefficients for Fan Airflow Model

FPTU	C1	C2	C3	C4	R^2
SCR_S8A	-1776	-0.0228	16.49	0.0036	0.989
SCR_S12A	-778.5	0.0091	6.918	0.0394	0.993
SCR_S8B	-1705	-0.0254	18.15	-0.0448	0.994
SCR_S8C	-1310	-0.0183	13.94	0.0677	0.997
SCR_S12C	-1903	-0.0105	16.78	0.0812	0.99

Table 5-5: Summary of ECM Settings

FPTU Manufacturer	ECM Settings			
	25%	50%	75%	100%
A	25%	50%	75%	100%
B	4 VDC	6 VDC	8 VDC	10 VDC
C	2.5 VDC	5 VDC	7.5 VDC	10 VDC

5.2. Series Terminal Unit Power Performance

Both power consumption and power quality were measured. A model was developed for the power consumption as a function of ECM setting and inlet air velocity pressure, Piav. Because the fan airflow was mainly controlled by the ECM setting, the model used the ECM setting rather than fan airflow as an input. Power consumption was also influenced by downstream static pressure and the primary airflow. Since downstream pressure remained constant, it was not used in the model. The impact of primary airflow on the power consumption was modeled by including Piav.

The power factor and power quality were varied by ECM setting. Although Cramlet (2008) did measure these data for one series SCR terminal unit, Furr (2006) did not, so there is very little comparison between ECM and SCR power quality performance.

5.2.1. Fan Power Consumption Analysis and Model. The power consumption of the VAV fan was mainly dependent on the airflow it produced. The airflow was almost entirely dependent on the ECM setting, and since the ECM setting was an input into the system, it was used for modeling rather than the airflow. It was also slightly dependent on primary airflow, which was represented by Piav. Figure 5-5 shows the power consumption of the fan versus the airflow of the fan for terminal unit ECM_S8A, while Figure 5-6 shows these data for terminal unit ECM_S12C-M1.

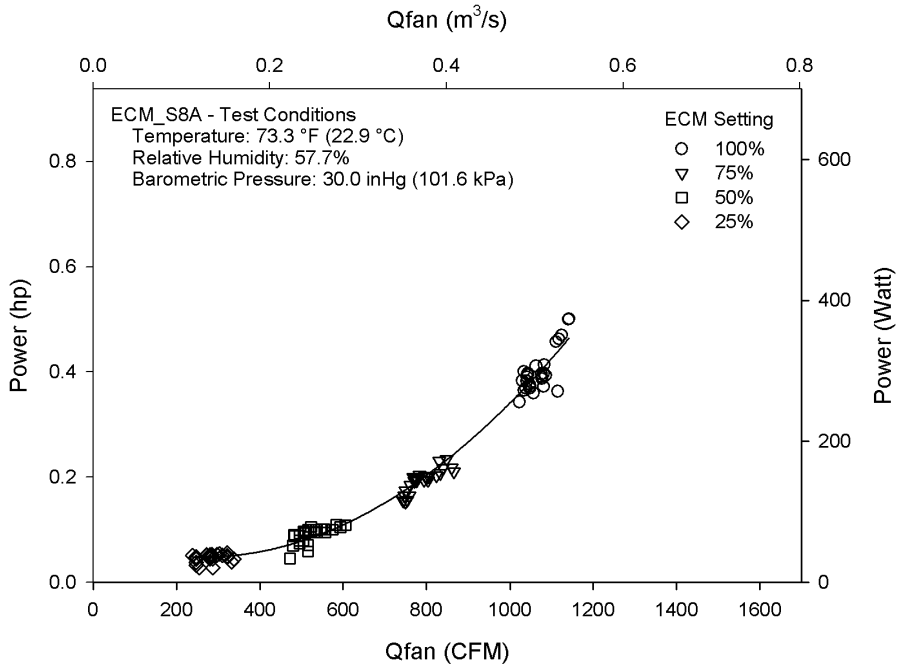

Figure 5-5: Power vs. Q_{fan} for ECM_ S8A

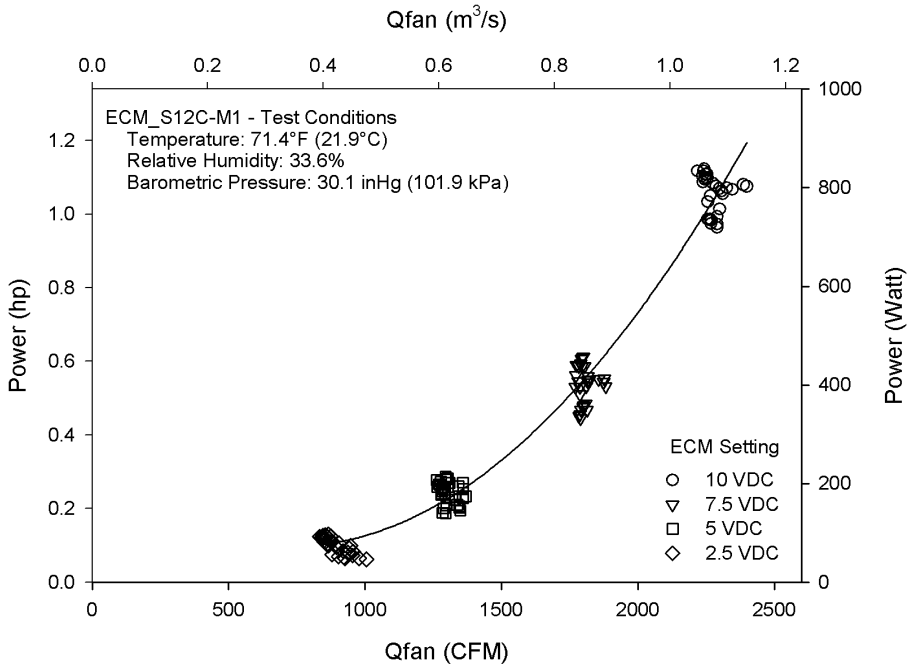

Figure 5-6: Power vs. Q_{fan} for ECM_ S12C-M1

These figures show the typical power curve for all ECM series terminal units tested. They were also consistent with the results obtained by Cramlet (2008). The main difference between these data and those obtained by Furr (2006) was that the power curve for the SCR motors was linear with respect to Qfan, while it was parabolic for the ECM motors. Figure 5-7 shows a comparison of power consumption for SCR_S8C (Furr 2006) and ECM_S8C-M1 (Cramlet 2008). At the lowest flow rates, the SCR unit consumed five times more power than the ECM unit. As the flow rates increased, the difference in power consumption narrowed.

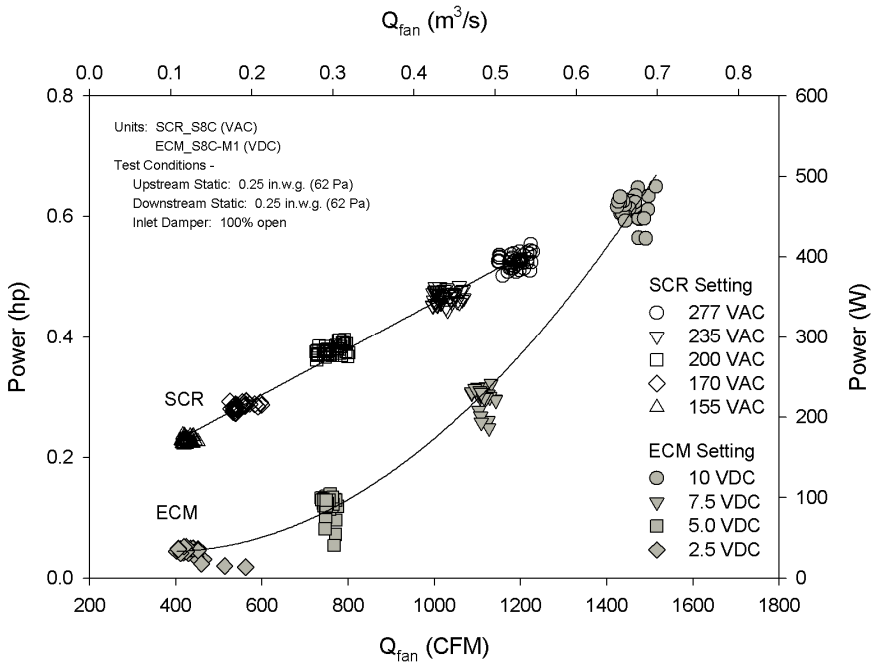

Figure 5-7: Power vs. Q_{fan} for SCR_S8C and ECM_S8C-M1

The fan power model used for the ECM controlled fans was similar to the model used for the SCR controlled units (Equation 5-3) except for the definition of the voltages, V. For the SCR units, V represented the AC voltage measured after the SCR controller. For the ECM units, it represented the percent of maximum ECM setting.

Table 5-6 presents the coefficients for the ECM terminal units, and Table 5-7 presents the results for the SCR units obtained by Furr (2006). The model produced satisfactory results for the ECM units, which were generally on par with those for the SCR units. For the ECM units, the lowest R^2 was 0.968, which meant the model fit the data well. For the SCR units, the lowest was 0.870, which was believed to be due to a faulty SCR controller (Furr 2006). For the properly functioning SCR units, the lowest R^2 was 0.983. Overall, this model appeared to correlate the power consumption of the motors with the independent variables without adding much complexity.

$$Power_{fan} = C_1 + C_2 * V^2 + C_3 * V + C_4 * P_{iav} \quad (5\text{-}3)$$

Table 5-6: Fan Power Model Coefficients for ECM Series Terminal Units

FPTU	C1	C2	C3	C4	R^2
ECM_S8A	70.343	0.049	-2.602	2.338	0.968
ECM_S12A	197.65	0.161	-9.589	24.376	0.989
ECM_S8B	8.89	0.061	-0.221	21.258	0.985
ECM_S12B	112.278	0.074	-3.657	-31.915	0.978
ECM_S8C-M1	78.998	0.07045	-3.1497	-12.993	0.998
ECM_S8C-M2	46.608	0.045	-1.165	-4.711	0.993
ECM_S12C-M1	145.834	0.111	-4.31	-45.401	0.998
ECM_S12C-M2	179.663	0.131	-7.303	-18.473	0.996

Table 5-7: Fan Power Model Coefficients for SCR Series Terminal Units

FPTU	C1	C2	C3	C4	R^2
SCR_S8A	-732.7	-0.0114	7.13	-2.12	0.989
SCR_S12A	-269.4	0.00854	1.80	19.05	0.997
SCR_S8B	-595.7	-0.0111	6.96	-13.25	0.983
SCR_S12B	125.9	0.00534	0.736	-16.36	0.870
SCR_S8C	-455.5	-0.00817	5.32	1.91	0.994
SCR_S12C	-917.0	-0.0129	9.86	97.73	0.99

5.2.2. Power Factor Analysis. The power factor of FPTUs was important for two main reasons. First, some utilities charge a penalty fee for power factors that fall below a certain value. Second, low power factor means that the electricity demand is higher than it needs to be, and also often results in a higher demand charge from the utility. Higher demand means the current is higher than necessary, so any losses due to resistance in the wire, known as I^2R losses, are increased as well.

On the ECM controlled fans, the power factor was generally between 0.4 and 0.6 regardless of the ECM setting. Each individual motor seemed to react differently to increasing ECM settings, with no consistent trend. Figure 5-8 shows the power factor at different ECM settings for ECM_S8A. Figure 5-9 the power factor at different ECM settings for ECM_S12C-M2. Each ECM setting also displayed a range of power factors, with some motors and settings having more or less variation than other settings. The variation affects different ECM settings in different ways. For terminal unit ECM_S8A, the highest power factors for low ECM settings were achieved with the highest primary

flow. However, at the maximum setting, the highest power factor was achieved at medium primary air flow rates.

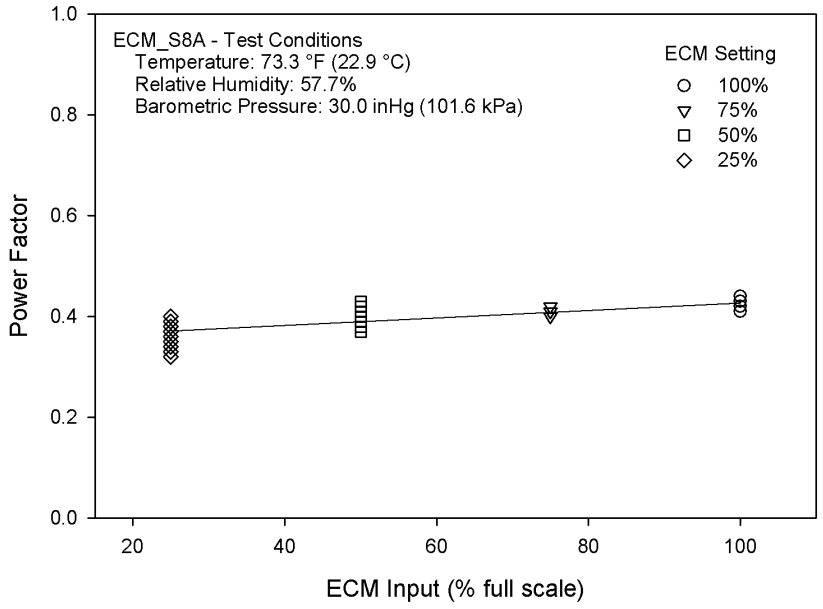

Figure 5-8: Power Factor vs. ECM Input for ECM_ S8A

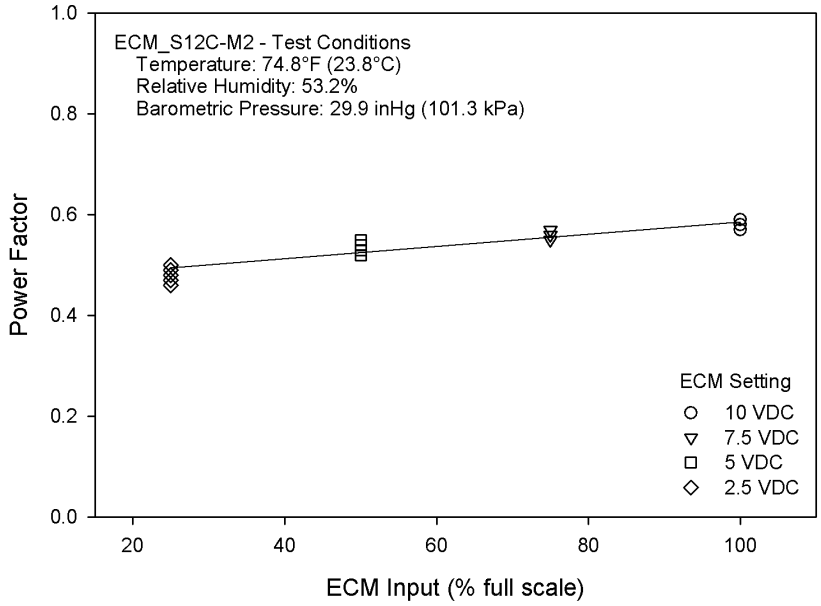

Figure 5-9: Power Factor vs. ECM Input for ECM_S12C-M2

Cramlet (2008) showed that SCR controllers behave completely differently. As the SCR controller is turned up, the power factor also approaches one. This behavior is shown in Figure 5-10, which also shows an almost linear increase in power factor for terminal unit SCR_S8C. In contrast, for the ECM controlled fan, the power factor stayed nearly constant. The SCR controller "chops" the sine wave to achieve lower voltages, and slows down the motor. At its maximum setting, there is almost no distortion to the sine wave, resulting in a much higher power factor.

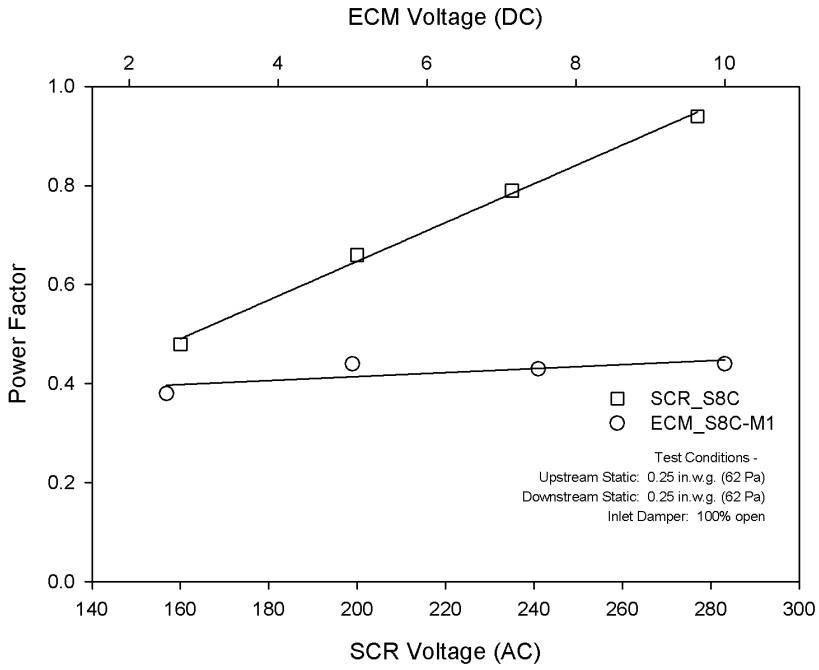

Figure 5-10: Power Factor vs. Controller Voltage for SCR_S8C and ECM_S8C-M1

Power factor was only one measure used to evaluate the impact of a FPTU. For example, a low power factor at very low power level did not have as much effect on demand as a slightly higher power factor at much higher power levels. Another useful quantity was the apparent power, which is related to real power by the power factor (Equation 5-4). Apparent power is the amount of demand seen on the supply side of the building. Figure 5-11 (Cramlet 2008) compares the apparent power of an ECM controlled fan and an SCR controlled fan, both in an S8C terminal unit, of identical design. This shows that at flow rates below 1050 CFM (0.496 m3/s), the ECM unit has as much as a four times advantage in apparent power, despite its lower power factor. As the flow rate increases, the SCR's power factor increases, which kept its apparent power

relatively constant. Since the ECM's power factor remains fairly constant, it's apparent power increased as the flow rate, and thus real power, increased. At approximately 1050 CFM (0.496 m3/s), the apparent power of the ECM became higher than the apparent power of the SCR (Cramlet 2008).

$$RealPower = ApparentPower * PowerFactor \tag{5-4}$$

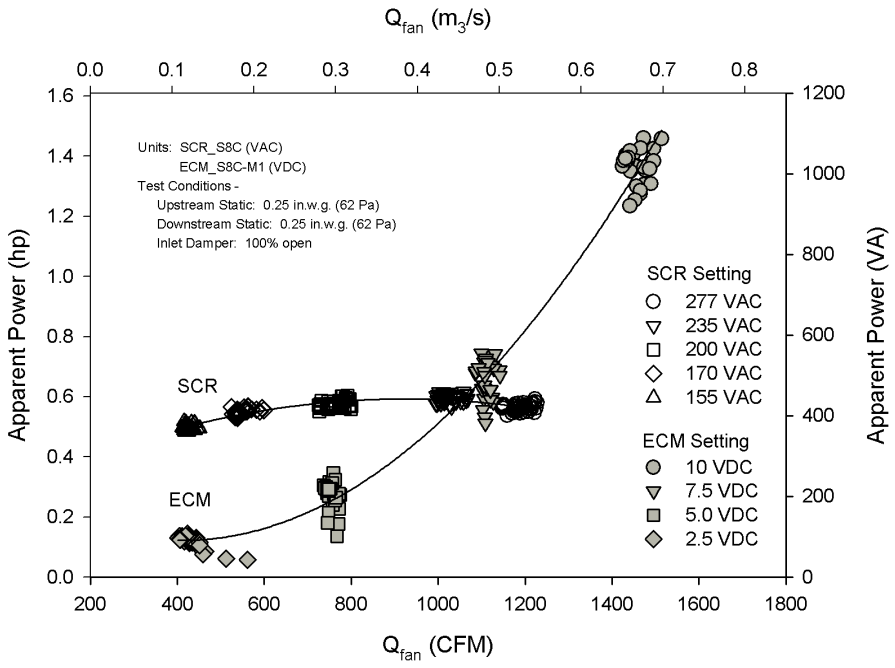

Figure 5-11: Comparison of Apparent Power for SCR and ECM Controlled FPTU

This behavior of the ECM was duplicated in this study. Because the power factor of the ECM did not vary significantly across its range of operation, the increase in apparent power was similar in shape, though not magnitude, to the increase in real power. Figure 5-12 shows the apparent power of terminal unit ECM_S8A plotted

against the airflow of the fan. The curve for apparent power was similar to the curve for real power for this same FPTU (Figure 5-5). A similar comparison can be made for terminal unit ECM_S12C-M1 in Figure 5-13 and Figure 5-6, respectively. ECM_S8A had similar apparent and real power requirements at about 1050 CFM (0.496 m3/s), as ECM_S12C-M1 did at approximately 1700 CFM (0.802 m3/s). In this case, the larger FPTU was more efficient than the smaller FPTU because it was producing more airflow at the same power.

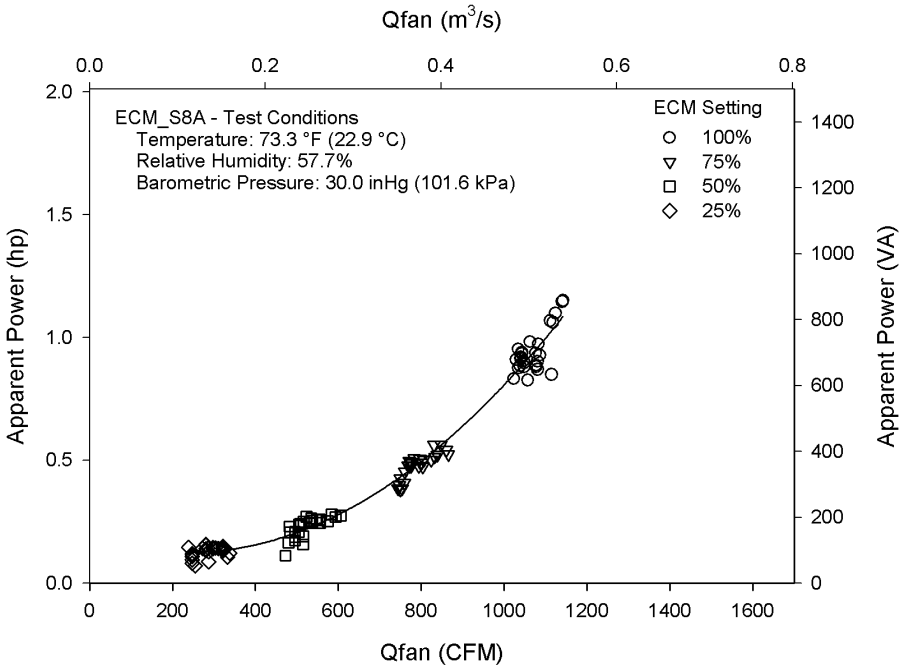

Figure 5-12: Apparent Power vs. Q_{fan} for ECM_ S8A

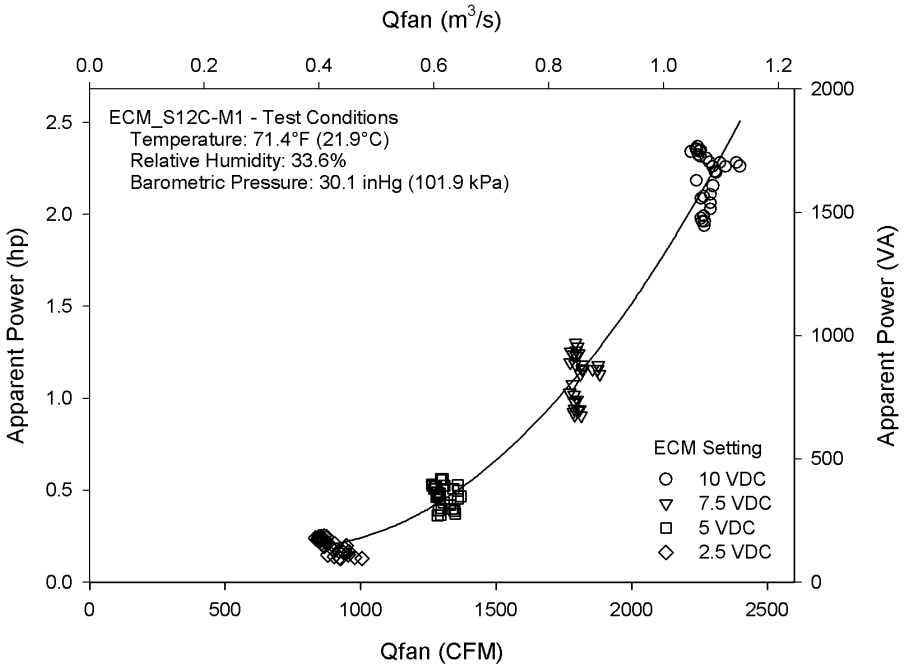

Figure 5-13: Apparent Power vs. Q_{fan} for ECM_ S12C-M1

5.2.3. Power Quality Analysis. Harmonic data for the first 25 harmonics of current, voltage, and power were recorded. The harmonic data represents the amount of distortion relative to a 60 Hz sine wave caused by the ECM and controller electronics. A complete set of harmonic data is found in the appendix. The harmonic data were recorded as a percentage of the fundamental, or first harmonic, value. It was then converted to volts, amps, or watts for reporting.

Figure 5-14 shows the real power harmonics, in percentage form, for ECM_S8A, Figure 5-15 shows the same harmonics in watts. Figure 5-16 and Figure 5-17 repeat the same two graphs for ECM_S12C-M2. The magnitude of the real power harmonics was below 1% of the fundamental harmonic. There did not appear to be any discernible

trend of the dependence on ECM setting with respect to harmonics in Figure 5-14 or Figure 5-16. The size of the unit also did not appear to be a factor. One noticeable attribute of the power harmonics was that some harmonics were negative. It was assumed that these harmonics were transferring power back to the voltage source. It should also be noted that there was very little real power consumed by harmonic distortion because the magnitudes were small (less than 1%) for all harmonics.

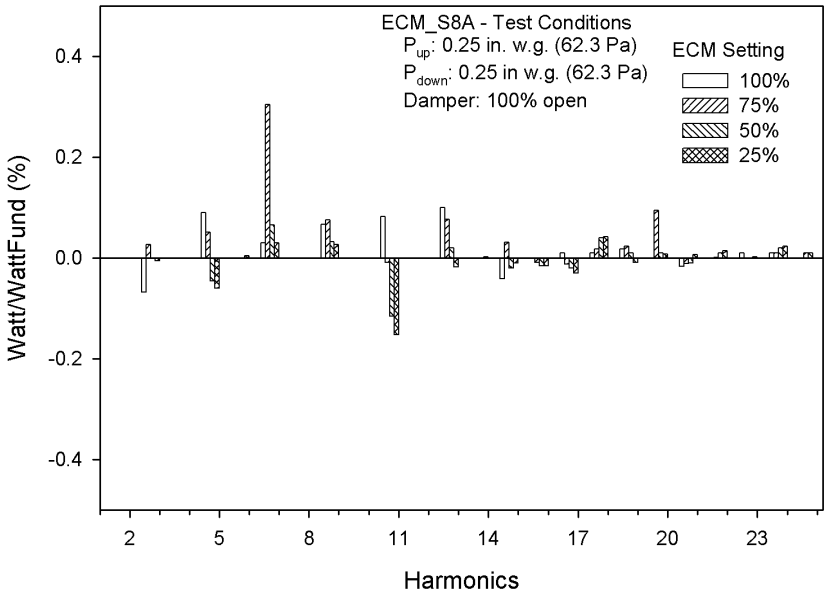

Figure 5-14: Real Power Harmonics (%) for ECM_ S8A

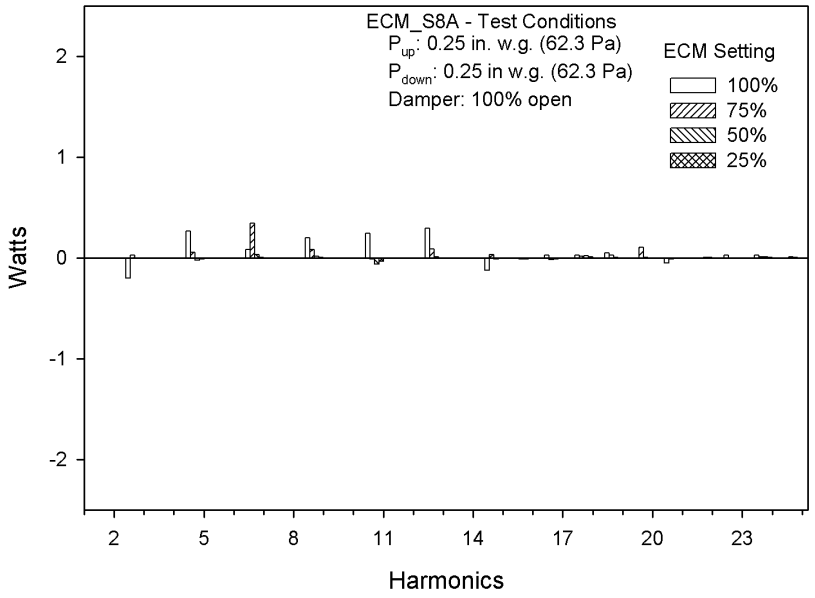

Figure 5-15: Real Power Harmonics (Watts) for ECM_ S8A

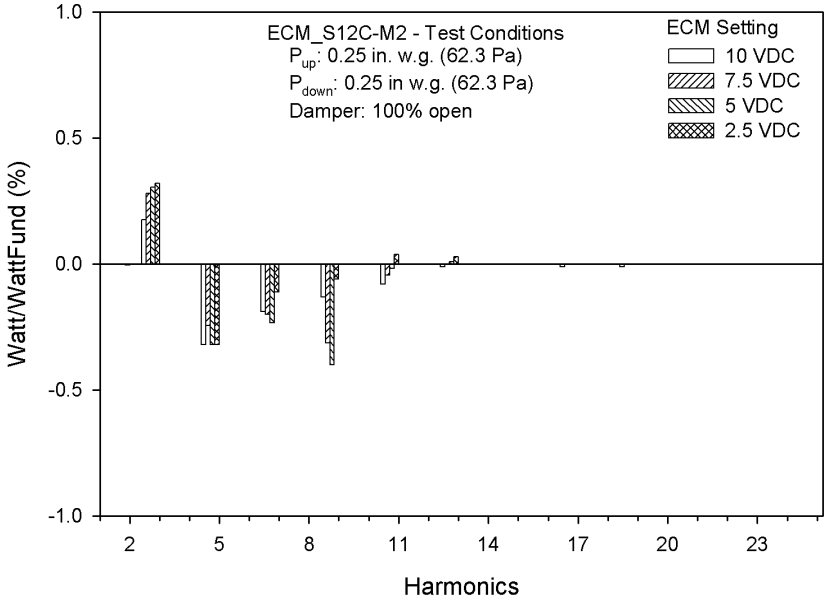

Figure 5-16: Real Power Harmonics (%) for ECM_ S12C-M2

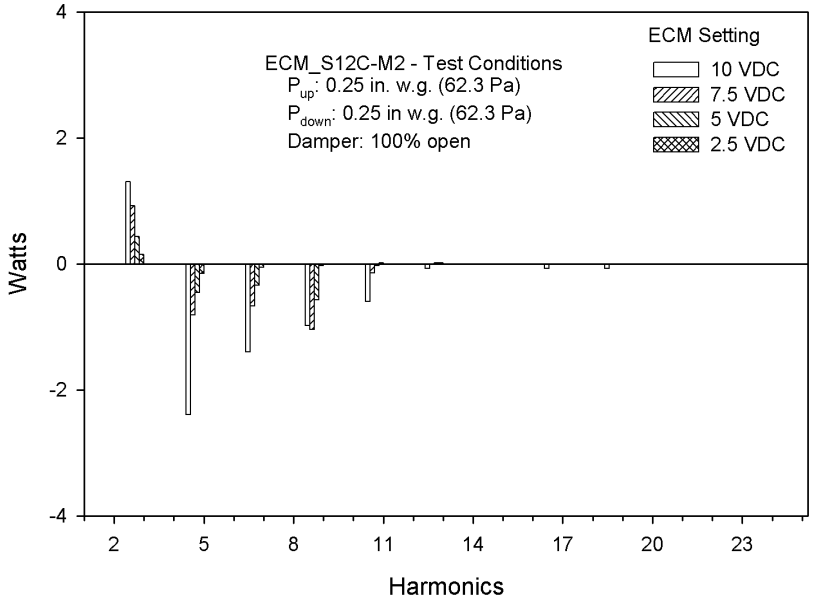

Figure 5-17: Real Power Harmonics (Watts) for ECM_S12C-M2

One problem with analyzing harmonic distortion by the individual harmonics was the difficulty in looking at a whole range of frequencies at one time. A more convenient approach to plot and analyze harmonic distortion was to look at their cumulative effect through the total harmonic distortion (THD), defined in Equation (5-5). THD was much easier to plot and analyze, though specific situations may warrant a more in depth analysis of individual harmonics. The THD for real power is reported here in its percentage form.

$$THD = \frac{\sum harmonic\ powers}{fundamental\ frequency\ power} = \frac{f_2 + f_3 + \ldots + f_n}{f_1} \qquad (5\text{-}5)$$

Figure 5-18 presents the THD for ECM_S8A, and Figure 5-19 presents it for ECM_S12C-M2. The THD was highest for 100% ECM setting for ECM_S8A, while it was at its highest at the lowest ECM setting for ECM_S12C-M2. This showed THD was not entirely dependent on ECM setting. It should be noted that if this value were plotted in Watts, the higher ECM settings would have higher THD due to their much higher power consumption. A summary of the real power THD for all terminal units tested is presented in Table 5-8.

Table 5-8: Real Power THD (%)

FPTU	ECM Setting				Average
	25%	50%	75%	100%	
ECM_S8A	0.62	0.54	0.75	0.84	0.69
ECM_S8B	0.93	0.73	0.87	0.89	0.86
ECM_S8C-M2	0.61	0.43	0.35	0.43	0.46
ECM_S12A	0.98	1.00	0.96	0.73	0.92
ECM_S12B	0.64	1.21	0.83	0.67	0.84
ECM_S12C-M1	1.46	1.33	1.22	1.38	1.35
ECM_S12C-M2	1.45	1.21	1.22	0.95	1.21

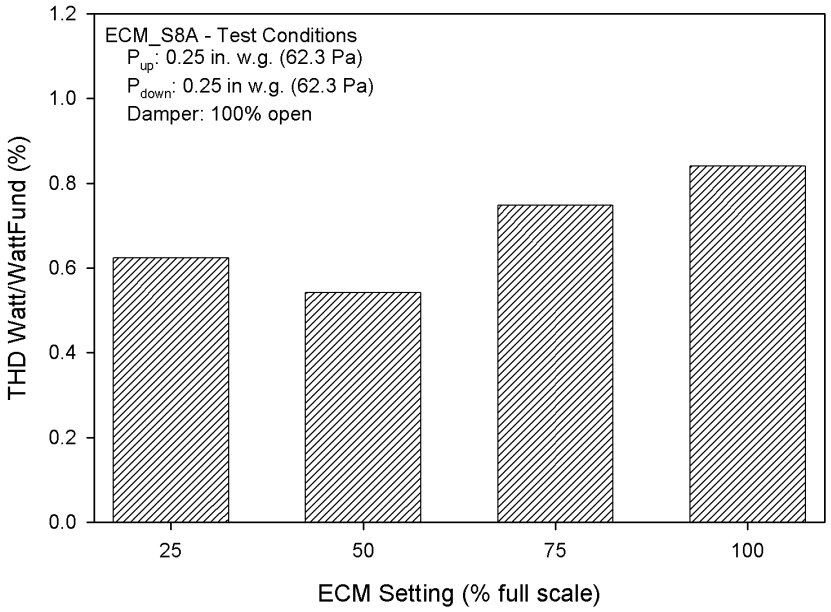

Figure 5-18: Real Power THD (%) for ECM_ S8A

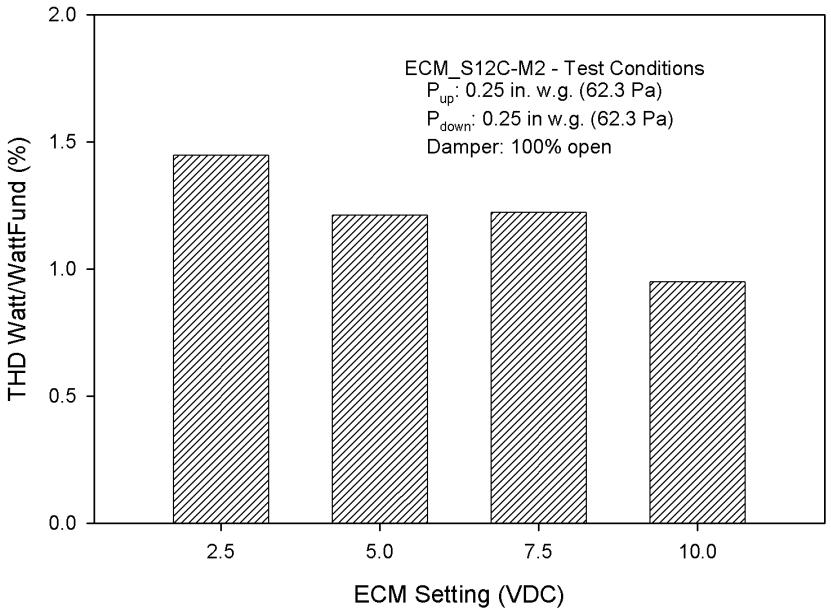

Figure 5-19: Real Power THD (%) for ECM_ S12C-M2

The distortion of the voltage sine wave was below 1.5% of the fundamental harmonic for all FPTUs tested. There was also little difference between different ECM settings, or FPTU size. Figure 5-20 shows the voltage harmonics for ECM_S8B as a percentage of the fundamental, while Figure 5-21 shows these harmonics as a voltage. Figure 5-22 shows the voltage harmonics for ECM_S12B as a percentage of the fundamental, and Figure 5-23 shows the harmonics as voltage. Similar results were also found for FPTUs from the other manufacturers. The THD for voltage was also a convenient way to quickly analyze the cumulative effect of the different harmonics without having to view a large number of separate harmonic values, and is presented in Table 5-9 for all terminal units tested.

Table 5-9: Voltage THD (%)

FPTU	ECM Setting				Average
	25%	50%	75%	100%	
ECM_S8A	0.78	0.75	0.8	0.78	0.78
ECM_S8B	0.86	0.82	0.82	0.91	0.85
ECM_S8C-M2	0.87	0.76	0.76	0.7	0.77
ECM_S12A	1.11	1.13	1.12	1.17	1.13
ECM_S12B	0.87	1.18	1.08	1.04	1.04
ECM_S12C-M1	1.33	1.21	1.33	1.22	1.27
ECM_S12C-M2	1.3	1.26	1.26	1.33	1.29

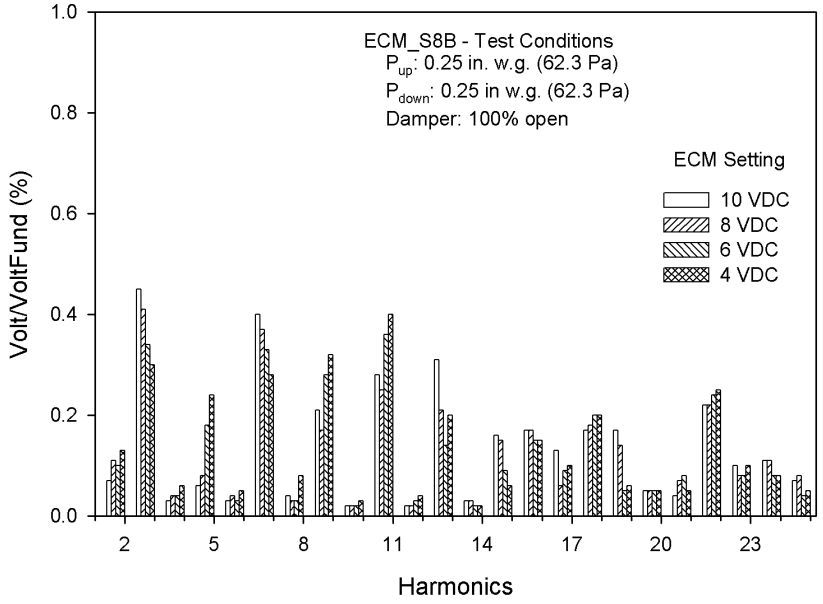

Figure 5-20: Voltage Harmonics for ECM_S8B (%)

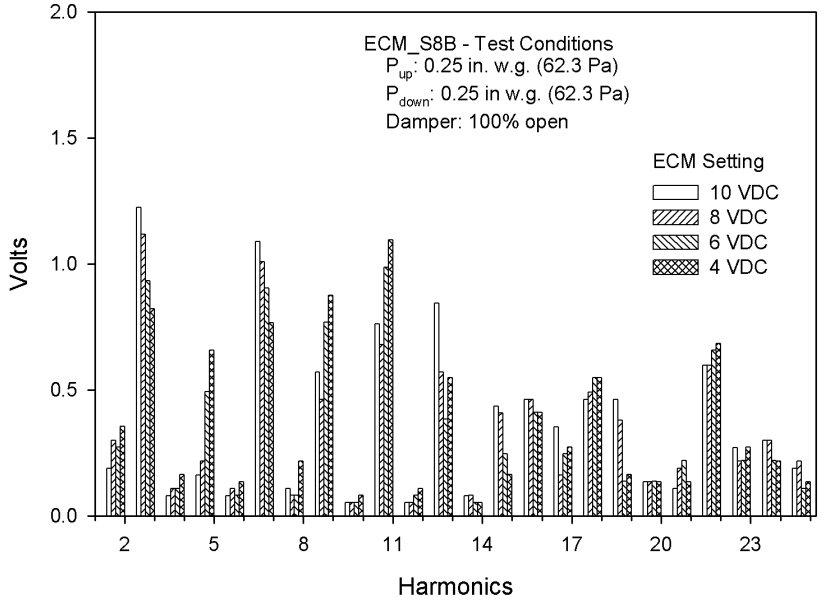

Figure 5-21: Voltage Harmonics for ECM_S8B (Volts)

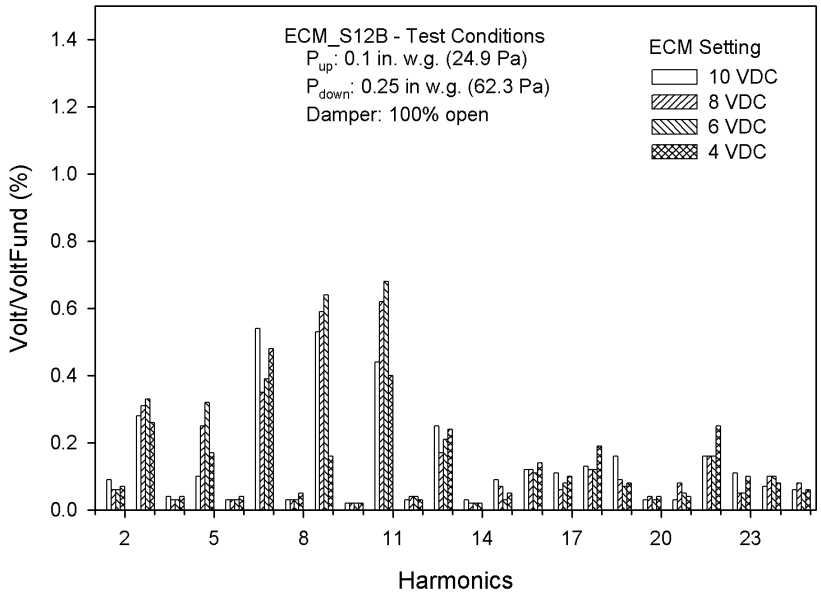

Figure 5-22: Voltage Harmonics for ECM_S12B (%)

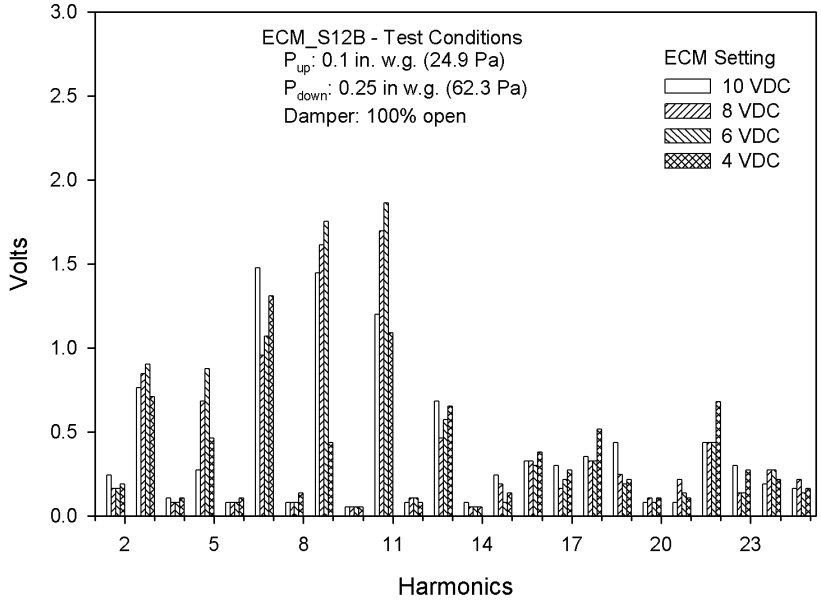

Figure 5-23: Voltage Harmonics for ECM_S12B (Volts)

The behavior of the harmonic distortion of the current was different from that of the voltage. First, the distortion of the current was much greater than the voltage. When looking at the magnitude of the harmonic distortion in amps, there was a difference both between ECM settings, as well as between different sizes of FPTUs. The difference was likely because the voltage was nearly constant for all of the tests, while the RMS current was highly dependent on ECM setting, and the 12 inch units often drew more power and current than their 8 inch counterparts. When viewed as a percentage, there was not as much difference between terminal unit size or ECM setting.

Figure 5-24 and Figure 5-25 compare the current harmonics for FPTU ECM_S8A as a percentage of fundamental and in amps, respectively. Figure 5-26 and Figure 5-27 repeat the comparison for FPTU ECM_S12A. In Figure 5-24, for a given harmonic, the difference was relatively small between ECM settings, but viewing that same harmonic in Figure 5-25 shows a very large difference. This was because at an ECM setting of 100%, the current was many times larger than the current at an ECM setting of 25%. Also notice that there was little difference in percentages between Figure 5-24 and Figure 5-26. For example, the 5th harmonic in both figures was around 80%, a little higher for ECM_S12A and a little lower for ECM_S8A. The 5th harmonic for ECM_S12A, in Figure 5-27, was over 4 amps, while the 5th harmonic for ECM_S8A, in Figure 5-25, was under 2 amps. These results illustrated that percentage distortion can sometimes be misleading because a high percentage at low current levels does not impact the overall system as much as the same percentage at higher current levels. Table 5-10 contains a summary of the current THD for all terminal units tested.

Table 5-10: Current THD

FPTU	ECM Setting				Average
	25%	50%	75%	100%	
ECM_S8A	89.34	89.55	91.24	90.32	90.11
ECM_S8B	90.39	89.52	89.68	89.08	89.67
ECM_S8C-M2	84.53	85.99	85.99	86.43	85.74
ECM_S12A	88.23	85.79	84.44	84.79	85.81
ECM_S12B	91.38	90.02	88.73	88.55	89.67
ECM_S12C-M1	168.52	155.25	159.83	164.98	162.15
ECM_S12C-M2	171.89	158.8	147.43	135.76	153.47

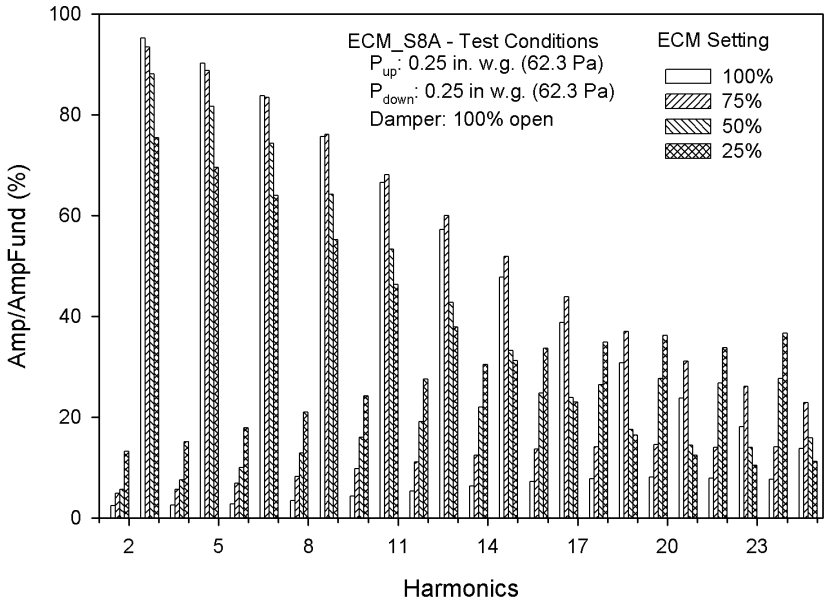

Figure 5-24: Current Harmonics for ECM_S8A (%)

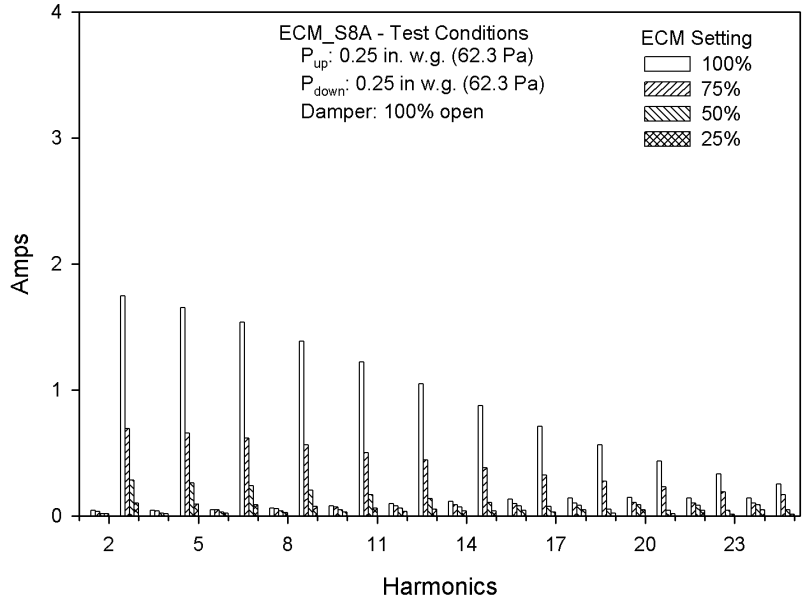

Figure 5-25: Current Harmonics for ECM_S8A (Amps)

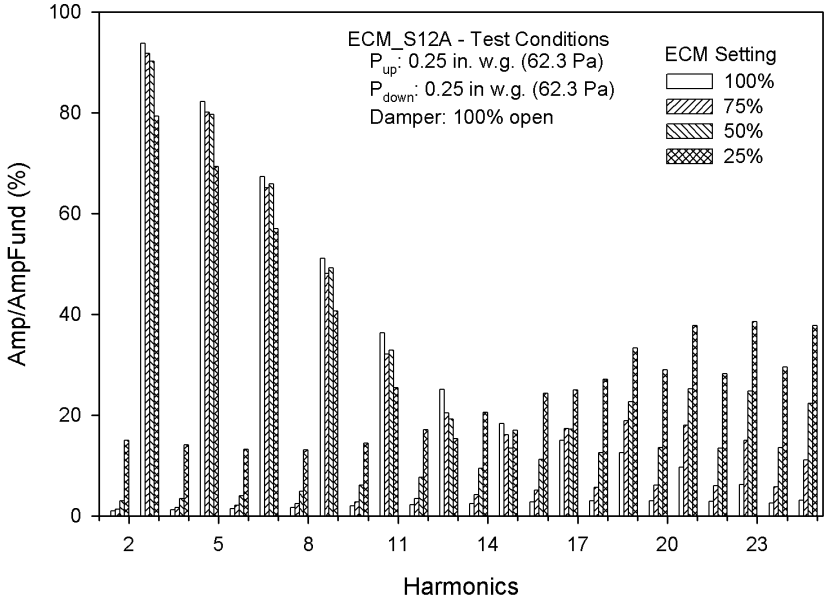

Figure 5-26: Current Harmonics for ECM_S12A (%)

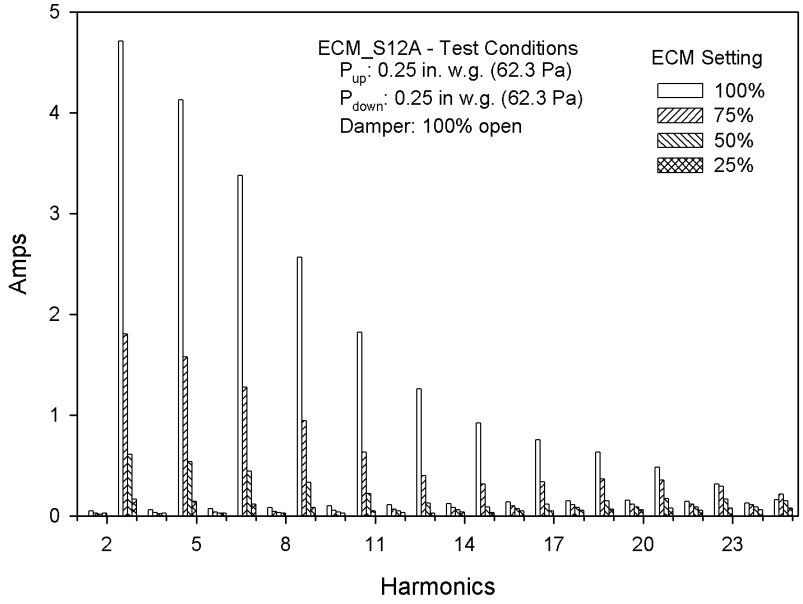

Figure 5-27: Current Harmonics for ECM_S12A (Amps)

When discussing current harmonics, the main concern is with the triplen harmonics, which are odd multiples of 3 of the fundamental. Triplen harmonics are in phase with the fundamental, and thus add to the peak current. Figure 5-28 shows the triplen harmonics of terminal unit ECM_S8A as percentage of the fundamental, and Figure 5-29 shows these harmonics in amps. Figure 5-30 and Figure 5-31 show the same graphs for terminal unit ECM_S12A. These harmonics are a subset of those discussed previously. It is important to note, that the percentages did not tell the whole story. If one only had the harmonics as a percentage, the conclusion may be made that lower ECM settings have as much of a problem with harmonic distortion as higher settings. This was not completely true, since the lower ECM settings had a much lower

current draw, so the harmonics produced at these settings contribute much less to the harmonic distortion in the overall system.

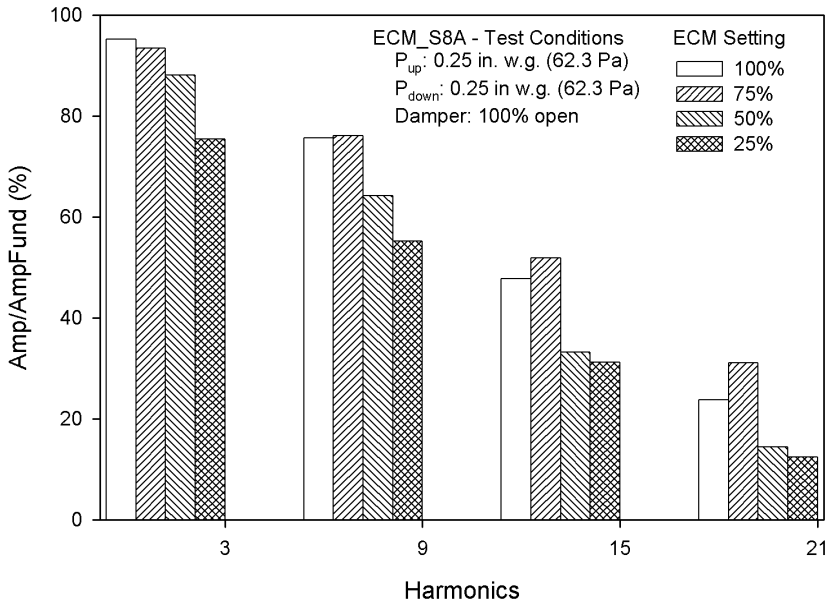

Figure 5-28: Current Triplen Harmonics for ECM_S8A (%)

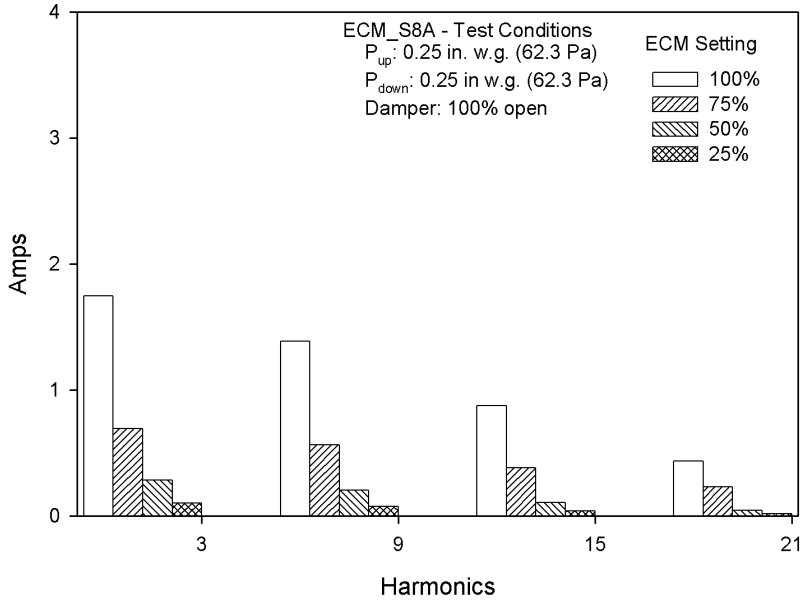

Figure 5-29: Current Triplen Harmonics for ECM_S8A (Amps)

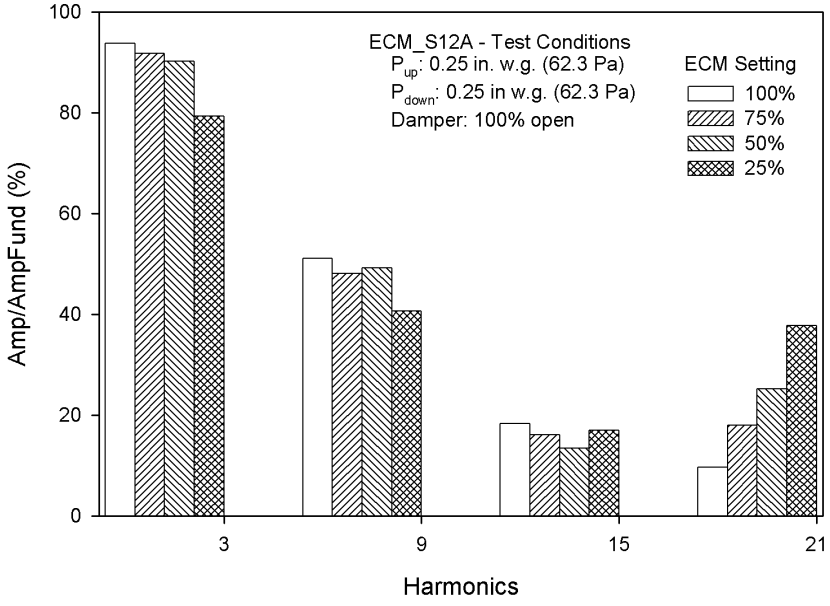

Figure 5-30: Current Triplen Harmonics for ECM_S12A (%)

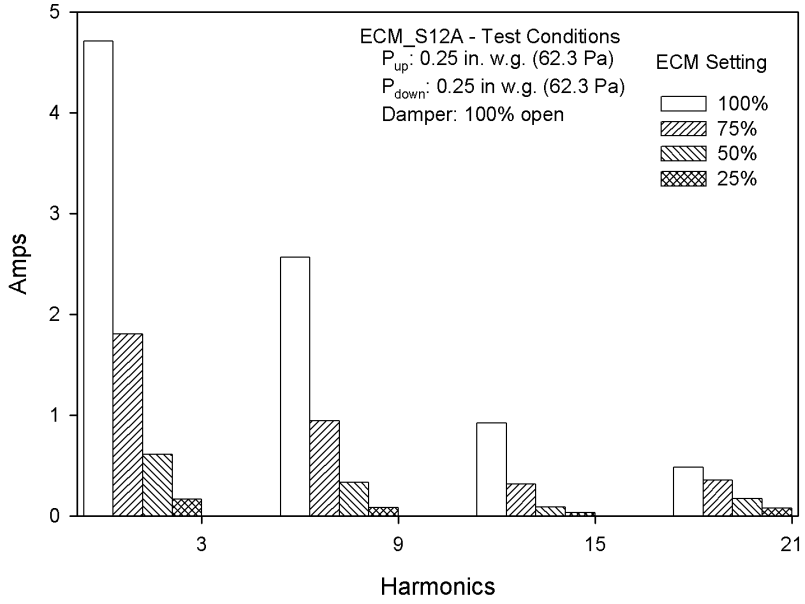

Figure 5-31: Current Triplen Harmonics for ECM_S12A (Amps)

CHAPTER VI

PARALLEL FAN POWERED TERMINAL UNITS RESULTS AND MODELS

Data were collected for seven ECM controlled parallel fan powered terminal units from three different manufacturers. Data were collected using the equipment described in Chapter III, following the procedure outlined in Chapter IV. Models were developed for airflow and power performance. Airflow and power will be discussed in separate sections in this chapter.

6.1. Parallel Terminal Unit Airflow

Several aspects of the airflow performance of the FPTU were analyzed and modeled. As with the series units, it was important to quantify the primary airflow delivered to the FPTU as well as the air supplied by the FPTU. The primary airflow behaved similarly to that of the series units, in that it depended on damper setting and the differential pressure across the terminal unit. The air supplied by the terminal unit depended on primary airflow, the airflow induced by the terminal unit fan, and leakage from the terminal unit.

6.1.1. Primary Airflow Analysis and Model. As with the series units, the primary airflow was dependent on the position of the primary air inlet damper and the differential pressure across the damper. The upstream and downstream static pressures were used to calculate the differential pressure across the damper. This pressure difference should be a better approximation than it was in the series units because the pressure rise across the terminal unit fan was not included in the downstream static pressure. There must be a

positive pressure differential for there to be airflow through the FPTU for normal operating conditions.

At very high airflows, it was observed that the downstream static pressure was sometimes higher than the upstream static pressure. As air moved from the smaller upstream duct into the larger downstream duct, it slowed down, increasing the static pressure. If this increase in static pressure was greater than the losses in the FPTU between the two static pressure taps, the downstream static pressure would be larger than the upstream static pressure. These conditions were generally outside the designed range of operation of the FPTUs, and were not reported in the data this study.

All of the manufacturers utilized a butterfly damper in the parallel units, so each FPTU was tested at settings of 0° (fully open), 22.5°, 45°, and 67.5°. Figure 6-1 shows the primary airflow plotted against DP ($P_{up} - P_{down}$) for terminal unit ECM_P8B. Figure 6-2 shows the same data for terminal unit ECM_P12C-M2. The curves were generated using a fit of the data to Equation (6-1).

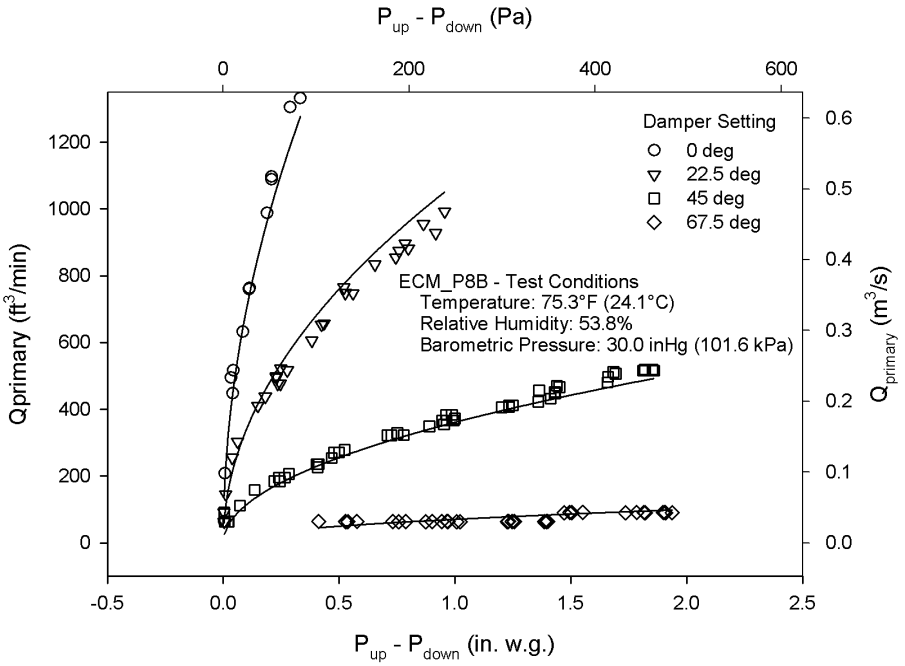

Figure 6-1: $Q_{primary}$ vs. DP for ECM_P8B

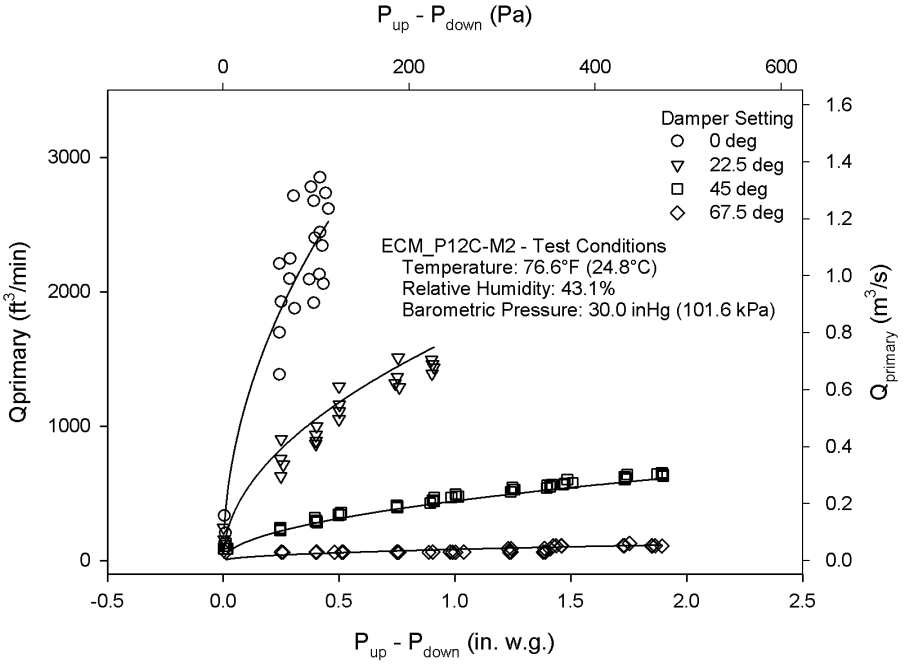

Figure 6-2: $Q_{primary}$ vs. DP for ECM_P12C-M2

$$Q_{primary} = C_1 * (1 + C_2 * S + C_3 * S^2) * \sqrt{DP} \quad (6\text{-}1)$$

The values for the coefficients and R^2 values for each terminal unit are presented in Table 6-1. The data for ECM_P8C-M1 were from Cramlet (2008). The data for the SCR controlled units were from Furr et al (2008) and presented in Table 6-2. The only differences in design between the ECM controlled FPTUs from manufacturer C were the motors and controllers used to vary fan speed. They were comparable to the FPTUs utilizing SCR controlled motors.

This model generally correlated well with the primary airflow data. All of the FPTUs had R^2 values of 0.96 or above. The only exception to this was the 12 inch FPTU from manufacturer B, which was at 0.872. It was difficult to set the damper position correctly for ECM_P12B due to an inaccurate analog display that was used to set the damper position. The results for this unit may possibly be improved by further testing. These results were generally higher than those obtained for the SCR units.

Table 6-1: Model Coefficients for ECM Controlled Units

FPTU	C1	C2	C3	R^2
ECM_P8A	1380	-2.03E-02	8.90E-05	0.982
ECM_P12A	3868	-1.54E-02	3.27E-05	0.961
ECM_P8B	2212	-2.71E-02	1.89E-04	0.988
ECM_P12B	6528	-2.84E-02	2.06E-04	0.872
ECM_P8C-M2	1469	-2.35E-02	1.38E-04	0.975
ECM_P8C-M1	1671	-2.53E-02	1.71E-04	0.978
ECM_P12C-M1	3380	-2.25E-02	1.22E-04	0.960
ECM_P12C-M2	3747	-2.98E-02	2.27E-04	0.969

Table 6-2: Model Coefficients for SCR Controlled Units

FPTU	C1	C2	C3	R^2
SCR_P8A	1363	-2.02E-02	9.87E-05	0.924
SCR_P12A	7425	-3.07E-02	2.45E-04	0.935
SCR_P8B	1935	-2.48E-02	1.91E-04	0.981
SCR_P12B	5781	-2.77E-02	2.04E-04	0.935
SCR_P8C	1594	-2.73E-02	1.91E-04	0.981
SCR_P12C	1838	-1.16E-02	1.63E-05	0.637

6.1.2. Fan Airflow Analysis and Model. Figure 6-3 shows the fan airflow for terminal unit ECM_P8A plotted against the downstream static pressure. This figure shows how ECM controlled fans were designed to operate, which was at a constant airflow at a given ECM setting across a wide range of operating conditions. Each ECM setting in this case shows a basically constant airflow at different downstream static pressures. Figure 6-4 shows the fan airflow for terminal unit ECM_P12B. At the lower ECM settings, the fan appeared to behave similar to that of unit ECM_P8A, with little variation at different downstream static pressures. At the highest setting there was a noticeable decrease in Qfan as the downstream pressure increased, with the fan output nearly identical to the next lower ECM setting at a downstream static pressure of 0.5 in. w.g. (125 Pa). These data were plotted to illustrate the behavior of ECM_P12B at the highest ECM setting, but were not included in the data analysis.

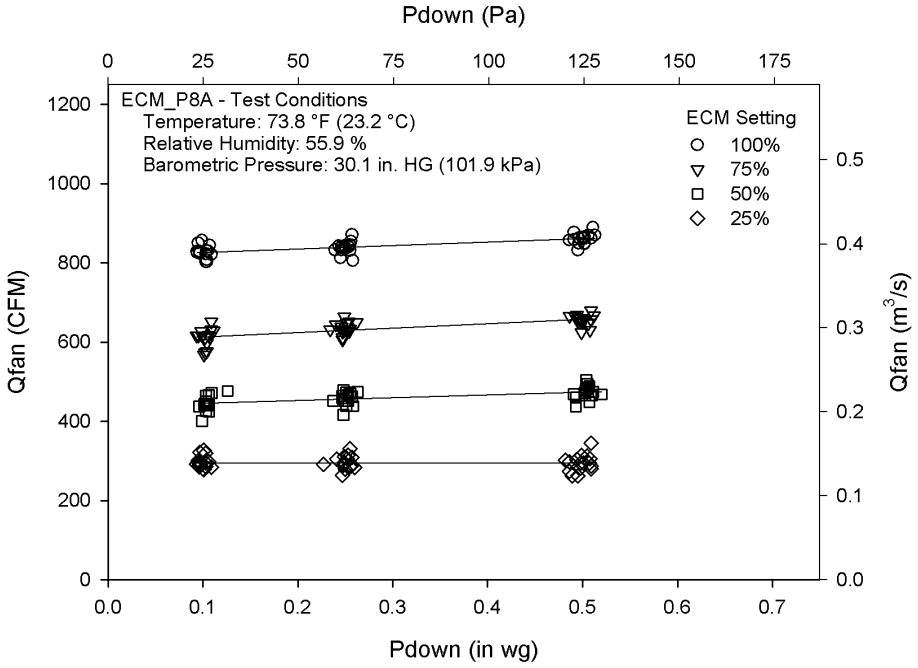

Figure 6-3: Q_{fan} vs. P_{down} for ECM_P8A

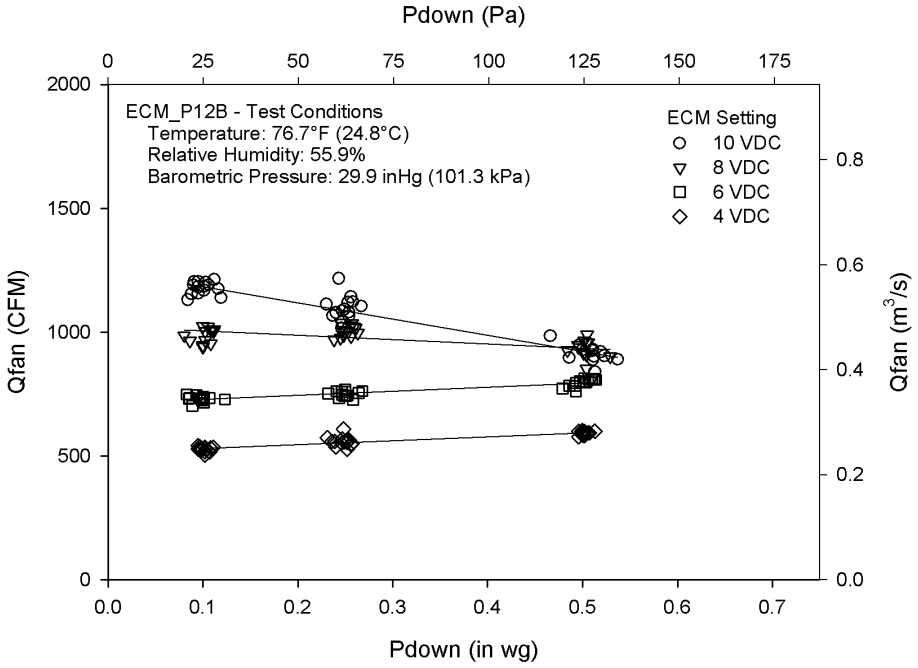

Figure 6-4: Q_{fan} vs. P_{down} for ECM_P12B

The airflow induced by the fan in a parallel unit was mainly a function of the ECM setting. As seen in Figure 6-4, the highest ECM setting sometimes performed differently than the other ECM settings. In ECM_P12B the difference in behavior for the 10 VDC setting was possibly due to using a somewhat undersized motor for the application. This unit used a ½ hp motor, while ECM_P12C-M1 and ECM_P12C-M2 used ¾ hp motors and ECM_P12A used a 1 hp motor. When the FPTUs were operating near their design limits, such as the 10 VDC setting for ECM_P12B, the ECM controller often performed erratically. These data were not included in the data analysis, though they were plotted to show the erratic behavior at the 10 VDC ECM setting.

The model for fan airflow is shown in Equation (6-2). It was the same form used by Furr (2006) and Cramlet (2008). All of the terminal units in this study used a gravity operated backdraft damper, while those from manufacturer A tested by Furr (2006) utilized a primary air operated backdraft damper. The different damper resulted in the addition of the term in parentheses in Equation (6-2).

$$Q_{fan} = C_1 + C_2 * V^2 + C_3 * V + C_4 * P_{down} + (C_5 * P_{iav}) \quad (6\text{-}2)$$

For the SCR units, V represented the AC voltage measured after the SCR controller. For the ECM units, V represented the ECM setting as a percent of maximum airflow. For unit ECM_P8C-M1 this required adjusting the C2 and C3 coefficients from CFM/V^2 and CFM/V to $CFM/\%^2$ and CFM/% respectively. Manufacturer A provided a controlled adjusted by turning a screw located on the controller to choose a setting from

zero to 100, so it simply represents the ECM setting. Manufacturer B used a 2 – 10 VDC signal, so the settings used were 4 VDC (25%), 6 VDC (50%), 8 VDC (75%), and 10 VDC (100%). Manufacturer C used a control signal of 0 – 10 VDC, so settings of 2.5 VDC (25%), 5 VDC (50%), 7.5 VDC (75%), and 10 VDC (100%) were used. Table 6-3 contains a summary of the ECM settings used.

Table 6-3: Summary of ECM Settings for Parallel FPTUs

FPTU Manufacturer	ECM Settings			
	25%	50%	75%	100%
A	25%	50%	75%	100%
B	4 VDC	6 VDC	8 VDC	10 VDC
C	2.5 VDC	5 VDC	7.5 VDC	10 VDC

The data for the SCR units was taken from Furr (2006), while that for unit ECM_P8C-M1 was taken from Cramlet (2008). The coefficients and R^2 values for the ECM units are presented in Table 6-4. All models for the ECM controlled FPTUs had R^2 values above 0.955, and most of them above 0.98. The coefficients and R^2 values for the SCR units are presented in Table 6-5. The SCR controlled FPTUs had a minimum R^2 of 0.931, with the rest of the models being above 0.978.

Table 6-4: ECM Coefficients for Parallel Fan Airflow Model

FPTU	C1	C2	C3	C4	C5	R^2
ECM_P8A	139.907	0.18	5.047	66.163	0	0.992
ECM_P12A	24.713	0.019	13.221	51.429	0	0.995
ECM_P8B	300.029	0.007	7.846	139.826	0	0.994
ECM_P12B	358.348	0.011	7.170	49.795	0	0.955
ECM_P8C-M1	-282.267	-.13841	25.7991	-290.917	0	0.982
ECM_P8C-M2	40.273	-0.011	11.015	-111.869	0	0.979
ECM_P12C-M1	-206.123	-0.083	22.925	-122	0	0.99
ECM_P12C-M2	-53.466	-0.039	16.115	-272.663	0	0.987

Table 6-5: SCR Coefficients for Parallel Fan Airflow Model

FPTU	C1	C2	C3	C4	C5	R^2
SCR_P8A	1108.5	0.028	-9.53	-516.9	-172.8	0.985
SCR_P12A	-1567.2	-0.0199	16.98	-407.4	-360.2	0.978
SCR_P8B	-988.5	-0.0197	11.85	-303	0	0.99
SCR_P12B	-1143	-0.0131	13.56	-364.8	0	0.998
SCR_P8C	-1725	-0.0328	19.79	-564.4	0	0.991
SCR_P12C	-2142.9	-0.0396	26.36	-1920.9	0	0.931

6.1.3. FPTU Leakage Analysis and Model. The fan airflows in the previous section were the net airflows induced by the terminal unit fan. The induced air provided by the terminal fan was equal to the difference between the supply air and the primary supplied to the terminal unit plus the leakage, Equation (6-3). Because there was not an easy way to directly measure the air induced by the fan with the laboratory equipment, leakage was measured by turning off the terminal fan so that the induced air, Q_{fan}, would be equal to zero. This meant the leakage was simply the difference between the primary air and the supply air.

$$Q_{fan} = (Q_{sup\ ply} - Q_{primary}) + Q_{leakage} \quad (6\text{-}3)$$

Figure 6-5 shows the leakage for terminal unit ECM_P8C-M2 plotted against the inlet velocity pressure. The data showed significant scatter with respect to inlet velocity pressure. The leakage in this terminal unit was primarily dependent on the internal static pressure of the FPTU, regardless of the airflow.

Figure 6-6 shows the leakage for unit ECM_P12A plotted against inlet velocity pressure. The leakage from this FPTU was several times higher than the leakage for terminal unit P8C-M2. In this study, both units from manufacturer A had much higher leakage than the other manufacturers. It appeared that the larger leakage was possibly due to the type of grommet used for the point of entry of the motor cabling into the terminal unit. There was little to no sealing between the grommet and the power/control cable bundle, Figure 6-7 and Figure 6-8.

For this FPTU, there was a strong positive correlation between inlet velocity pressure and leakage. This was assumed to be due to two main factors. One was the power/control cable bundle strung directly through the primary air stream (Figure 6-9), which would redirect some of the air through the entry point of the cabling. The other factor was the location of punch-outs for non-included accessories being directly opposite the primary air inlet, so that as primary airflow was increased, there would be increased stagnation pressure at the end of the terminal unit where the punch-outs were located (Figure 6-10). This resulted in increased air leakage through the punch-outs. Both of these factors were observed during the tests.

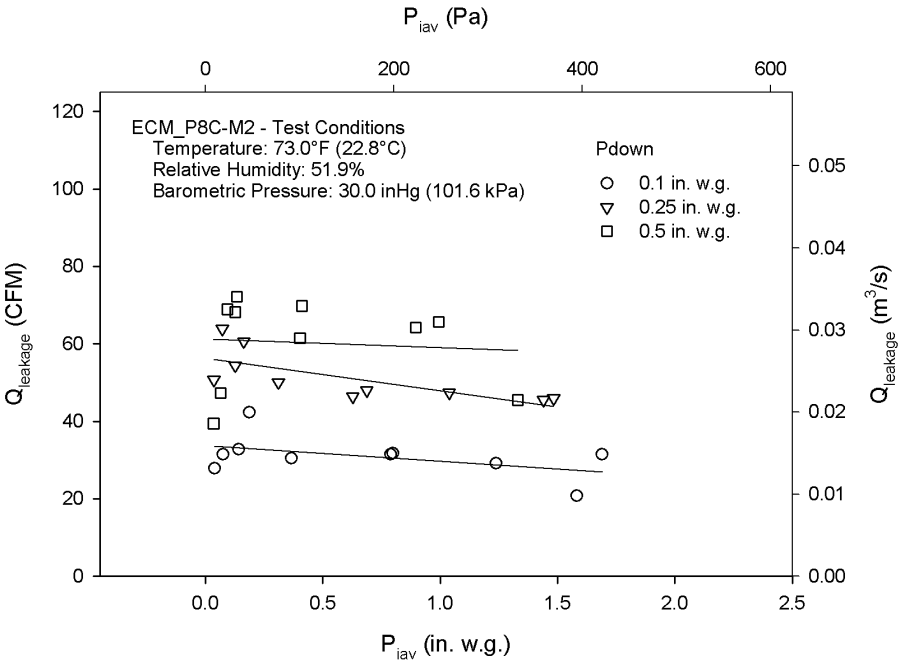

Figure 6-5: Leakage vs. P_{iav} for ECM_P8C-M2

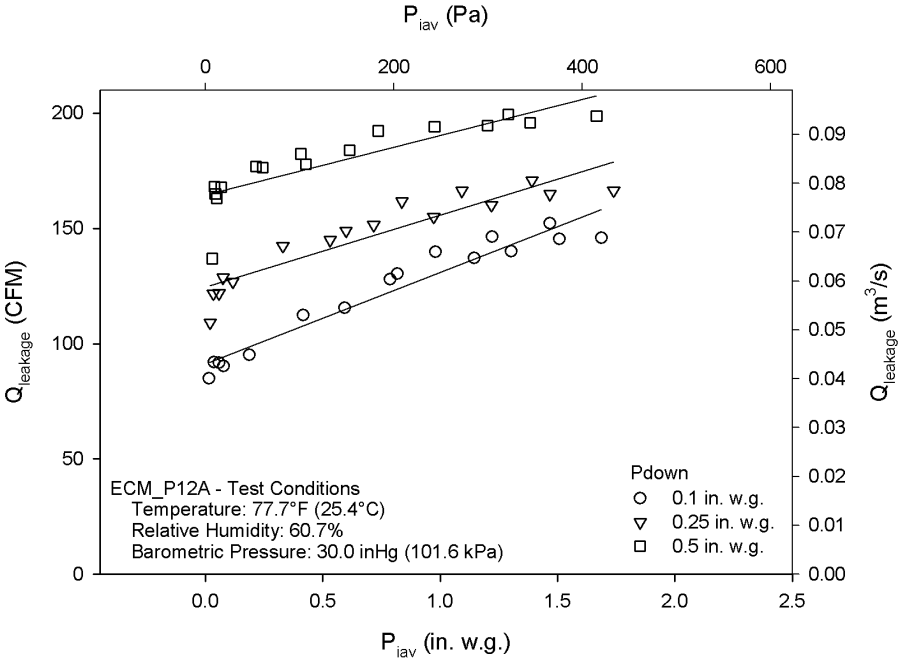

Figure 6-6: Leakage vs. P_{iav} for ECM_P12A

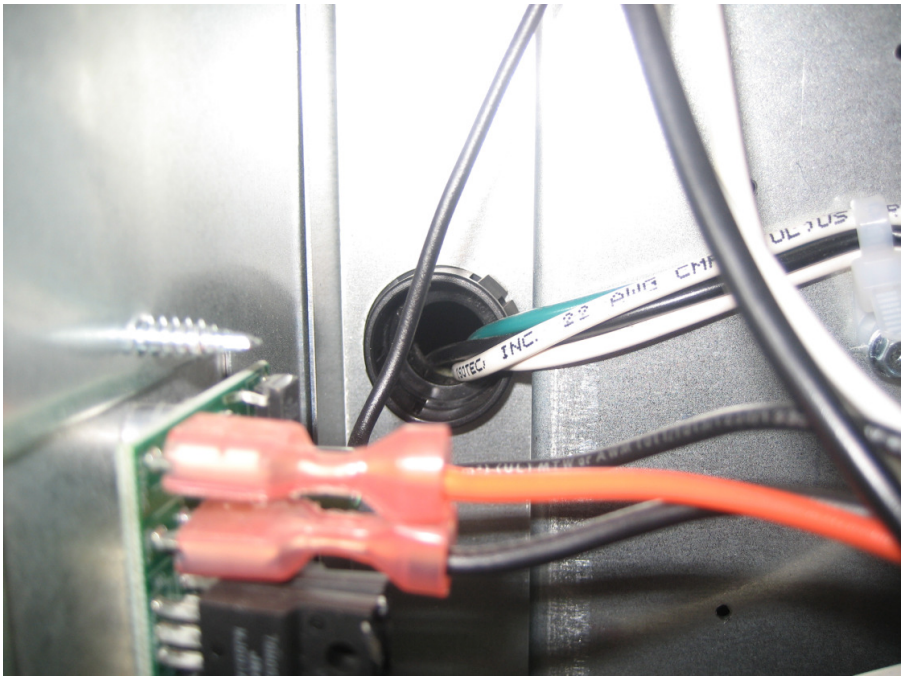

Figure 6-7: Grommet and Cable Bundle for ECM_P12A

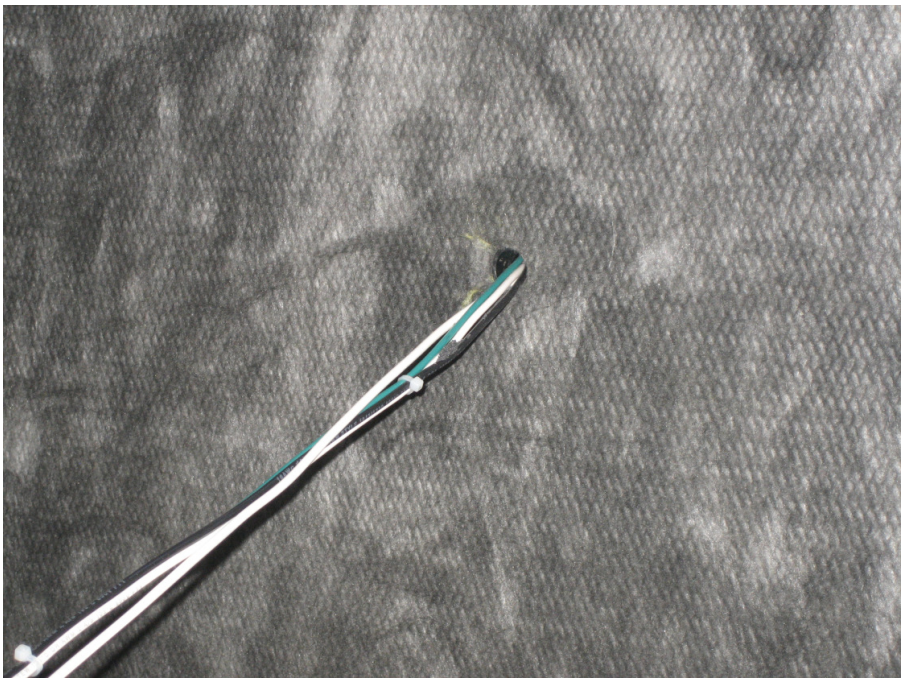

Figure 6-8: Entry Point of Cable Bundle into FPTU ECM_P12A

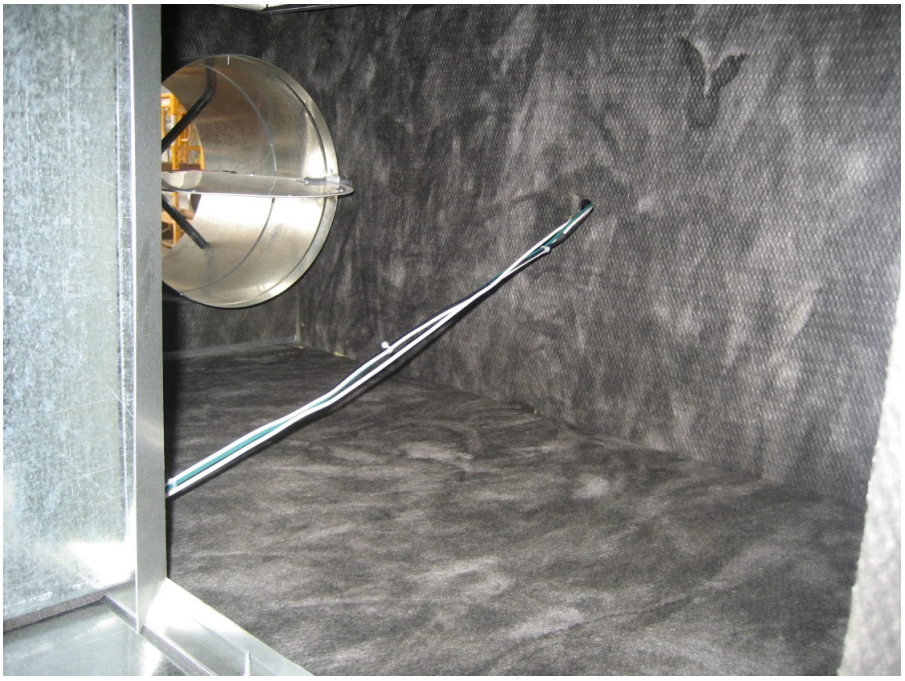

Figure 6-9: Cable Bundle Through Primary Air Stream for ECM_P12A

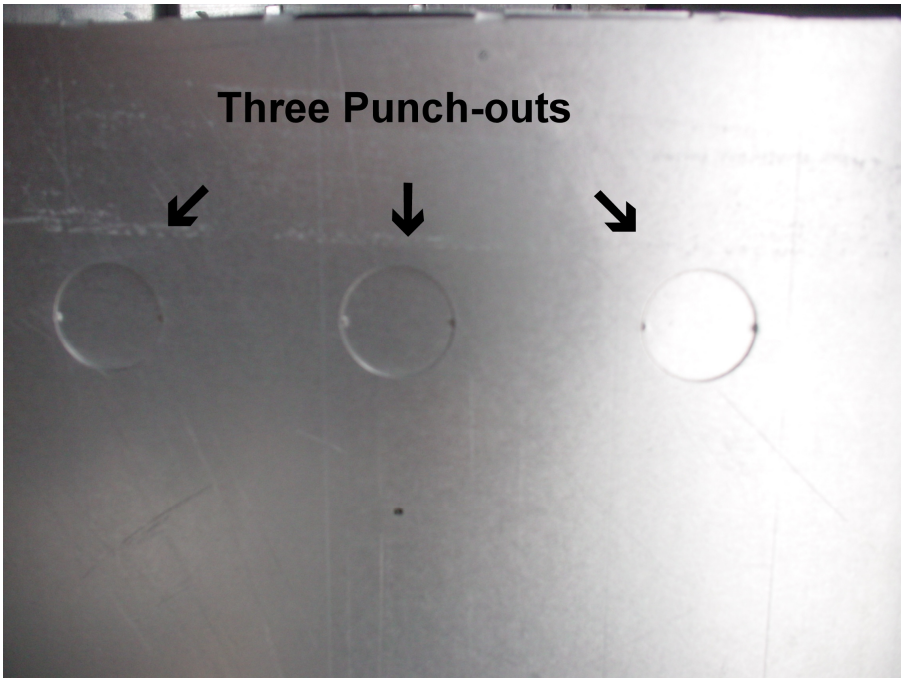

Figure 6-10: Punch-outs Opposite Primary Air Inlet for ECM_P12A

Figure 6-11 and Figure 6-12 show the leakage for ECM_P8C-M2 and ECM_P12A, respectively, plotted versus P_{down}. The leakage for ECM_P8C-M2 varied almost linearly with downstream static pressure and showed little dependence on P_{iav}. This variation was different from ECM_P12A where an increase in P_{iav} from 0.25 in. w.g. (62.3 Pa) to 1.25 in. w.g. (311.4 Pa) resulted in an approximately 75 CFM (0.0354 m^3/s) increase in leakage at a downstream static pressure of 0.1 in. w.g. (24.9 Pa). Both figures show leakage at three different inlet velocity pressures to illustrate the effect of increasing primary airflow on leakage from the terminal units. Notice that increasing P_{iav} affected each unit differently. ECM_P8C-M2 showed little or slightly negative dependence on P_{iav}. Leakage for ECM_P12A showed a increase in leakage with respect to P_{iav}.

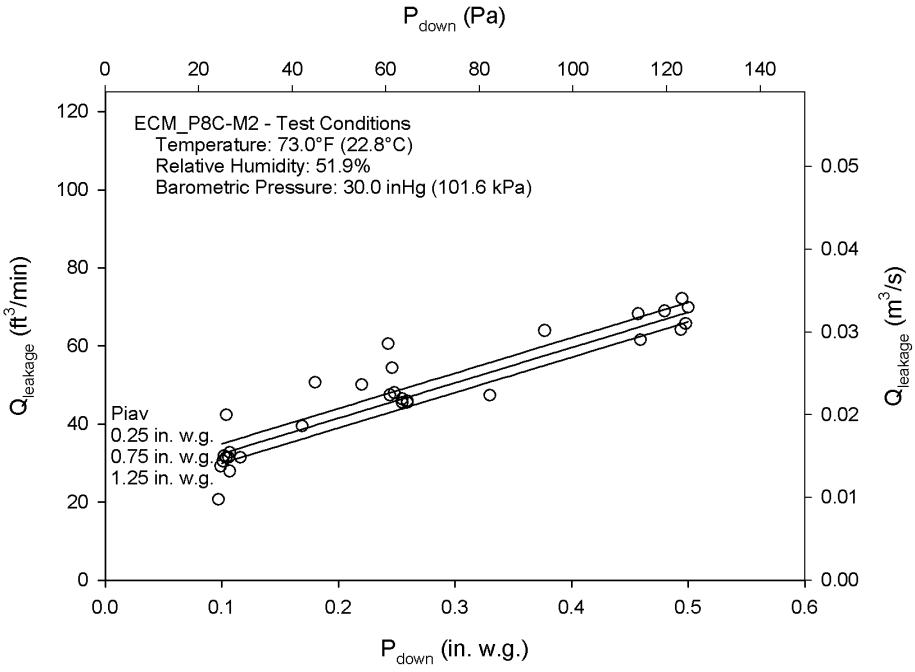

Figure 6-11: Leakage vs. P_{down} for ECM_P8C-M2

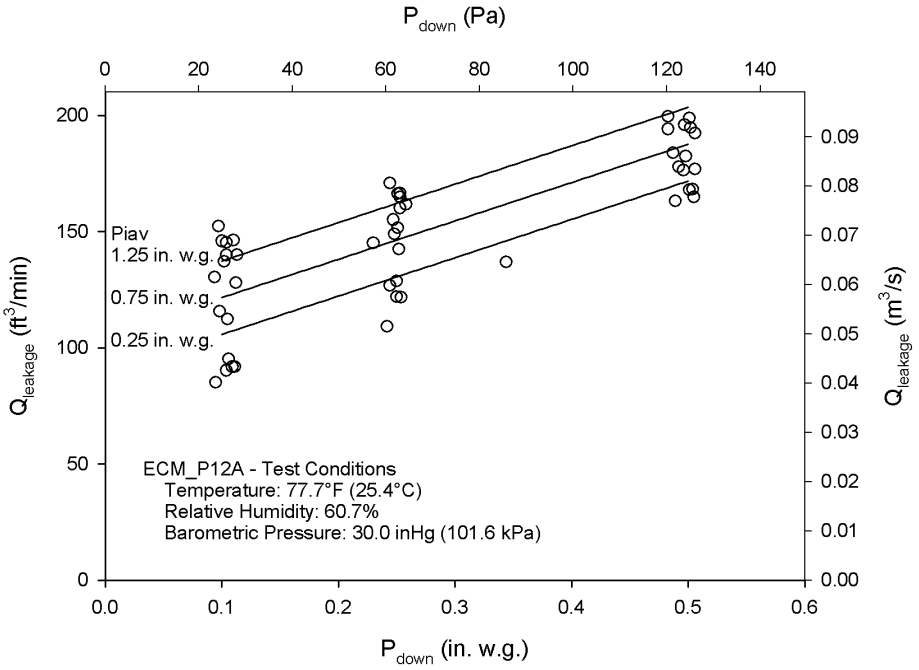

Figure 6-12: Leakage vs. P_{down} for ECM_P12A

The equation used to model the air leakage was taken from Furr (2006), and is shown in Equation (6-4). The coefficients for the ECM controlled terminal units are presented in Table 6-6, and the data for ECM_P8C-M1 was taken from Cramlet (2008). The coefficients for the SCR controlled terminal units were taken from Furr (2006) and are presented in Table 6-7. All of the FPTUs from Manufacturer C were of the same design. Manufacturer A used a primary air operated backdraft damper on the SCR units, but switched to a gravity operated damper for the ECM units. The R^2 values were generally lower than those for the other models, and ranged from 0.826 to 0.972 for the ECM FPTUs and from 0.767 to 0.989 for the SCR FPTUs. The variation and low values were likely due to measuring leakage as a small difference between two large numbers.

$$Q_{leakage} = C_1 + C_2 * P_{down} + C_3 * P_{iav} \quad (6\text{-}4)$$

Table 6-6: ECM Coefficients for FPTU Leakage Model

FPTU	C1	C2	C3	R^2
ECM_P8A	43.287	121.922	11.878	0.972
ECM_P12A	81.339	165.046	31.638	0.948
ECM_P8B	8.705	72.872	-4.472	0.887
ECM_P12B	15.997	78.834	-13.244	0.856
ECM_P8C-M1	37.87	119.98	3.213	0.918
ECM_P8C-M2	27.127	90.5	-4.985	0.895
ECM_P12C-M1	28.996	72.274	-6.628	0.927
ECM_P12C-M2	35.044	76.499	-4.948	0.826

Table 6-7: SCR Coefficients for FPTU Leakage Model

FPTU	C1	C2	C3	R^2
SCR_P8A	16.47	138.1	-6.16	0.97
SCR_P12A	14.4	97.94	-37.9	0.858
SCR_P8B	13.8	37.41	0	0.767
SCR_P12B	17.83	58.26	-27.16	0.945
SCR_P8C	16.86	77.55	-10.76	0.97
SCR_P12C	22.3	100.83	-15.02	0.989

6.2. Parallel Terminal Unit Power Performance

One of the main reasons for choosing parallel fan powered terminal units instead of series fan powered terminal units is the perceived lower energy requirements of parallel units. To model the energy use of a FPTU, the power of the FPTU must be

characterized over the whole range of operating conditions of each FPTU. In addition, comparisons of series and parallel FPTUs must also include the power required to supply the primary air. The real power consumption of each terminal unit was measured and modeled. In addition to the real power consumption, the apparent power and power factor, and power quality were also measured and analyzed. Equations were developed to model the real power consumption.

6.2.1. Fan Power Consumption Analysis and Model. The fan power consumption in a parallel FPTU is dependent on the airflow produced and the downstream static pressure. Figure 6-13 shows the power consumption of terminal unit ECM_P8B plotted versus Qfan. For the most part, this unit operated with airflow independent of downstream static pressure. As downstream pressure increased, power consumption also increased. For example, at an ECM setting of 4 VDC, the fan was producing an airflow around 500 – 600 CFM (0.236 – 0.283 m3/s). There were three distinct power consumption levels, one at about 75 Watts, one at about 100 Watts, and the highest at about 150 Watts. These three power values corresponded directly with P_{down} levels of 0.1 in. w.g. (24.9 Pa), 0.25 in. w.g. (62.3 Pa), and 0.5 in. w.g. (124.5 Pa). At an ECM setting of 10 VDC, when P_{down} was raised to 0.5 in. w.g. (124.5 Pa), the fan airflow and power consumption were reduced to the same levels as an ECM setting of 8 VDC at 0.5 in. w.g. (124.5 Pa) downstream static pressure. These reductions in airflow and power consumption were possibly due to operating the FPTU outside its designed rang of operation. These data were not used in the data analysis.

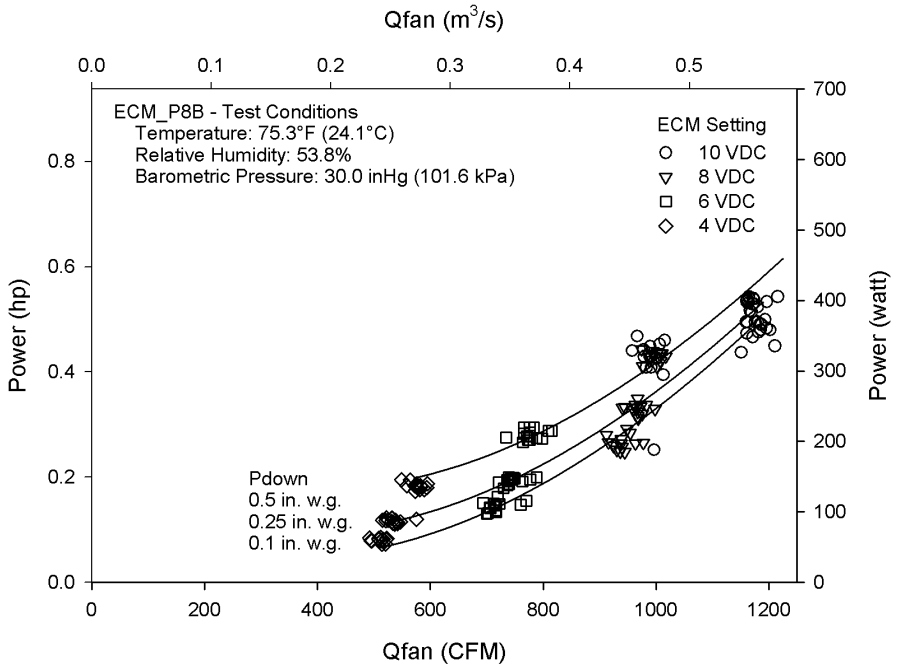

Figure 6-13: Real Power vs. Q_{fan} for ECM_P8B

Figure 6-14 shows the real power consumption of terminal unit P12C-M1 plotted against Q_{fan}. At ECM settings of 5 VDC and 7.5 VDC, fan airflow remained constant at different levels of P_{down} with power consumption increasing with increasing downstream static pressure. At ECM settings of both 2.5 VDC and 10 VDC, which were on the limit of recommended operation, increasing P_{down} resulted in increased power consumption with decreased airflow.

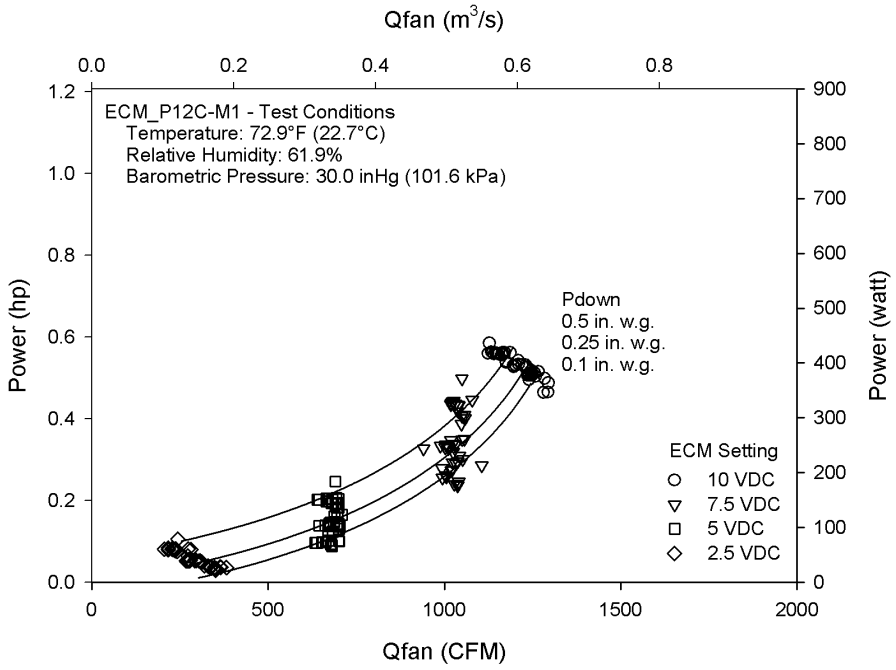

Figure 6-14: Power vs. Q_{fan} for ECM_P12C-M1

These results were fairly typical of the ECM terminal units tested in this study. Terminal unit ECM_P8C-M1, which was tested by Cramlet (2008), did not show a difference in airflow or power consumption between ECM settings of 7.5 VDC and 10 VDC. The reason for this difference appeared to be in the programming of that particular ECM motor/controller combination. One difference between SCR and ECM controlled units was that fan airflow depended more on the downstream static pressure in SCR units than it did in ECM units. The other main difference was that the power consumption of SCR models increased linearly with increasing airflow, while the increase was parabolic in ECM units. The power consumption versus fan airflow is shown for SCR_P8C and ECM_P8C-M1 in Figure 6-15 (Furr 2006 and Cramlet 2008).

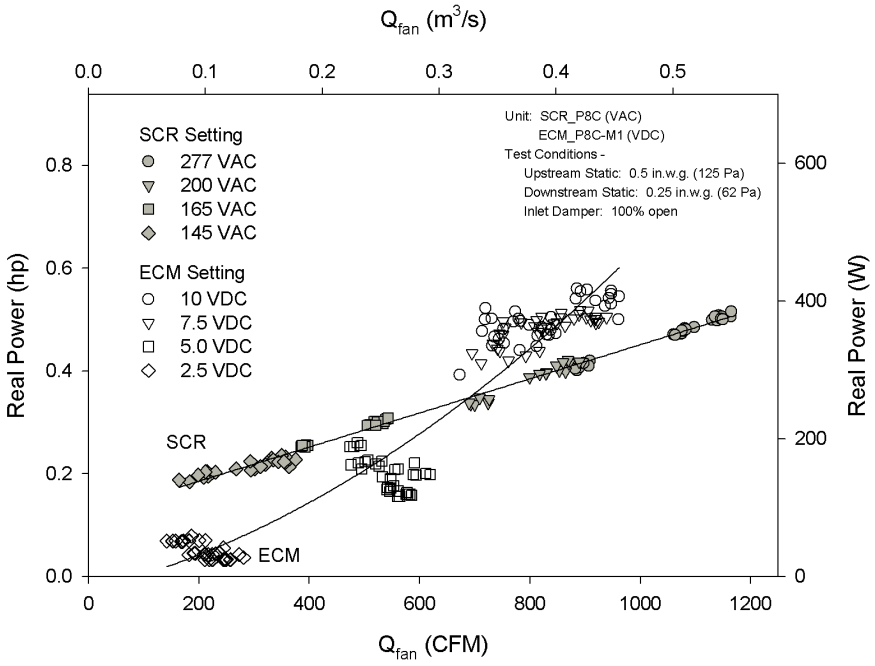

Figure 6-15: Real Power vs. Q_{fan} for SCR_P8C and ECM_P8C-M1

The form of the equation used to model power consumption was adopted from Furr (2006), and is shown in Equation (6-5). The coefficients for ECM_P8C-M1 (Cramlet 2008) have been adapted to the new scale for ECM setting. Furr (2006) also required an additional term for SCR terminal unit P8A, which was the inlet air velocity pressure. Since each manufacturer's controller utilized a different control signal, it was determined that the best way to compare different ECM units was to use the percentage from minimum to maximum ECM setting explained in section 6.1.2. The coefficients for the ECM units are presented in Table 6-8, while those for the SCR units are in Table 6-9. All of the models for the ECM FPTUs were above 0.919 indicating the models correlated well with the measured performance.

$$Power_{fan} = C_1 + C_2 * V^2 + C_3 * V + C_4 * P_{down} + C_5 * P_{iav} \quad (6\text{-}5)$$

Table 6-8: ECM Coefficients for Fan Power Model

FPTU	C1	C2	C3	C4	C5	R^2
ECM_P8A	11.698	0.025	-0.919	203.915	0	0.953
ECM_P12A	3.345	0.06	-1.987	358.335	0	0.922
ECM_P8B	11.463	0.036	-0.35	245.189	0	0.990
ECM_P12B	29.067	0.042	-0.521	196.659	0	0.955
ECM_P8C-M1	-202.61	-.041	9.994	-8.424	0	0.919
ECM_P8C-M2	55.736	0.074	-3.739	172.102	0	0.943
ECM_P12C-M1	-59.413	0.027	1.347	167.824	0	0.977
ECM_P12C-M2	22.523	0.043	-1.318	114.355	0	0.976

Table 6-9: SCR Coefficients for Fan Power Model

FPTU	C1	C2	C3	C4	C5	R^2
SCR_P8A	5.86	0.000895	0.304	-89.3	-31.9	0.908
SCR_P12A	-631	-0.0039	6.22	-142	0	0.956
SCR_P8B	-258	-0.006	3.65	-82.3	0	0.989
SCR_P12B	-403	-0.00515	5.15	-128.7	0	0.996
SCR_P8C	-363	-0.0088	5.18	-145	0	0.99
SCR_P12C	-622	-0.0159	9.48	-638	0	0.923

6.2.2. Power Factor Analysis. As with the series terminal units, the ECM controlled fans on the parallel terminal units also had power factors that were generally between 0.4 and 0.6. Figure 6-16 shows the power factor of terminal unit ECM_P8A, and was

generally around 0.4. At an ECM setting of 7.5 VDC, this unit displayed a spread in power factor of just below 0.4 to about 0.5. This showed a spread in power factors that was common among the ECM controlled units. Figure 6-17 shows the power factor for ECM_P12C-M2. This unit had a slightly higher power factor of generally around 0.5.

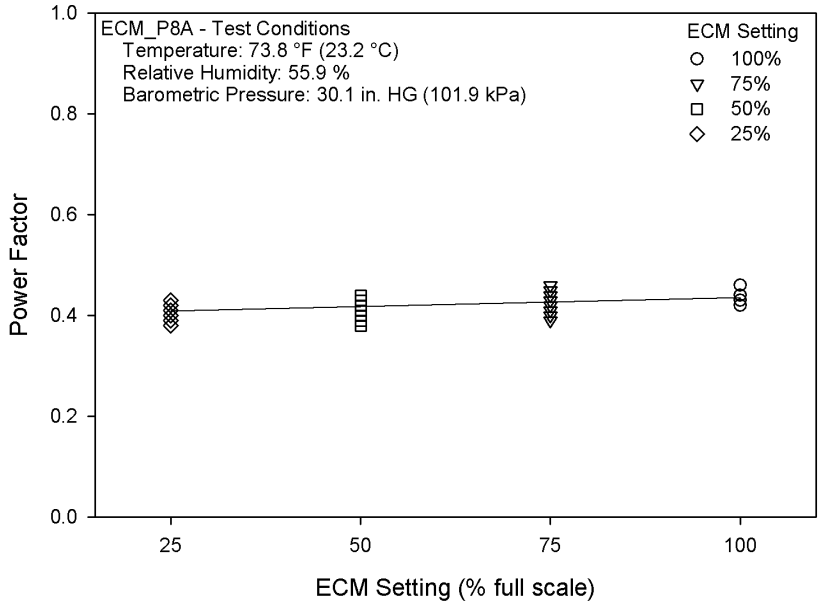

Figure 6-16: Power Factor for ECM_P8A

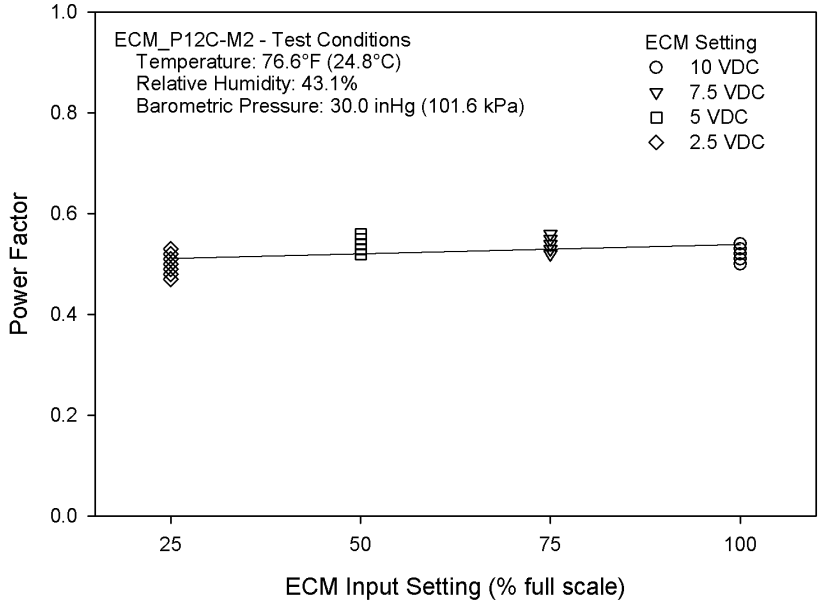

Figure 6-17: Power Factor for ECM_P12C-M2

The apparent power performance of the terminal units was another important quantity used to evaluate the impact of ECM controlled FPTUs on electrical demand. The relationship between real power, apparent power, and power factor is shown in (5-4). Figure 6-18 shows the apparent power for terminal unit ECM_P8A plotted versus Q_{fan}. It shows that there were distinct levels of apparent power at each ECM setting, which corresponded to different levels of P_{down}, similar to the real power consumption. No attempt was made to quantify the relationship between real power, P_{down}, power factor, and apparent power in this study. Figure 6-19 shows the apparent power for terminal unit ECM_P12C-M2 plotted against Q_{fan}. At a level of about 900 CFM (0.425

m3/s), ECM_P8A had an apparent power of approximately 700 VA. ECM_P12C-M2 did not reach this level of apparent power until about 1100 CFM (0.519 m3/s).

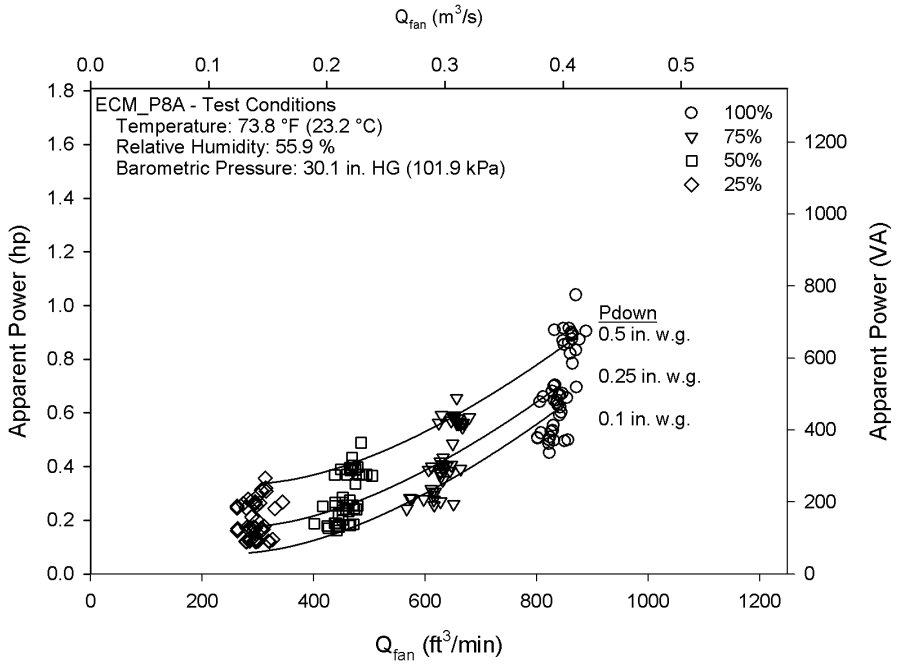

Figure 6-18: Apparent Power vs. Q_{fan} for ECM_P8A

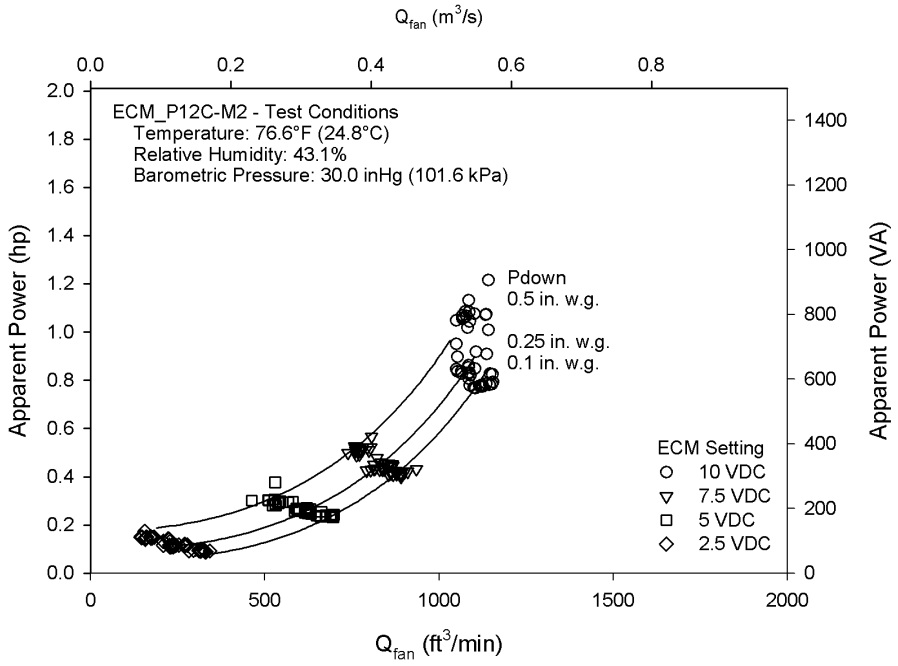

Figure 6-19: Apparent Power vs. Q_{fan} for ECM_P12C-M2

Cramlet (2008) showed a comparison of the apparent power of an ECM and SCR controlled terminal unit. This comparison is shown in Figure 6-20. Only at the lowest flow levels did the ECM motor have a lower apparent power than the SCR motor. At approximately 500 CFM (0.236 m3/s), both types of motor had an apparent power of approximately 400 VA. Figure 6-15 shows the real power comparison for these same units. The ECM unit had an average power consumption of about 150 Watts while the SCR unit had an average power consumption over 200 Watts. For these two units, the ECM unit had a real power consumption advantage at flow rates below about 700 CFM (0.330 m^3/s), but required more apparent power when airflow was above about 450 CFM

(0.212 m^3/s). The higher apparent power of the ECM could negate its real power advantage over the SCR controlled unit in some applications.

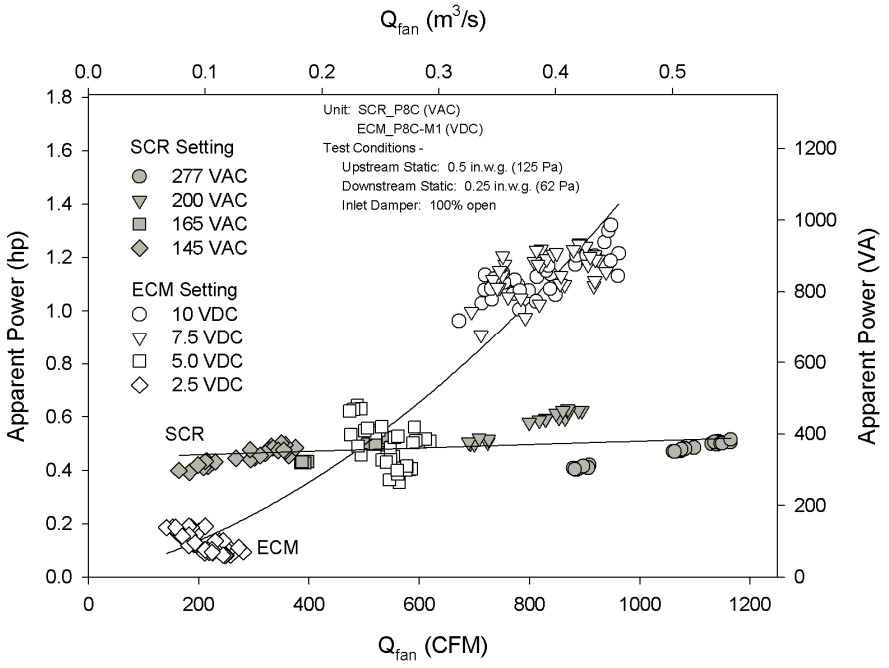

Figure 6-20: Apparent Power vs. Q_{fan} for SCR_P8C and ECM_P8C-M1

Figure 6-21 compares the power factor for SCR_P8C and ECM_P8C-M1. As with the series units, the SCR controlled parallel unit showed an increase in power factor with an increase in SCR setting. Likewise, the power factor of the ECM controlled unit was relatively flat with respect to ECM setting. The increase in power factor of the SCR unit would help explain why the apparent power was relatively constant throughout the entire range of airflow. Likewise, the relatively constant power factor of the ECM unit would help explain the increase in apparent power with an increase in airflow.

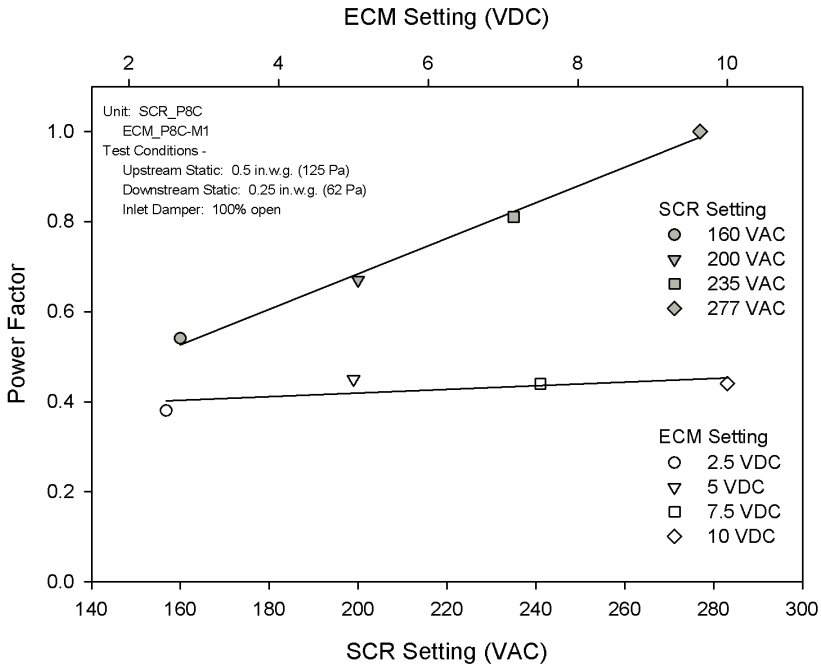

Figure 6-21: Power Factor Comparison for SCR_P8C and ECM_P8C-M1

6.2.3. Power Quality Analysis. The power quality is also an important aspect of the performance of fan powered terminal units. The harmonic distortion can cause problems for sensitive electronic equipment, decrease power factor, increase apparent power, overload neutral lines, and increase losses in the power distribution system (Kennedy 2000 and Gosbell 2000). Harmonics are often analyzed by looking at the percent distortion compared to the fundamental value, and also by looking at the magnitude of the distortion in units of amps, volts, or watts as the case may be.

The real power harmonics are important because they provide a direct indication of the amount of distortion in the power. Figure 6-22 shows the power harmonics for ECM_P8B in percentage form, with the harmonics shown in watts in Figure 6-23.

Figure 6-24 shows the power harmonics in percentage form for ECM_P12C-M1, with harmonics shown in watts in Figure 6-25. In contrast to the current and voltage harmonics, some of the watt harmonics were negative, which indicated that the distortion at these frequencies transferred power back to the voltage source. In percentage form, the highest distortion for any single harmonic was about 0.5%, reached at an ECM setting of 8 VDC at the 5th harmonic for ECM_P8B, and at an ECM setting of 10 VDC at the 9th harmonic for ECM_P12C-M1. In the case of ECM_P8A, this resulted in a distortion magnitude of about 1.25 watts. For ECM_P12C-M1, the magnitude in watts of the 9th harmonic at an ECM setting of 10 VDC was about 1.75 watts.

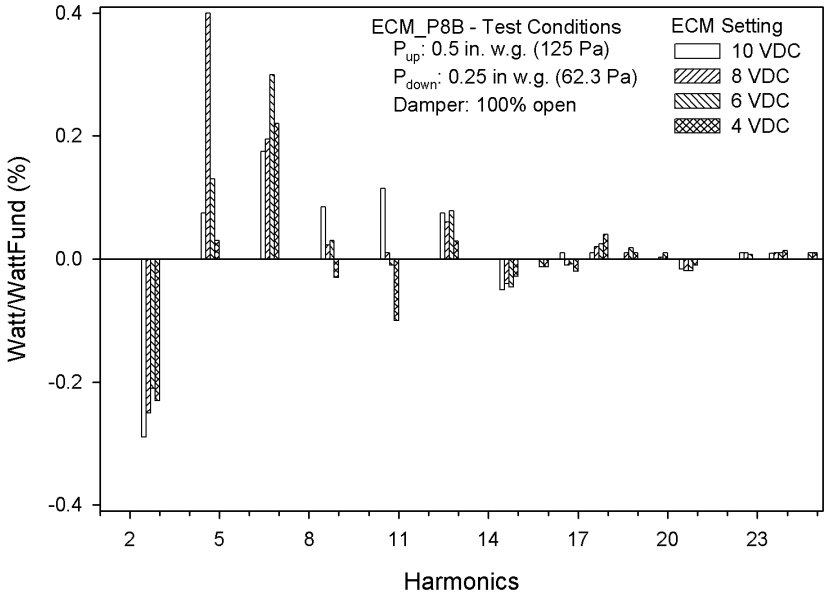

Figure 6-22: Real Power Harmonics for ECM_P8B (%)

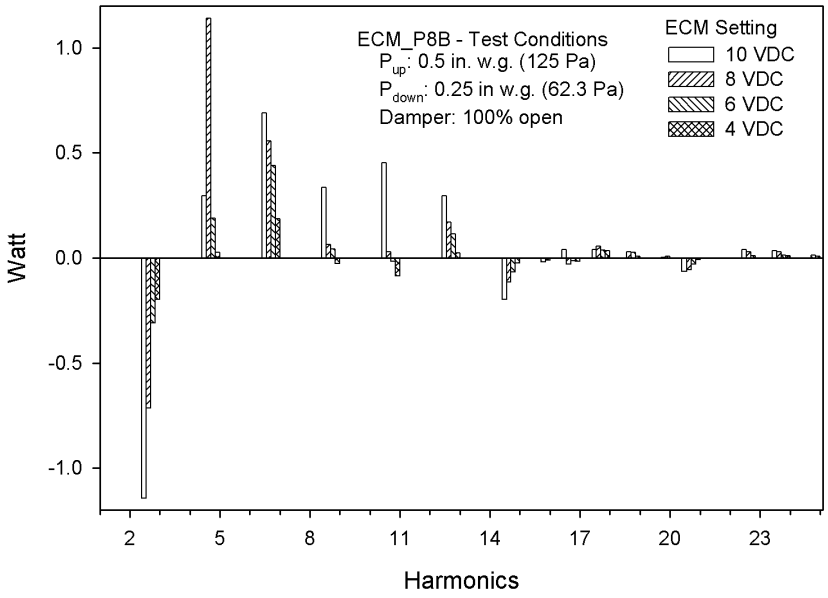

Figure 6-23: Real Power Harmonics for ECM_P8B (Watts)

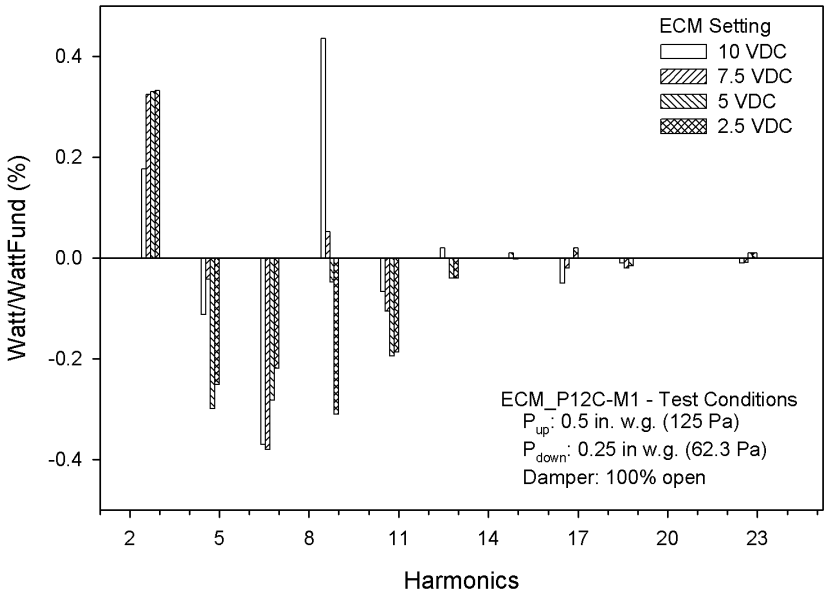

Figure 6-24: Real Power Harmonics for ECM_P12C-M1 (%)

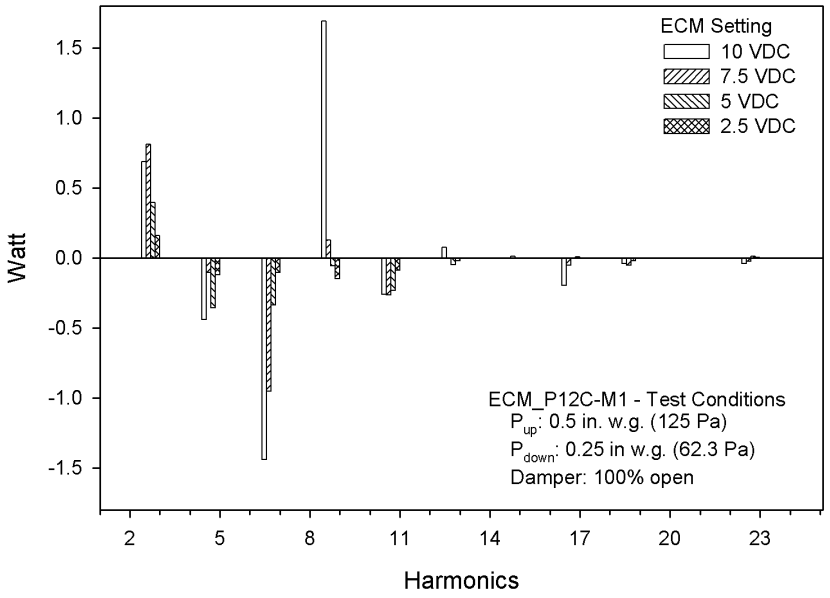

Figure 6-25: Real Power Harmonics for ECM_P12C-M1 (Watts)

Another method used to analyze the cumulative effect of harmonic distortion is the Total Harmonic Distortion (THD). The THD of real power is presented here in percentage form. Figure 6-26 shows the real power THD for ECM_P8B. Figure 6-27 shows the real power THD for ECM_P12C-M1. Both of these graphs show that there seemed to be little dependence of percent THD on ECM setting. If the THDs of these units were viewed in watts, the higher ECM settings would have higher THD since they have higher real power consumption. ECM_P12C-M1 had higher THD than ECM_P8B, though overall, there did not appear to be any dependence of THD on terminal unit size. A complete summary of real power THD results are found in Table 6-10.

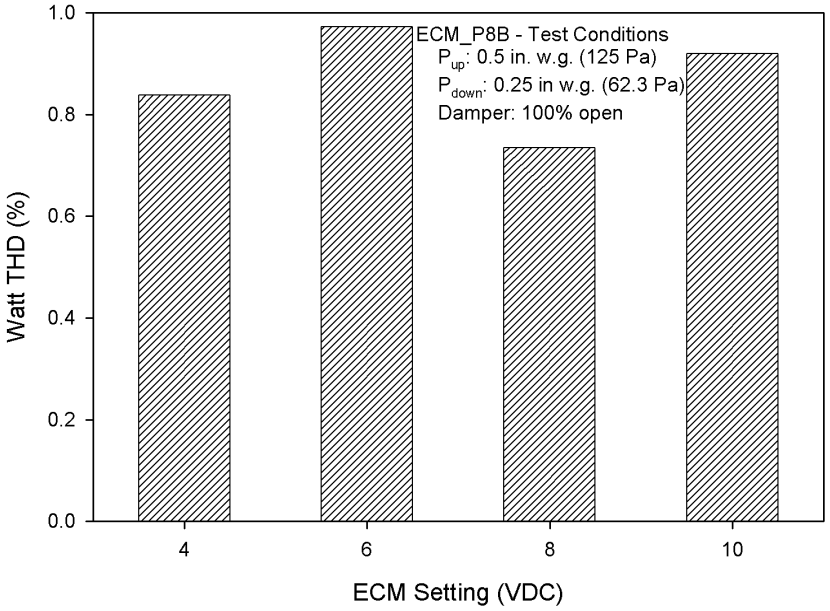

Figure 6-26: Real Power THD for ECM_P8B (%)

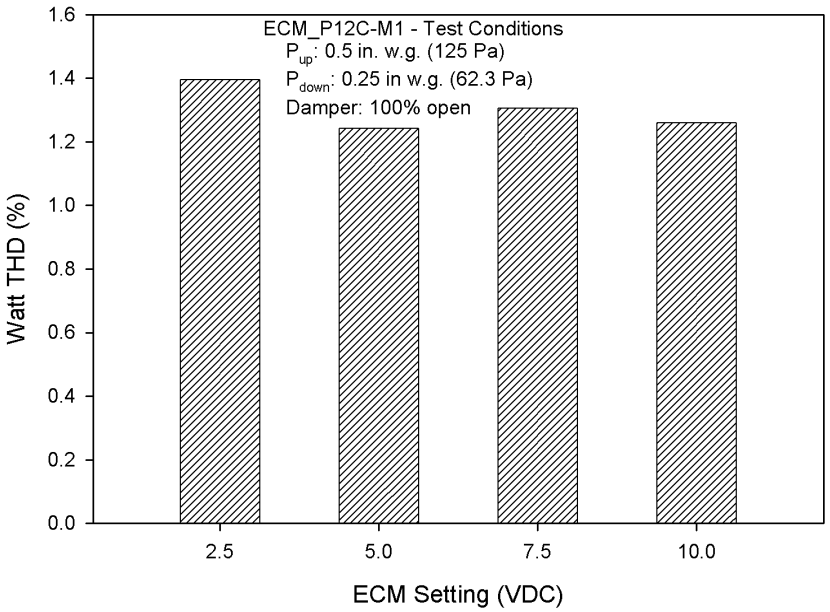

Figure 6-27: Real Power THD for ECM_P12C-M1 (%)

Table 6-10: Summary of Real Power THD (%)

FPTU	ECM Setting				Average
	25%	50%	75%	100%	
ECM_P8A	0.62	0.58	0.53	0.76	0.62
ECM_P8B	0.84	0.97	0.74	0.92	0.87
ECM_P8C-M2	0.60	0.88	0.62	0.65	0.69
ECM_P12A	0.91	0.96	0.71	0.59	0.79
ECM_P12B	0.84	0.77	0.63	1.21	0.86
ECM_P12C-M1	1.40	1.24	1.31	1.26	1.30
ECM_P12C-M2	1.21	1.11	1.03	0.61	0.99

Harmonic distortion in the current signal is important because current spikes can damage electrical equipment. Figure 6-28 shows the percent harmonic distortion for ECM_P8C-M2, and Figure 6-29 shows the percent harmonic distortion for P12B. The maximum setting for P8C-M2 is 9.5 VDC due to problems operating the motor above this level. These graphs show the typical behavior of current harmonic distortion which was higher at the lower harmonics and decreased as the harmonic frequency increased. Table 6-11 contains a summary of the current THD for all units tested.

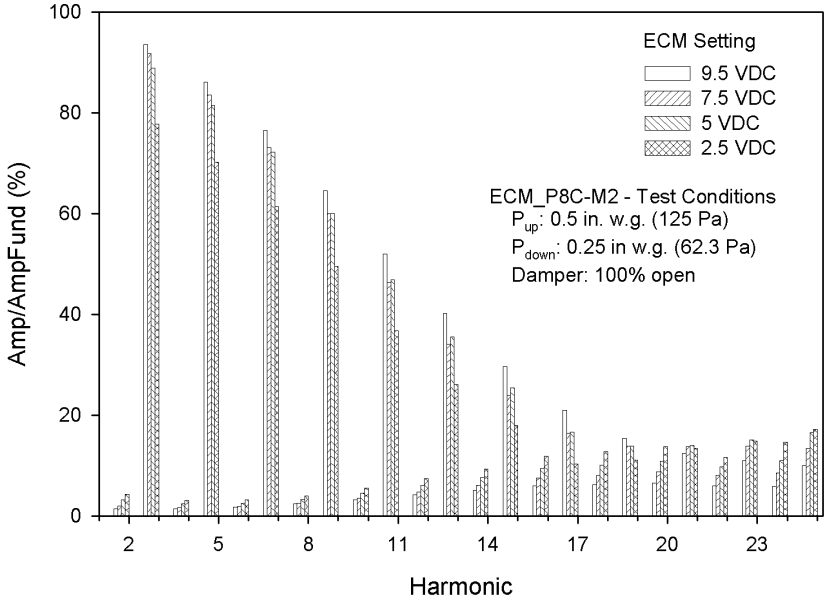

Figure 6-28: Current Harmonics for ECM_P8C-M2 (%)

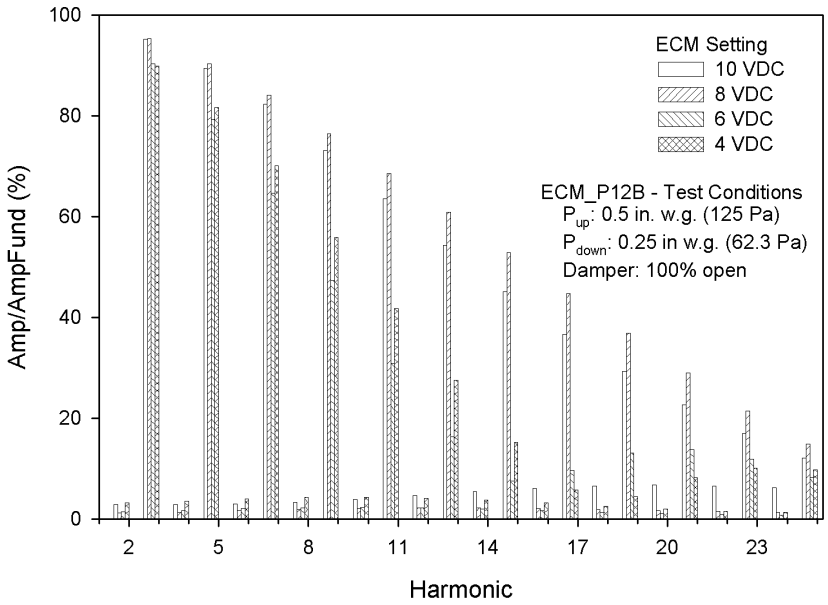

Figure 6-29: Current Harmonics for ECM_P12B (%)

Table 6-11: Summary of Current THD (%)

FPTU	ECM Setting				Average
	25%	50%	75%	100%	
ECM_P8A	90.24	90.28	90.28	90.65	90.36
ECM_P8B	89.74	90.35	90.14	89.90	90.03
ECM_P8C-M2	83.60	86.76	86.66	87.57	86.15
ECM_P12A	153.7	155.8	140.7	142.6	148.2
ECM_P12B	85.03	83.45	90.71	89.85	87.26
ECM_P12C-M1	170.4	175.6	179.8	182.7	177.1
ECM_P12C-M2	144.1	141.9	151.5	159.1	149.1

Though the percentages are very high, they only tell part of the story, since the real danger of harmonic distortion of the current signal is high amperage in the system damaging electrical equipment. Figure 6-30 shows the harmonic distortion of ECM_P8C-M2 in terms of amps, rather than percent. Figure 6-31 shows this for ECM_P12B. This shows that at the lower ECM settings, where the ECM controlled FPTUs had their greatest advantage in power consumption compared to SCR units, the magnitude of the current distortion was actually quite low. The highest ECM setting resulted in similar magnitude of current harmonics despite different size terminal units.

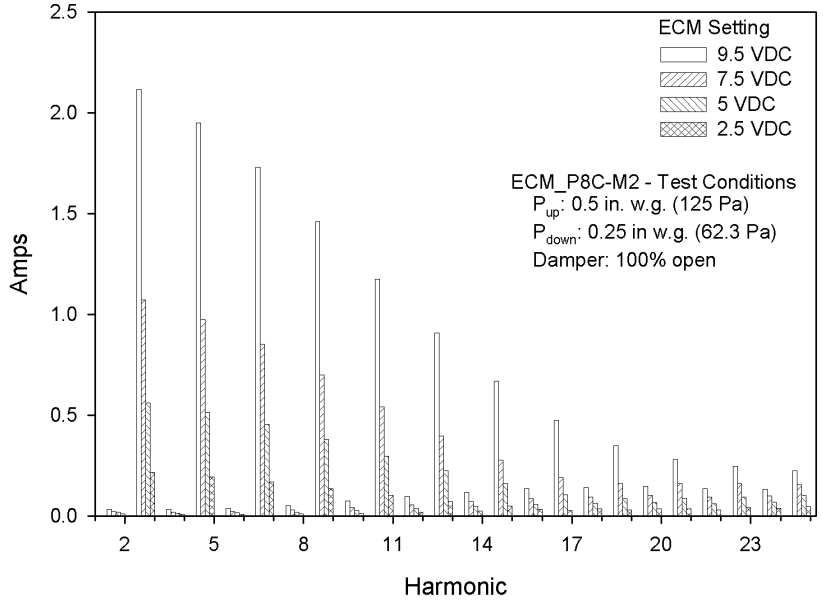

Figure 6-30: Current Harmonics for ECM_P8C-M2 (Amps)

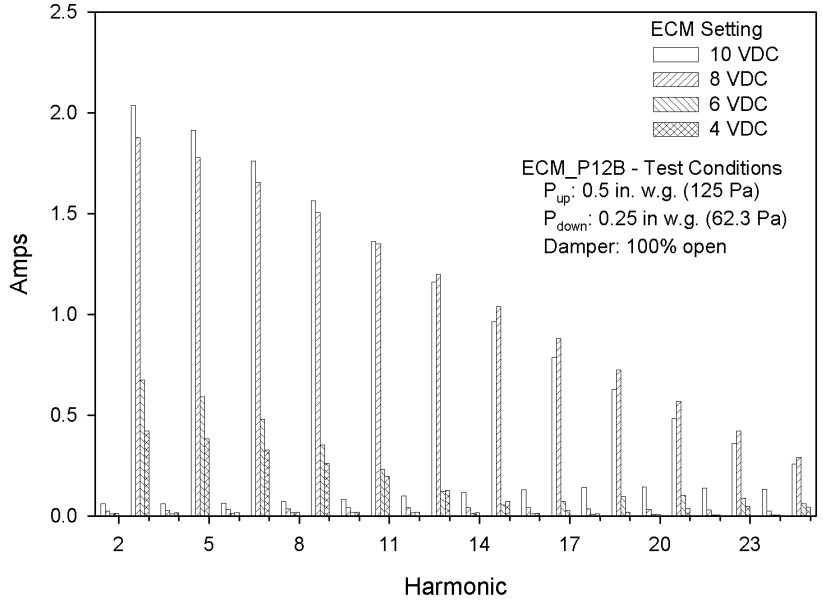

Figure 6-31: Current Harmonics for ECM_P12B (Amps)

Of special importance when discussing current harmonics are the triplen harmonics, which are odd multiples of three of the fundamental frequency. The triplen harmonics are important because they are in phase with the fundamental, and thus add to the peak current. Figure 6-32 shows the triplen harmonics in percentage form for ECM_P8C-M2, and Figure 6-33 shows these harmonics in amps. Figure 6-34 shows the triplen harmonics in percentage form for ECM_P12B, and Figure 6-35 shows them in amps. For both FPTUs, the triplen harmonic plots in percentage form showed similar distortion for all of the ECM settings. For the raw current data (in amps), the higher ECM settings had significantly higher current distortion, which was due to the much higher current draw at these settings. There was little difference in current harmonics between the two terminal unit sizes.

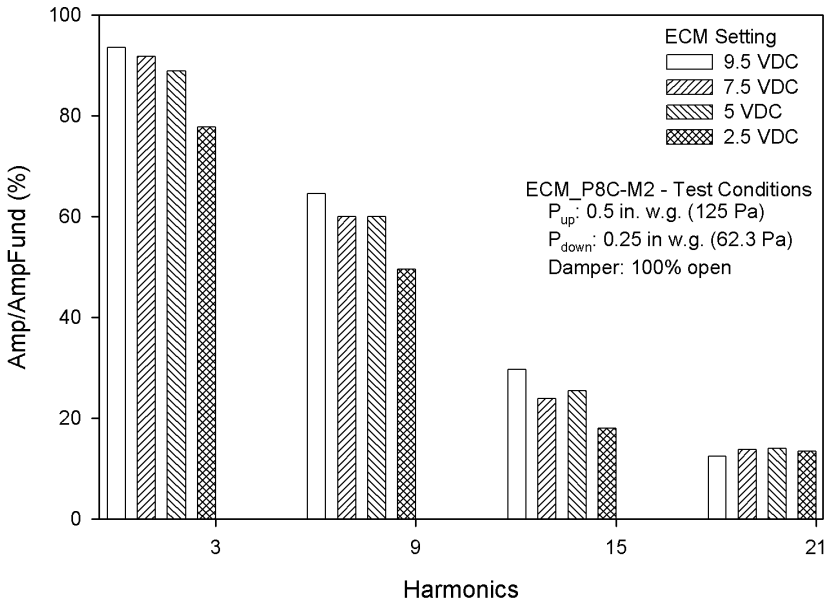

Figure 6-32: Current Triplen Harmonics for ECM_P8C-M2 (%)

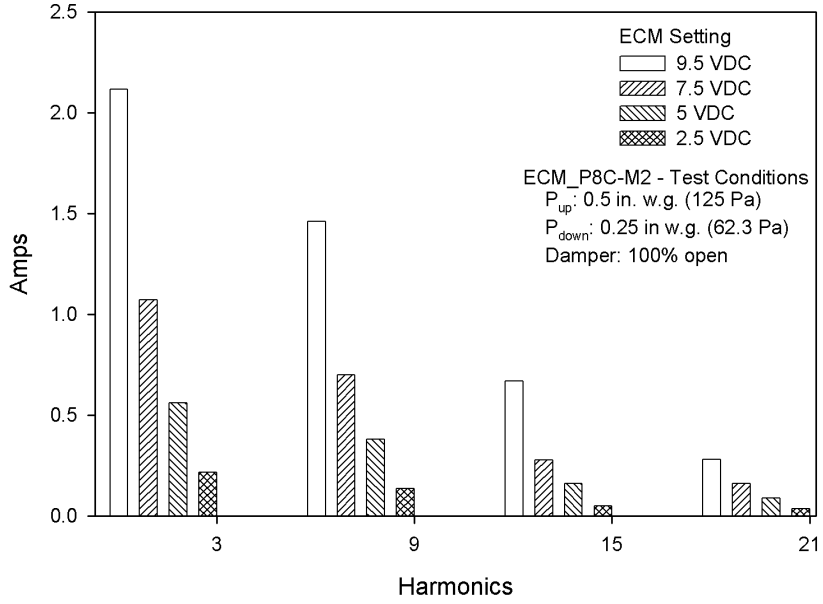

Figure 6-33: Current Triplen Harmonics for ECM_P8C-M2 (Amps)

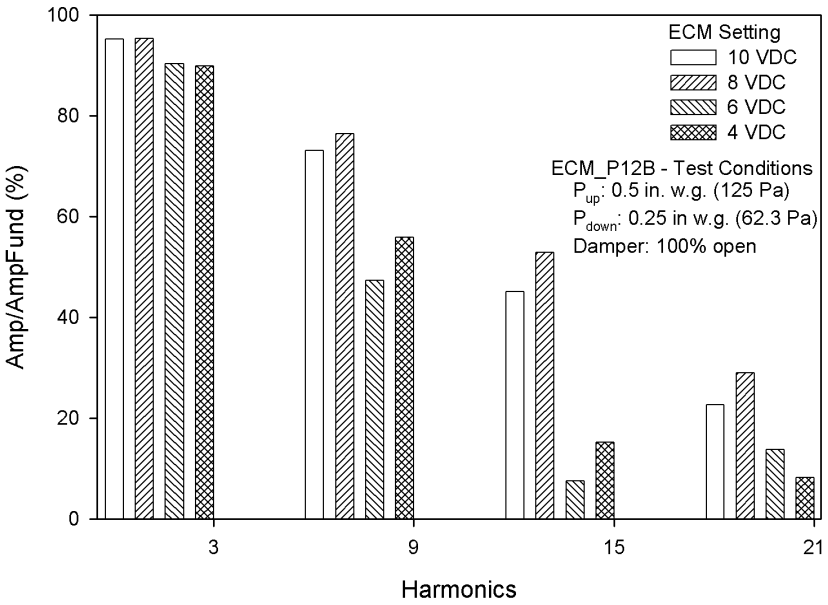

Figure 6-34: Current Triplen Harmonics for ECM_P12B (%)

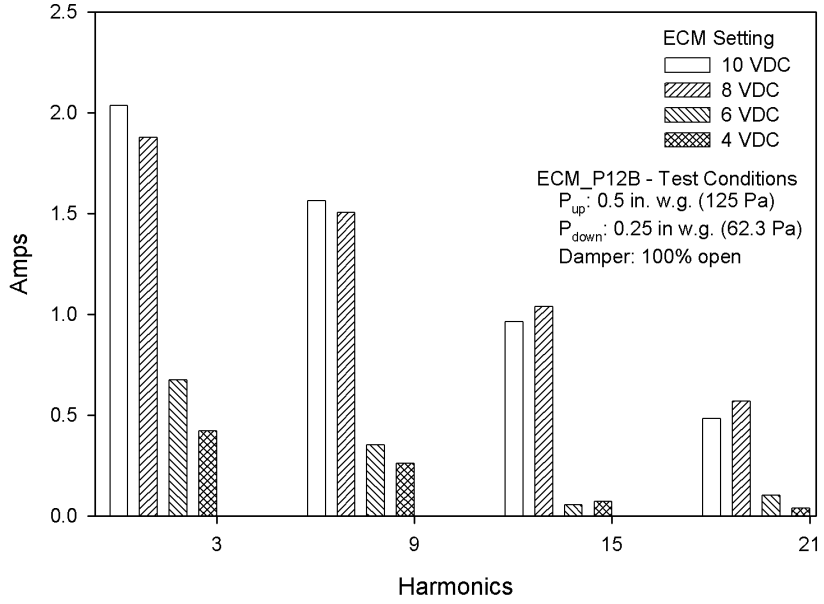

Figure 6-35: Current Triplen Harmonics for ECM_P12B (Amps)

Harmonic distortion of the voltage signal can also cause problems with electrical equipment. Figure 6-36 shows the voltage harmonics in percentage form for ECM_P8A, and Figure 6-37 shows the voltage harmonics for ECM_P8A in voltage form. Figure 6-38 shows the voltage harmonics for ECM_P12C-M2 in percentage form, with these harmonics in voltage form shown in Figure 6-39. In percentage form, the harmonics were generally less than 1%, and appeared to show little dependence on ECM setting. Because the voltage was 277 VAC, several of the harmonics for both FPTUs were higher than one volt. ECM_P12C-M2 had the 9th harmonic higher than 2 VAC, and the 5VDC ECM setting reached almost 3 VAC at the 9th harmonic. Table 6-12 contains a summary of the voltage THD for all terminal units tested.

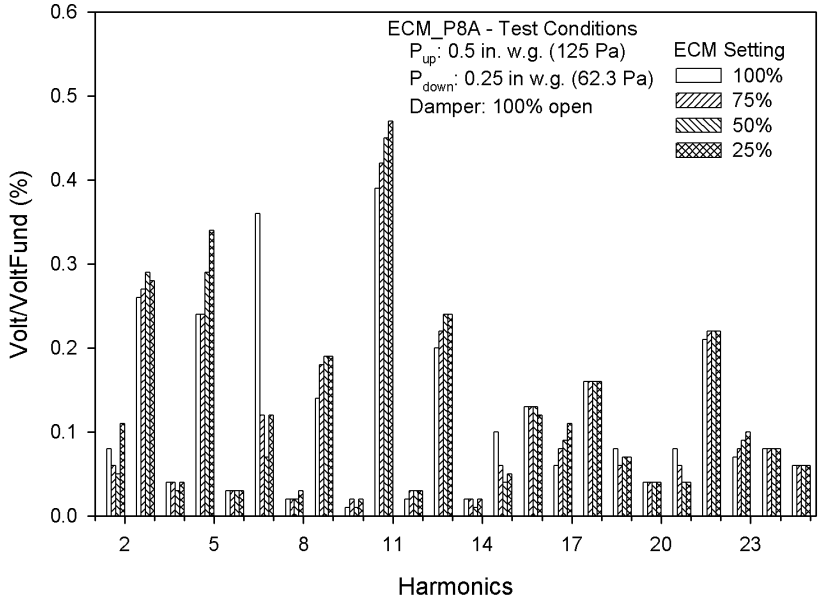

Figure 6-36: Voltage Harmonics for ECM_P8A (%)

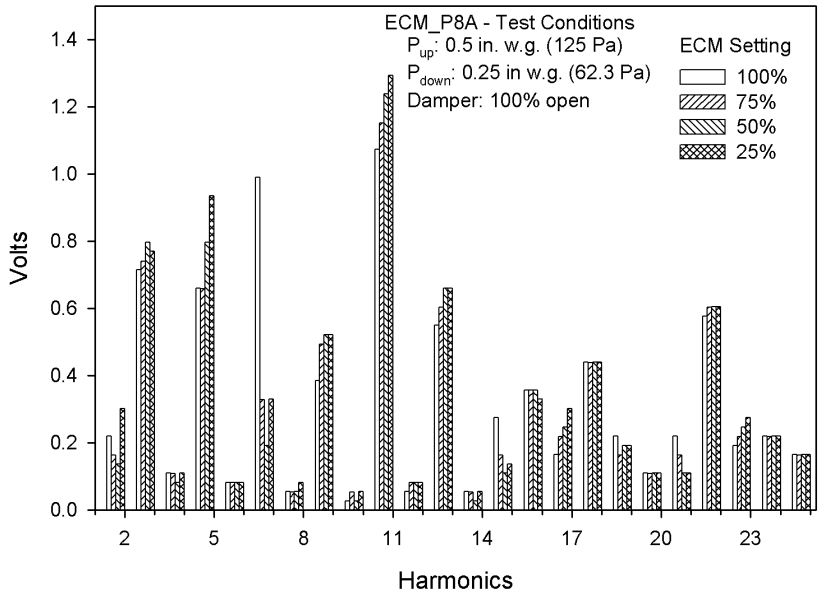

Figure 6-37: Voltage Harmonics for ECM_P8A (Volts)

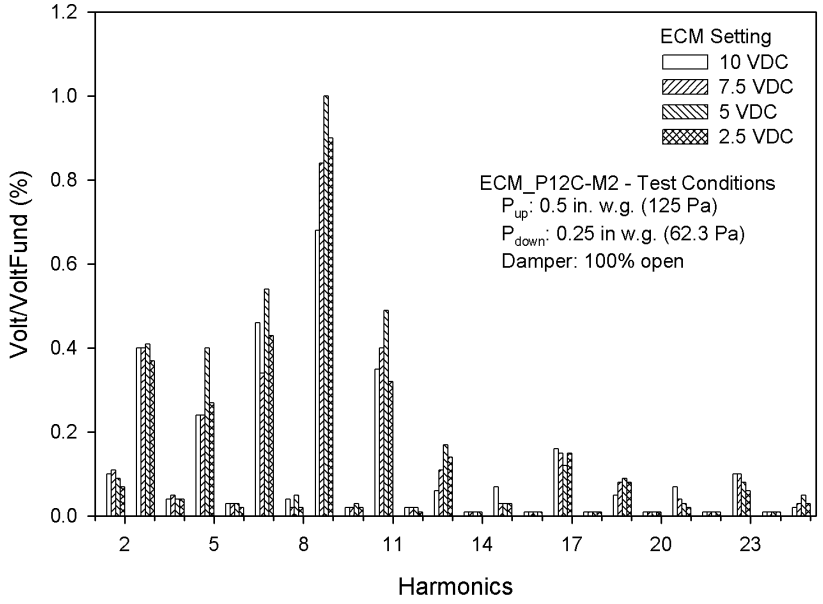

Figure 6-38: Voltage Harmonics for ECM_P12C-M2 (%)

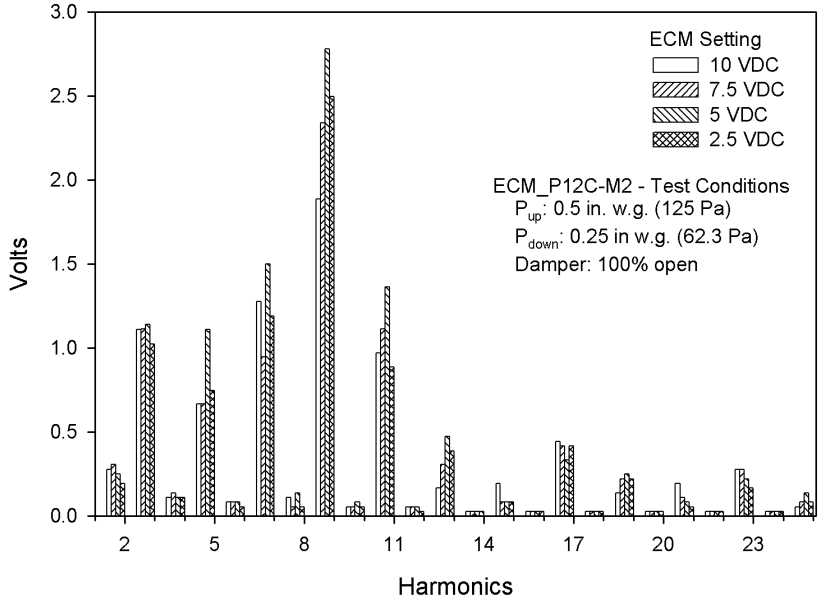

Figure 6-39: Voltage Harmonics for ECM_P12C-M2 (Volts)

Table 6-12: Summary of Voltage THD (%)

FPTU	ECM Setting				Average
	25%	50%	75%	100%	
ECM_P8A	0.83	0.78	0.74	0.79	0.79
ECM_P8B	0.84	0.89	0.93	0.93	0.90
ECM_P8C-M2	0.87	0.99	0.86	0.85	0.89
ECM_P12A	1.24	1.35	1.38	1.32	1.32
ECM_P12B	0.94	1.04	1.03	1.32	1.08
ECM_P12C-M1	1.19	1.19	1.27	1.13	1.20
ECM_P12C-M2	1.18	1.40	1.13	1.05	1.19

CHAPTER VII

SUMMARY AND CONCLUSIONS

Previous studies have shown that VAV systems use less energy than the older constant volume systems. An integral part of every VAV system is the terminal unit. Some applications use fan powered terminal units, which come in either series or parallel configurations. Some researchers have found that parallel FPTUs used less energy than systems with series FPTUs in some applications. These studies have focused on office buildings in specific climates, but lack general applicability to other building types and climates. One limitation of these studies was the lack of accurate performance models of fan powered terminal units. Furr (2006) developed these models for fan powered terminal units with SCR controlled motors.

While Furr's study was an important step in characterizing FPTUs, many manufacturers sell units with ECM controlled motors. These motors are assumed to be superior to the older SCR controlled motors in terms of energy consumption. There had been little to no experimental validation of this assumption when the ECM controllers were applied to fan powered terminal units. Cramlet (2008) developed experimental data and a preliminary model for one parallel and one series ECM controlled FPTU.

This study extends the work of Cramlet (2008) to seven series and seven parallel ECM controlled fan powered terminal units from three different manufacturers. The overall trends in performance of the ECM controlled FPTUs were similar with respect to different FPTU manufacturers, controller types, and motor manufacturers. Models of

the same form used by Furr (2006) were applied in this study to satisfactorily represent the different performance characteristics of the ECM controlled FPTUs.

Each series unit had three models developed to characterize its performance. The first was the primary air performance, which was independent of fan voltage. This model had R^2 values that ranged from 0.895 to 0.962 for the ECM units and 0.920 to 0.987 for the SCR units. The series model could possibly be improved by using the internal FPTU static pressure to calculate the differential pressure used in the model instead of the static pressure downstream of the fan.

The second model developed for the series fan powered terminal units was the airflow provided by the terminal unit fan. For the ECM controlled units, the R^2 values of this model ranged from 0.987 to 0.997. This model also correlated highly for the SCR controlled units, with R^2 values ranging from 0.989 to 0.997 for properly function SCR controllers. The high R^2 values for this form of the model demonstrate it explains most of the variability in the data.

The last model developed for the series units was that of fan power consumption. This is perhaps the most important model of the three because ECM controlled fans are expected to perform much better than their SCR counterparts. This model also correlated the data well for the ECM units. R^2 values ranged from 0.968 to 0.988. These R^2 values were similar to units with SCR controllers. Even a malfunctioning SCR was well represented by this model with an R^2 value of 0.87. This model can be used in conjunction with the fan airflow model to compare the power consumption of ECM and SCR controlled units at different operating conditions.

Due to their design, parallel fan powered terminal units were more complicated to model. The air supplied by the terminal unit was dependent on both the primary air supplied to the terminal unit and the air induced by the terminal fan. In contrast, for a series unit, the air supplied by the terminal unit is the airflow of the fan. Another reason is that parallel terminal units can be operated with the fan completely off whereas the fan in a series unit is always on. Parallel terminal units also have the added problem of air leakage from the FPTU which reduces the amount of air supplied by the terminal unit. As a consequence, parallel FPTUs required four different models to characterize their performance.

The first model developed for the parallel FPTUs was for the primary supplied to the terminal unit. Six of the seven models had R^2 values between 0.96 and 0.988. One model only had an R^2 value of 0.872 which could likely be improved by further testing of this unit. Six of the seven SCR units had R^2 values from 0.893 to 0.981, which were similar to those of the ECM units. One SCR unit had a low R^2 value of 0.637. Overall, this primary air model provided excellent correlation of the data for both ECM and SCR units.

The second model developed for ECM units was that for fan airflow. This model represented the effective airflow induced by the terminal fan. This model provided high correlation to the data for the ECM units. R^2 values ranged from 0.955 to 0.995, with all but one above 0.979. This model had a slightly different form for two of the SCR units, due to a different type of back draft damper. This difference was not present in the ECM

units due to all units having the same type of damper. The SCR units also conformed well with R^2 values from 0.931 to 0.998, with all but one above 0.978.

The third model developed for parallel units was for leakage. This model was important because it represented the amount of conditioned primary air lost to the return air plenum that was unavailable for conditioning the zone. The model was developed by testing the terminal unit with the terminal fan switched off. The correlation to the data of this model varied widely between different ECM terminal units, with R^2 values ranging 0.826 to 0.972, with only three of the seven above 0.9. The variation in R^2 values was possibly due to differences in back draft damper operation with some being stuck open when the fan was turned off, or even due to gaps between the blower assembly and mounting flange. This model performed better for the SCR units with four of six units tested having an R^2 above 0.945, though one unit was at 0.858, and one unit at 0.767. Overall, this model seems to represent fairly well the leakage from the terminal unit.

The final model developed was that for fan power consumption. This model was very important for several reasons. First, some manufacturers believe ECM controlled fans do not have as much of an impact on the power consumption of parallel units as they do on series units. Second, many of the models currently used for fan powered terminal units have not been tested in physical terminal units. Third, parallel fan powered terminal units are widely believed to be the energy efficient choice when fan powered units are used. A model of fan power consumption is needed to adequately

characterize the overall system energy consumption. Such a model would allow comparisons of systems with parallel units to systems with series units.

With the exception of one SCR unit that did not perform similarly to the other units of the same type, this model had the same form both ECM and SCR units. This model correlated well to the data for ECM units with R^2 values from 0.919 to 0.99. It also correlated well for the SCR units with R^2 values ranging from 0.908 to 0.996. It is believed that the R^2 values of the model may be improved for the ECM terminal units if the power data were measured in sync with the airflow data.

These models will allow better simulations to determine if fan powered terminal units will perform better than non powered units in wider variety of climates and building types. It will also allow simulations to determine if series or parallel fan powered terminal units would be more energy efficient for a given application, and which type would provide better comfort control, allowing a designer to make the optimum decision based on comfort and energy needs. By having models for SCR and ECM controlled units, simulations will be able to determine if and how much benefit is gained by using ECM controlled fans instead of SCR controlled fans. This will allow designers to make better decisions based on customer needs.

Similar to previous research, the leakage model is still only applicable to a full-cool mode. If a leakage model could be developed that was applicable even when the fan is in operation, it may lead to better terminal unit design. It may also allow whole system simulations to better predict the overall performance over a wider range of operating conditions.

REFERENCES

Alexander, J. and D. Int-Hout. 1998. Assuring zone IAQ. White paper. Titus. http://www.titus-hvac.com/tech_papers.asp.

AMCA. 1999. *ANSI/AMCA standard 210-99. Laboratory methods of testing fans for aerodynamic performance rating*. Arlington Heights, IL: Air Movement and Control Association.

Ardehali, M.M. and T.F. Smith. 1996. Evaluation of variable volume and temperature HVAC system for commercial and residential buildings. *Energy Conversion Management*. 37(9): 1469-1479.

ASHRAE. 1999. *ANSI/ASHRAE standard 120-1999, Method of testing to determine flow resistance of HVAC ducts and fittings.* Atlanta: American Society of Heating, Refrigerating, and Air-Conditioning Engineers, Inc.

ASHRAE. 2004. *ANSI/ASHRAE standard 90.1-2004, Energy standard for buildings except low-rise residential buildings*. Atlanta: American Society of Heating, Refrigerating and Air-Conditioning Engineers, Inc.

ASHRAE. 2006. *ANSI/ASHRAE standard 130-1996 (RA 2006), Methods of testing for rating ducted air terminal units*. Atlanta: American Society of Heating, Refrigerating and Air-Conditioning Engineers, Inc.

Chen, S.Y.S, and S.J. Demster. 1996. *Variable air volume systems for environmental Quality.* New York: McGraw-Hill.

Cramlet, A. 2008. Performance of ECM Controlled VAV Fan Power Terminal Units. M.S. Thesis, Texas A&M University, College Station, TX.

Elleson, J.S. 1993. Energy use of fan-powered mixing boxes with cold air distribution. *ASHRAE Transactions* 99(1):1349-1358.

Energy Information Administration (EIA). 2008. 2003 Commercial Buildings Energy Consumption Survey. Table E3A. Washington D.C.: United States Department of Energy.

EnergyIdeas Clearinghouse. 2002. Reducing power factor cost. Washington State University Cooperative Extension Energy Program. Pullman, WA: Washington State University.

Fluke. 2008. Power Log, Version 2.7. Everett, Wa: Fluke Corporation.

Fluke Corporation. 2005. Fluke i5s AC Current Clamp Instruction Sheet. Everett, WA: Fluke Corporation.

Fluke Corporation. 2000. Fluke i1000s AC Current Probe for Oscilloscopes Users Manual. Everett, WA: Fluke Corporation.

Furr, J. 2006. Development of Models for Series and Parallel Fan Variable Air Volume Terminal Units. M.S. Thesis, Texas A&M University, College Station, TX.

Furr, J., O'Neal, D.L., Davis, M., Bryant, J., and Cramlet, A. 2008. Performance of VAV parallel fan powered terminal units: experimental results and models. *ASHRAE Transactions*, 114(1): 83-90.

Gosbell, V.J. 2000. Power Quality Centre. Technical Note No. 3. University of Wollongong, NSW Australia.

HASP/ACLD 7101 [Computer Software]. 1971. Tokyo: Japan Building Mechanical Engineers Association.

Hydeman, M., S. Taylor, and J. Stein. 2003. Advanced Variable Air Volume System Design Guide. *Integrated energy systems: productivity and building science.* San Francisco: California Energy Commission.

Inoue, U. and T. Matsumoto. 1979. A study on energy savings with variable air volume systems by simulation and field measurement. *Energy and Buildings* 2:27-36.

Kennedy, Barry W. 2000. *Power quality primer.* New York: McGraw-Hill Professional.

Khoo, I., G.J. Levermore, and K.M. Letherman. 1998. Variable-air-volume terminal units I: steady state models. *Building Services Engineering Research & Technology* 19(3): 155-162.

Kolderup, E., T. Hong, M. Hydeman, S. Taylor, and J. Stein. 2003. Integrated design of large commercial HVAC systems. *Integrated energy systems: productivity and building science.* San Francisco: California Energy Commission.

Lawrence Berkeley National Laboratory (LBNL). 1998. DOE-2, Version 2.2. Lawrence Berkeley National Laboratory, Berkeley, CA.

Microsoft. 1998. *Microsoft Visual Studio 6*. Redmond, WA: Microsoft Corporation.

Microsoft. 2007. *Microsoft Visual Studio 2008*. Redmond, WA: Microsoft Corporation.

Montgomery, D.C., E.A. Peck, and G.G. Vining. 2001. *Introduction to linear regression analysis: third edition*. New York: John Wiley & Sons, Inc.

Sekhar, S.C. 1997. A critical evaluation of variable air volume systems in hot and humid climates. *Energy and Buildings* 26: 223-232.

SPSS. 2008. *SPSS for Windows 17*. Chicago, IL: SPSS, Inc.

TRACE® 600: Load Design and Economics Simulation Program. 1993. La Cross, WI: The Trane Company, American Standard Company.

Wendes, H. 1994. *Variable air volume manual*. Lilburn, GA: The Fairmont Press, Inc.

APPENDIX A

SERIES TERMINAL UNITS RESULTS

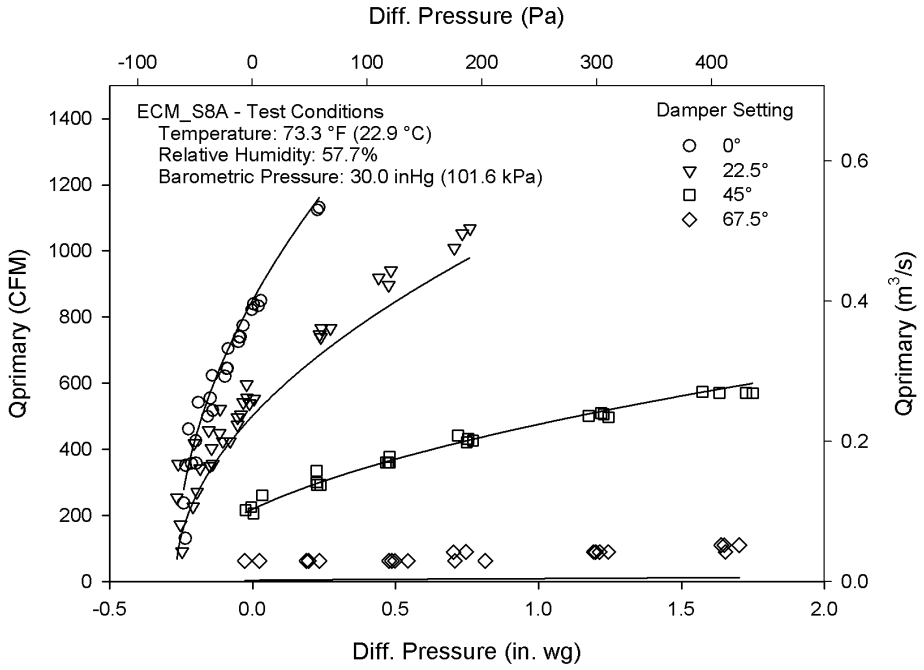

Figure A-1: $Q_{primary}$ vs. DP for ECM_S8A

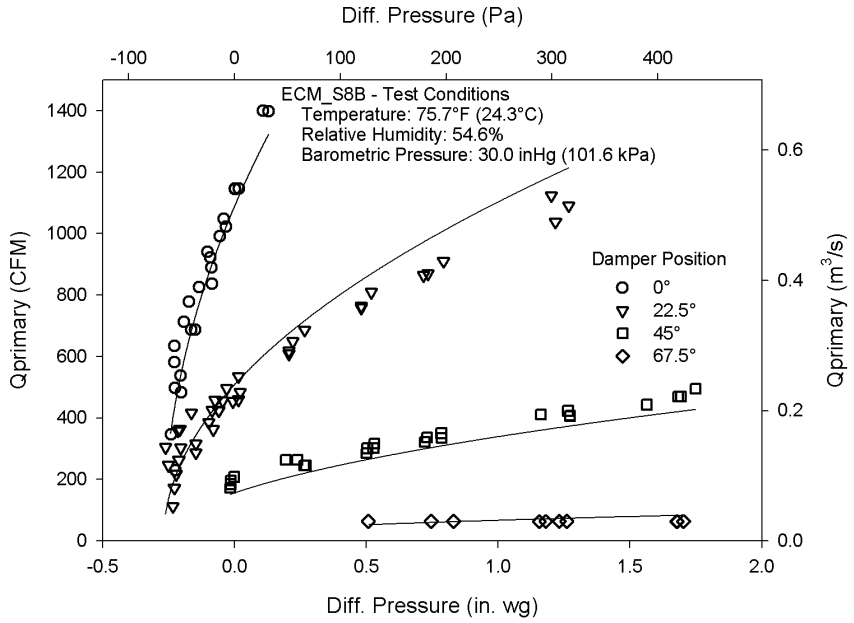

Figure A-2: $Q_{primary}$ vs. DP for ECM_S8B

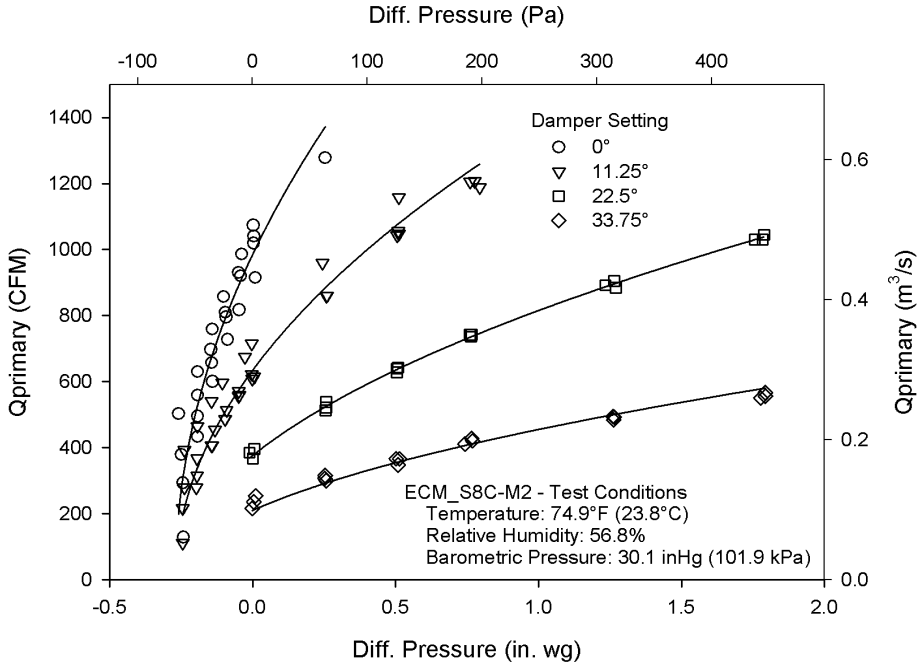

Figure A-3: $Q_{primary}$ vs. DP for ECM_S8C-M2

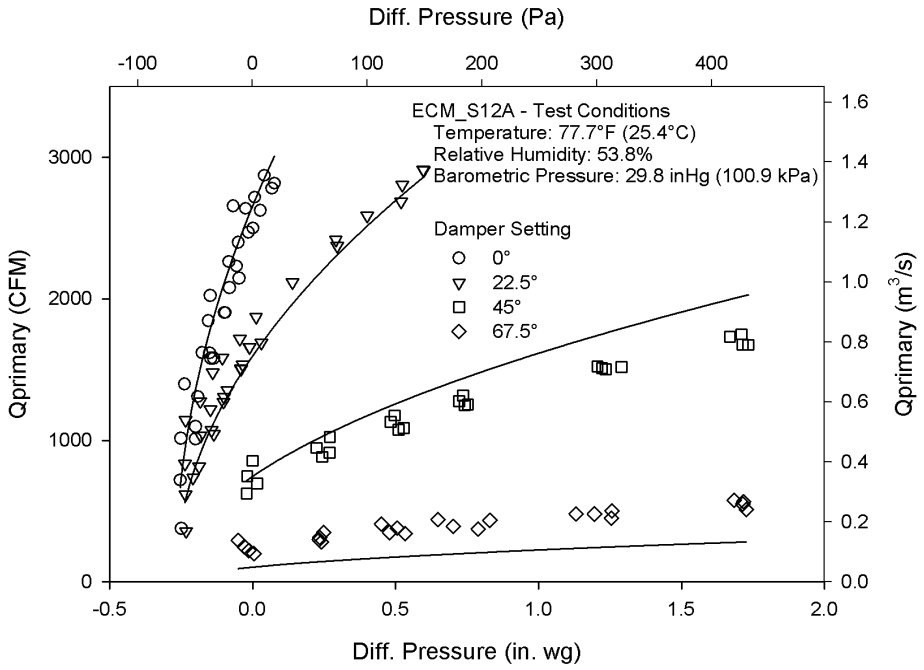

Figure A-4: $Q_{primary}$ vs. DP for ECM_S12A

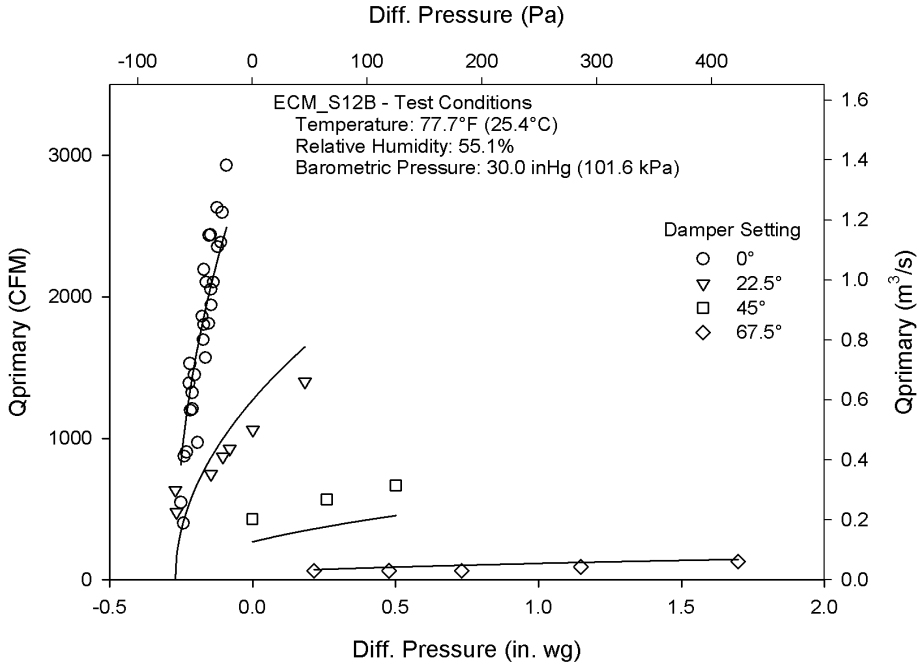

Figure A-5: $Q_{primary}$ vs. DP for ECM_S12B

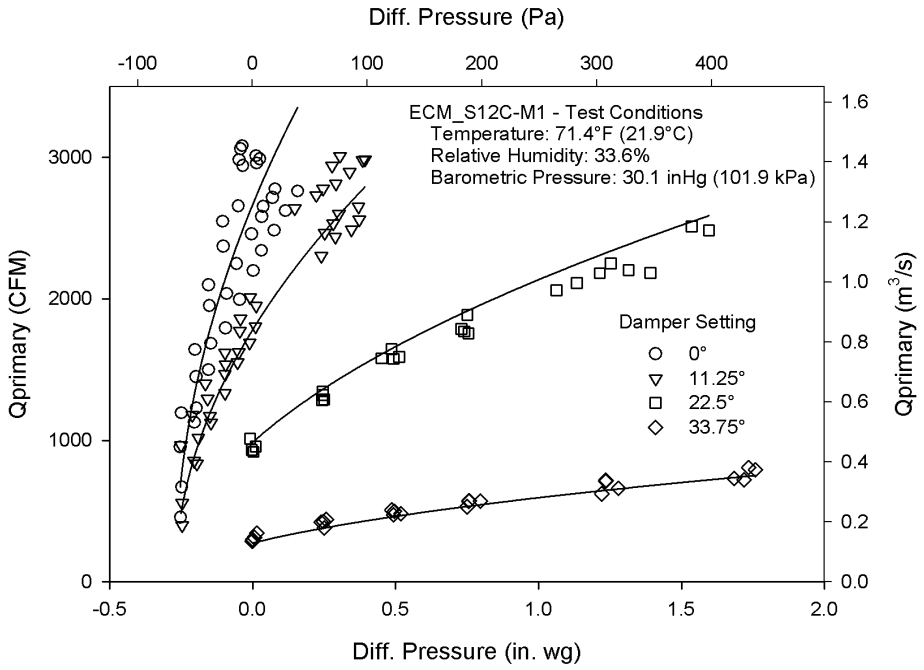

Figure A-6: $Q_{primary}$ vs. DP for ECM_S12C-M1

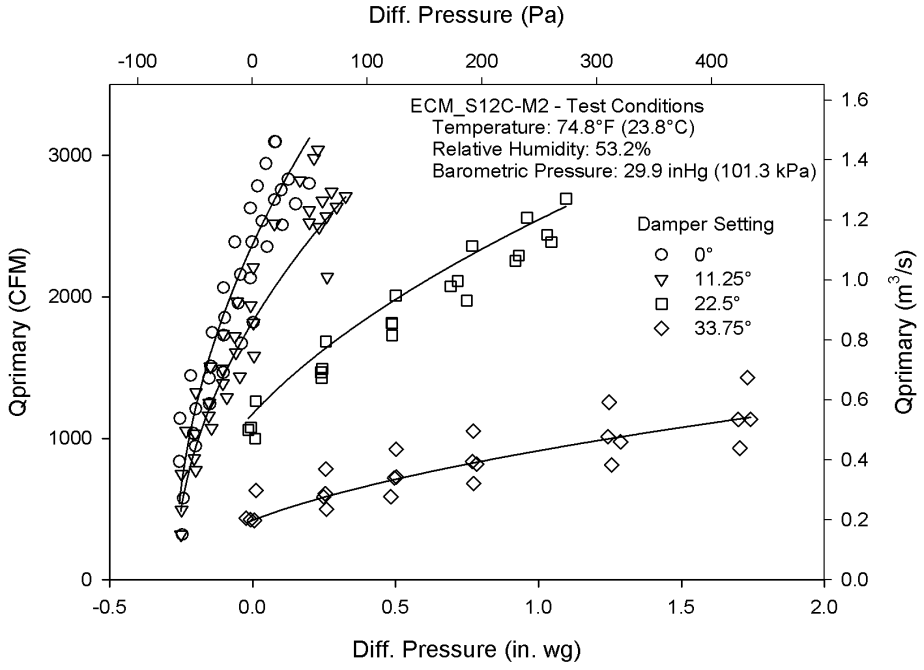

Figure A-7: $Q_{primary}$ vs. DP for ECM_S12C-M2

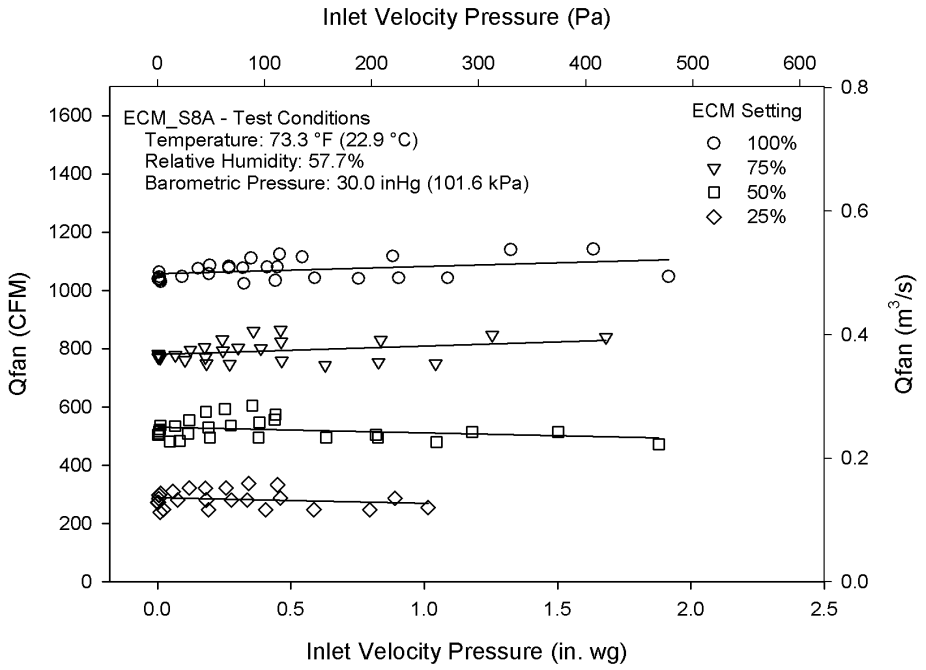

Figure A-8: Q_{fan} vs. P_{iav} for ECM_S8A

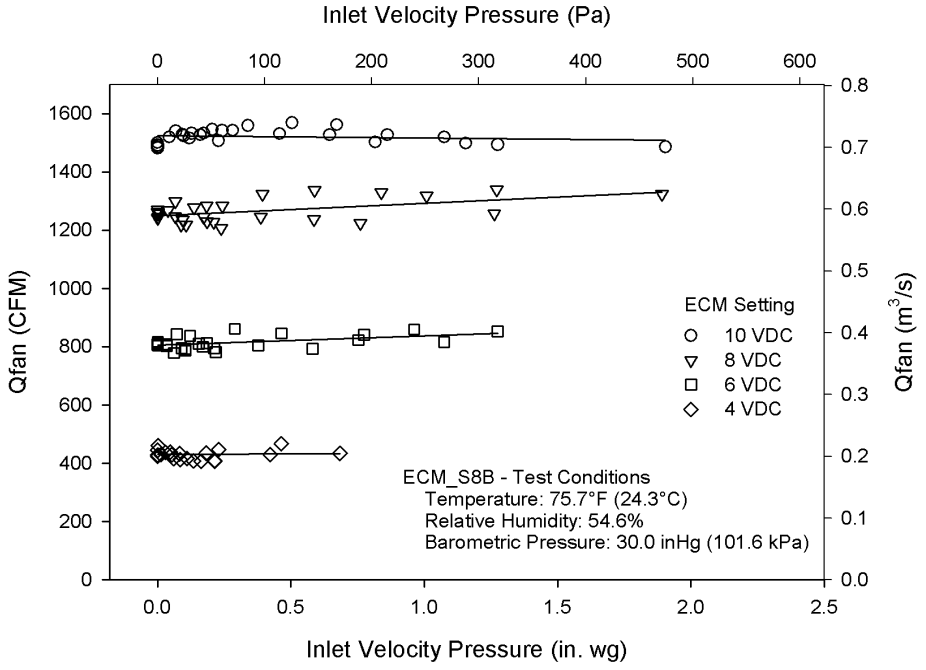

Figure A-9: Q_{fan} vs. P_{iav} for ECM_S8B

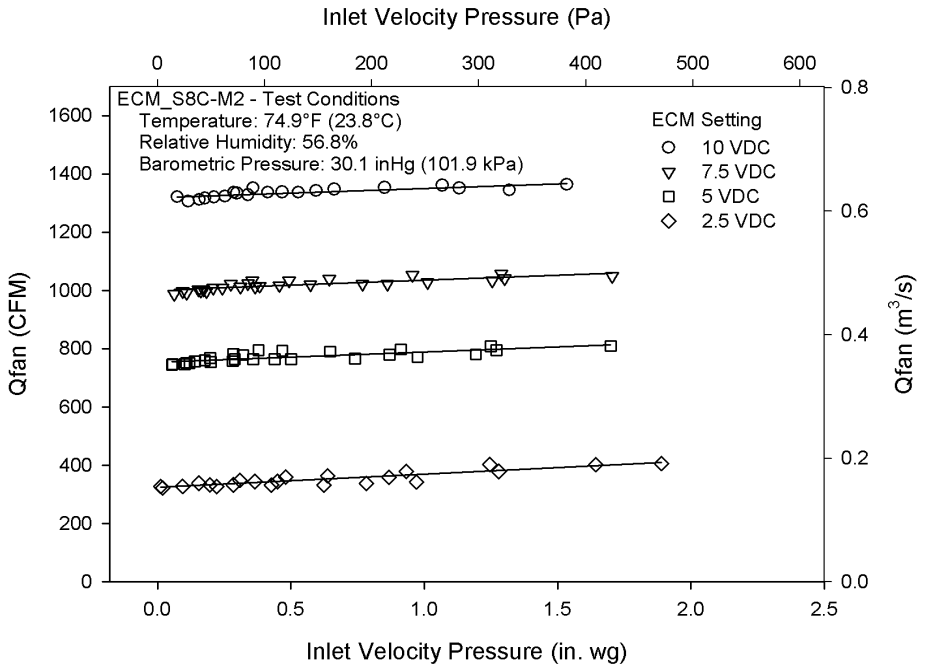

Figure A-10: Q_{fan} vs. P_{iav} for ECM_S8C-M2

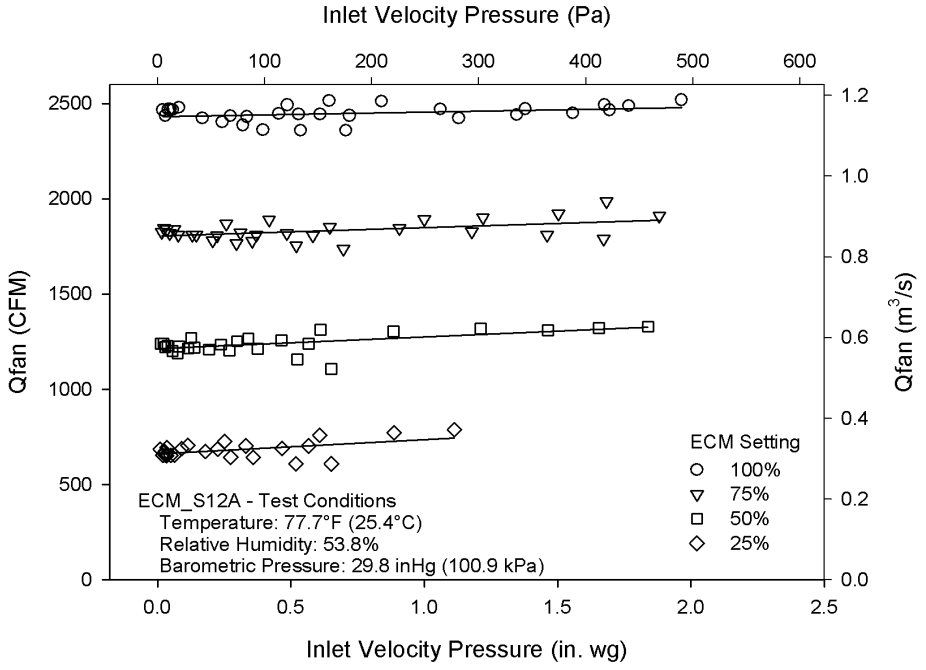

Figure A-11: Q_{fan} vs. P_{iav} for ECM_S12A

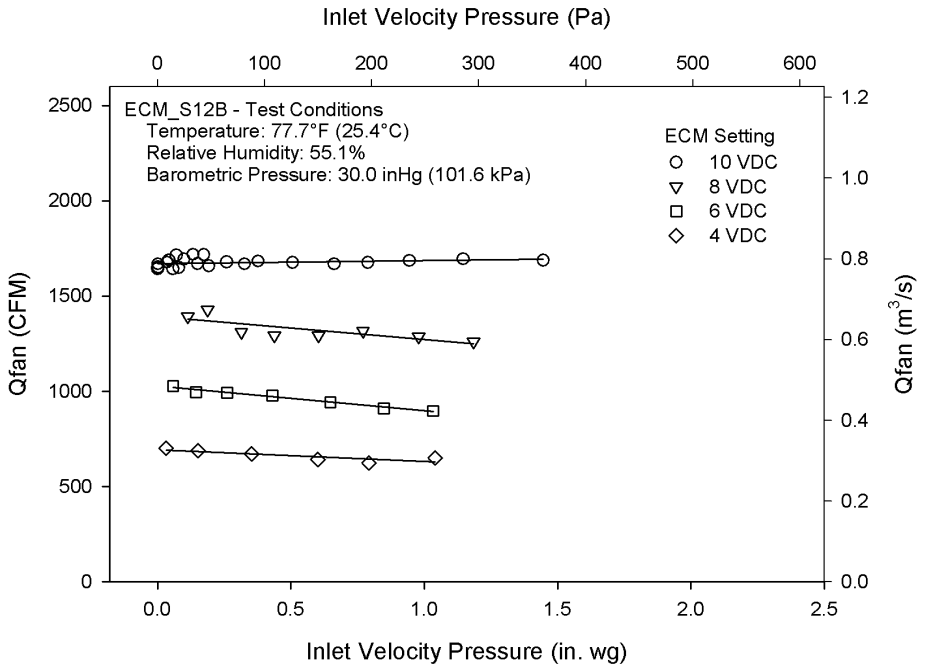

Figure A-12: Q_{fan} vs. P_{iav} for ECM_S12B

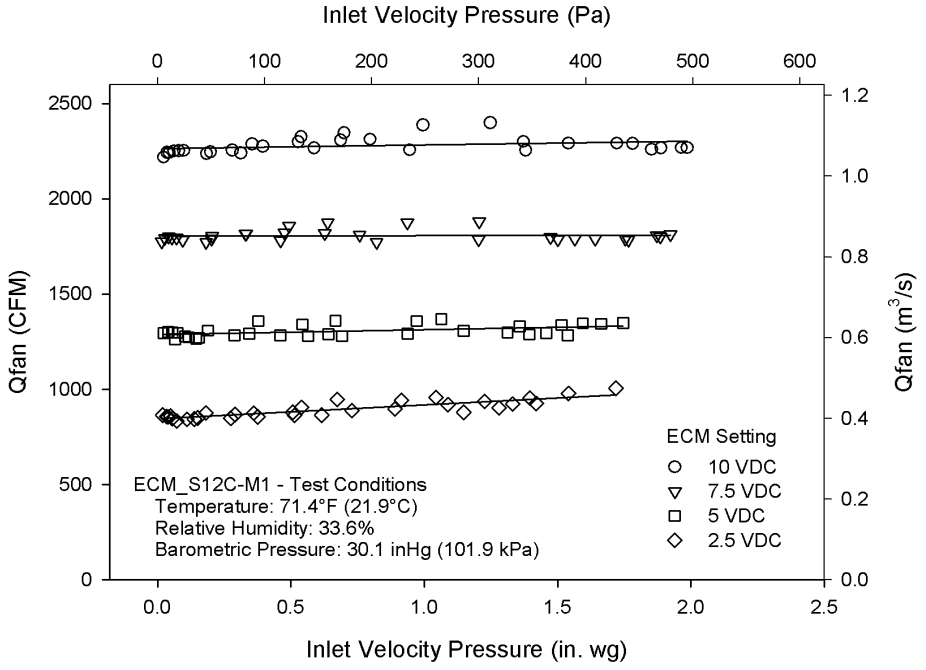

Figure A-13: Q_{fan} vs. P_{iav} for ECM_S12C-M1

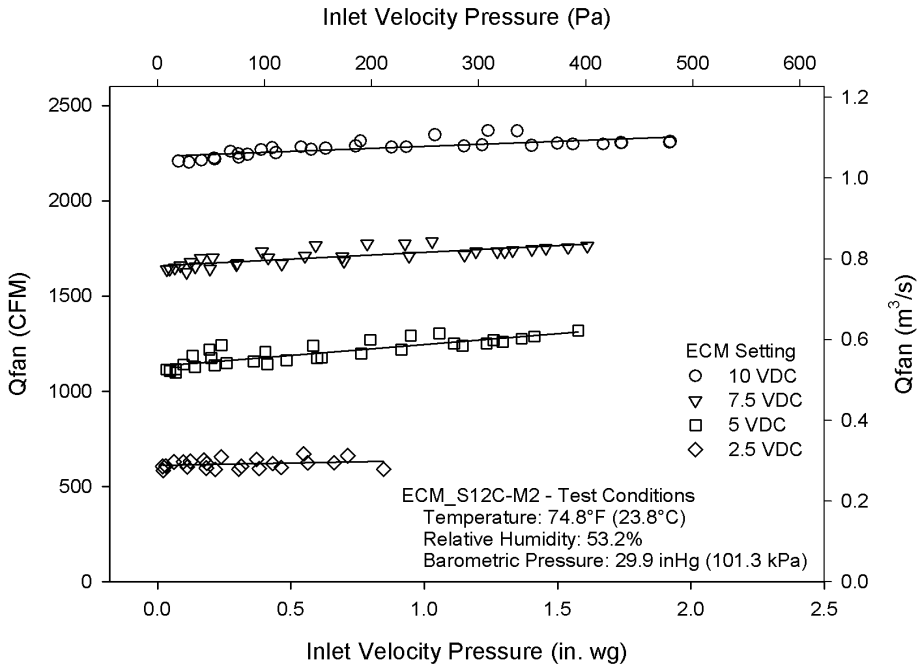

Figure A-14: Q_{fan} vs. P_{iav} for ECM_S12C-M2

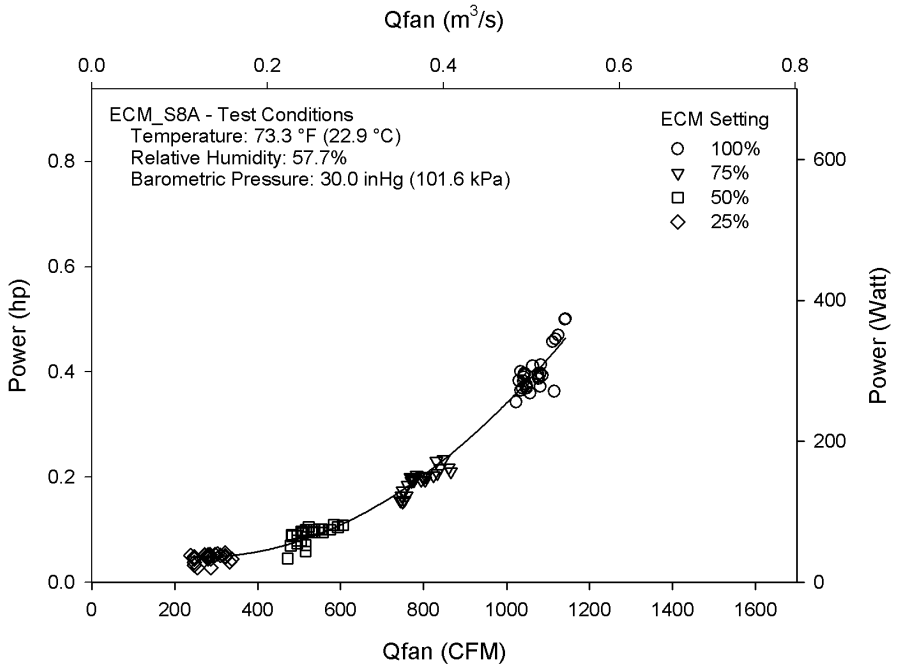

Figure A-15: Power vs. Q_{fan} for ECM_S8A

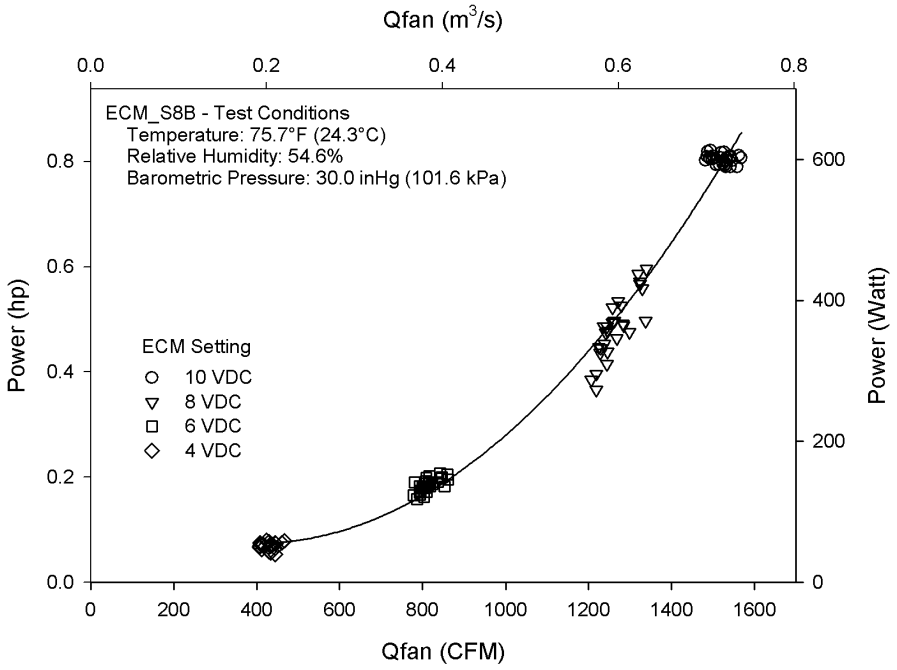

Figure A-16: Power vs. Q_{fan} for ECM_S8B

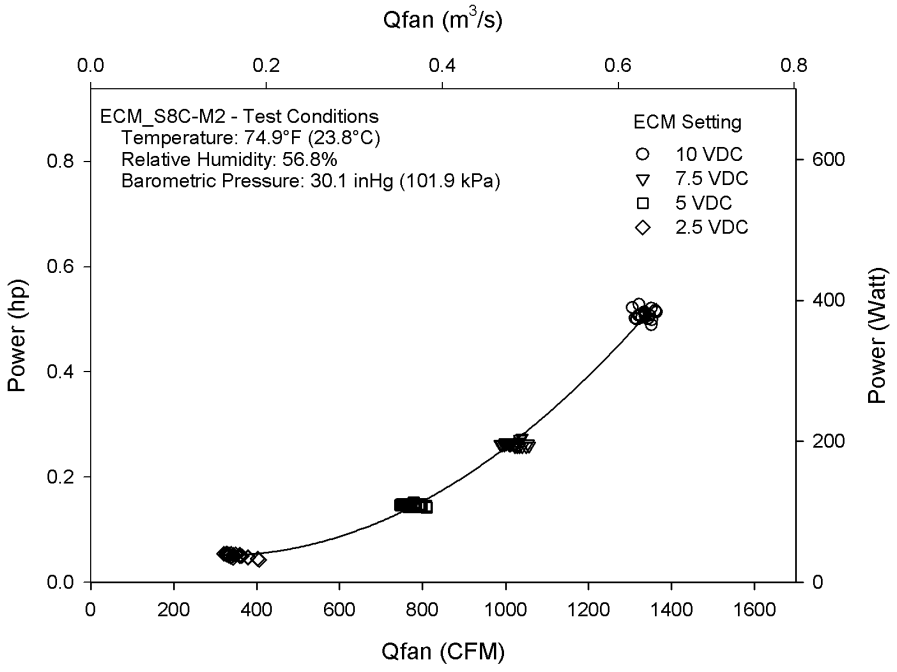

Figure A-17: Power vs. Q_{fan} for ECM_S8C-M2

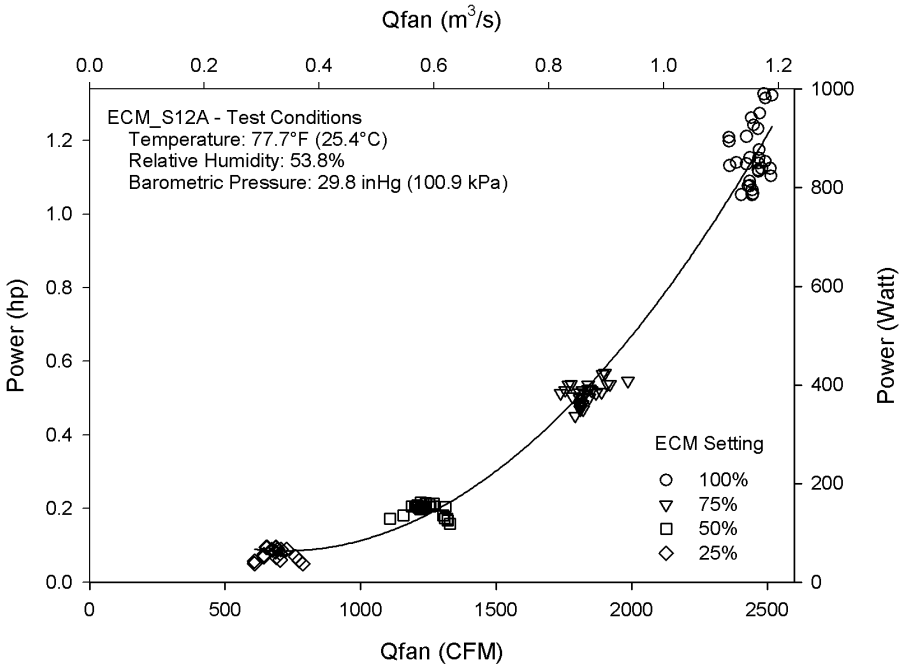

Figure A-18: Power vs. Q_{fan} for ECM_S12A

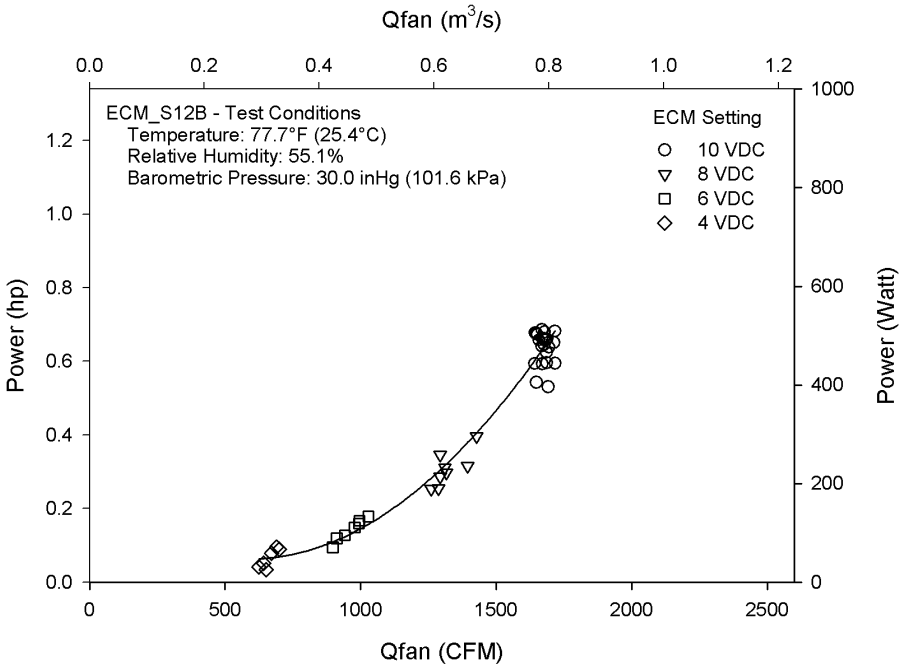

Figure A-19: Power vs. Q_{fan} for ECM_S12B

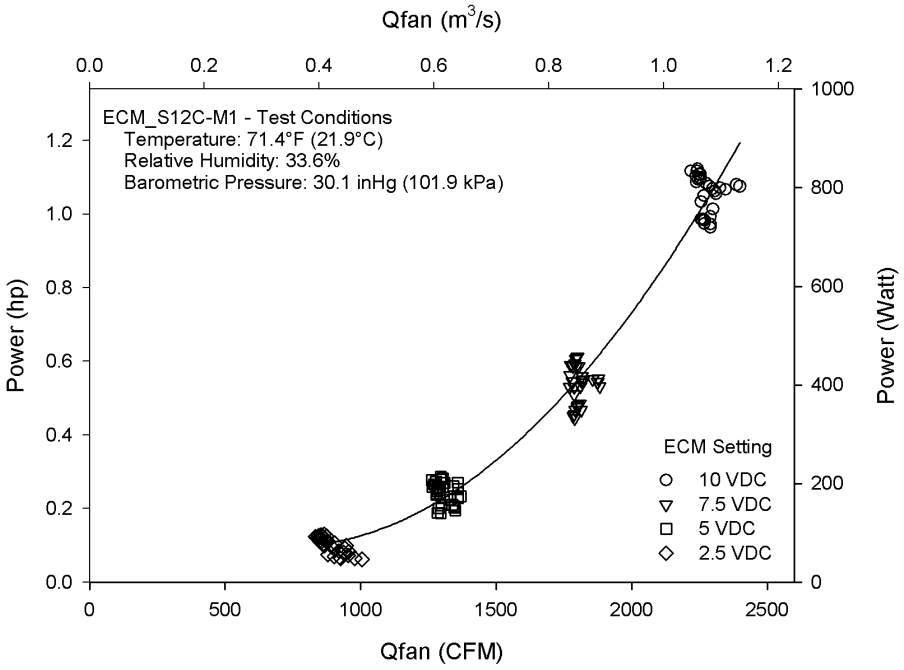

Figure A-20: Power vs. Q_{fan} for ECM_S12C-M1

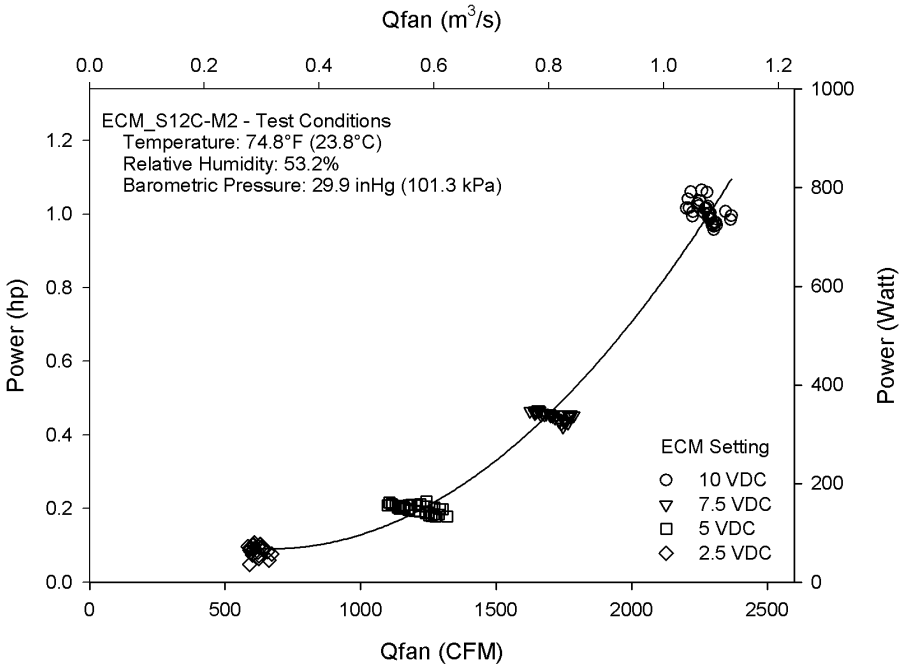

Figure A-21: Power vs. Q_{fan} for ECM_S12C-M2

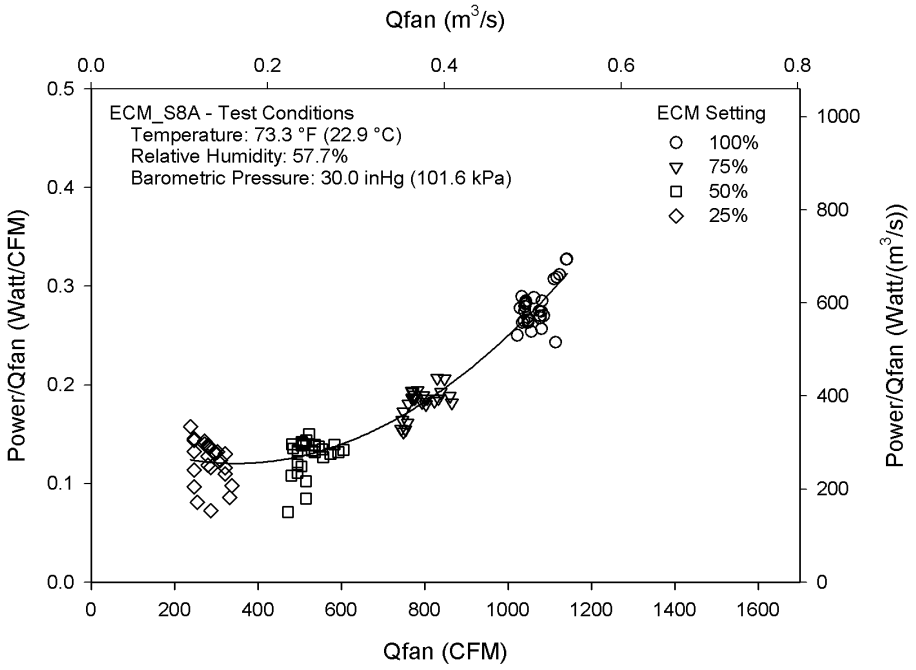

Figure A-22: Watt/CFM vs. Q_{fan} for ECM_S8A

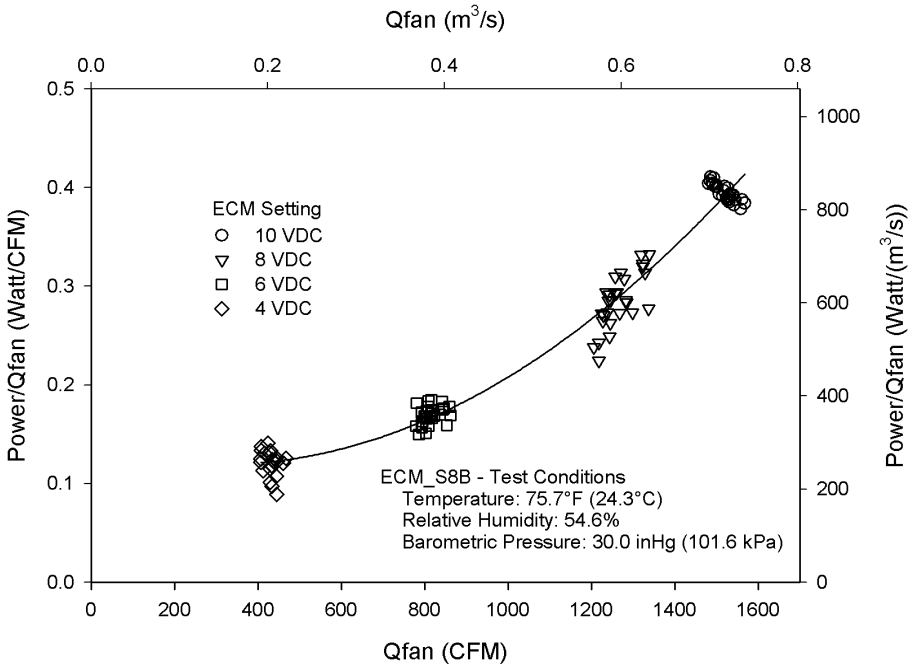

Figure A-23: Watt/CFM vs. Q_{fan} for ECM_S8B

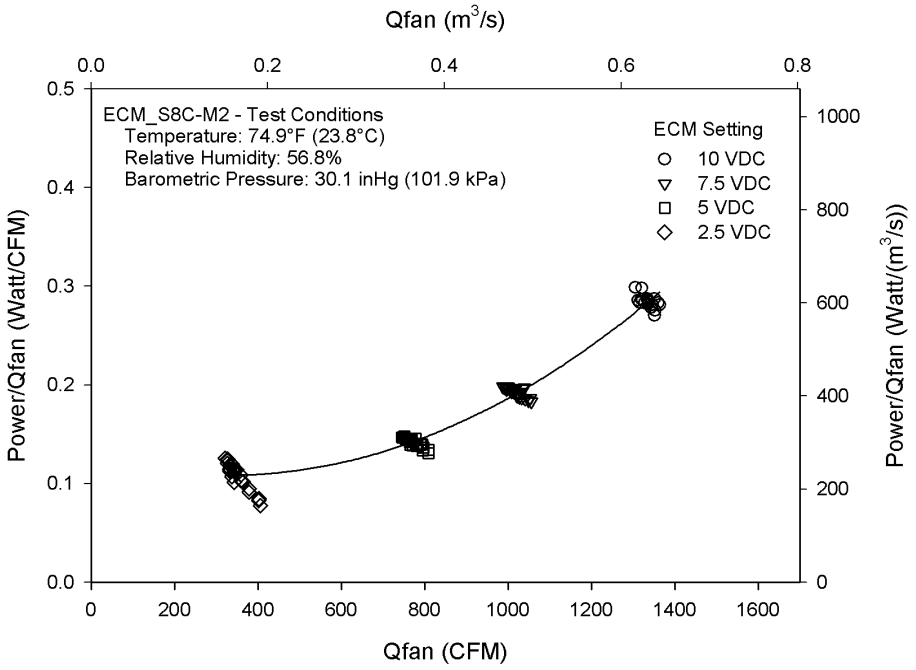

Figure A-24: Watt/CFM vs. Q_{fan} for ECM_S8C-M2

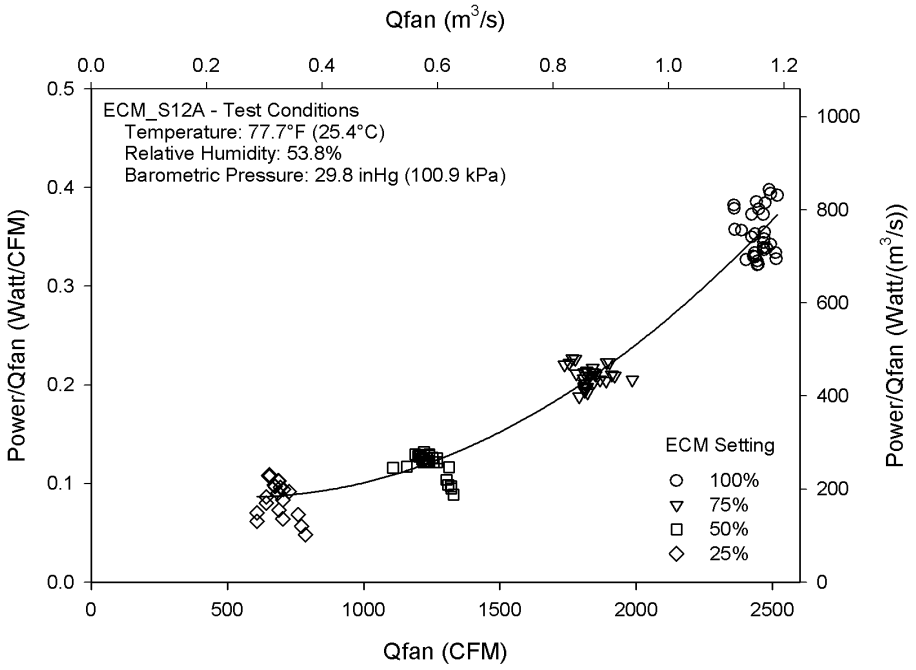

Figure A-25: Watt/CFM vs. Q_{fan} for ECM_S12A

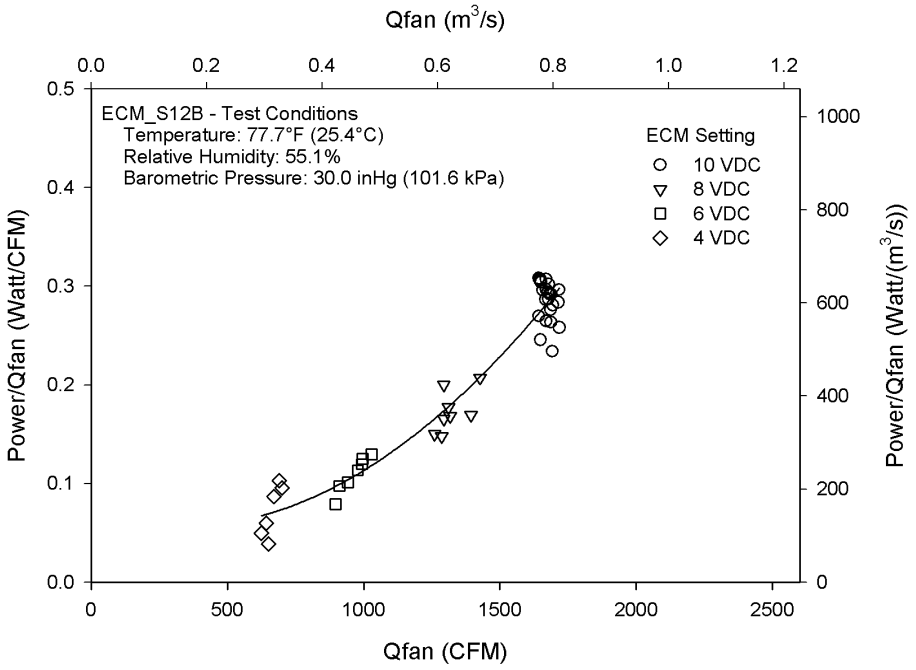

Figure A-26: Watt/CFM vs. Q_{fan} for ECM_S12B

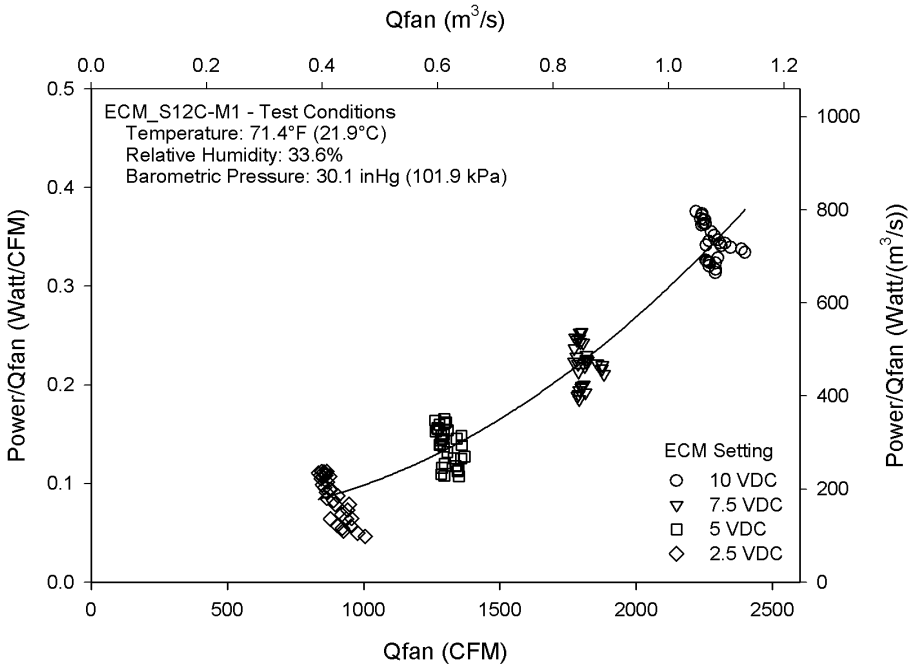

Figure A-27: Watt/CFM vs. Q_{fan} for ECM_S12C-M1

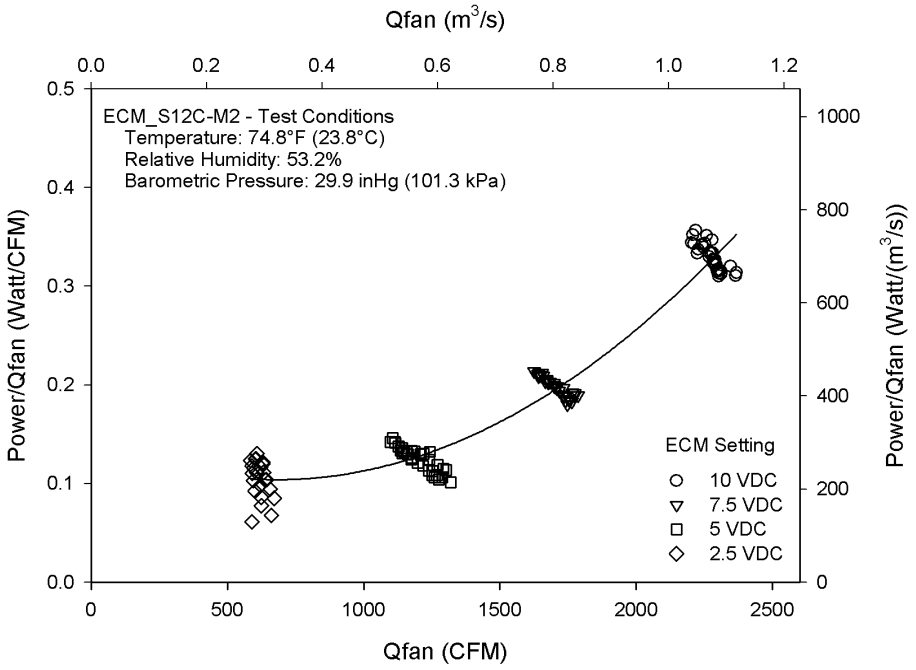

Figure A-28: Watt/CFM vs. Q_{fan} for ECM_S12C-M2

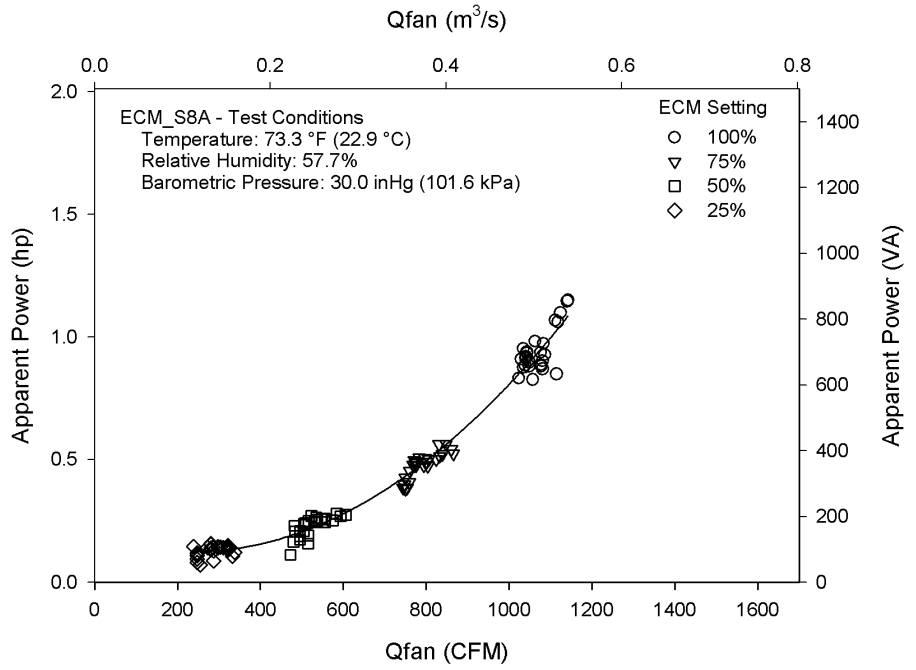

Figure A-29: Apparent Power vs. Q_{fan} for ECM_S8A

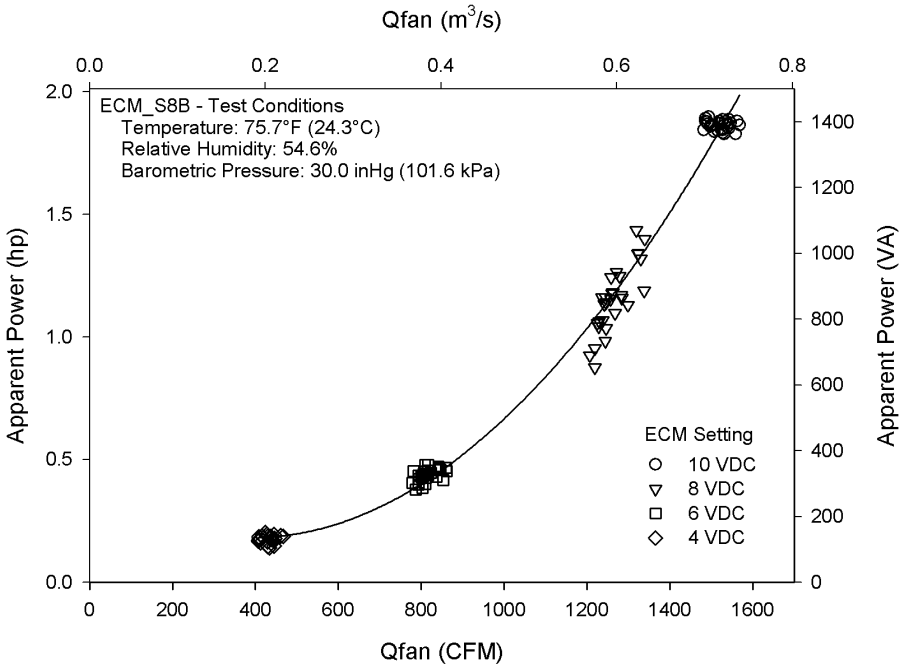

Figure A-30: Apparent Power vs. Q_{fan} for ECM_S8B

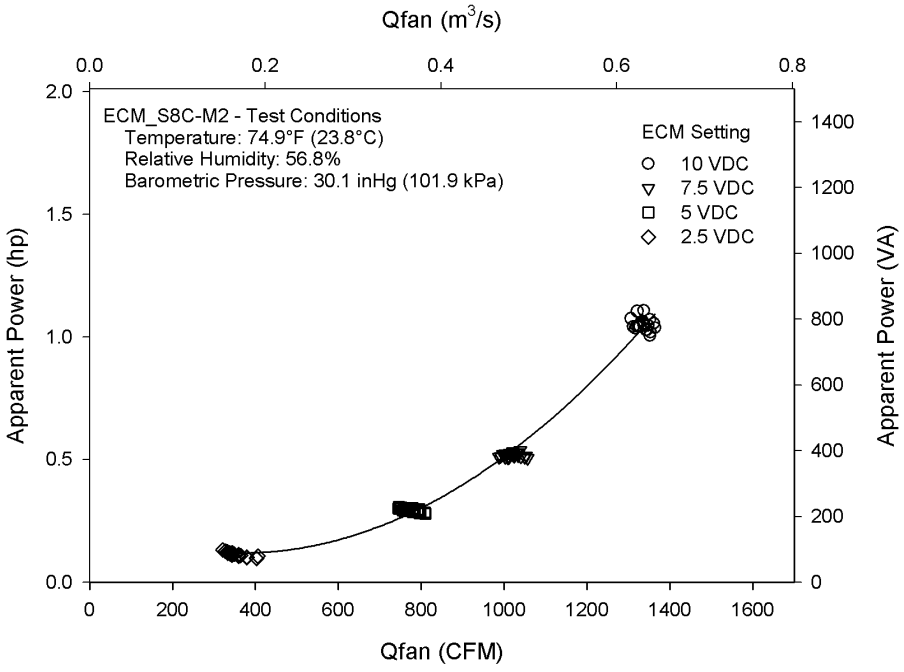

Figure A-31: Apparent Power vs. Q_{fan} for ECM_S8C-M2

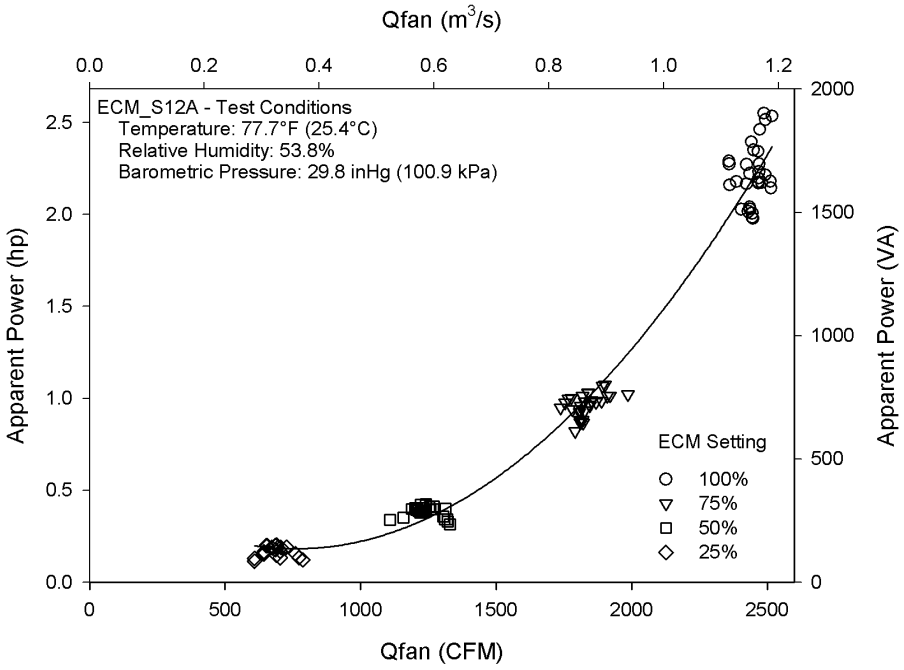

Figure A-32: Apparent Power vs. Q_{fan} for ECM_S12A

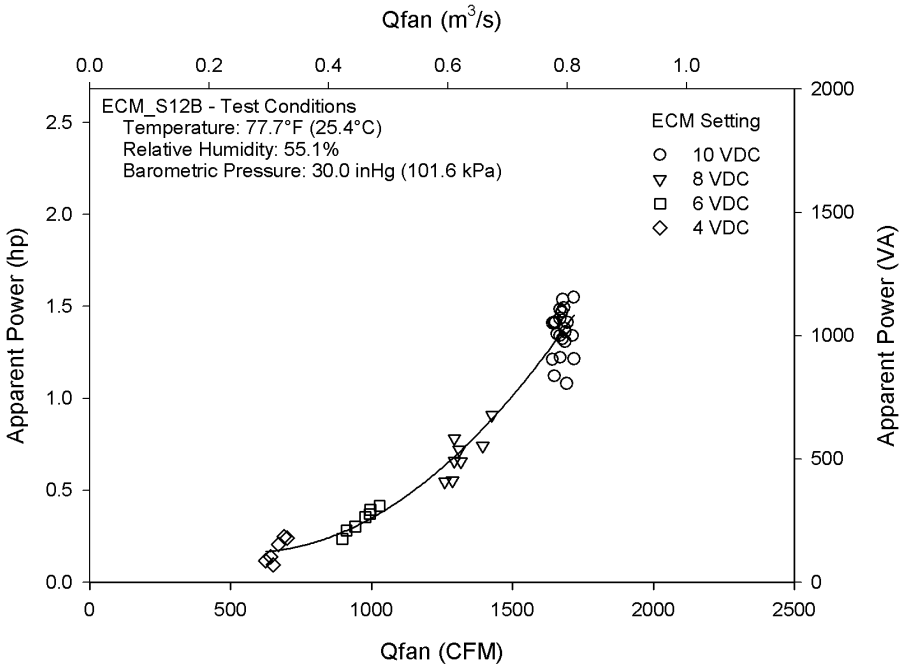

Figure A-33: Apparent Power vs. Q_{fan} for ECM_S12B

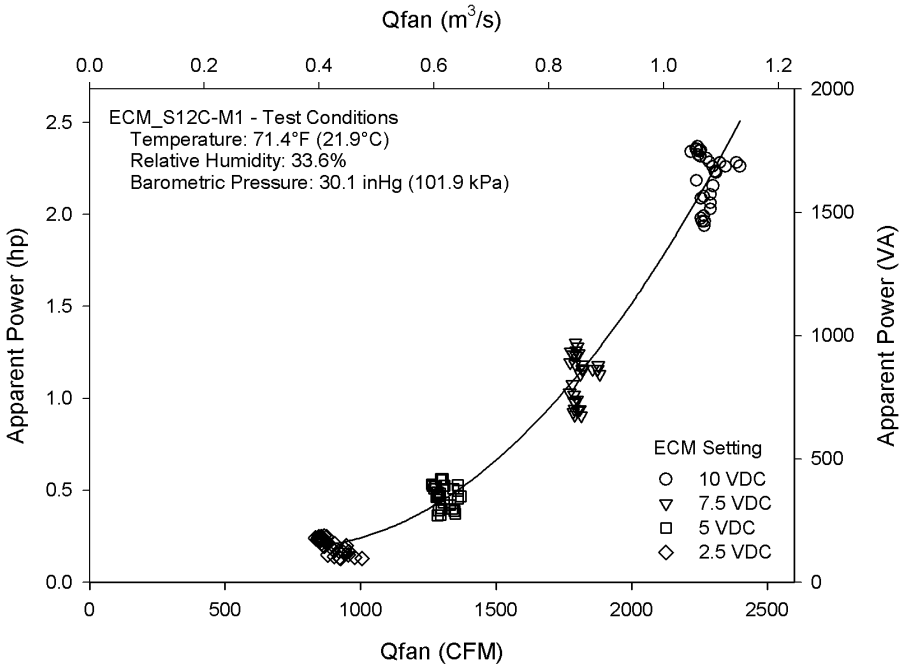

Figure A-34: Apparent Power vs. Q_{fan} for ECM_S12C-M1

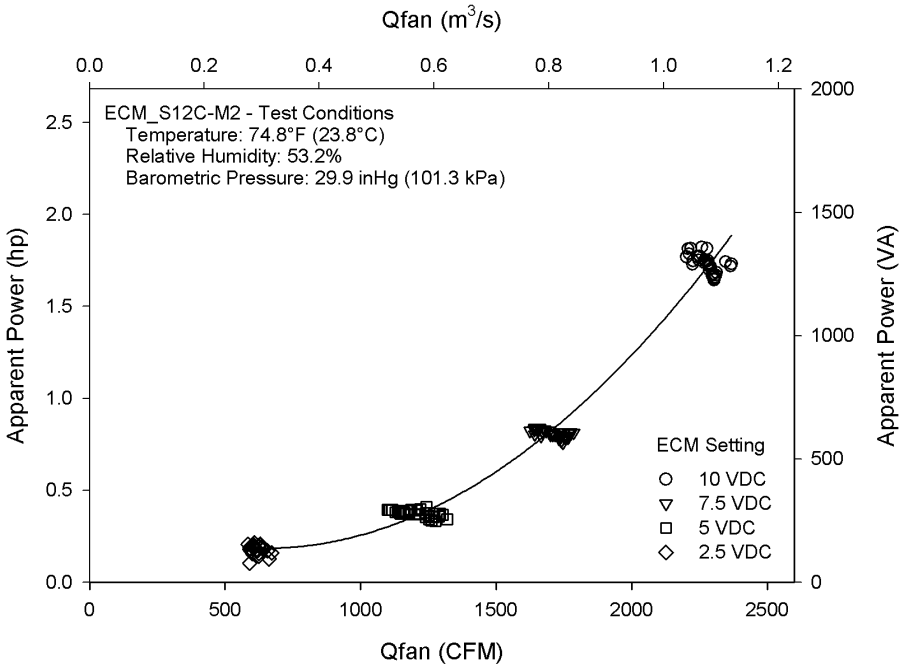

Figure A-35: Apparent Power vs. Q_{fan} for ECM_S12C-M2

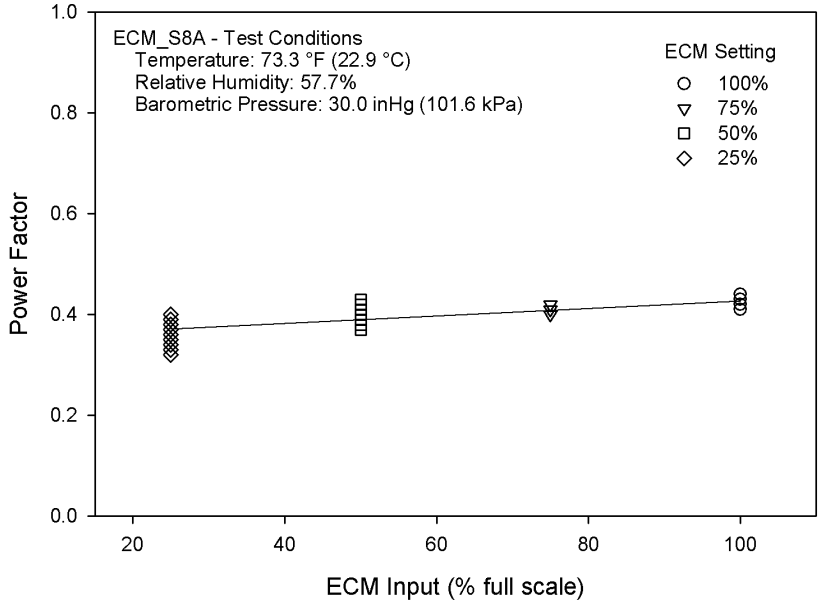

Figure A-36: Power Factor vs. ECM Input Setting for ECM_S8A

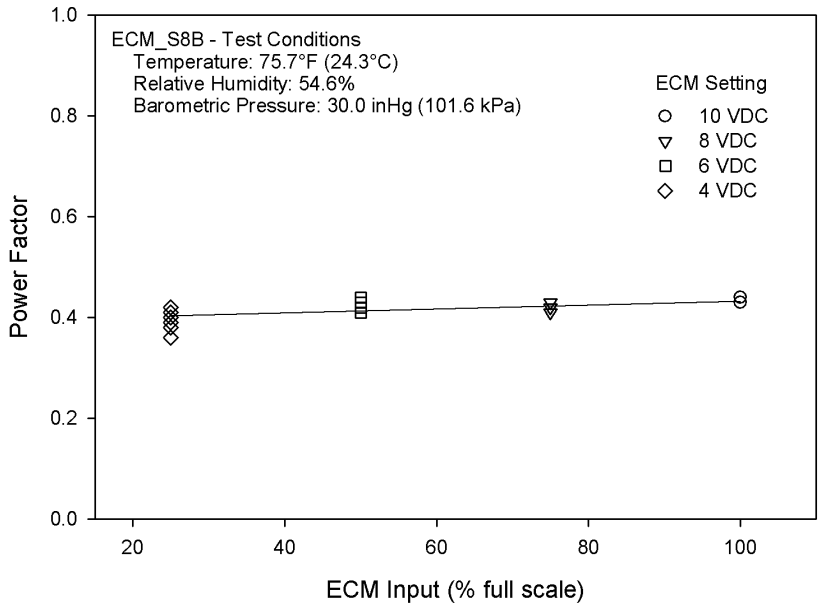

Figure A-37: Power Factor vs. ECM Input Setting for ECM_S8B

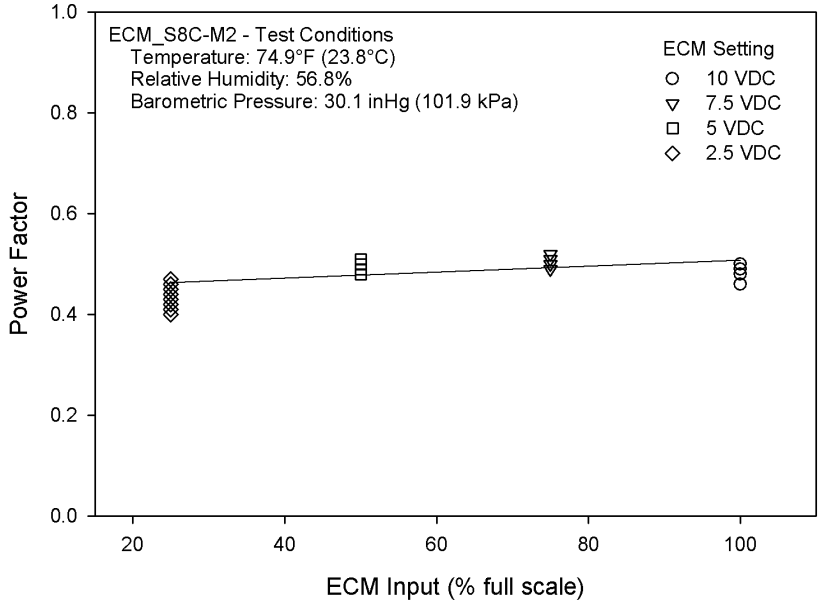

Figure A-38: Power Factor vs. ECM Input Setting for ECM_S8C-M2

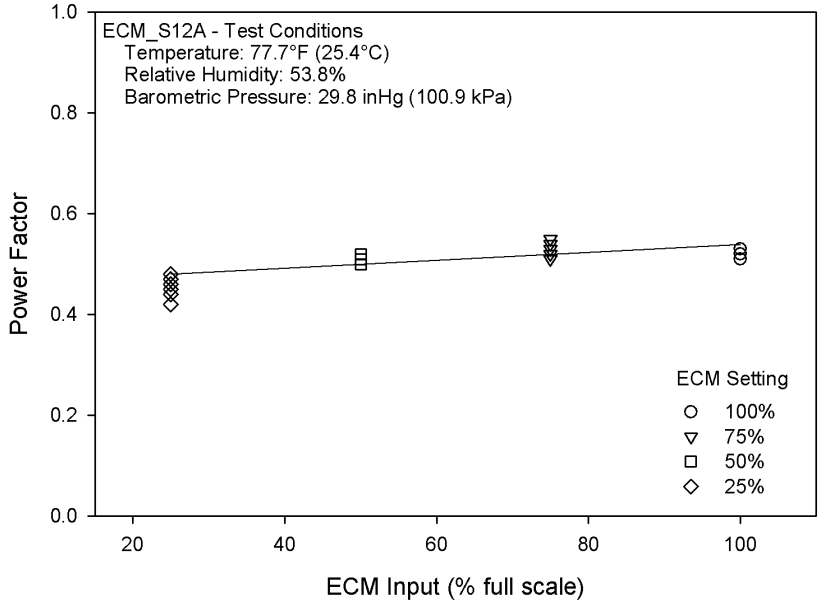

Figure A-39: Power Factor vs. ECM Input Setting for ECM_S12A

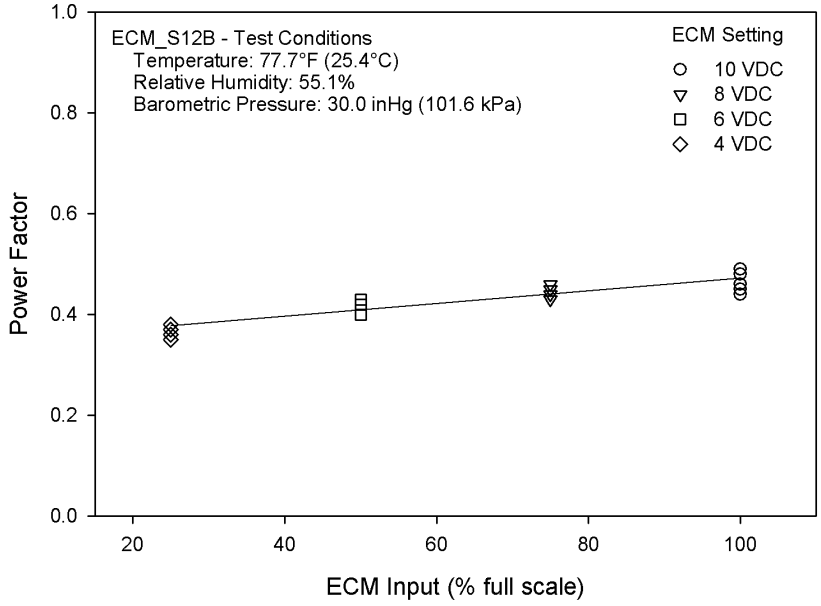

Figure A-40: Power Factor vs. ECM Input Setting for ECM_S12B

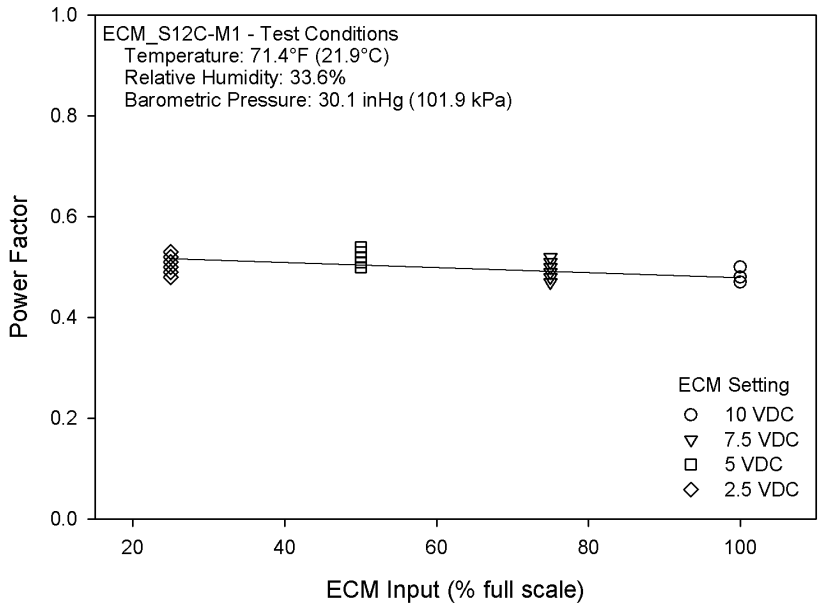

Figure A-41: Power Factor vs. ECM Input Setting for ECM_S12C-M1

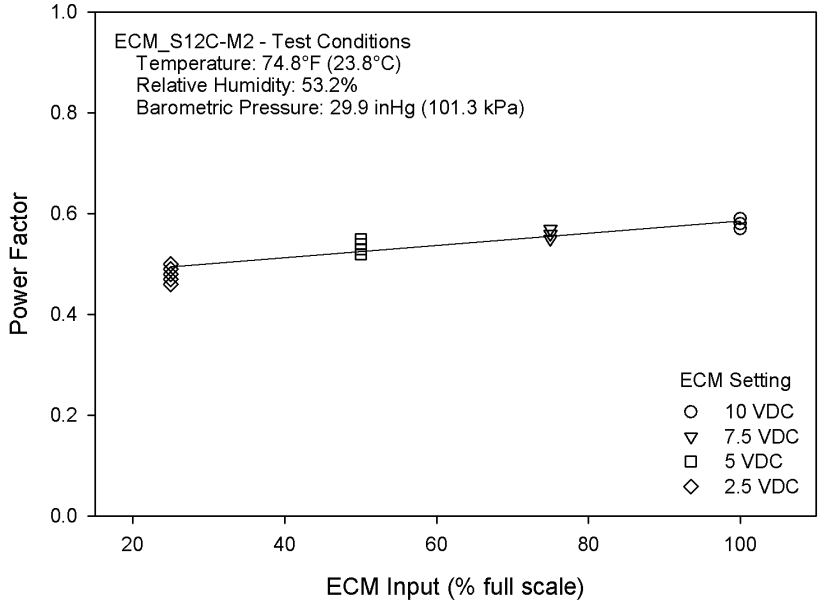

Figure A-42: Power Factor vs. ECM Input Setting for ECM_S12C-M2

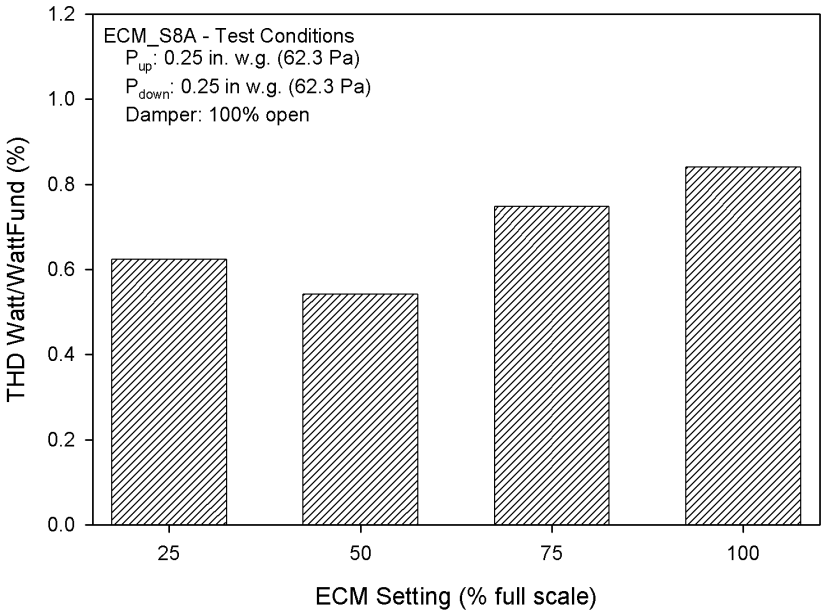

Figure A-43: Real Power THD (%) vs. ECM Input Setting for ECM_S8A

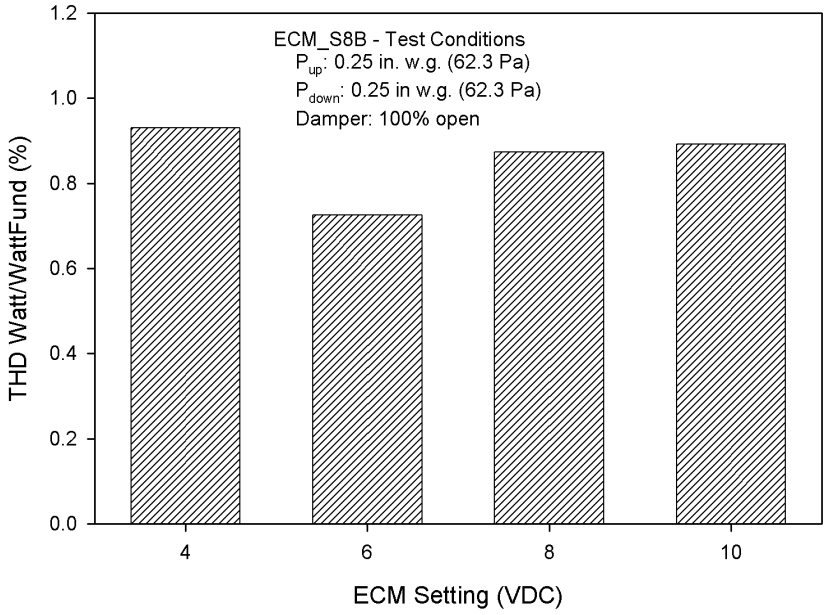

Figure A-44: Real Power THD (%) vs. ECM Input Setting for ECM_S8B

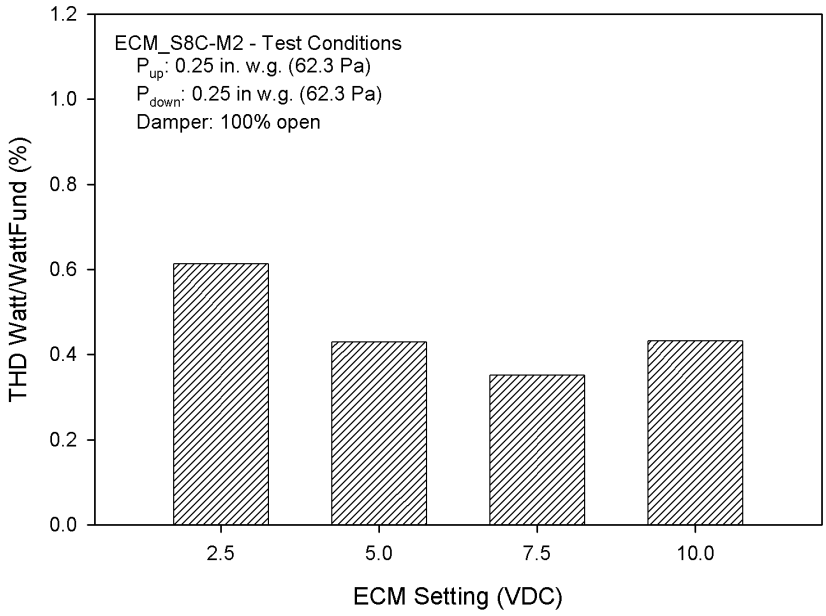

Figure A-45: Real Power THD (%) vs. ECM Input Setting for ECM_S8C-M2

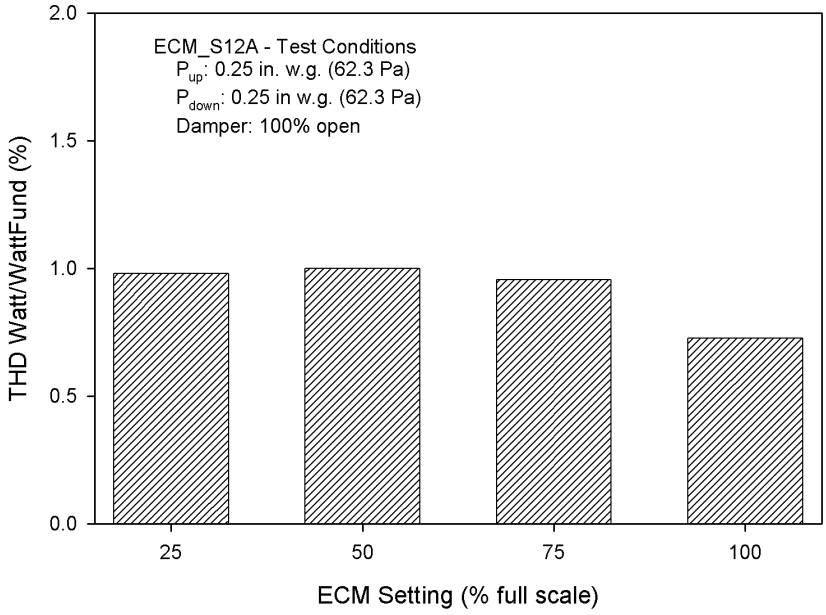

Figure A-46: Real Power THD (%) vs. ECM Input Setting for ECM_S12A

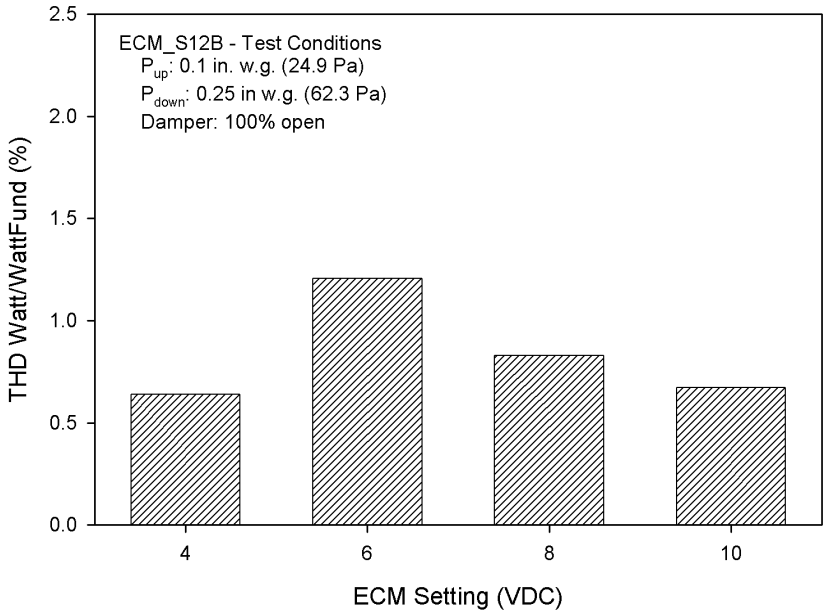

Figure A-47: Real Power THD (%) vs. ECM Input Setting for ECM_S12B

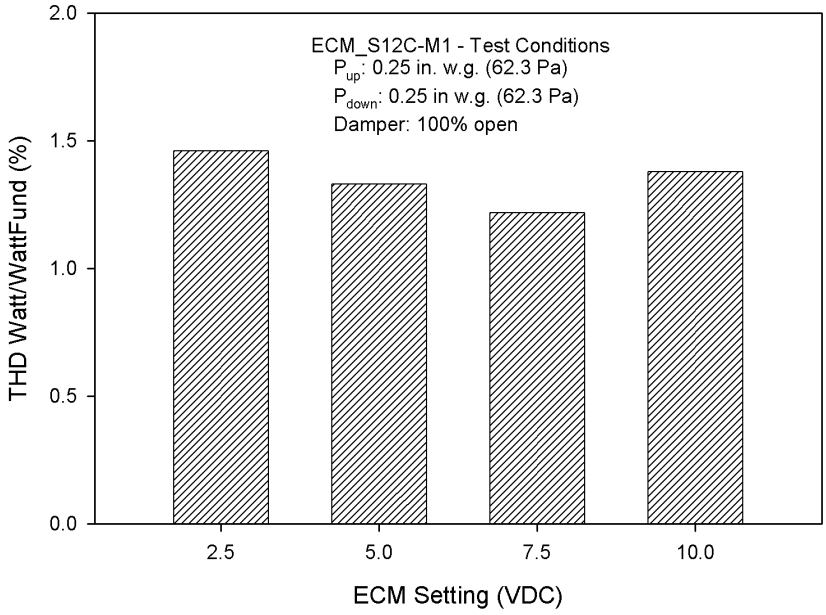

Figure A-48: Real Power THD (%) vs. ECM Input Setting for ECM_S12C-M1

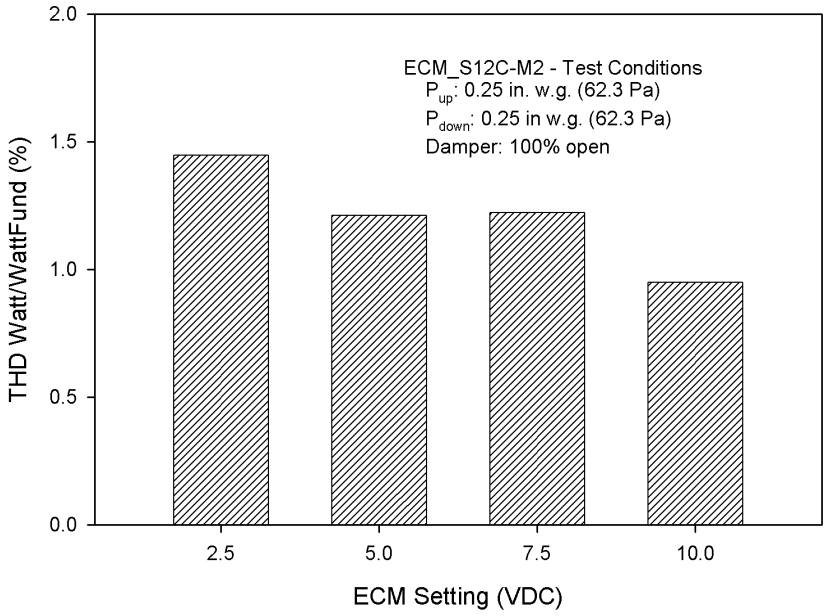

Figure A-49: Real Power THD (%) vs. ECM Input Setting for ECM_S12C-M2

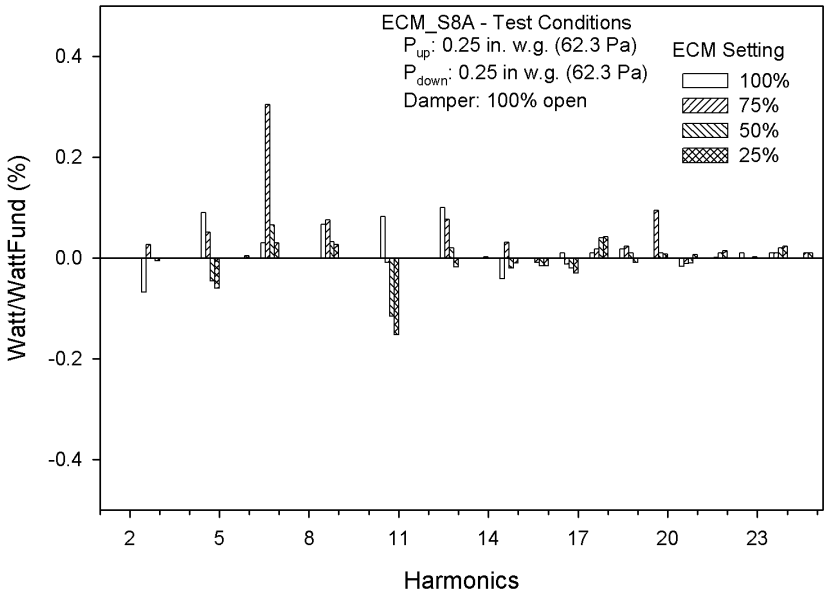

Figure A-50: Real Power Harmonics (%) for ECM_S8A

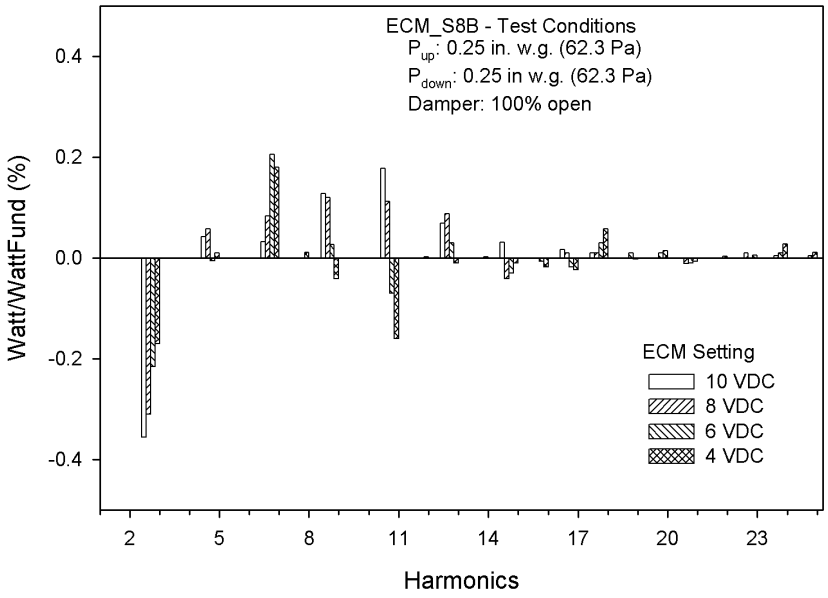

Figure A-51: Real Power Harmonics (%) for ECM_S8B

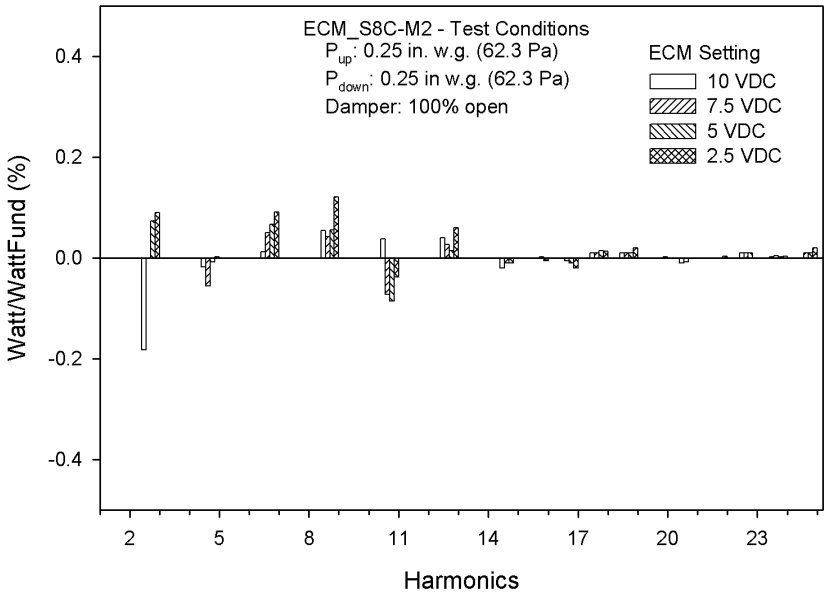

Figure A-52: Real Power Harmonics (%) for ECM_S8C-M2

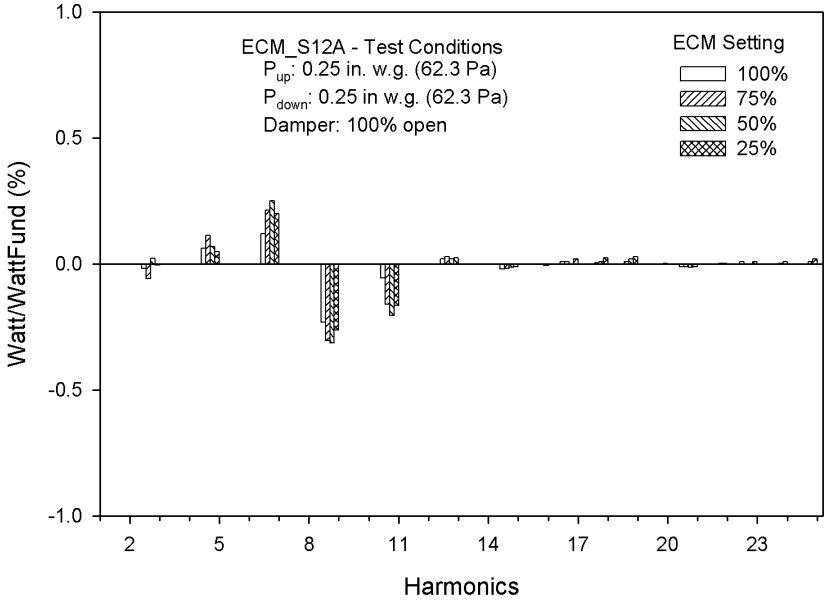

Figure A-53: Real Power Harmonics (%) for ECM_S12A

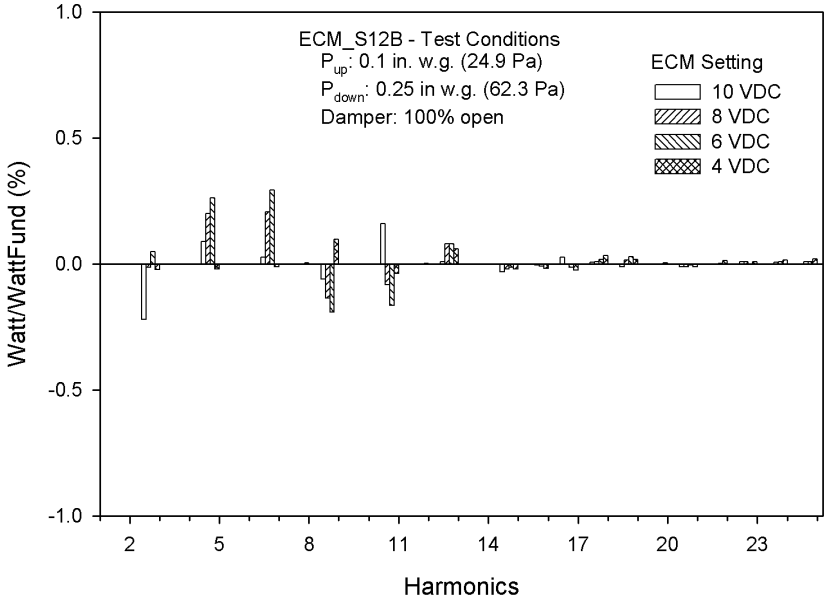

Figure A-54: Real Power Harmonics (%) for ECM_S12B

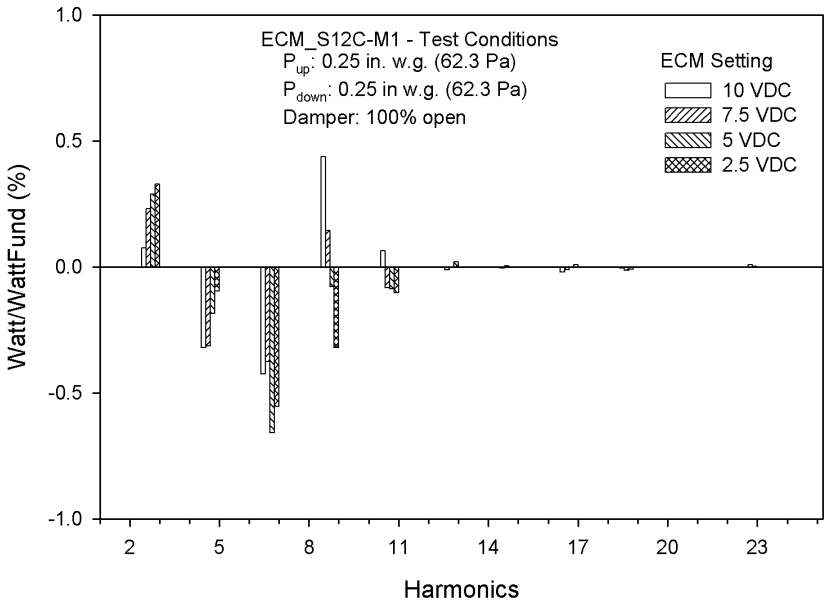

Figure A-55: Real Power Harmonics (%) for ECM_S12C-M1

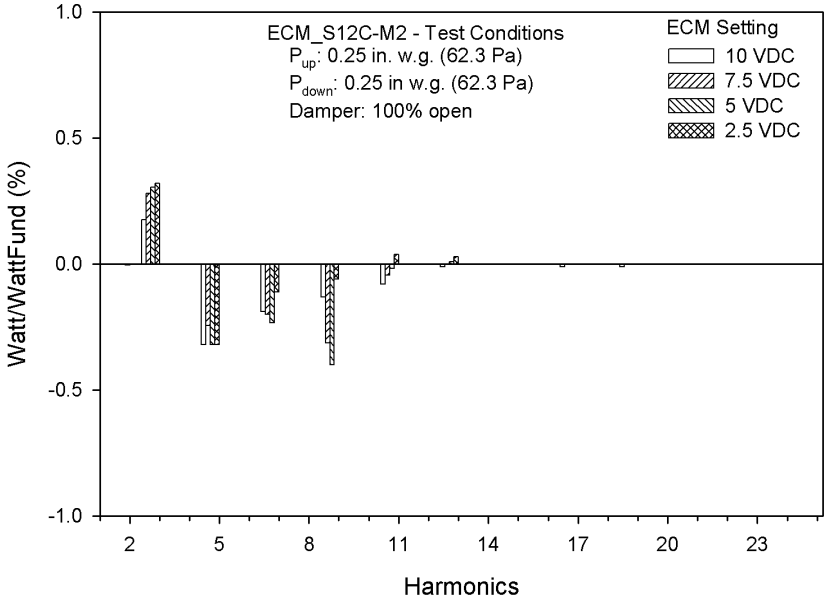

Figure A-56: Real Power Harmonics (%) for ECM_S12C-M2

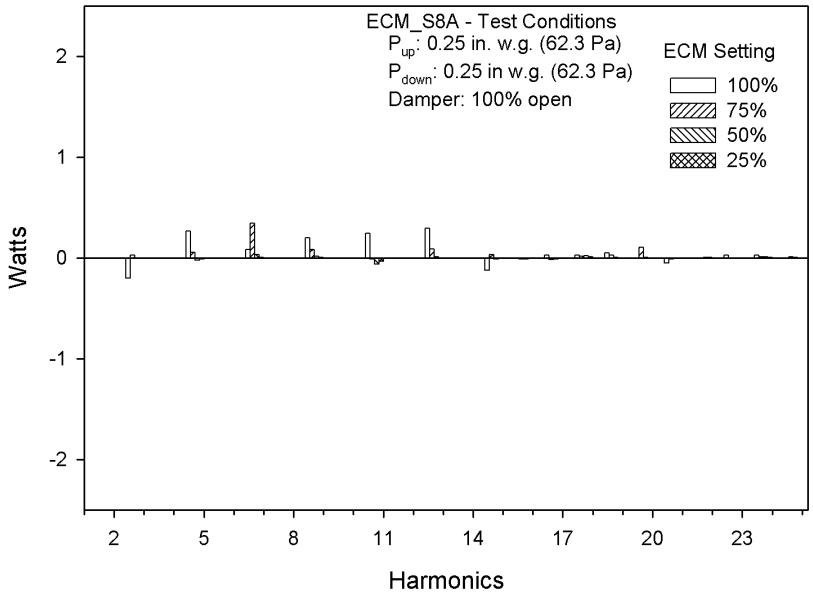

Figure A-57: Real Power Harmonics (Watts) for ECM_S8A

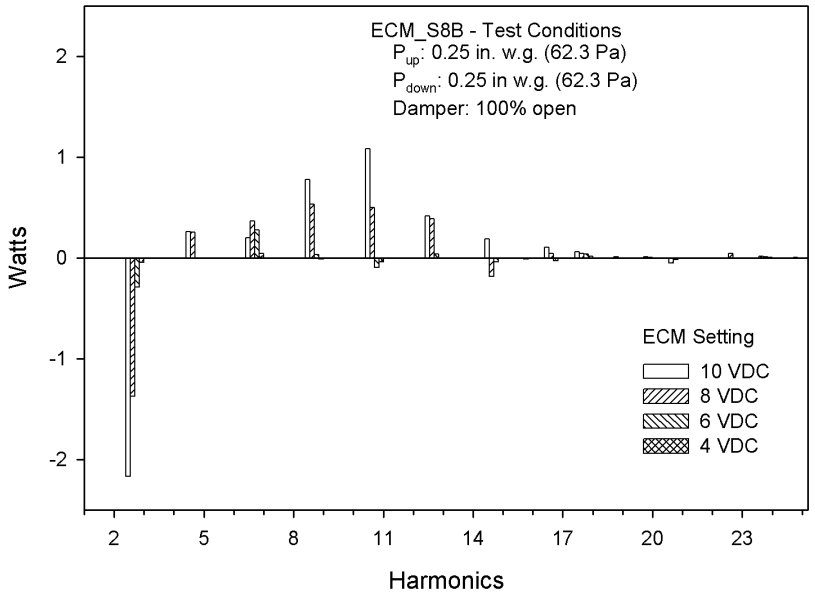

Figure A-58: Real Power Harmonics (Watts) for ECM_S8B

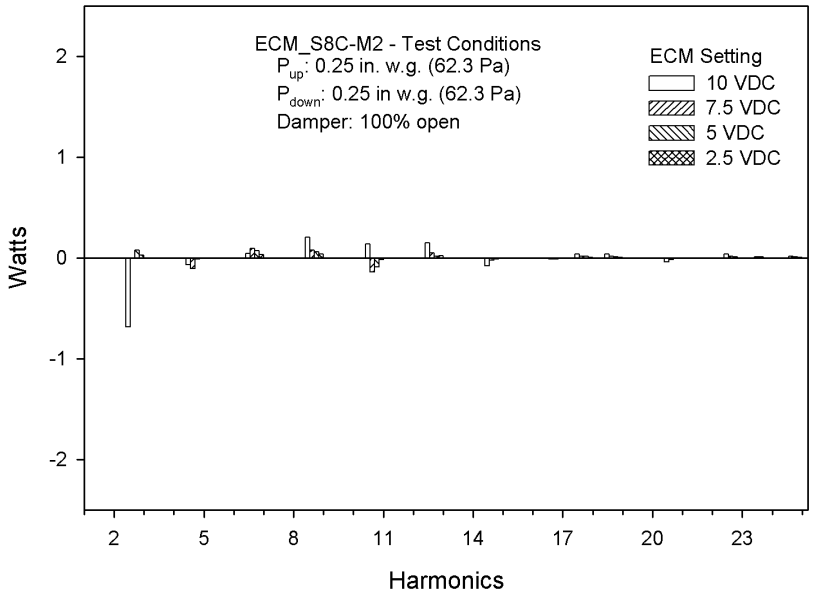

Figure A-59: Real Power Harmonics (Watts) for ECM_S8C-M2

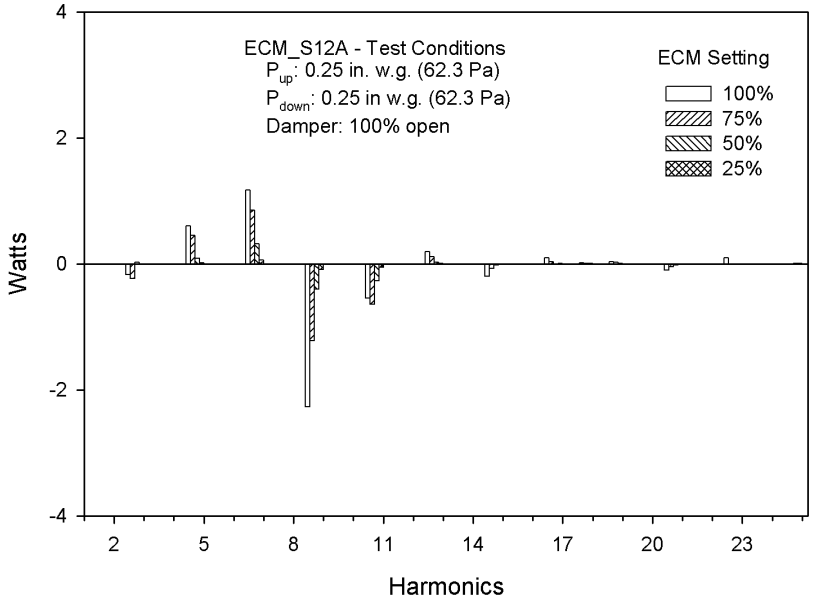

Figure A-60: Real Power Harmonics (Watts) for ECM_S12A

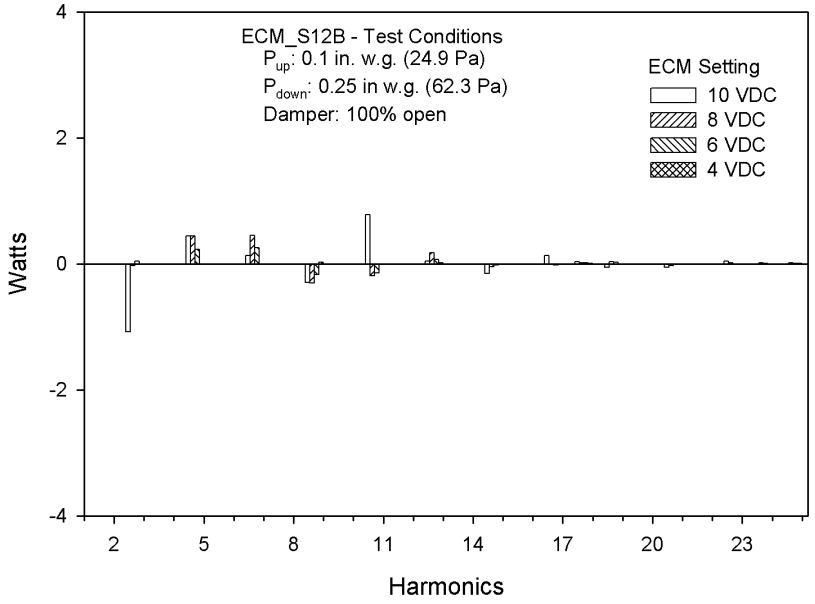

Figure A-61: Real Power Harmonics (Watts) for ECM_S12B

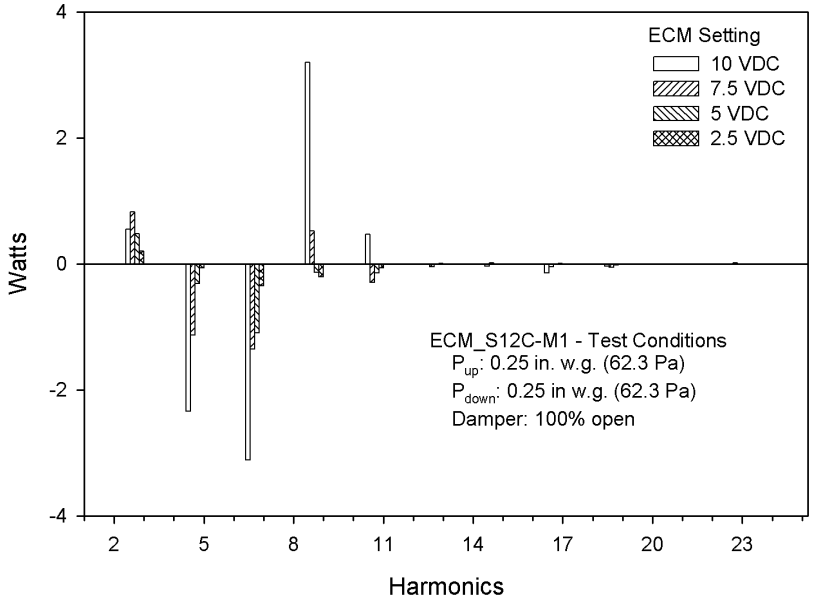

Figure A-62: Real Power Harmonics (Watts) for ECM_S12C-M1

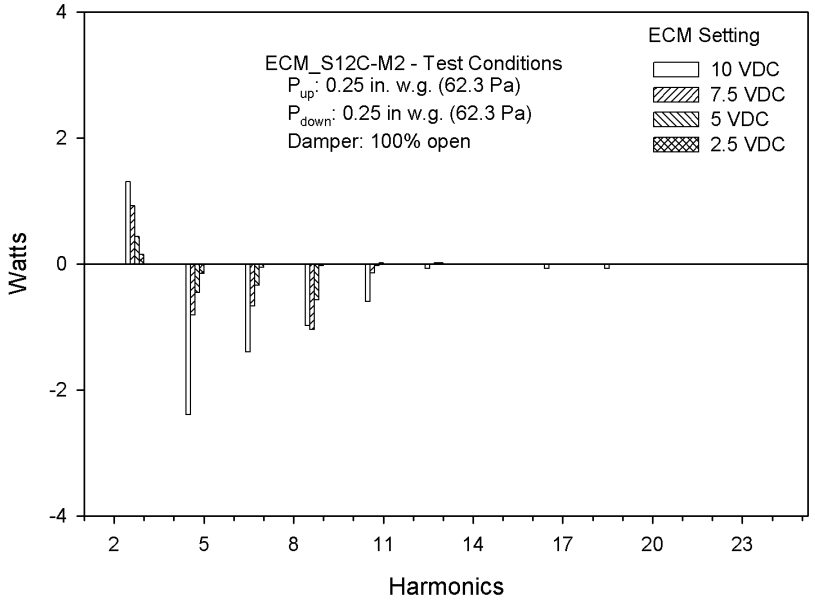

Figure A-63: Real Power Harmonics (Watts) for ECM_S12C-M2

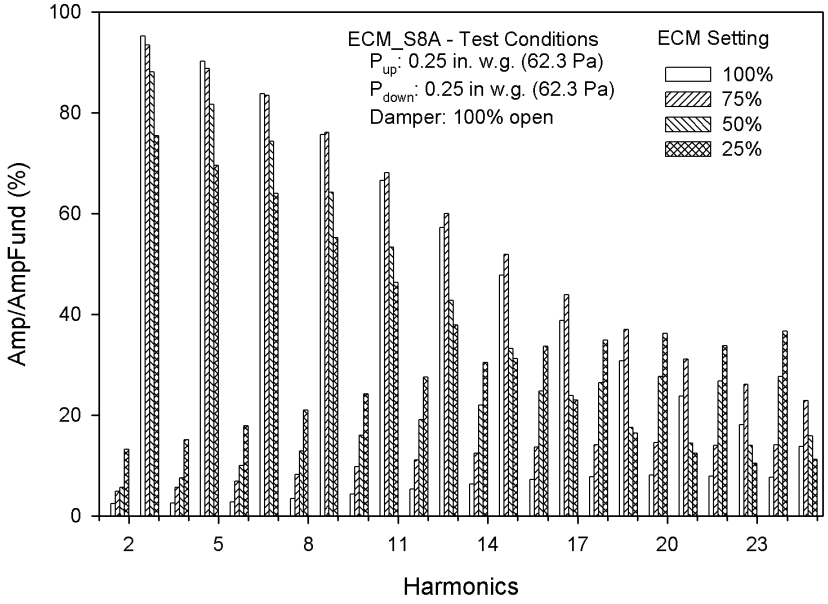

Figure A-64: Current Harmonics (%) for ECM_S8A

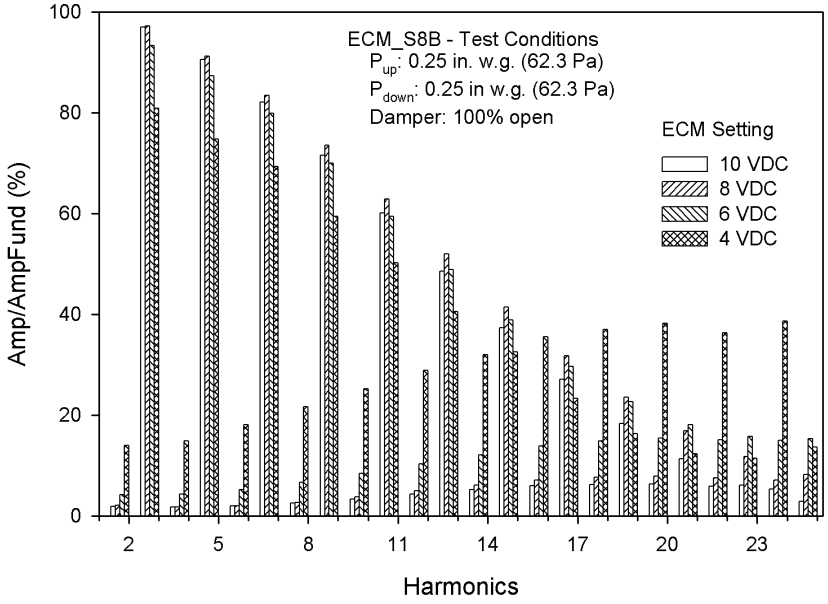

Figure A-65: Current Harmonics (%) for ECM_S8B

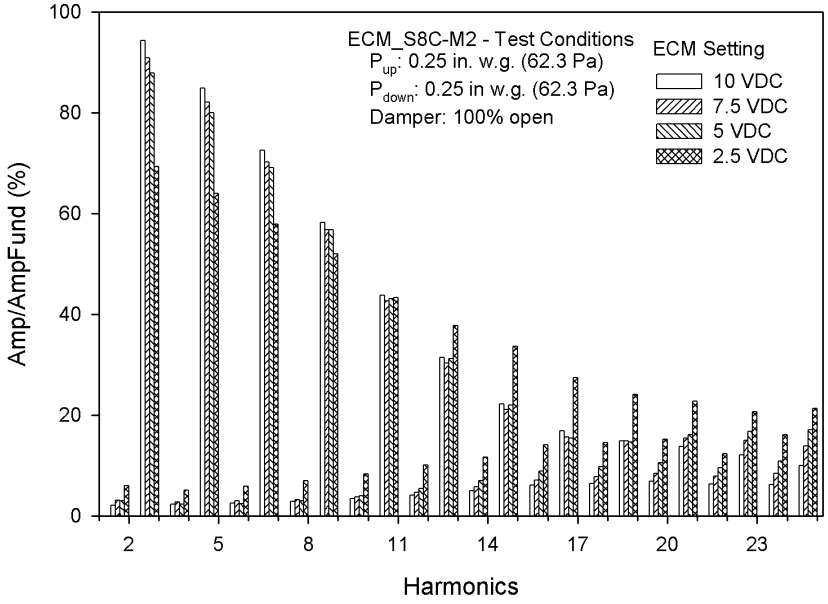

Figure A-66: Current Harmonics (%) for ECM_S8C-M2

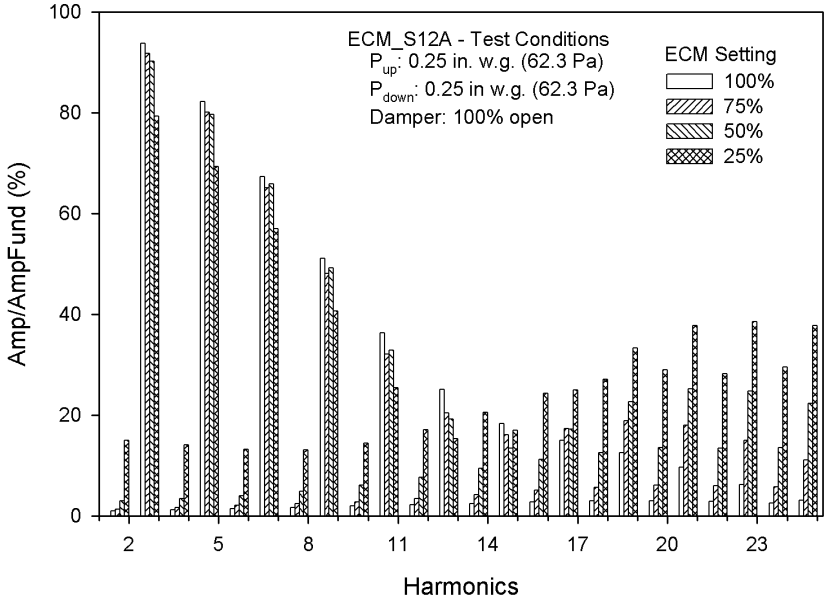

Figure A-67: Current Harmonics (%) for ECM_S12A

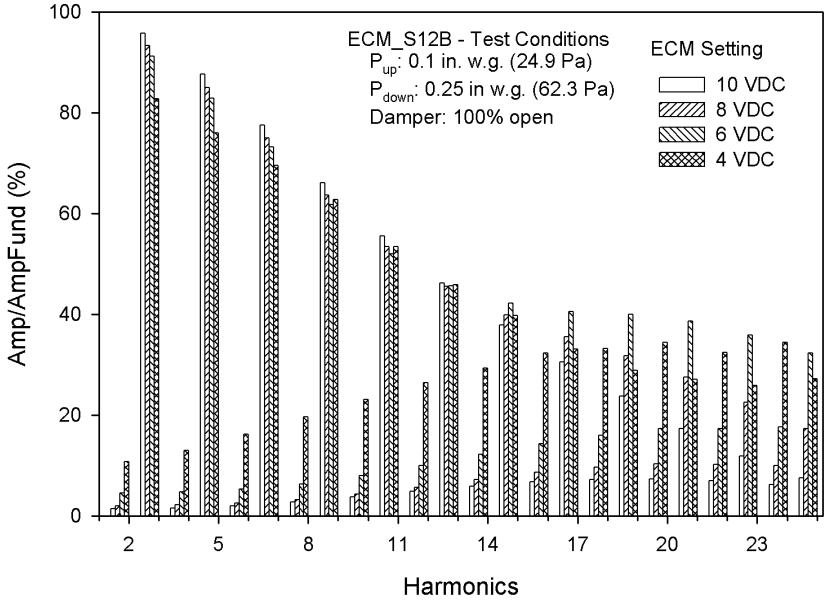

Figure A-68: Current Harmonics (%) for ECM_S12B

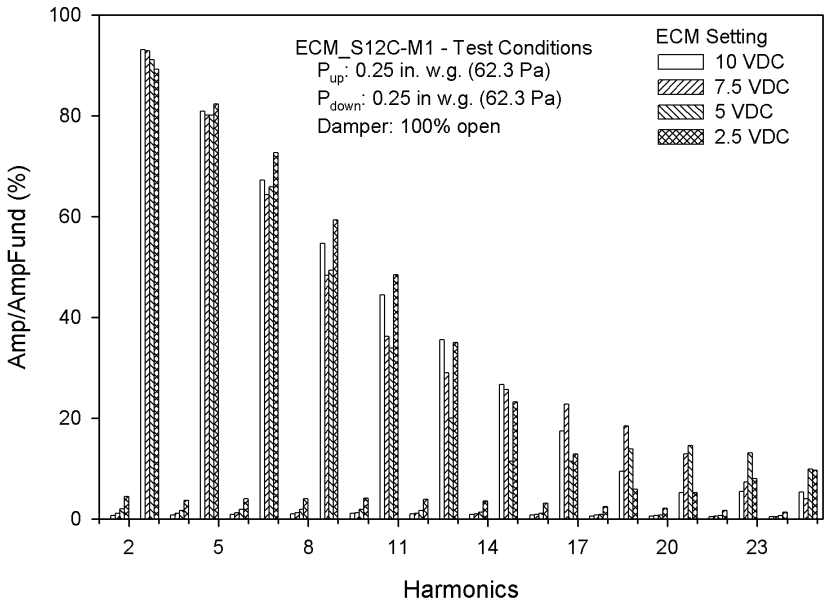

Figure A-69: Current Harmonics (%) for ECM_S12C-M1

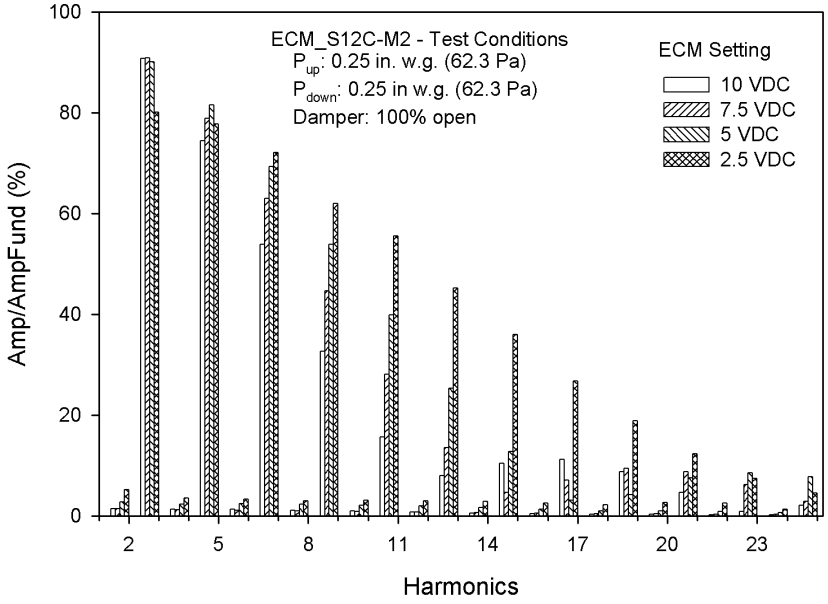

Figure A-70: Current Harmonics (%) for ECM_S12C-M2

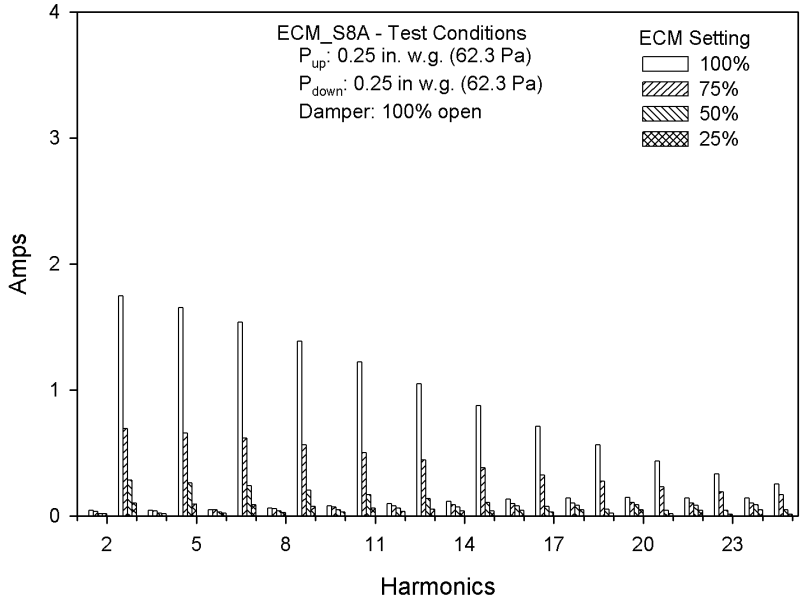

Figure A-71: Current Harmonics (Amps) for ECM_S8A

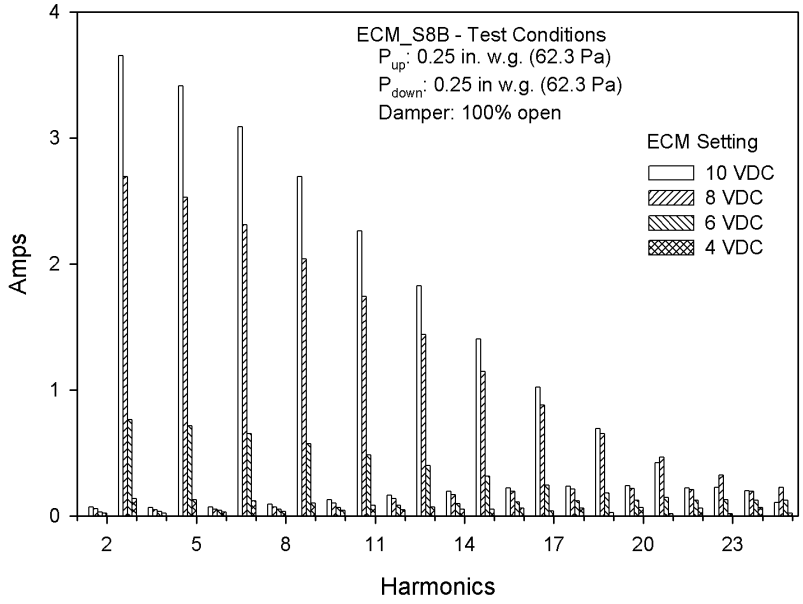

Figure A-72: Current Harmonics (Amps) for ECM_S8B

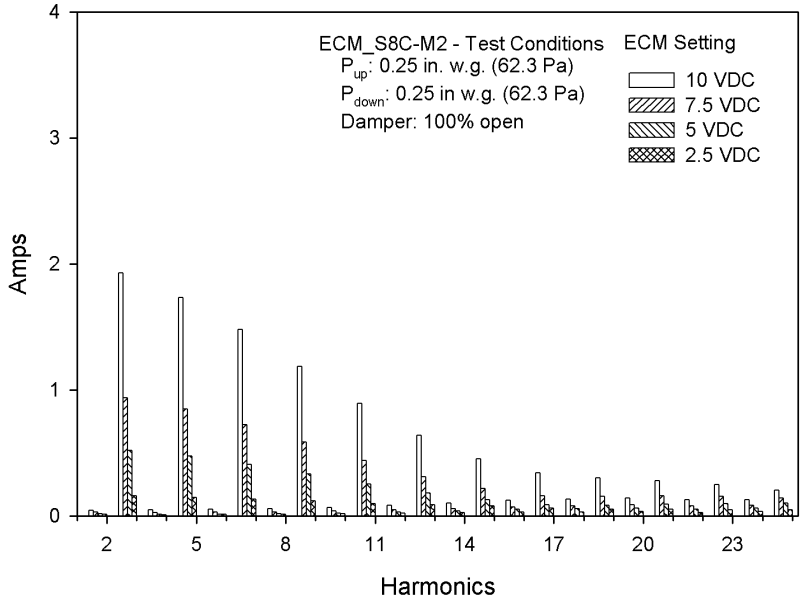

Figure A-73: Current Harmonics (Amps) for ECM_S8C-M2

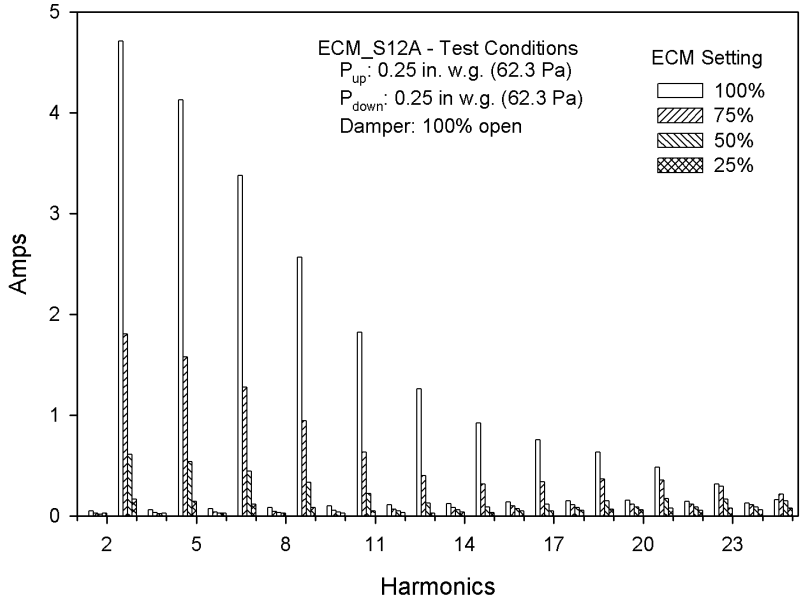

Figure A-74: Current Harmonics (Amps) for ECM_S12A

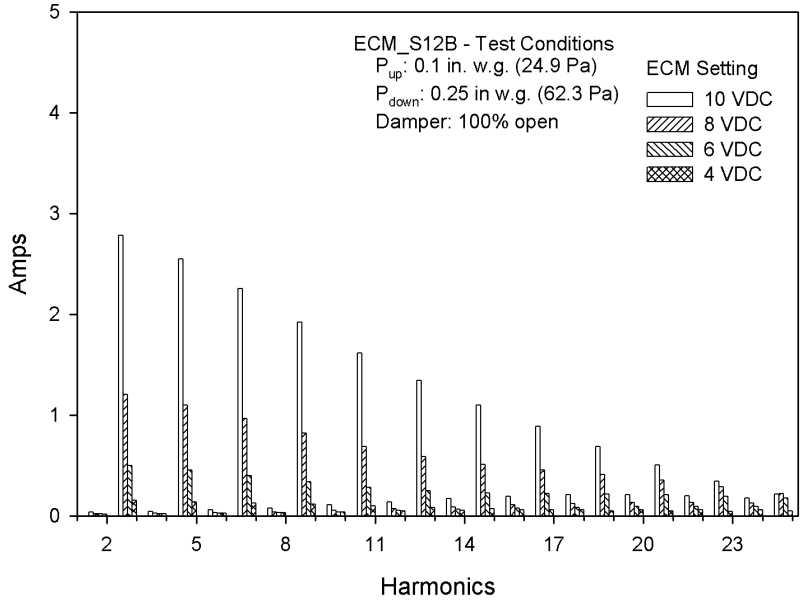

Figure A-75: Current Harmonics (Amps) for ECM_S12B

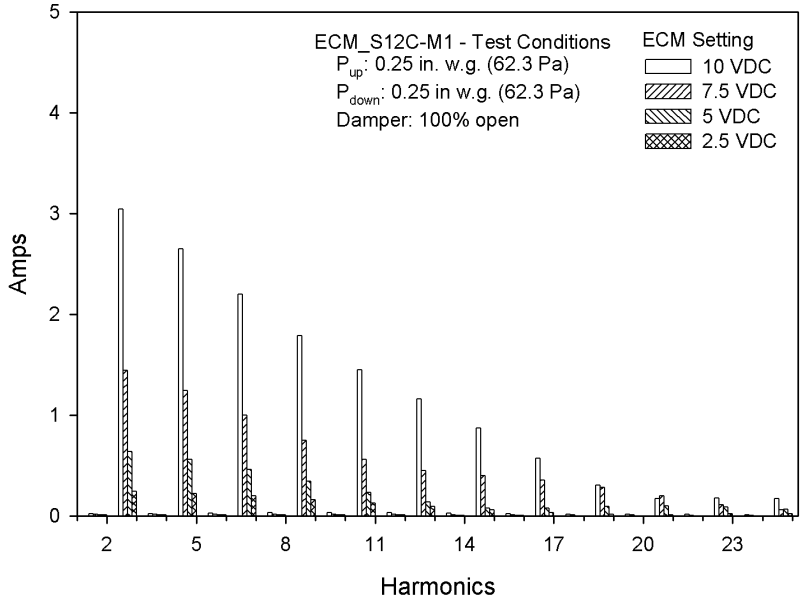

Figure A-76: Current Harmonics (Amps) for ECM_S12C-M1

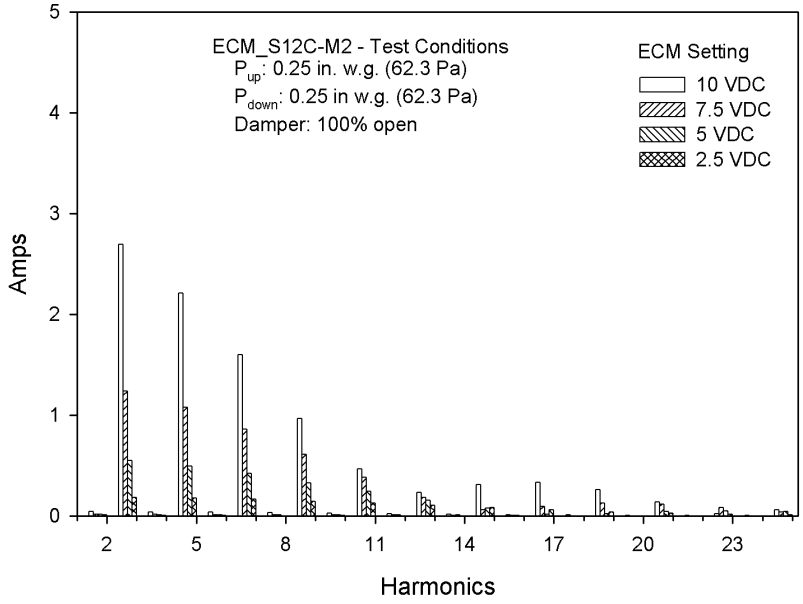

Figure A-77: Current Harmonics (Amps) for ECM_S12C-M2

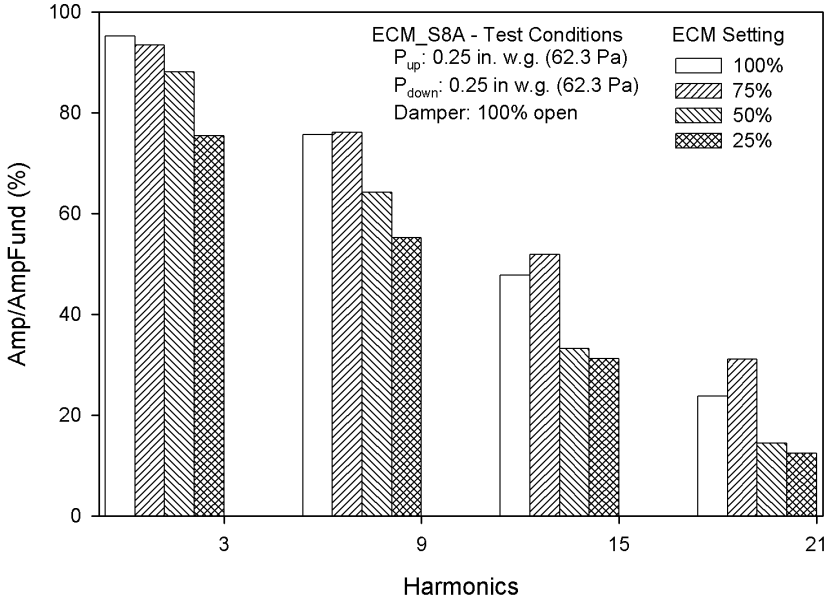

Figure A-78: Current Triplen Harmonics (%) for ECM_S8A

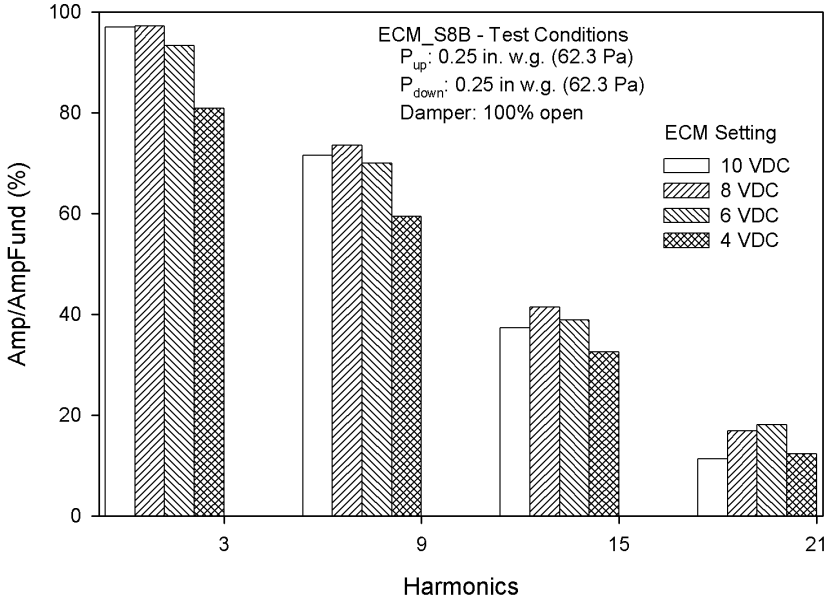

Figure A-79: Current Triplen Harmonics (%) for ECM_S8B

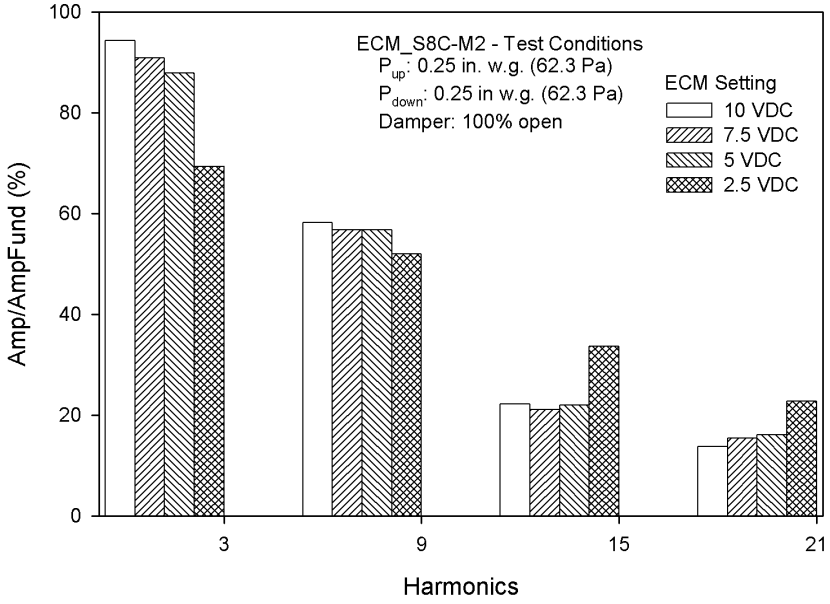

Figure A-80: Current Triplen Harmonics (%) for ECM_S8C-M2

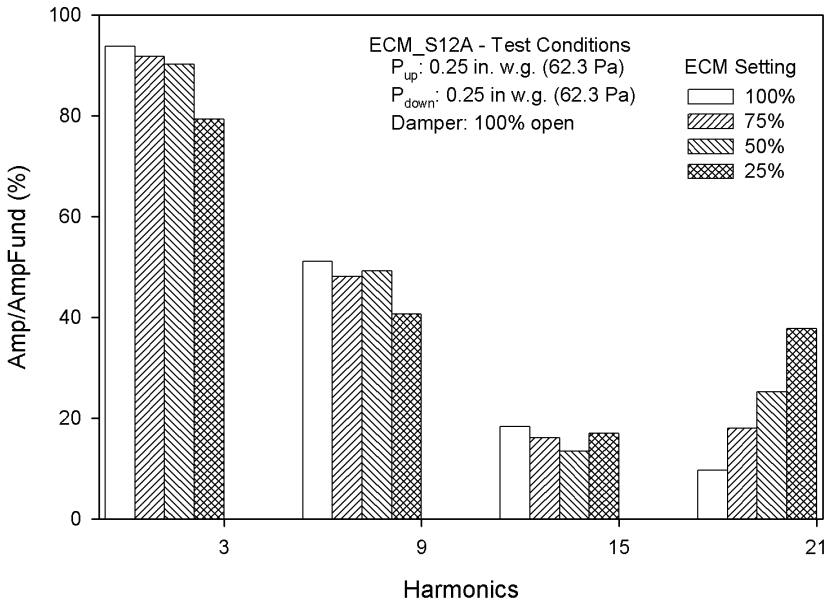

Figure A-81: Current Triplen Harmonics (%) for ECM_S12A

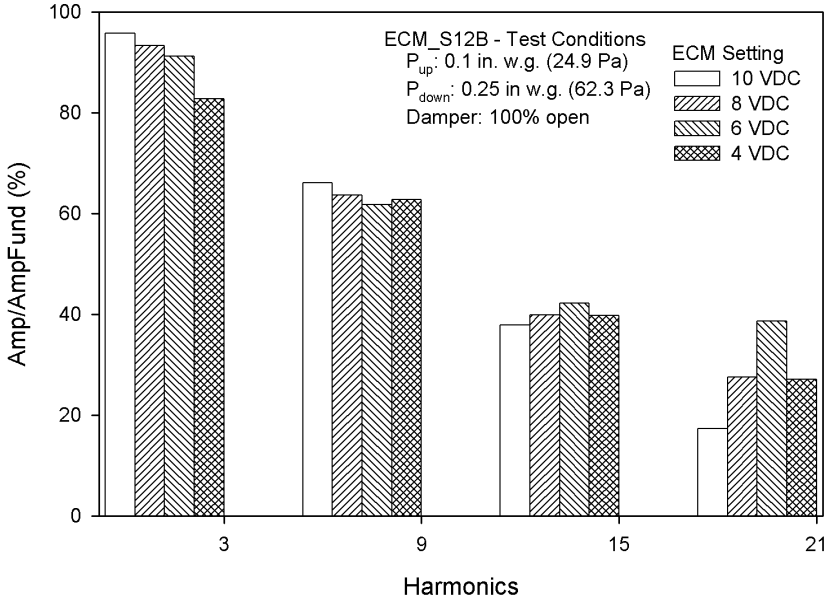

Figure A-82: Current Triplen Harmonics (%) for ECM_S12B

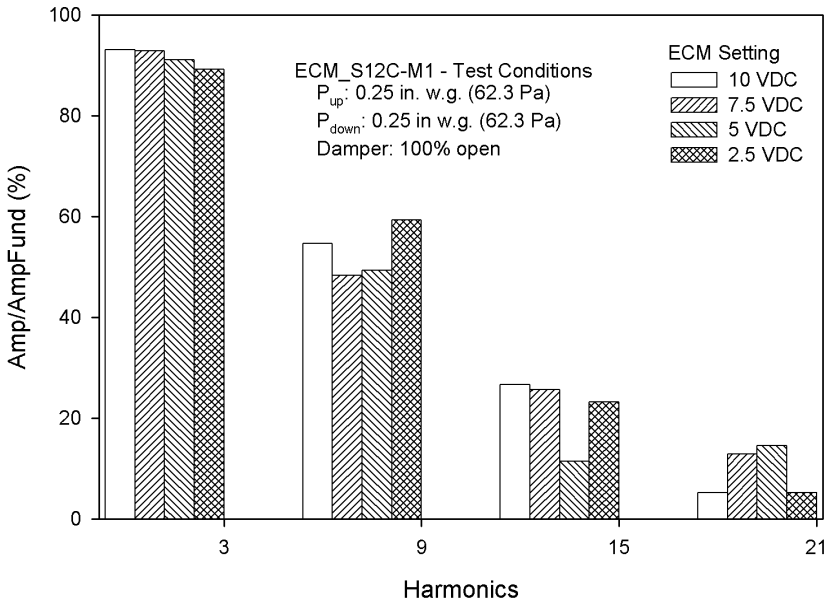

Figure A-83: Current Triplen Harmonics (%) for ECM_S12C-M1

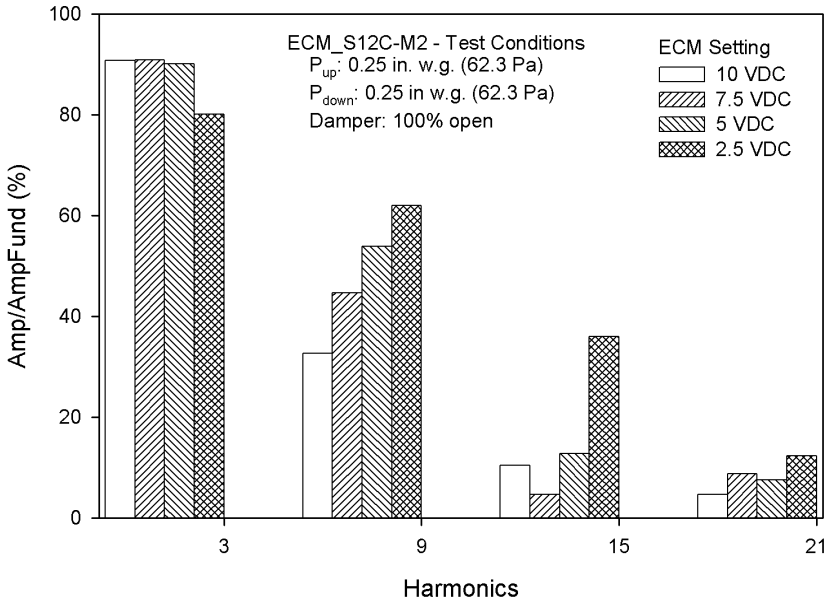

Figure A-84: Current Triplen Harmonics (%) for ECM_S12C-M2

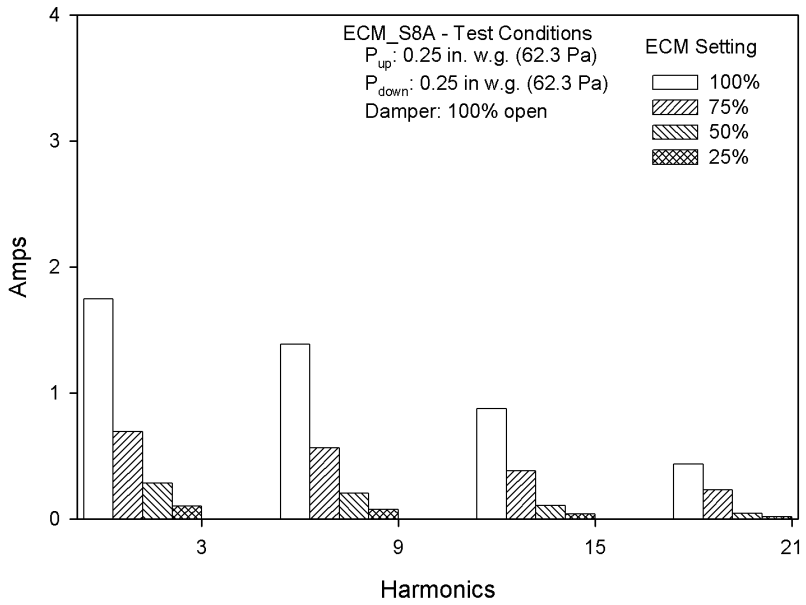

Figure A-85: Current Triplen Harmonics (Amps) for ECM_S8A

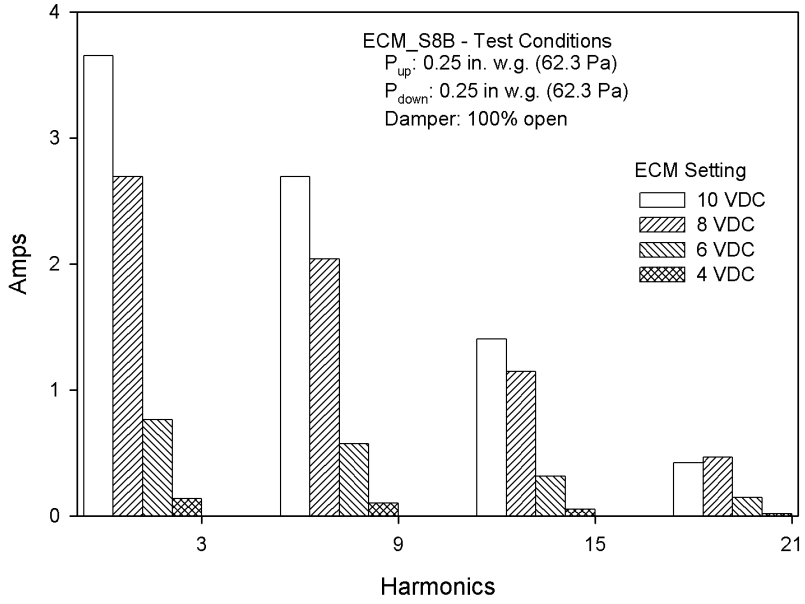

Figure A-86: Current Triplen Harmonics (Amps) for ECM_S8B

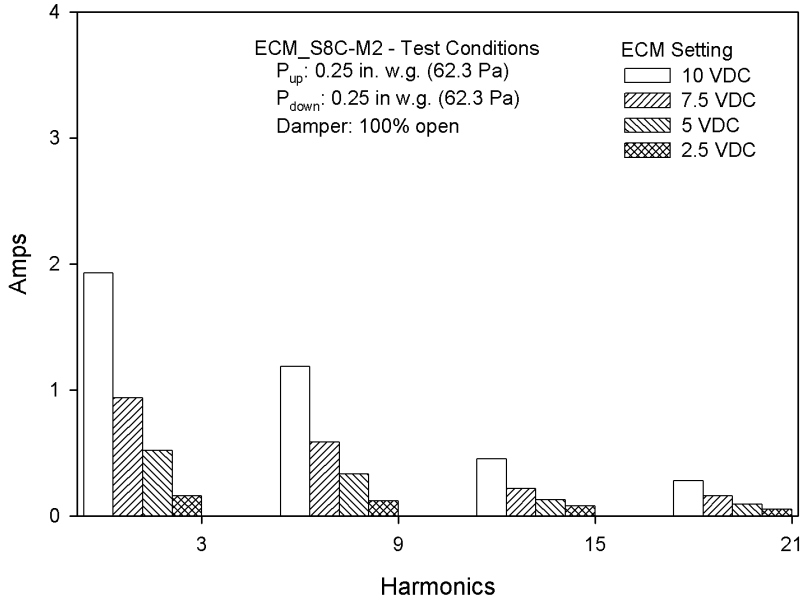

Figure A-87: Current Triplen Harmonics (Amps) for ECM_S8C-M2

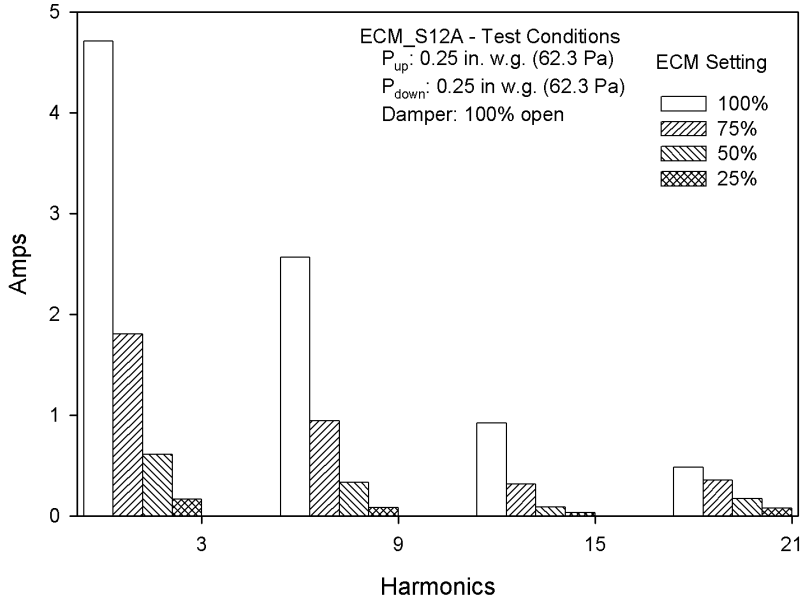

Figure A-88: Current Triplen Harmonics (Amps) for ECM_S12A

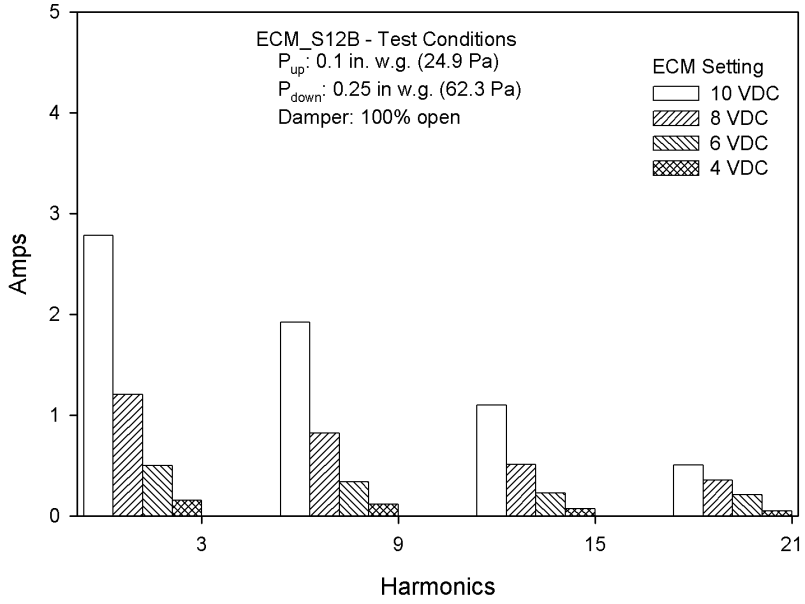

Figure A-89: Current Triplen Harmonics (Amps) for ECM_S12B

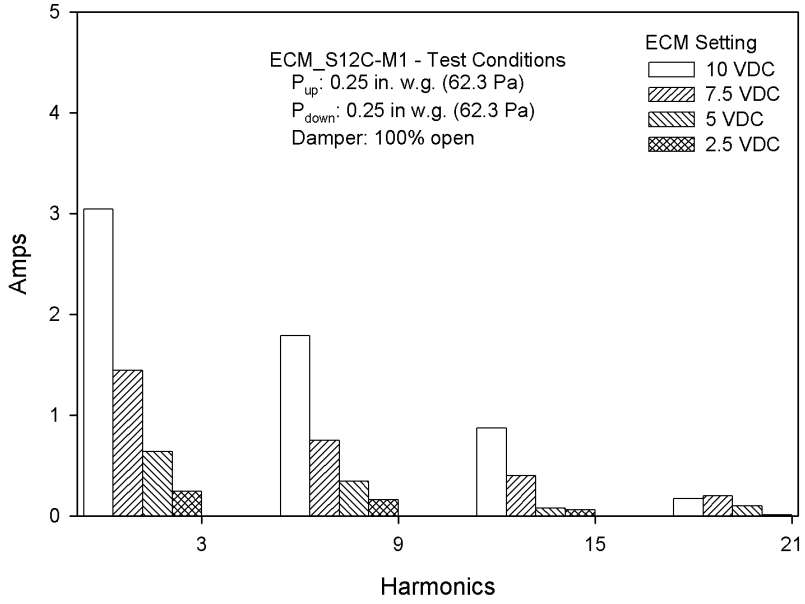

Figure A-90: Current Triplen Harmonics (Amps) for ECM_S12C-M1

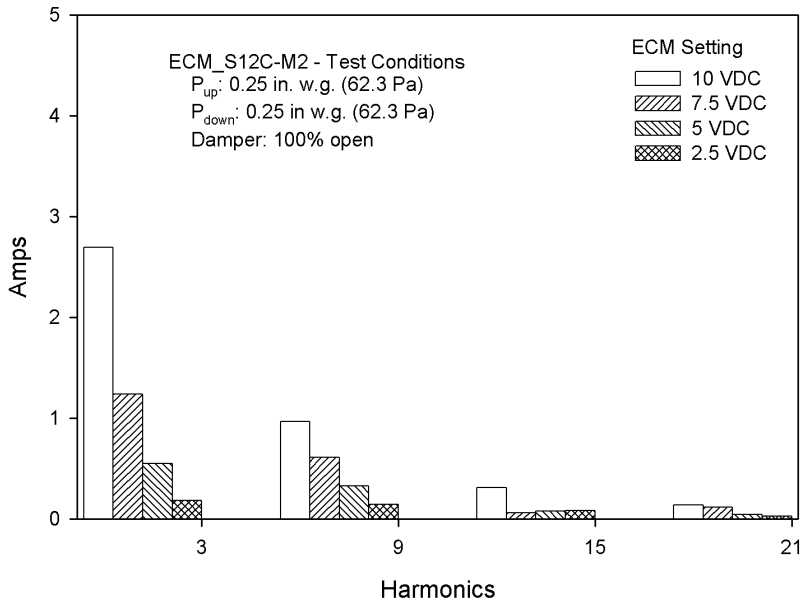

Figure A-91: Current Triplen Harmonics (Amps) for ECM_S12C-M2

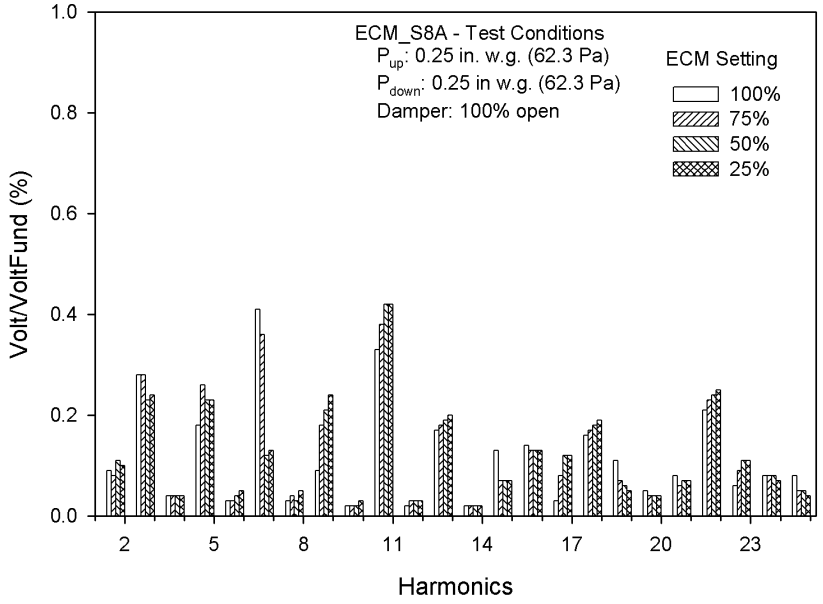

Figure A-92: Voltage Harmonics (%) for ECM_S8A

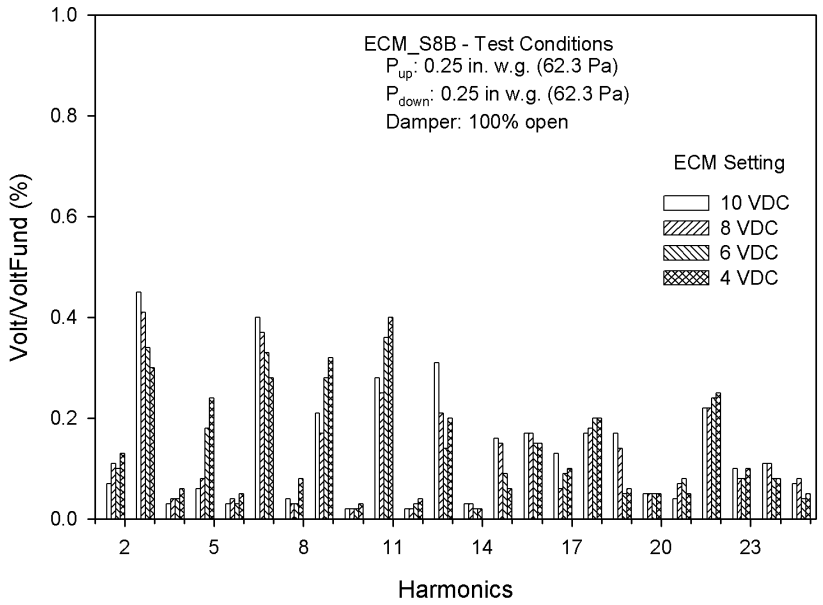

Figure A-93: Voltage Harmonics (%) for ECM_S8B

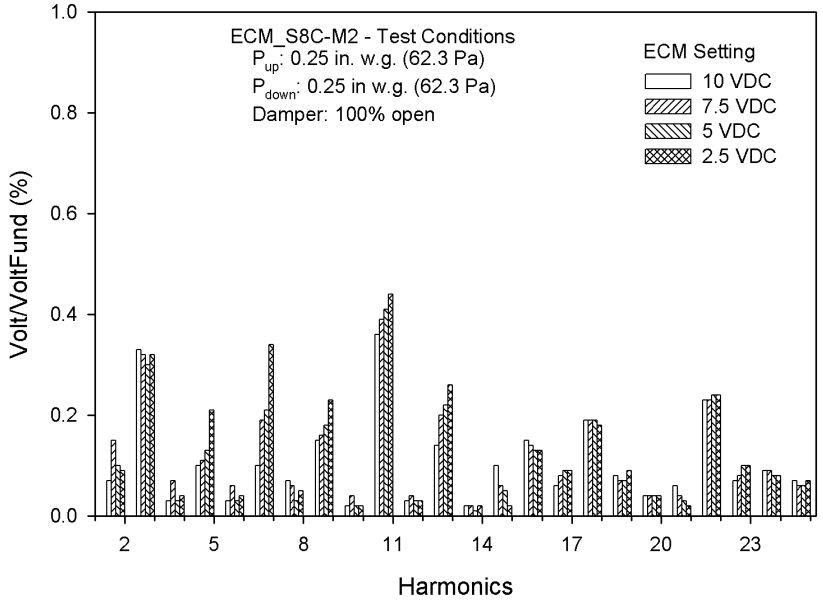

Figure A-94: Voltage Harmonics (%) for ECM_S8C-M2

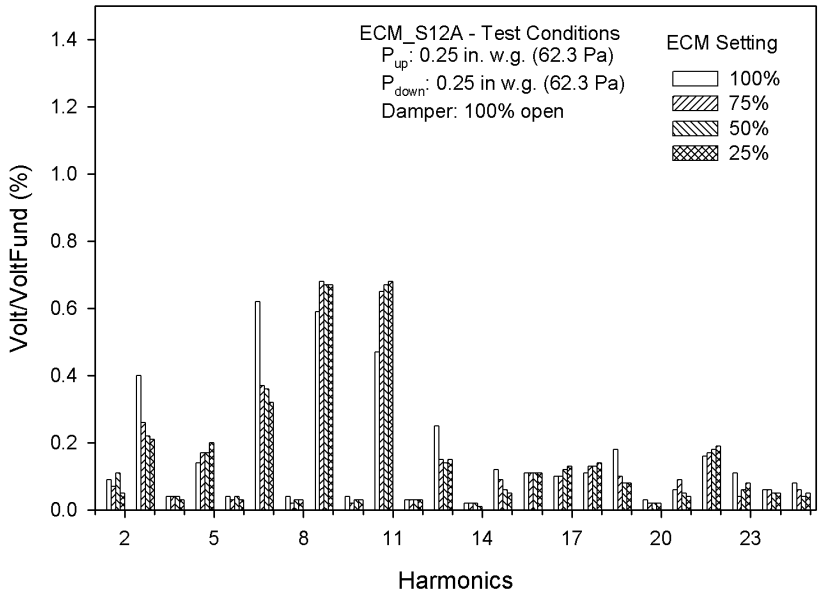

Figure A-95: Voltage Harmonics (%) for ECM_S12A

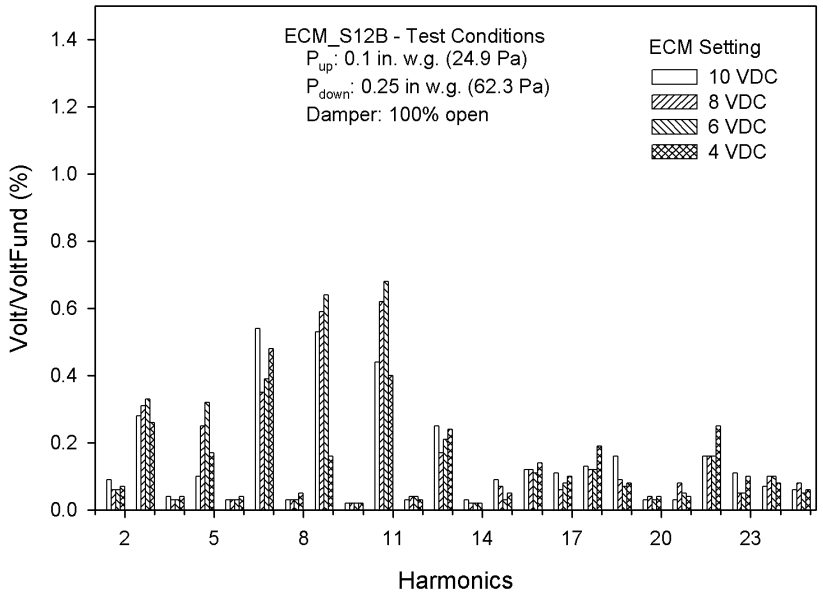

Figure A-96: Voltage Harmonics (%) for ECM_S12B

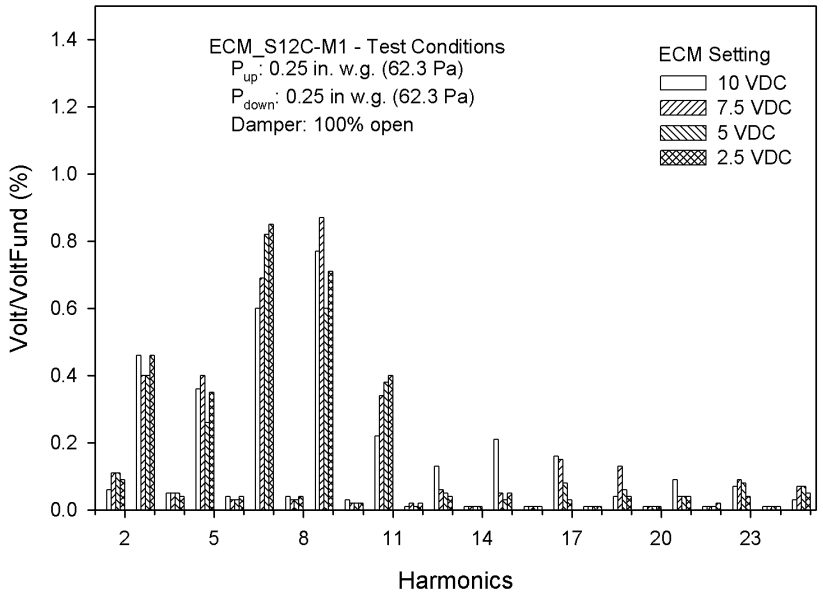

Figure A-97: Voltage Harmonics (%) for ECM_S12C-M1

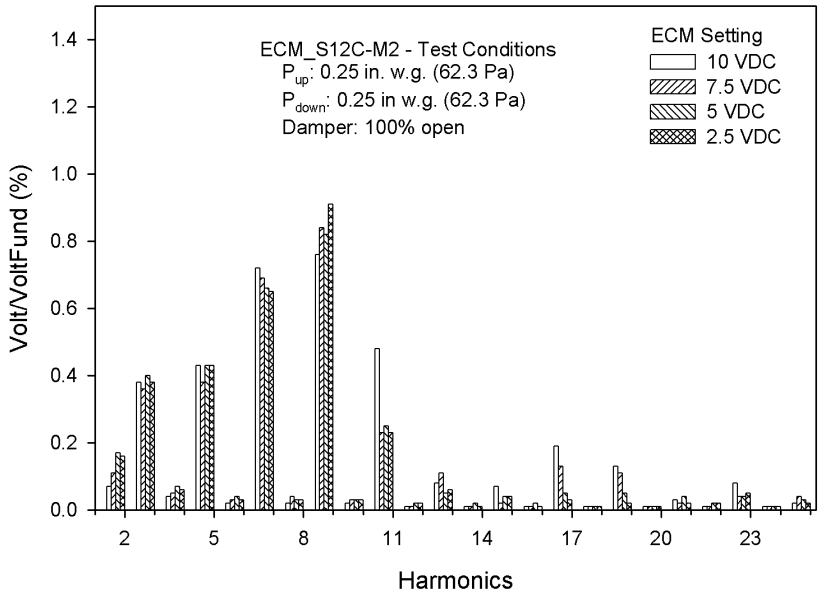

Figure A-98: Voltage Harmonics (%) for ECM_S12C-M2

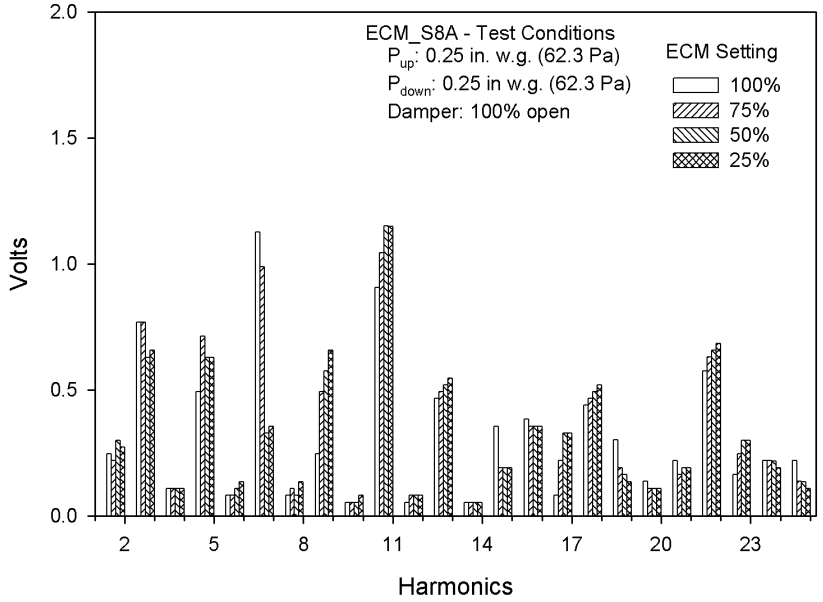

Figure A-99: Voltage Harmonics (Volts) for ECM_S8A

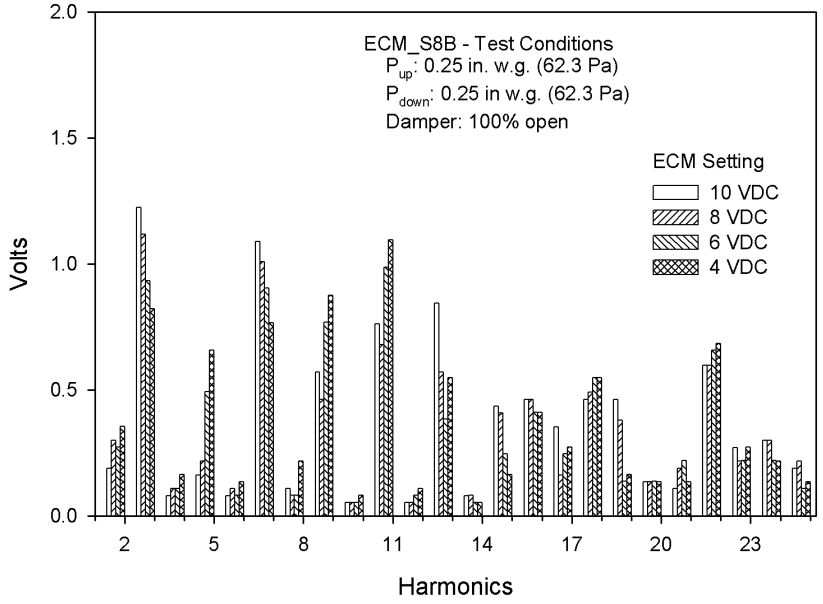

Figure A-100: Voltage Harmonics (Volts) for ECM_S8B

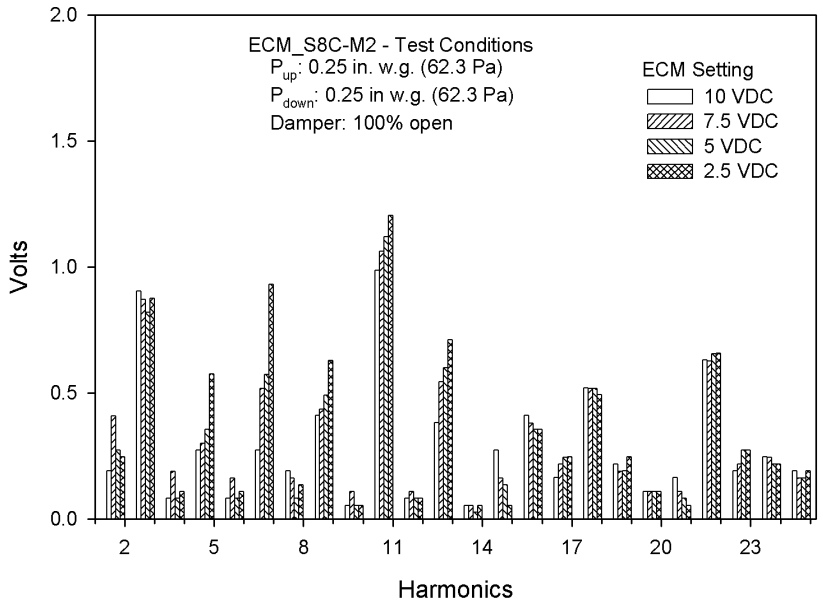

Figure A-101: Voltage Harmonics (Volts) for ECM_S8C-M2

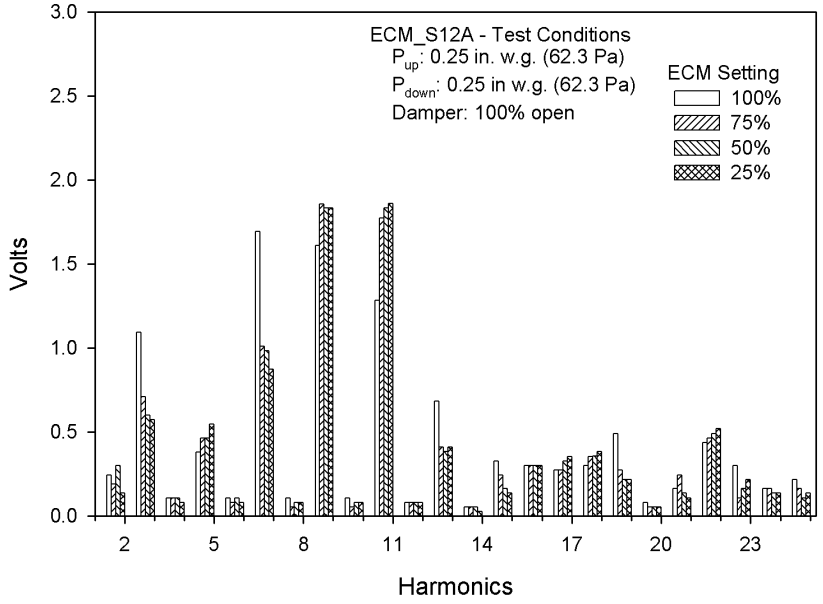

Figure A-102: Voltage Harmonics (Volts) for ECM_S12A

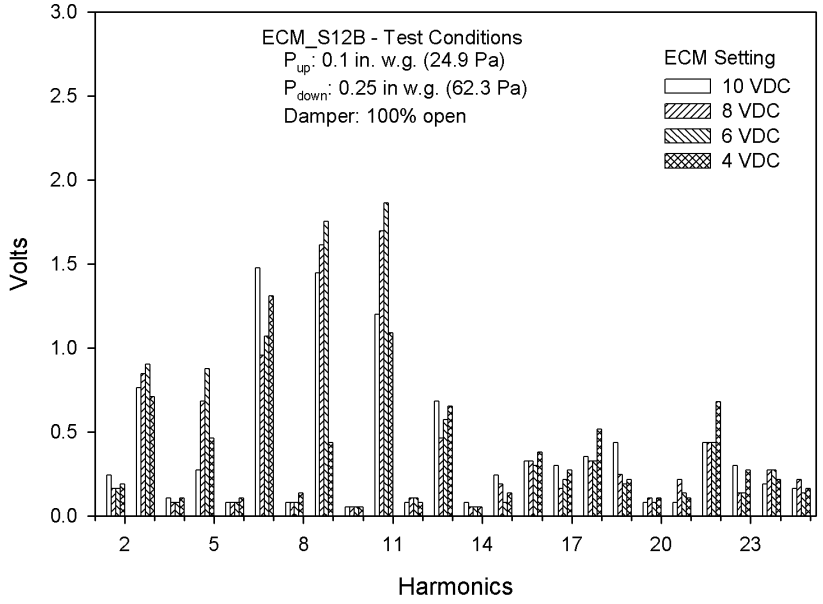

Figure A-103: Voltage Harmonics (Volts) for ECM_S12B

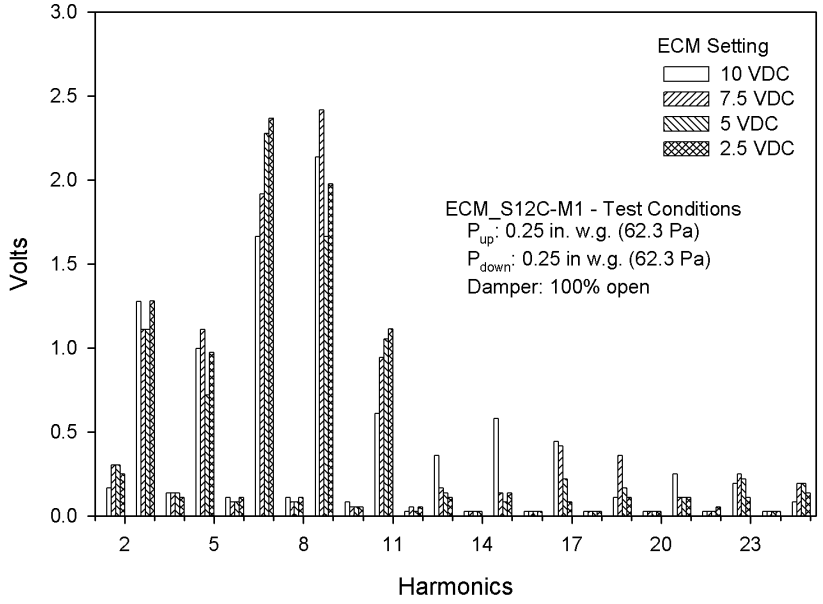

Figure A-104: Voltage Harmonics (Volts) for ECM_S12C-M1

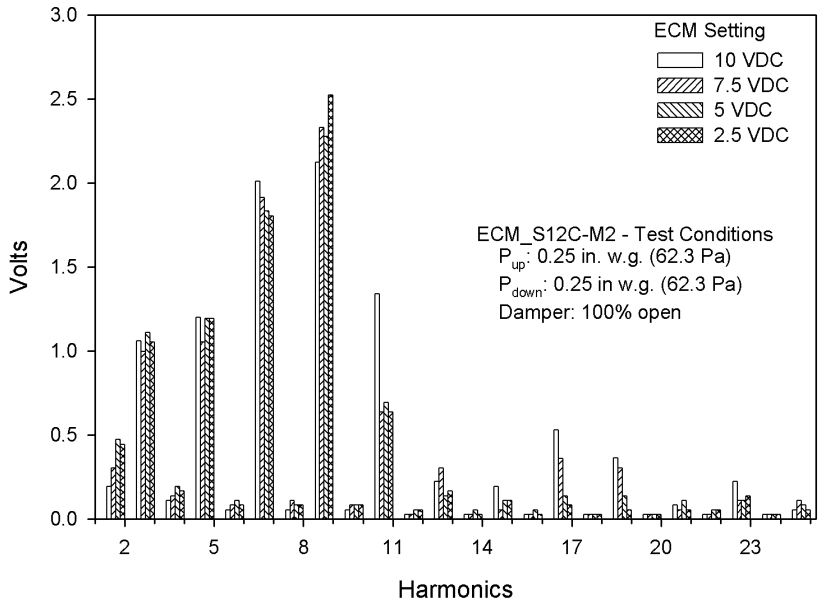

Figure A-105: Voltage Harmonics (Volts) for ECM_S12C-M2

APPENDIX B

PARALLEL TERMINAL UNITS RESULTS

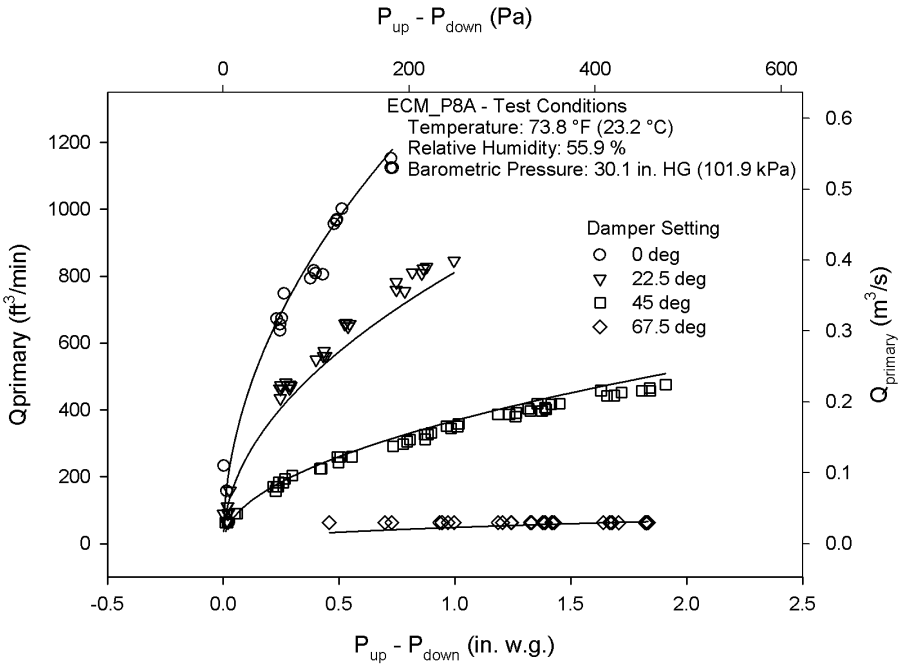

Figure B-1: $Q_{primary}$ vs. DP for ECM_P8A

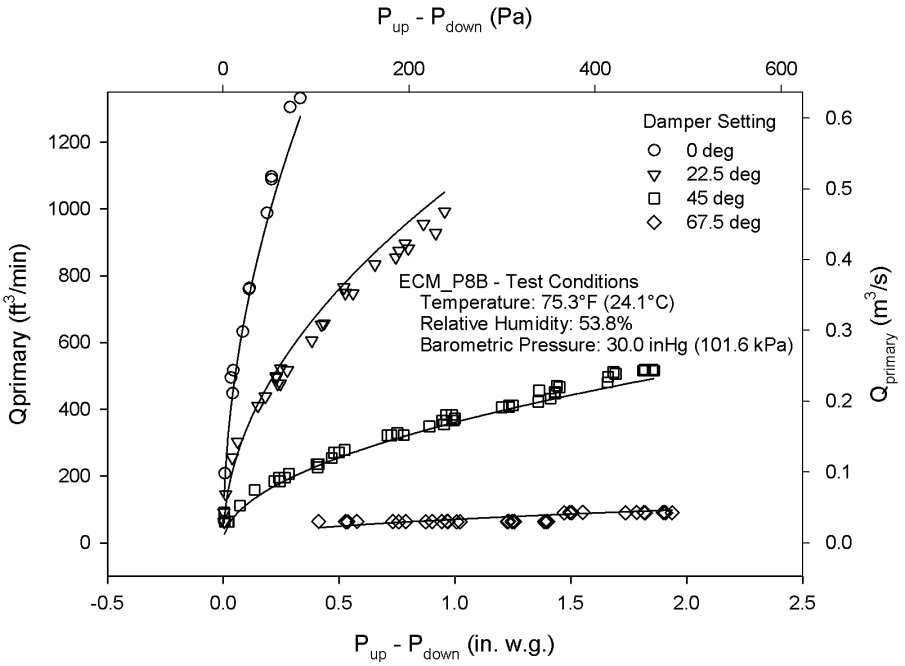

Figure B-2: $Q_{primary}$ vs. DP for ECM_P8B

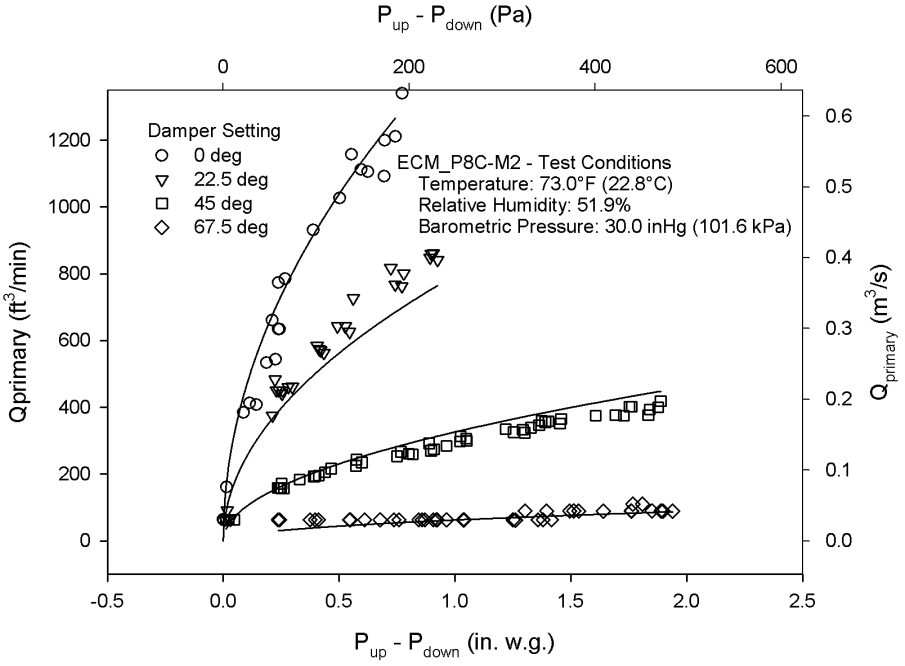

Figure B-3: $Q_{primary}$ vs. DP for ECM_P8C-M2

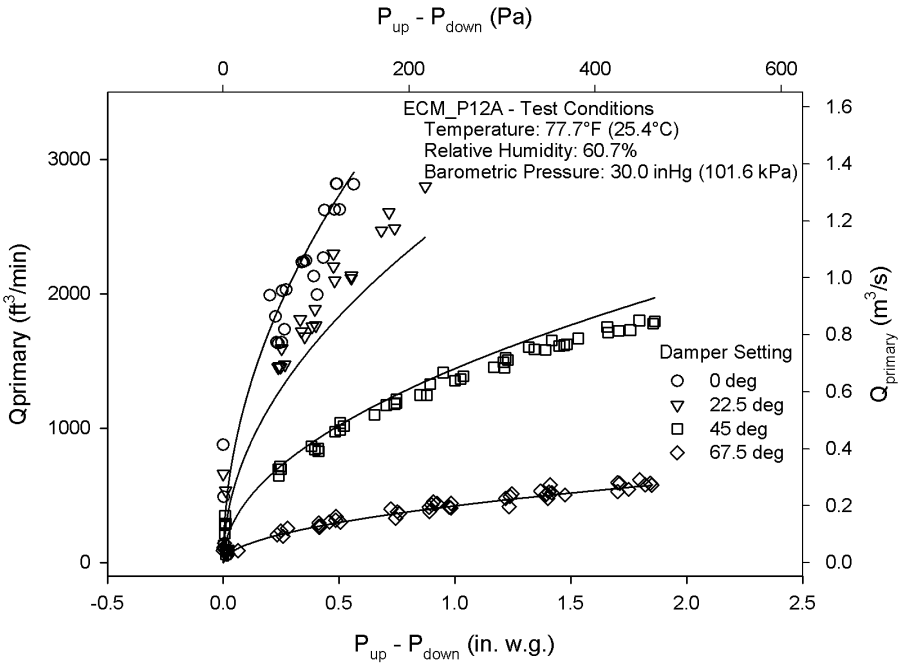

Figure B-4: $Q_{primary}$ vs. DP for ECM_P12A

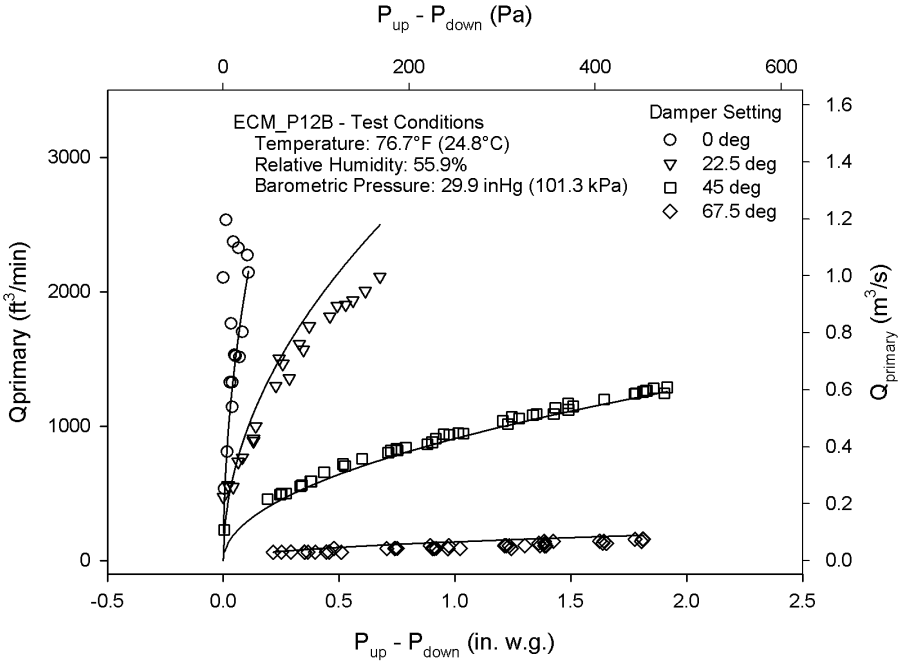

Figure B-5: $Q_{primary}$ vs. DP for ECM_P12B

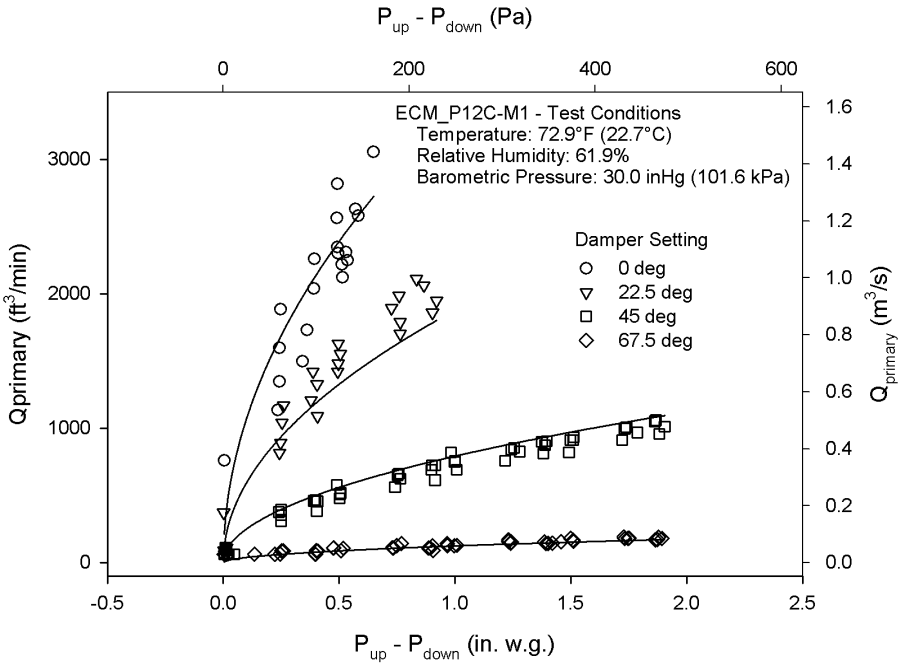

Figure B-6: $Q_{primary}$ vs. DP for ECM_P12C-M1

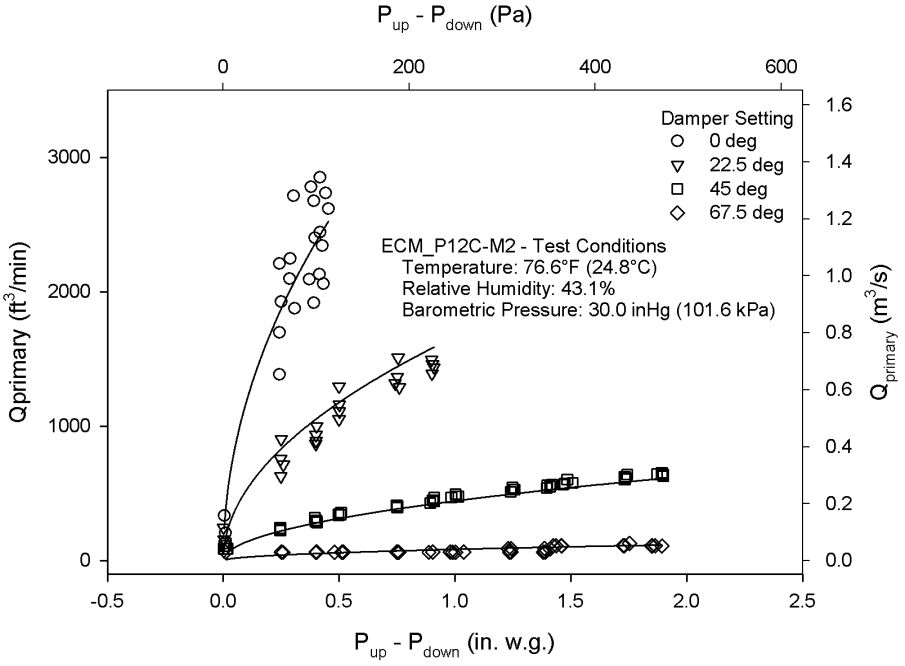

Figure B-7: $Q_{primary}$ vs. DP for ECM_P12C-M2

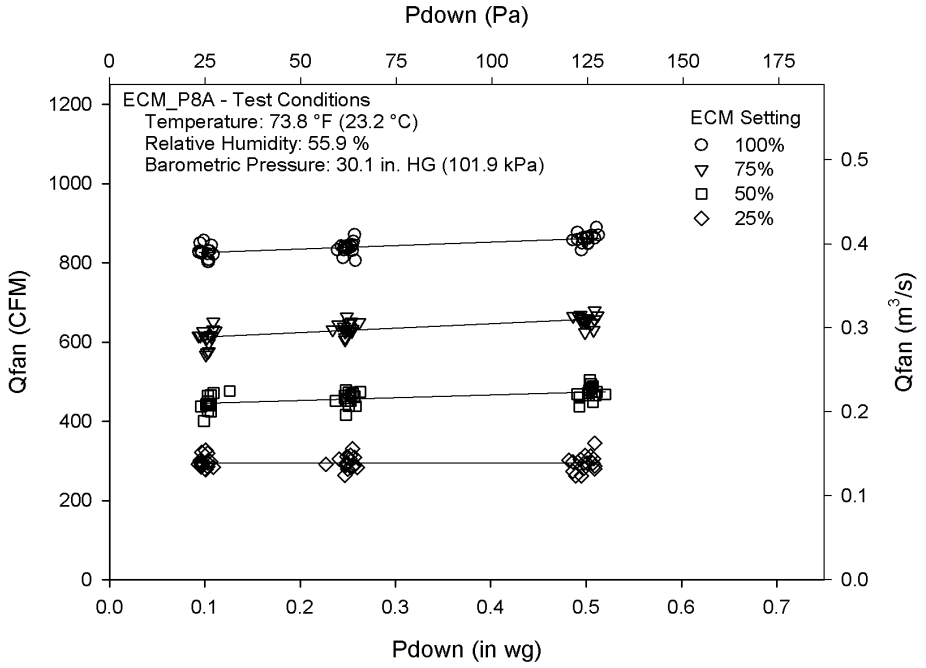

Figure B-8: Q_{fan} vs. P_{down} for ECM_P8A

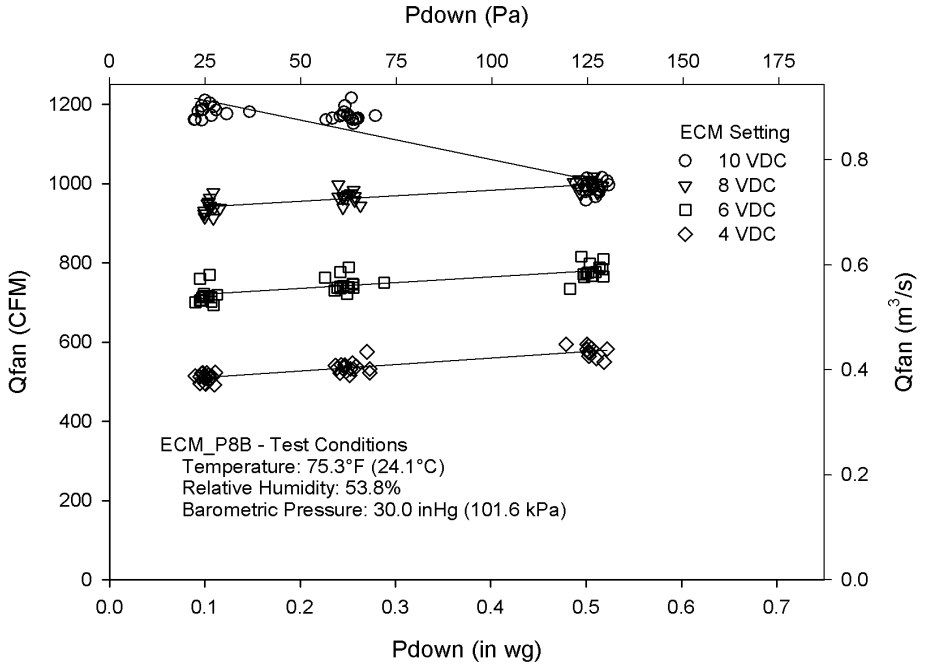

Figure B-9: Q_{fan} vs. P_{down} for ECM_P8B

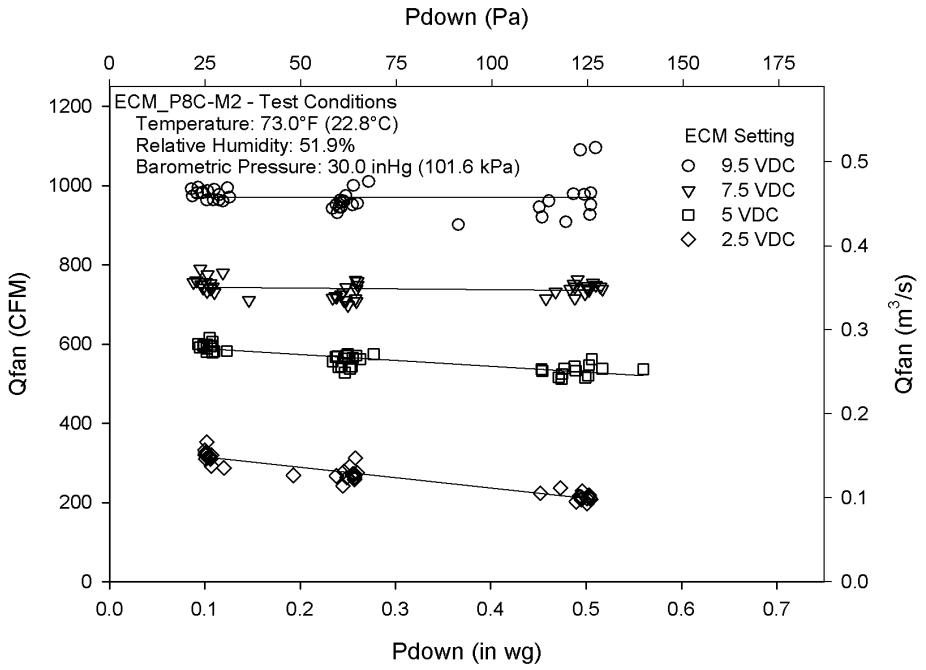

Figure B-10: Q_{fan} vs. P_{down} for ECM_P8C-M2

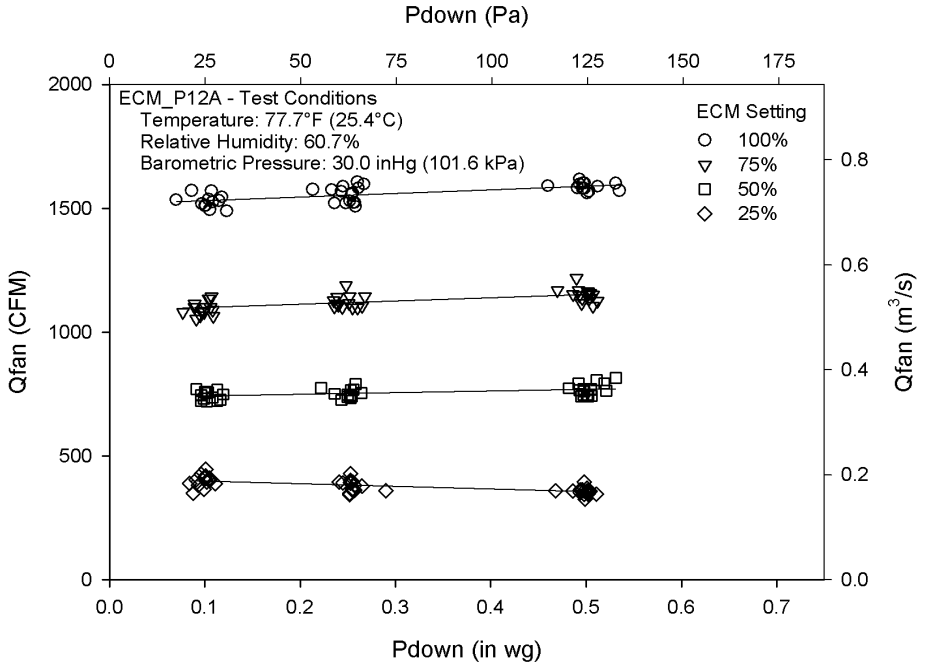

Figure B-11: Q_{fan} vs. P_{down} for ECM_P12A

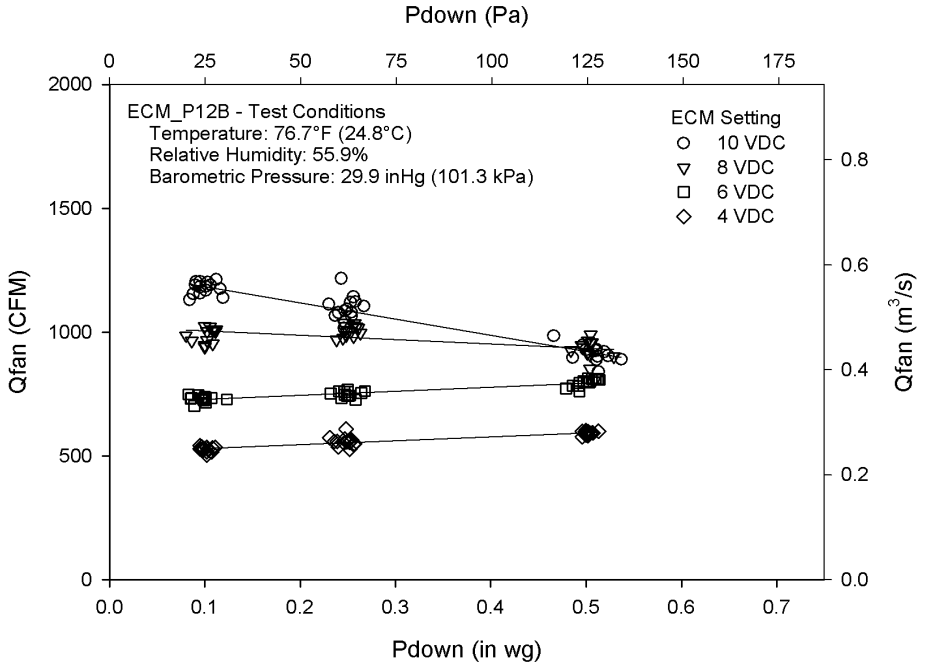

Figure B-12: Q_{fan} vs. P_{down} for ECM_P12B

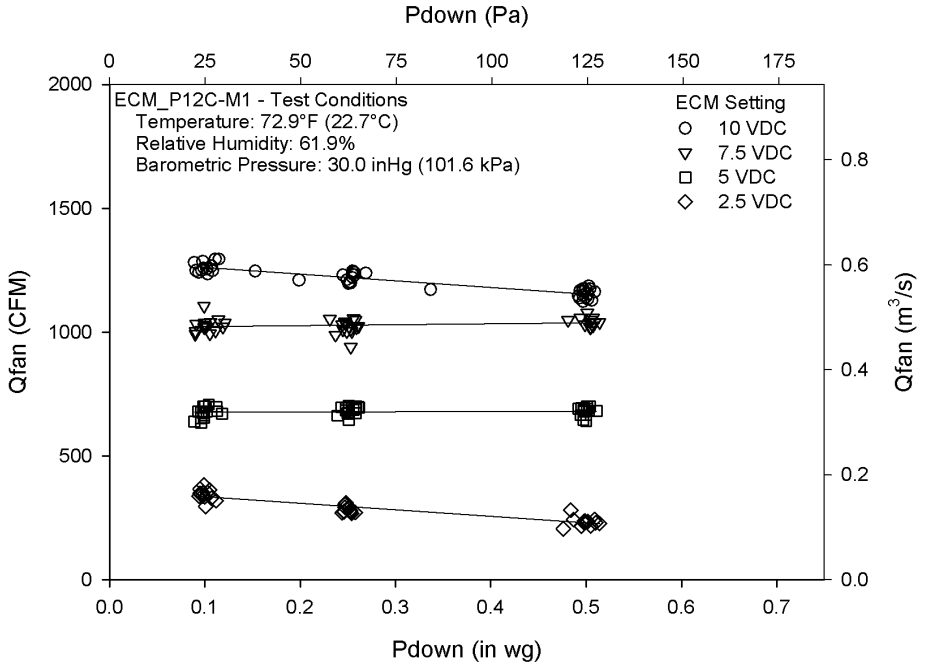

Figure B-13: Q_{fan} vs. P_{down} for ECM_P12C-M1

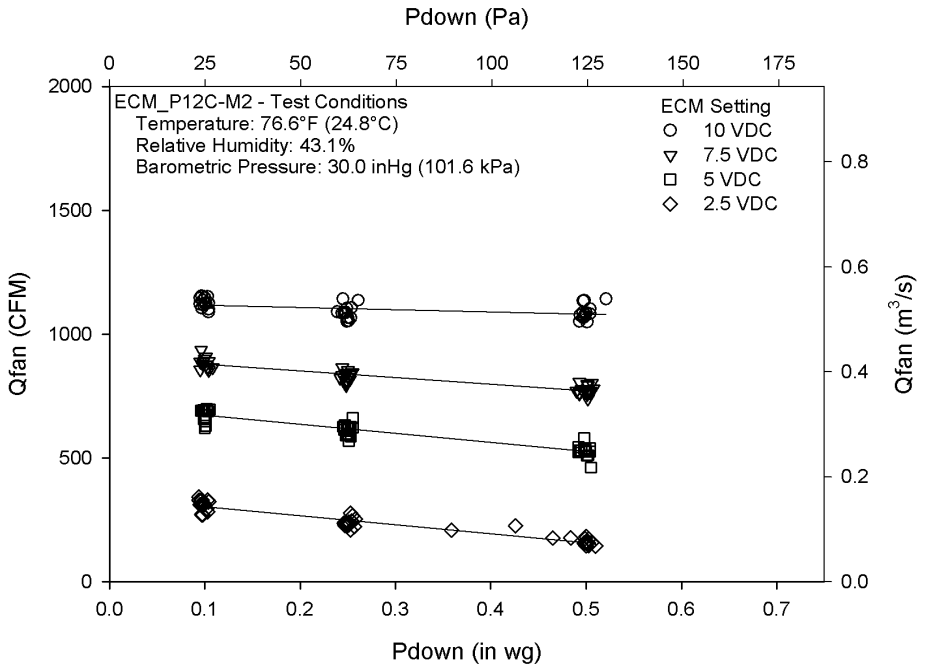

Figure B-14: Q_{fan} vs. P_{down} for ECM_P12C-M2

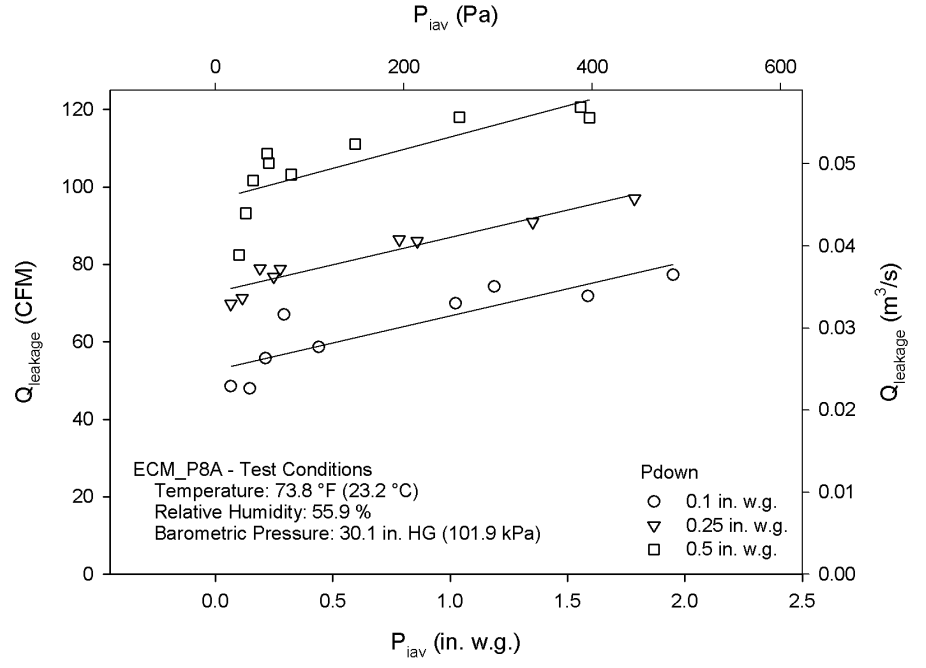

Figure B-15: Leakage vs. P_{iav} for ECM_P8A

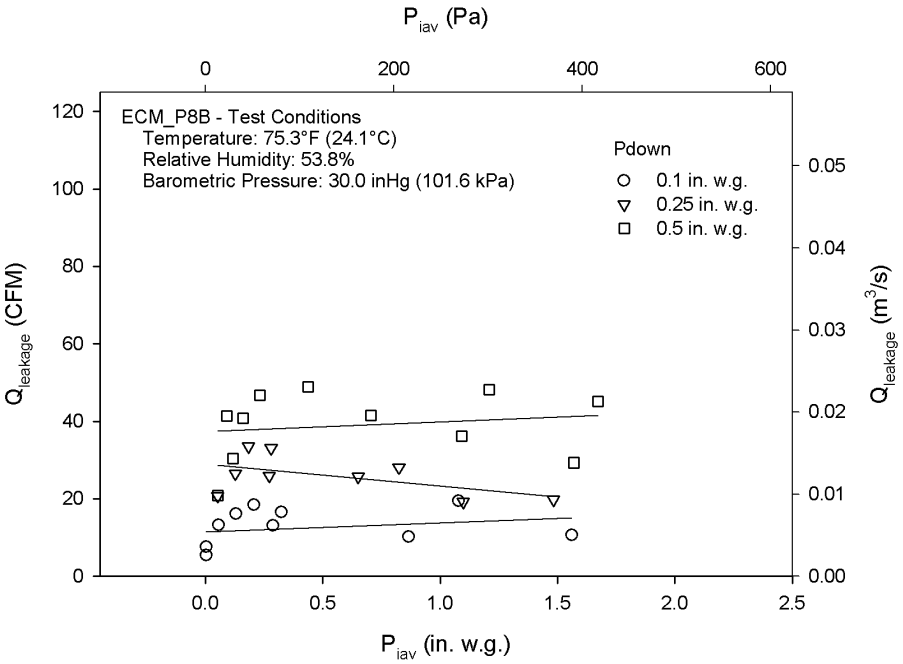

Figure B-16: Leakage vs. P_{iav} for ECM_P8B

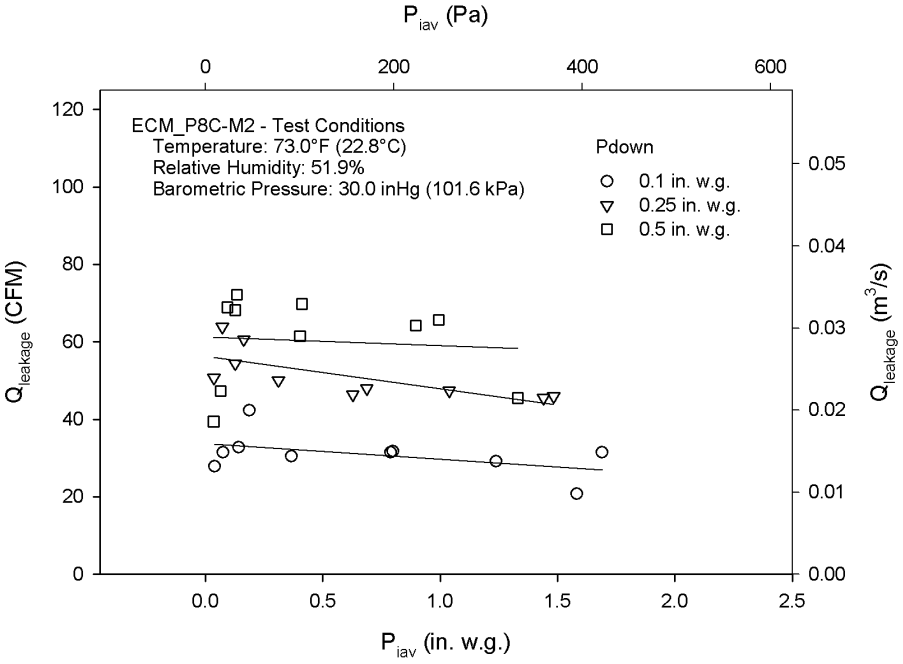

Figure B-17: Leakage vs. P_{iav} for ECM_P8C-M2

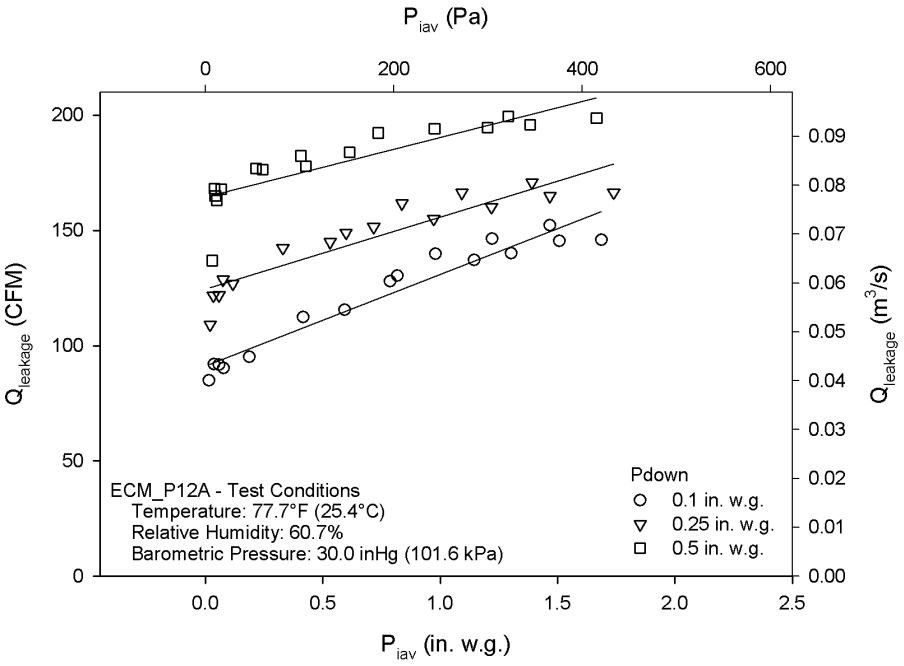

Figure B-18: Leakage vs. P_{iav} for ECM_P12A

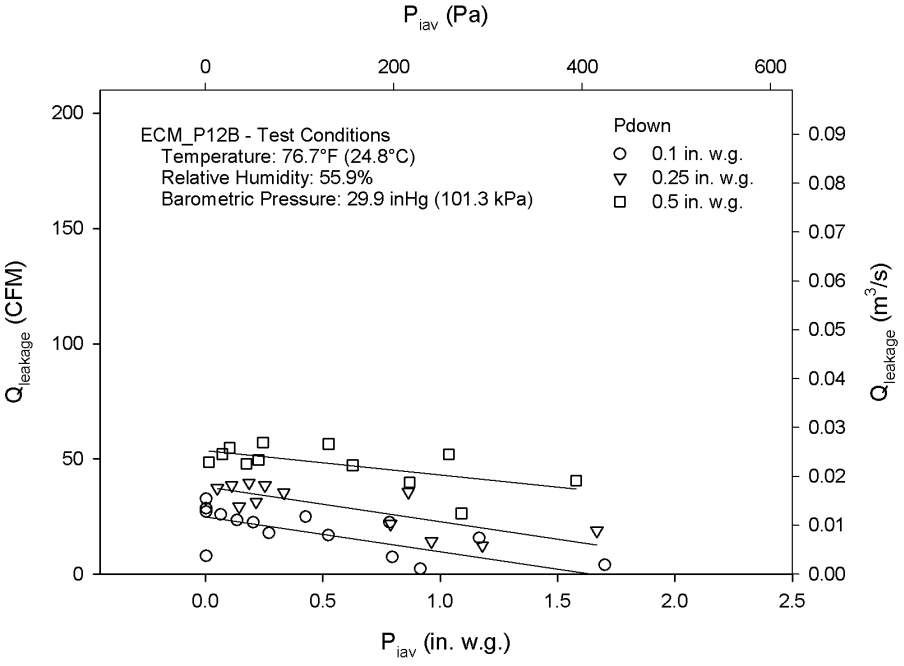

Figure B-19: Leakage vs. P_{iav} for ECM_P12B

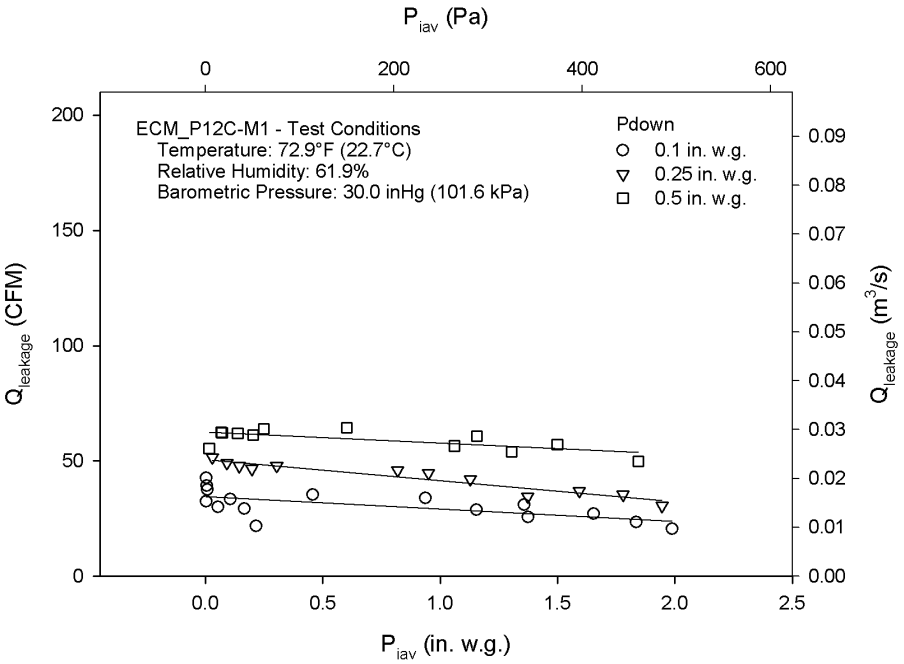

Figure B-20: Leakage vs. P_{iav} for ECM_P12C-M1

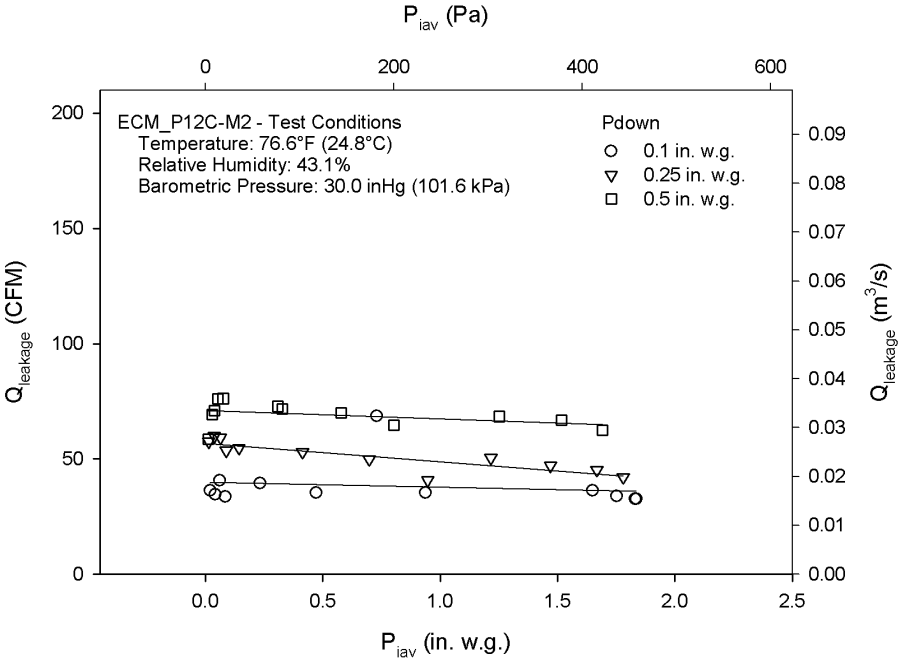

Figure B-21: Leakage vs. P_{iav} for ECM_P12C-M2

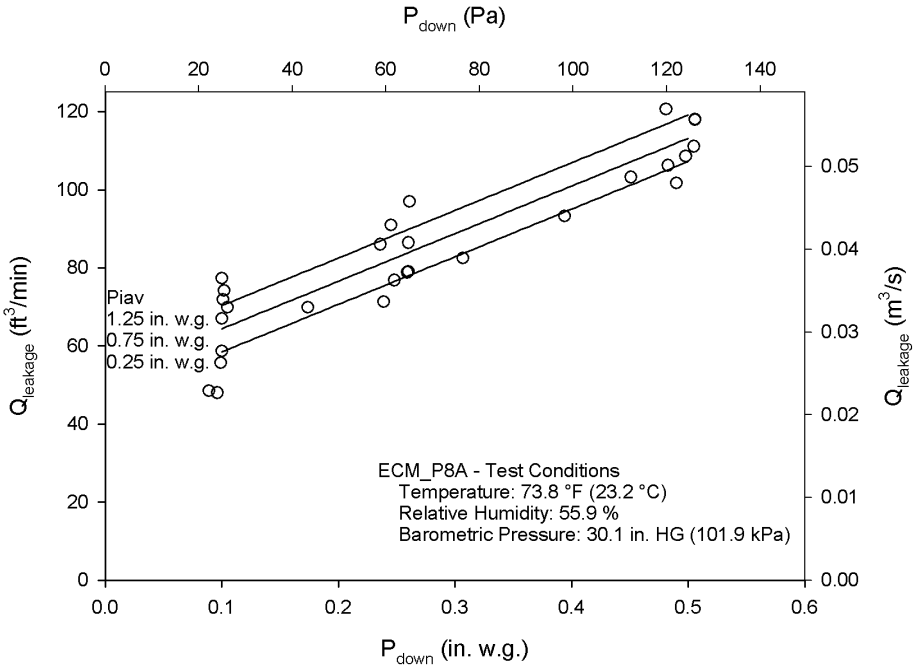

Figure B-22: Leakage vs. P_{down} for ECM_P8A

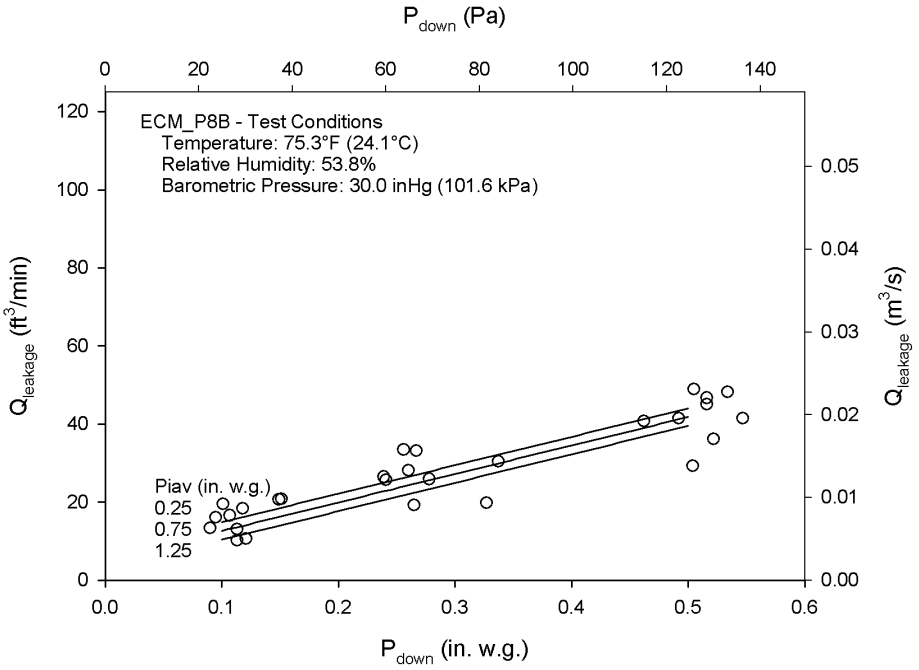

Figure B-23: Leakage vs. P_{down} for ECM_P8B

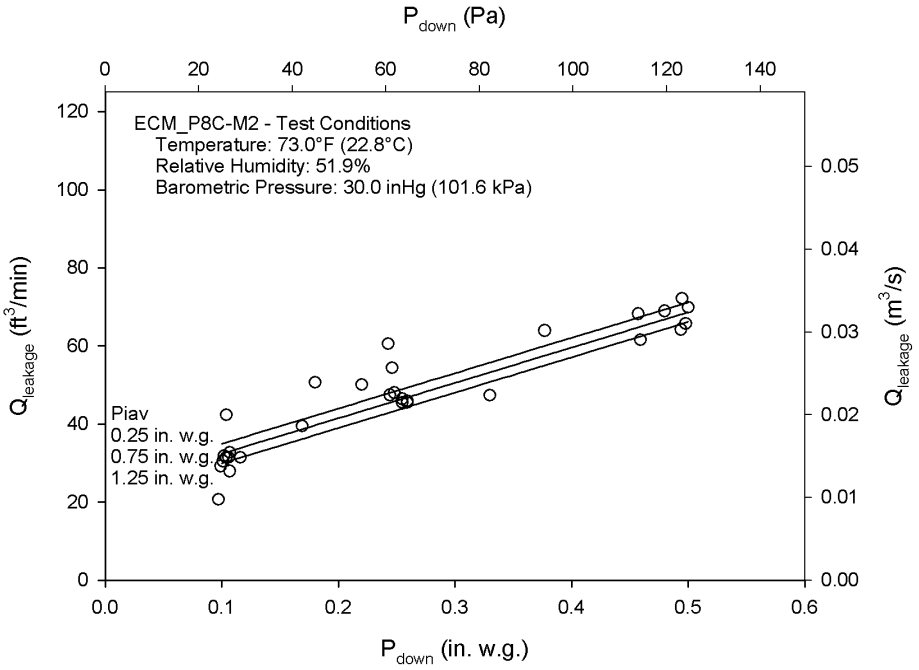

Figure B-24: Leakage vs. P_{down} for ECM_P8C-M2

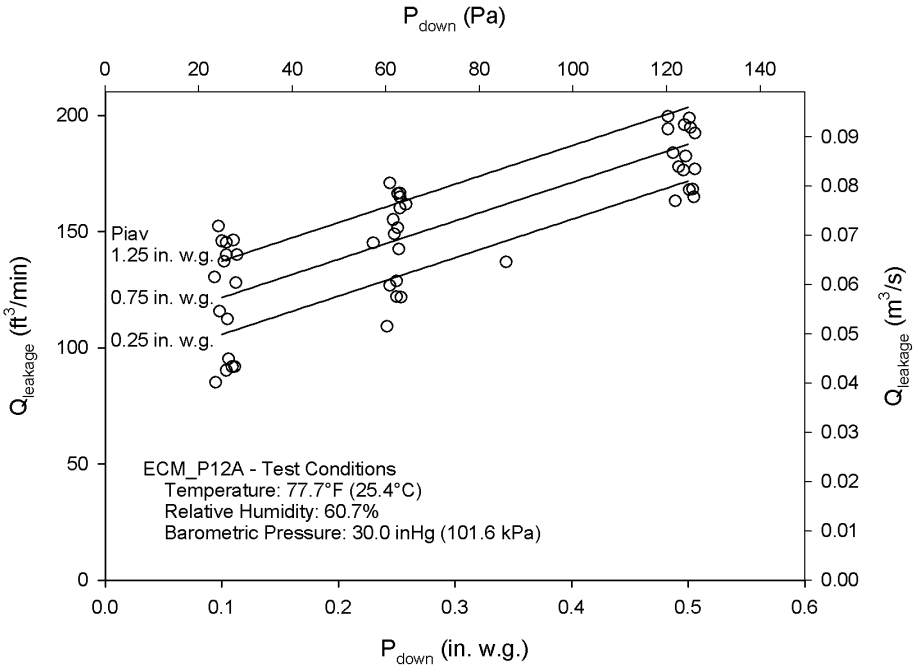

Figure B-25: Leakage vs. P_{down} for ECM_P12A

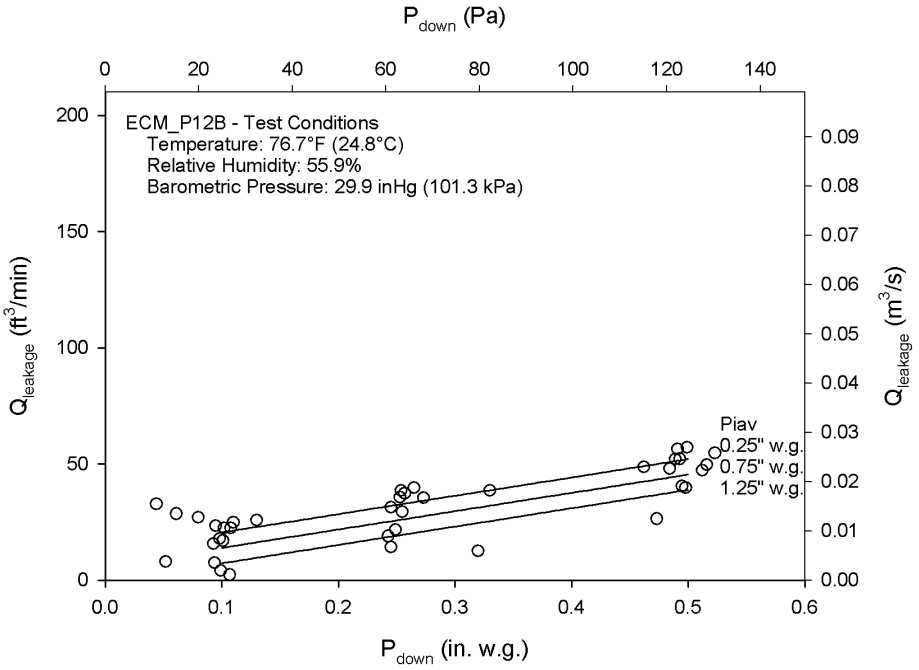

Figure B-26: Leakage vs. P_{down} for ECM_P12B

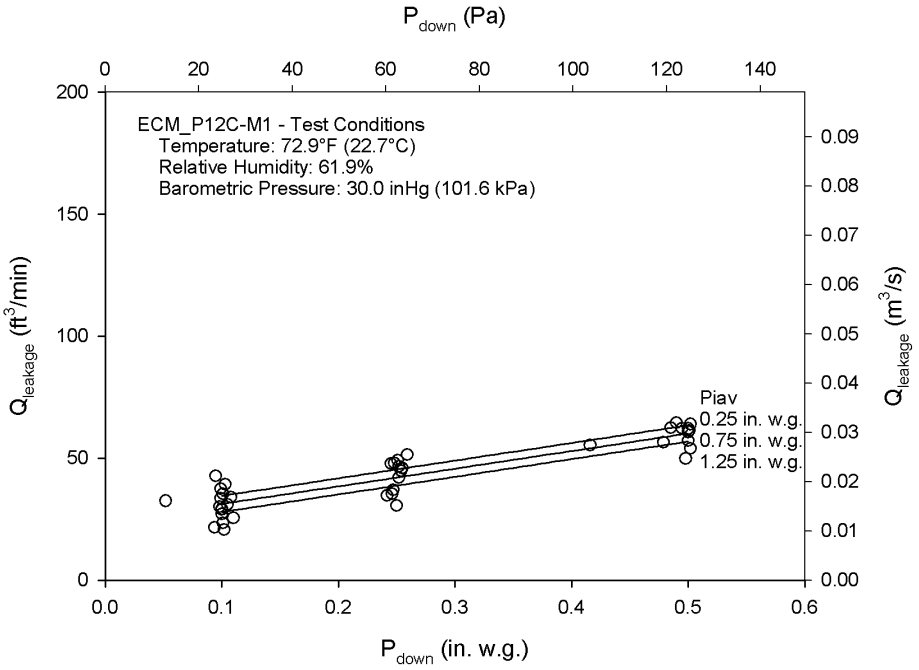

Figure B-27: Leakage vs. P_{down} for ECM_P12C-M1

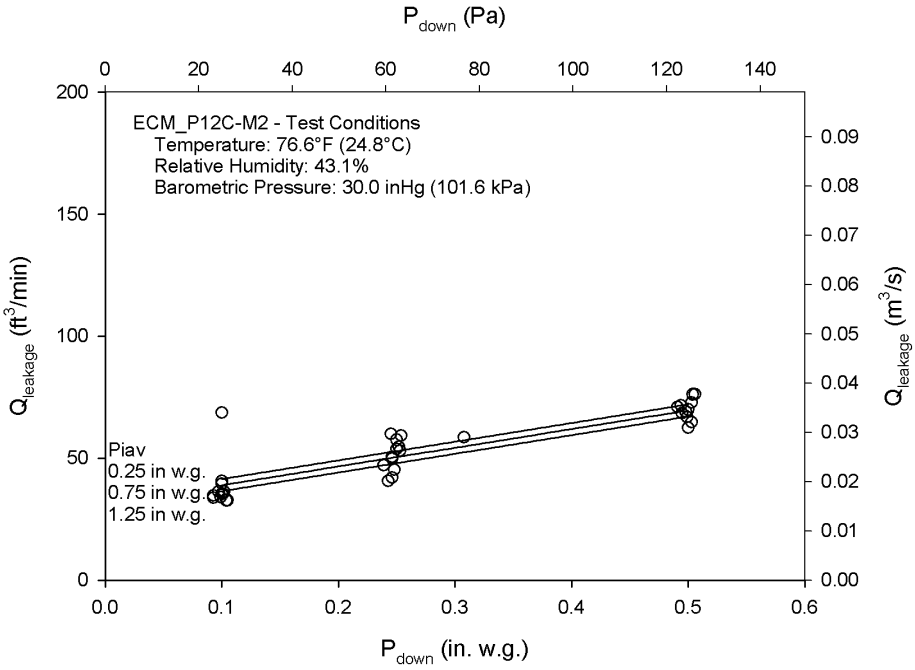

Figure B-28: Leakage vs. P_{down} for ECM_P12C-M2

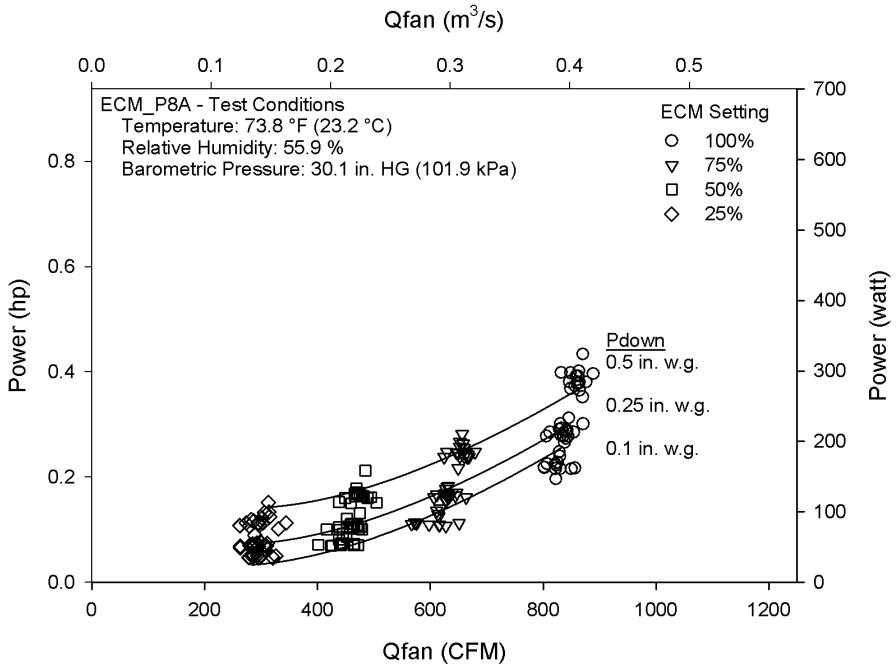

Figure B-29: Power vs. Q_{fan} for ECM_P8A

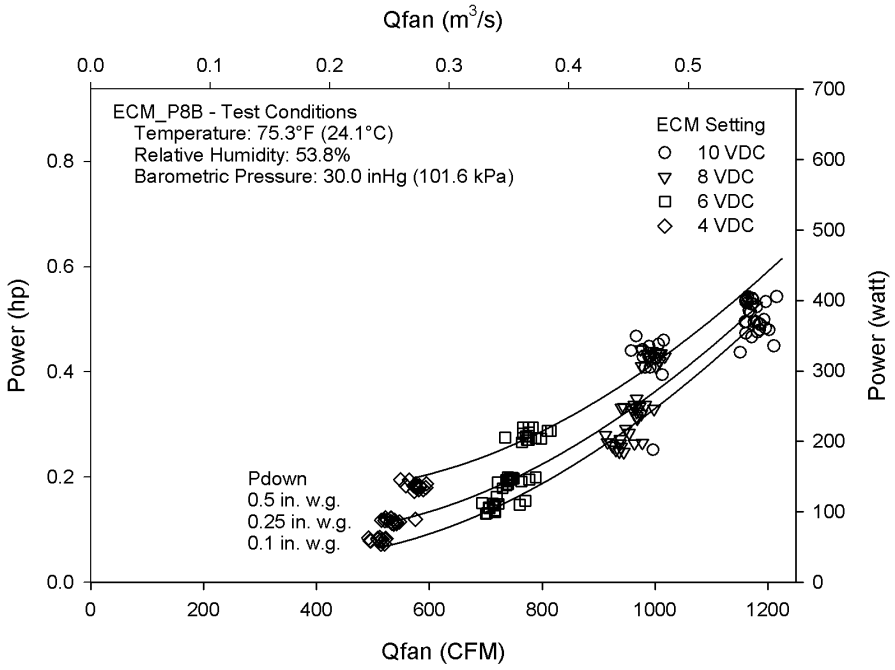

Figure B-30: Power vs. Q_{fan} for ECM_P8B

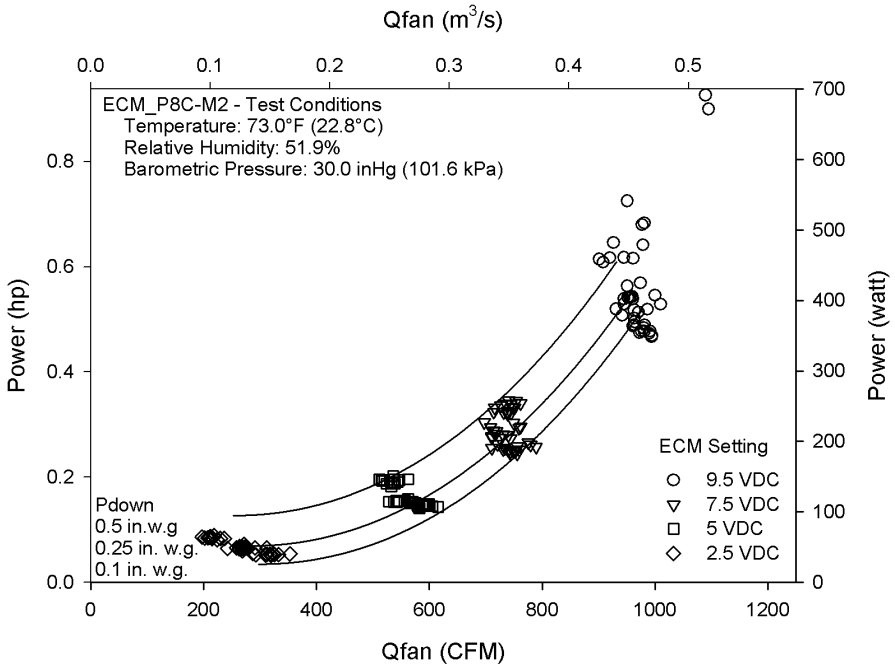

Figure B-31: Power vs. Q_{fan} for ECM_P8C-M2

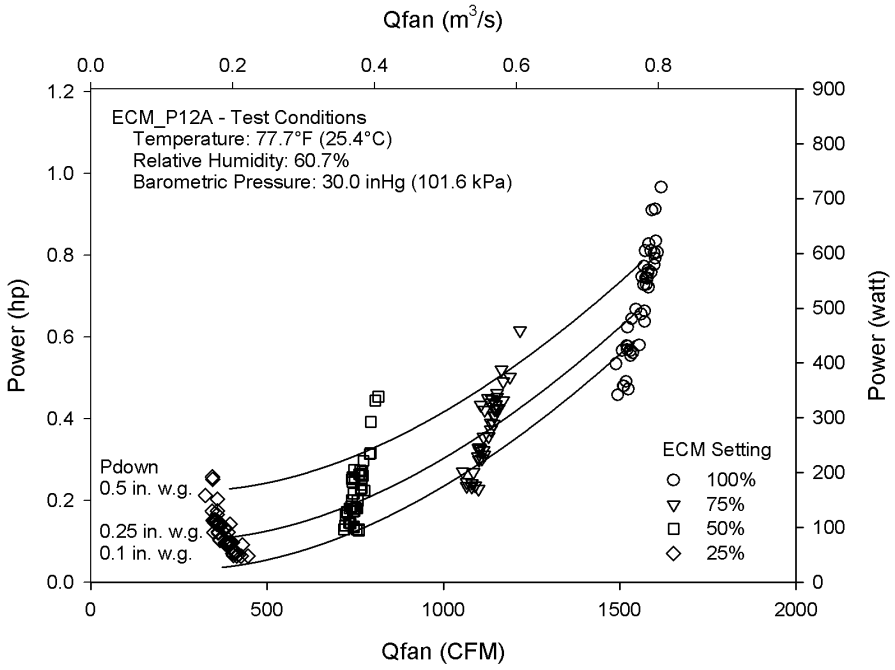

Figure B-32: Power vs. Q_{fan} for ECM_P12A

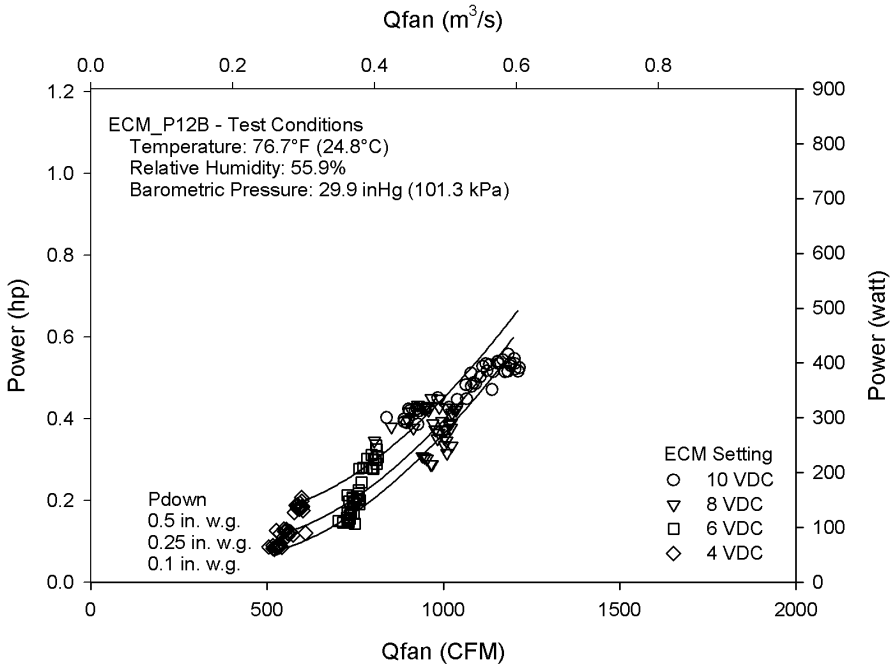

Figure B-33: Power vs. Q_{fan} for ECM_P12B

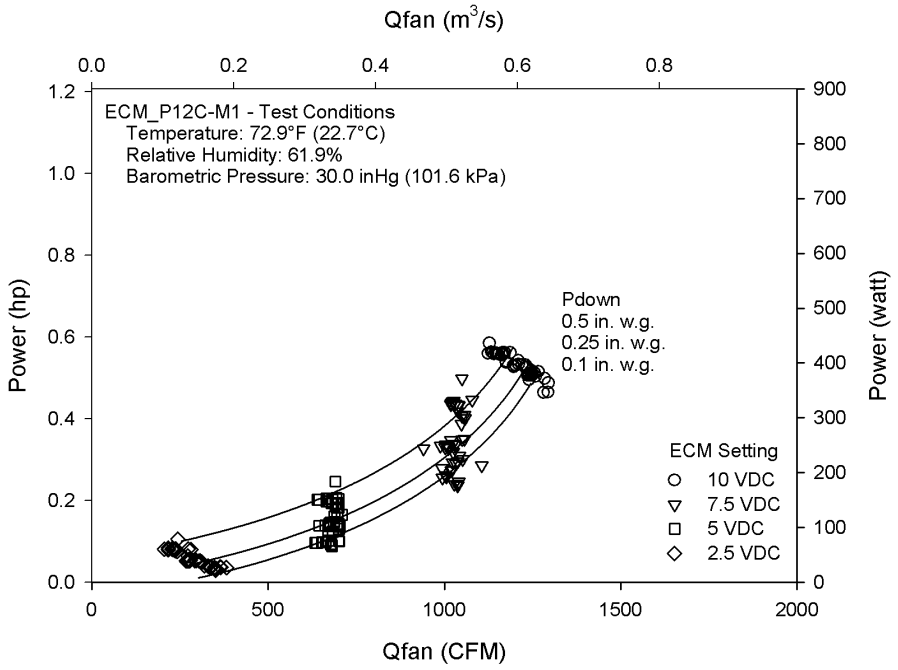

Figure B-34: Power vs. Q_{fan} for ECM_P12C-M1

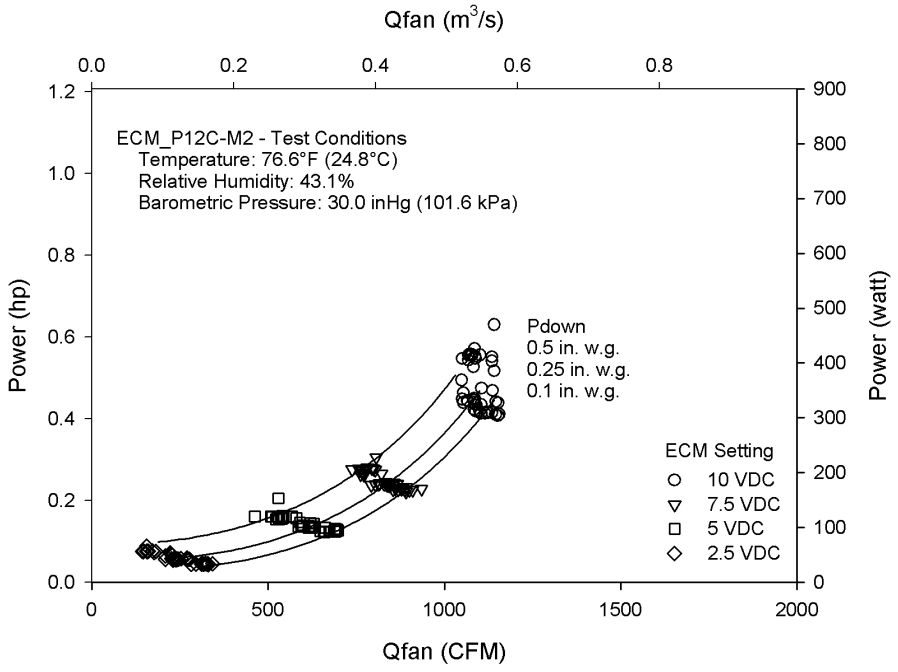

Figure B-35: Power vs. Q_{fan} for ECM_P12C-M2

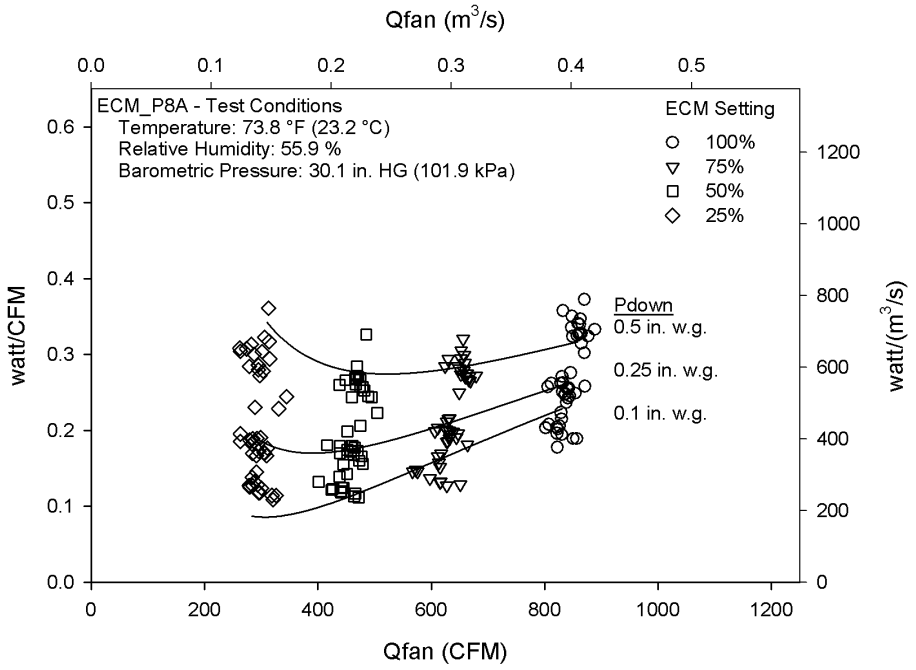

Figure B-36: Watt/CFM vs. Q_{fan} for ECM_P8A

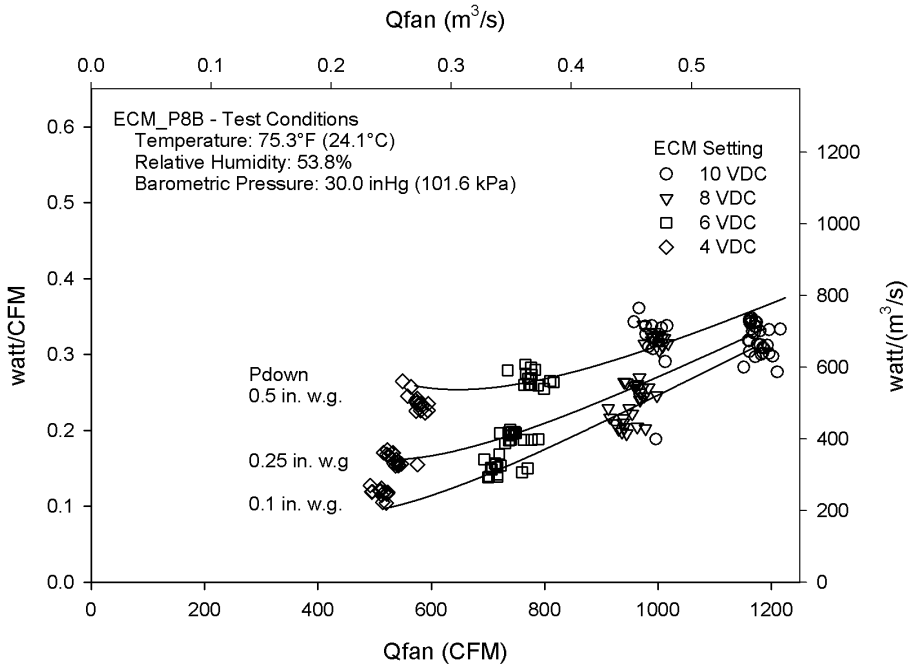

Figure B-37: Watt/CFM vs. Q_{fan} for ECM_P8B

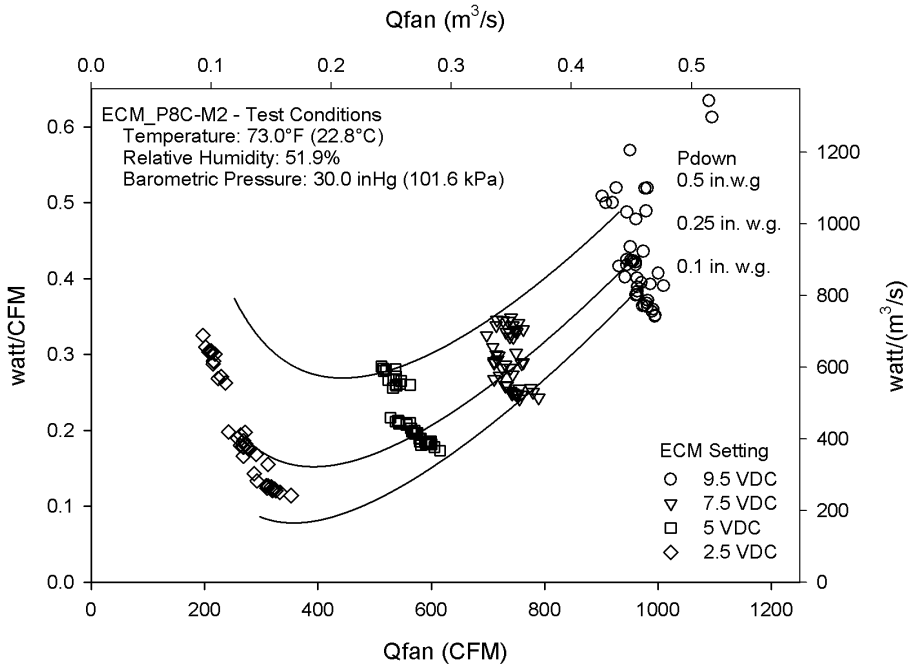

Figure B-38: Watt/CFM vs. Q_{fan} for ECM_P8C-M2

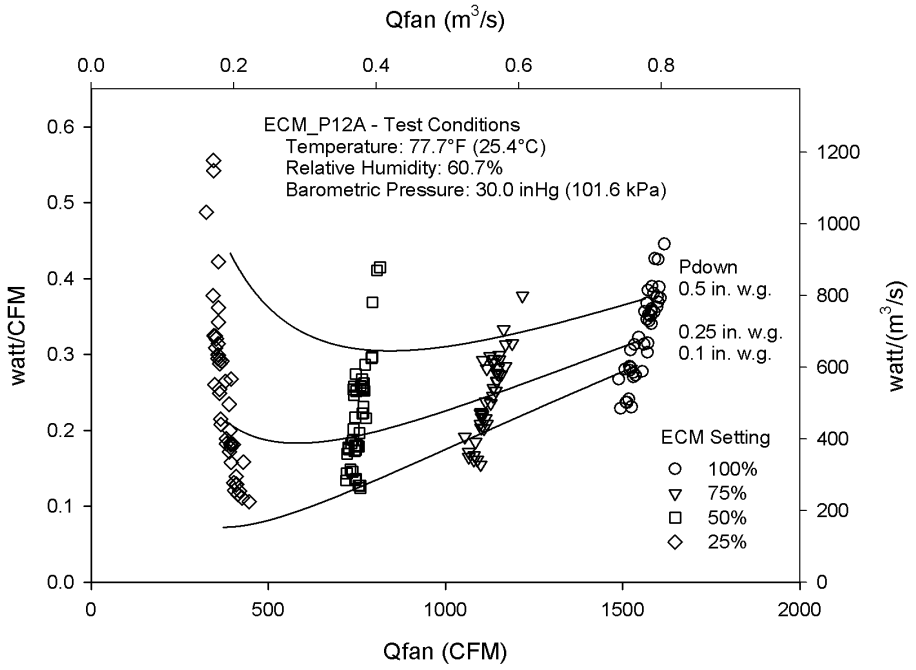

Figure B-39: Watt/CFM vs. Q_{fan} for ECM_P12A

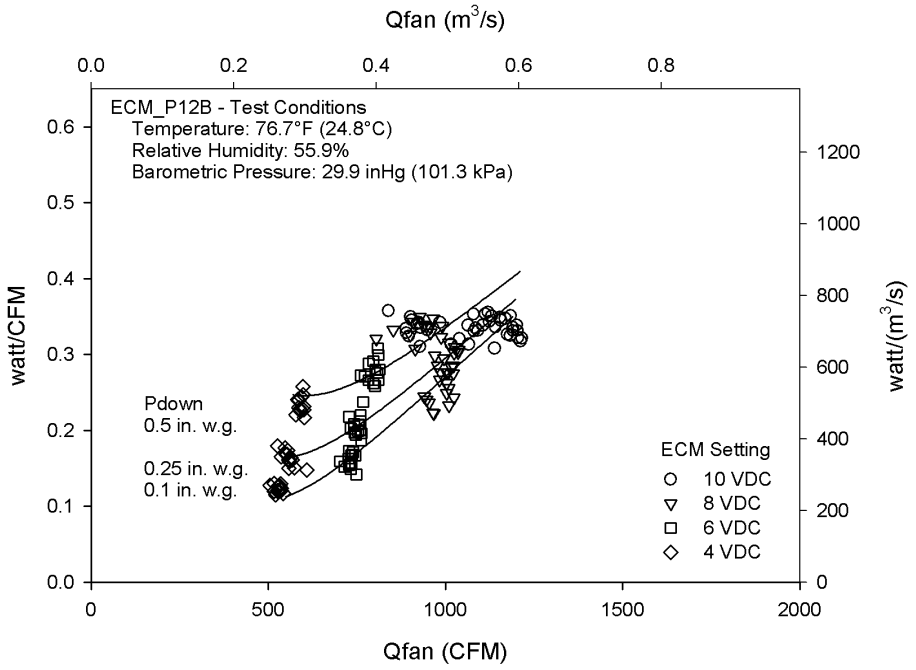

Figure B-40: Watt/CFM vs. Q_{fan} for ECM_P12B

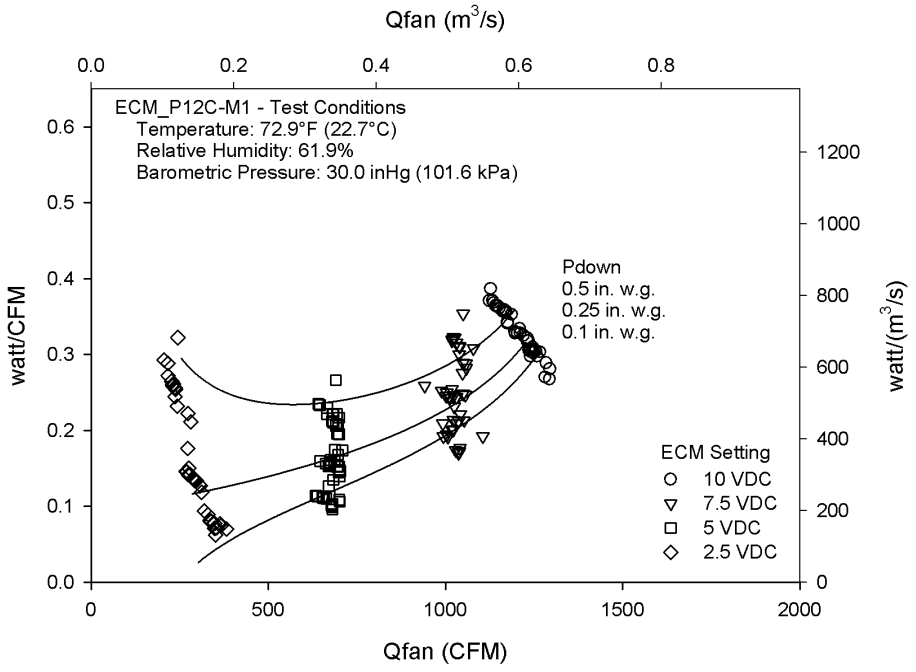

Figure B-41: Watt/CFM vs. Q_{fan} for ECM_P12C-M1

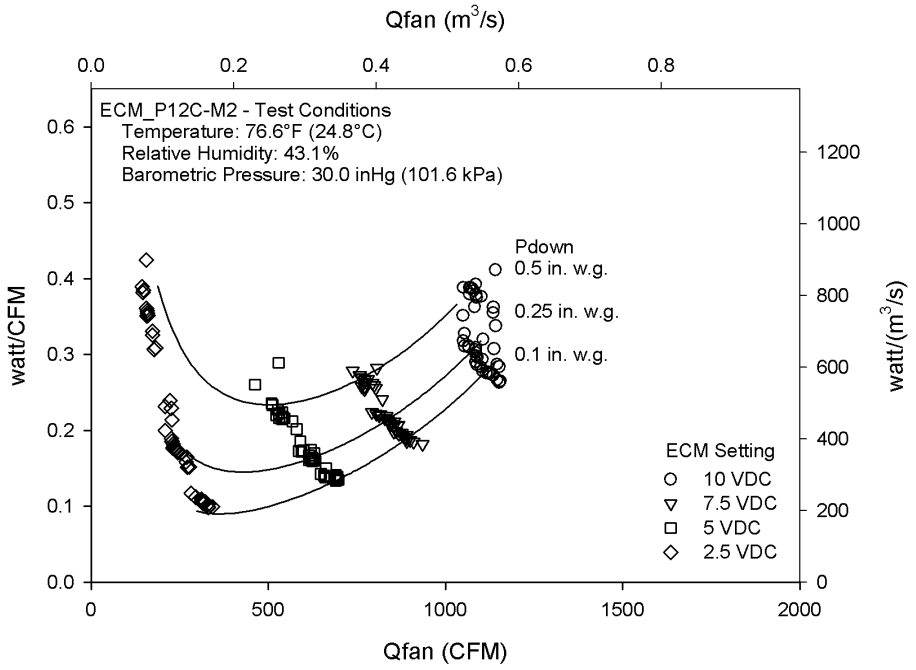

Figure B-42: Watt/CFM vs. Q_{fan} for ECM_P12C-M2

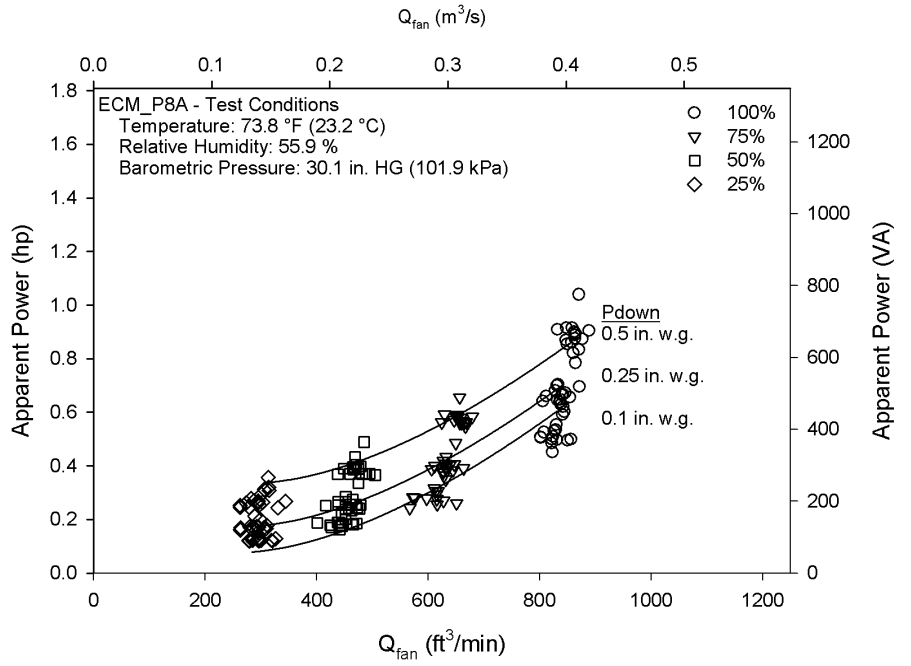

Figure B-43: Apparent Power vs. Q_{fan} for ECM_P8A

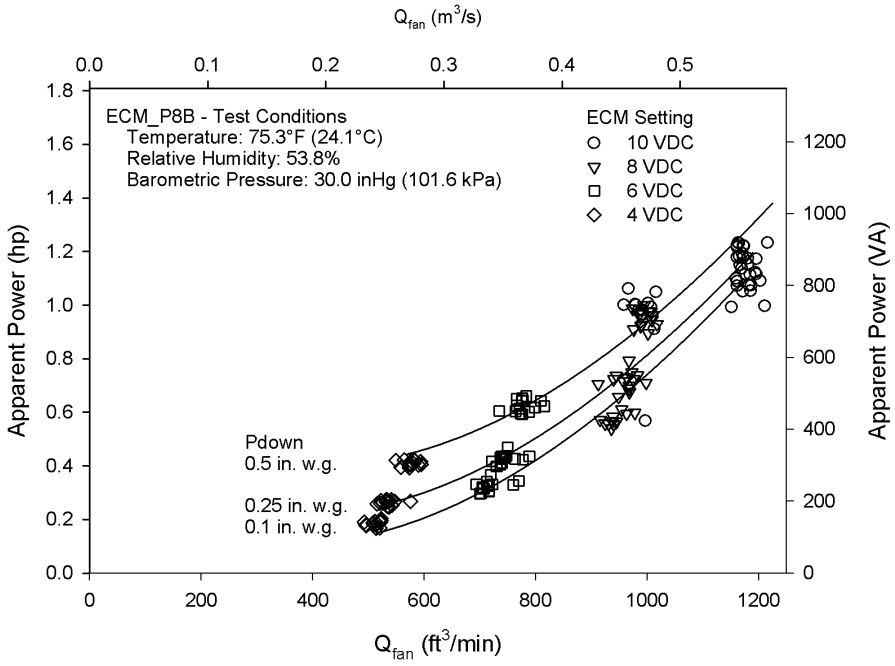

Figure B-44: Apparent Power vs. Q_{fan} for ECM_P8B

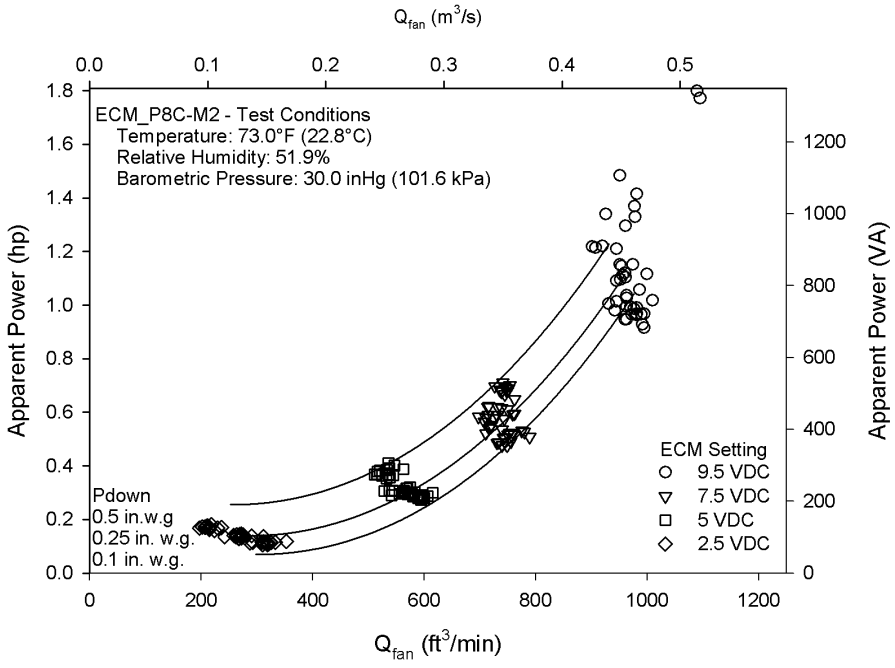

Figure B-45: Apparent Power vs. Q_{fan} for ECM_P8C-M2

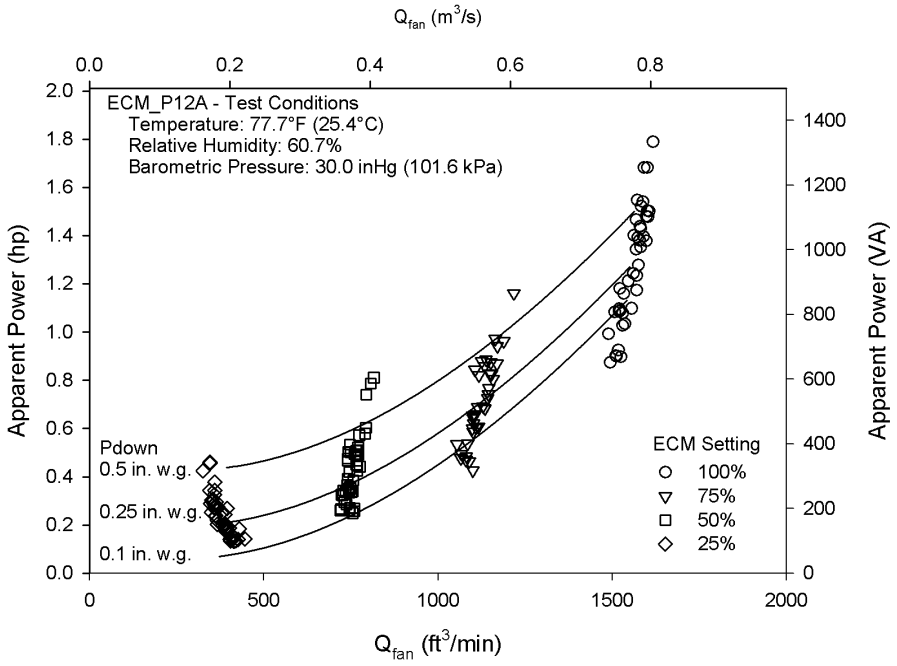

Figure B-46: Apparent Power vs. Q_{fan} for ECM_P12A

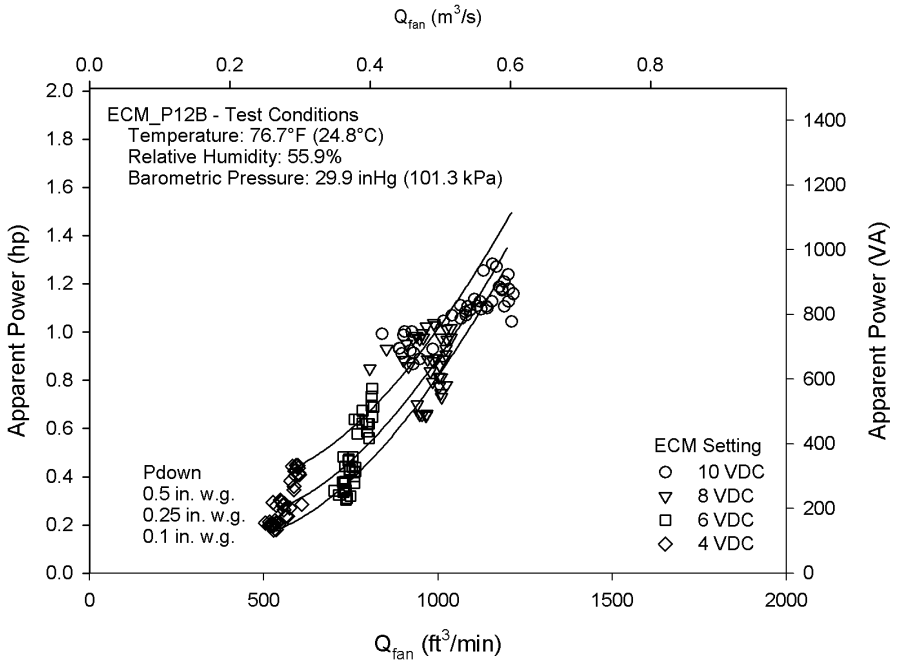

Figure B-47: Apparent Power vs. Q_{fan} for ECM_P12B

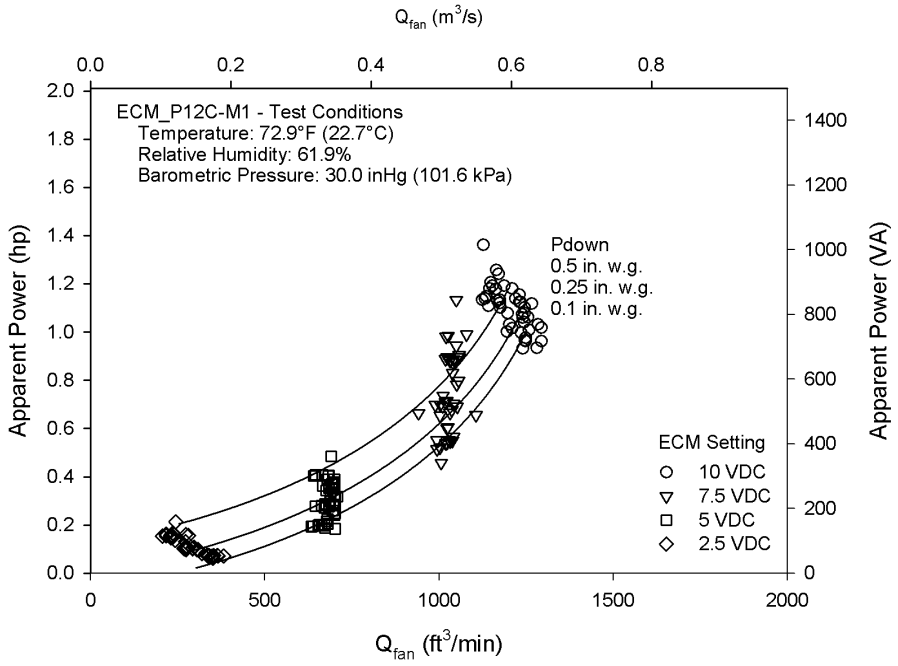

Figure B-48: Apparent Power vs. Q_{fan} for ECM_P12C-M1

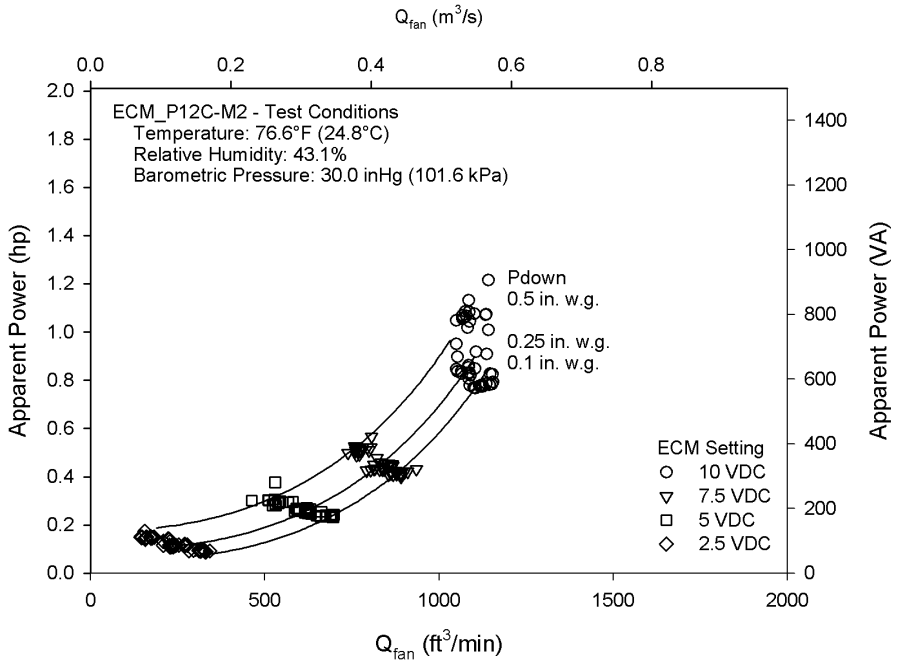

Figure B-49: Apparent Power vs. Q_{fan} for ECM_P12C-M2

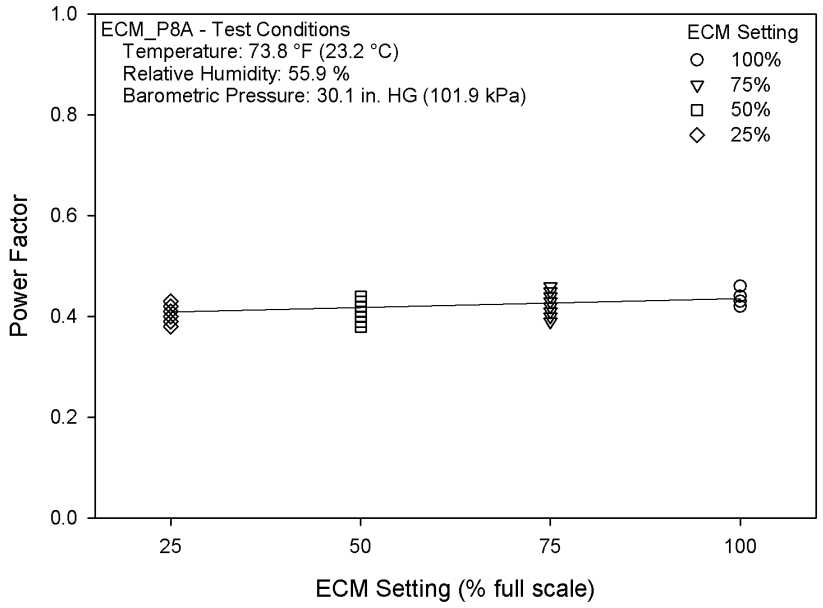

Figure B-50: Power Factor vs. ECM Input Setting for ECM_P8A

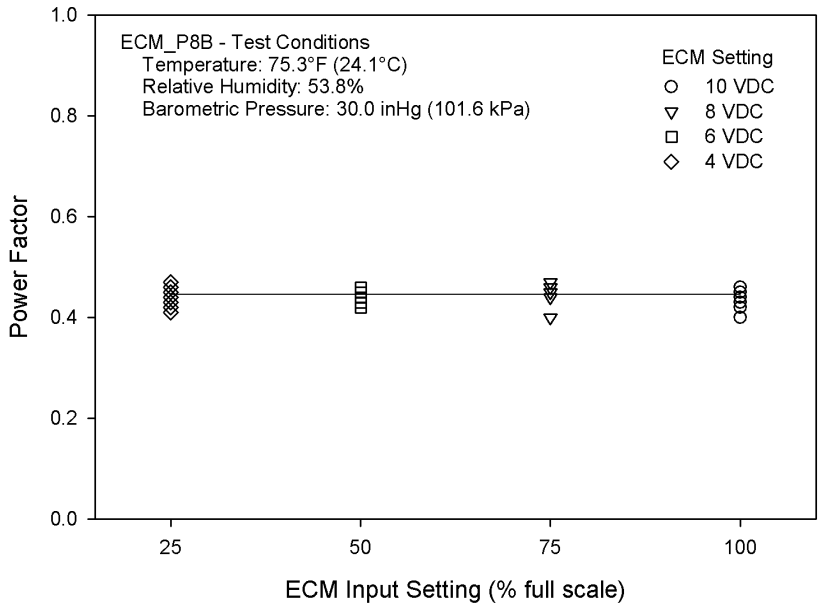

Figure B-51: Power Factor vs. ECM Input Setting for ECM_P8B

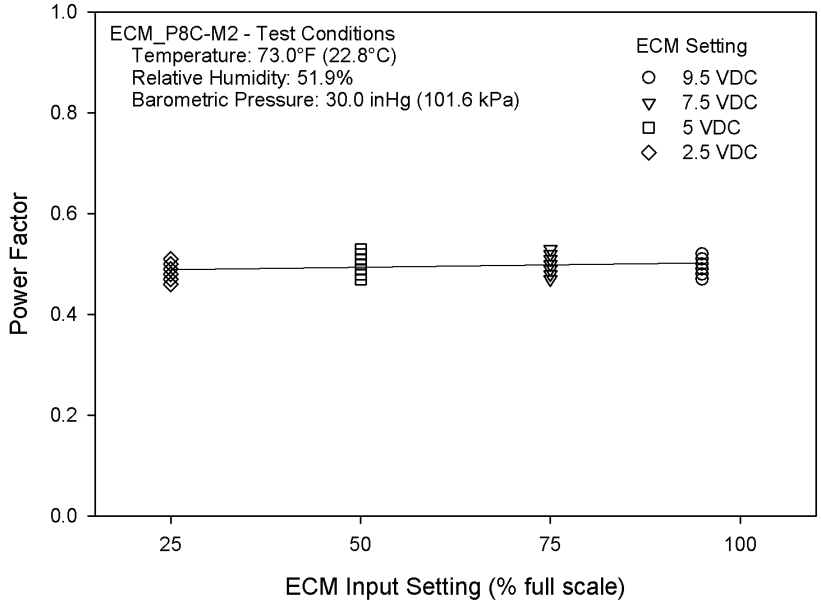

Figure B-52: Power Factor vs. ECM Input Setting for ECM_P8C-M2

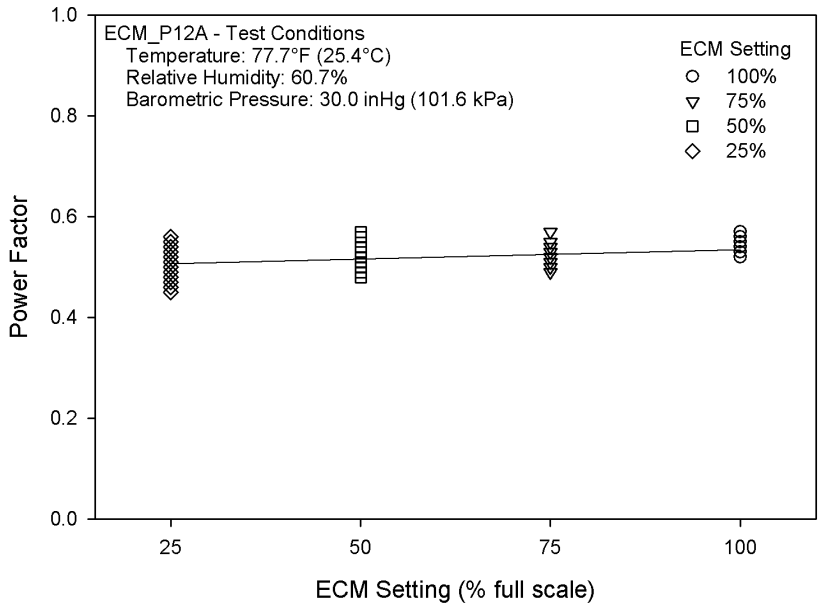

Figure B-53: Power Factor vs. ECM Input Setting for ECM_P12A

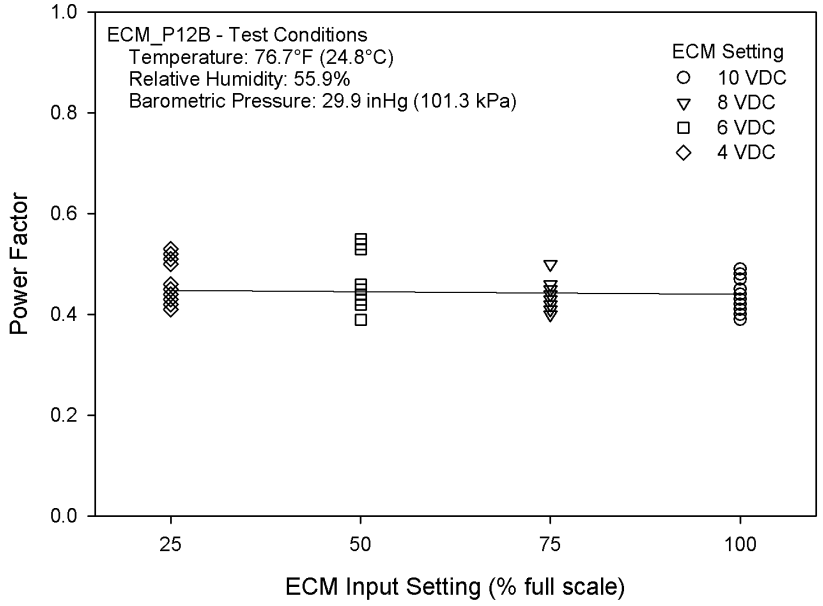

Figure B-54: Power Factor vs. ECM Input Setting for ECM_P12B

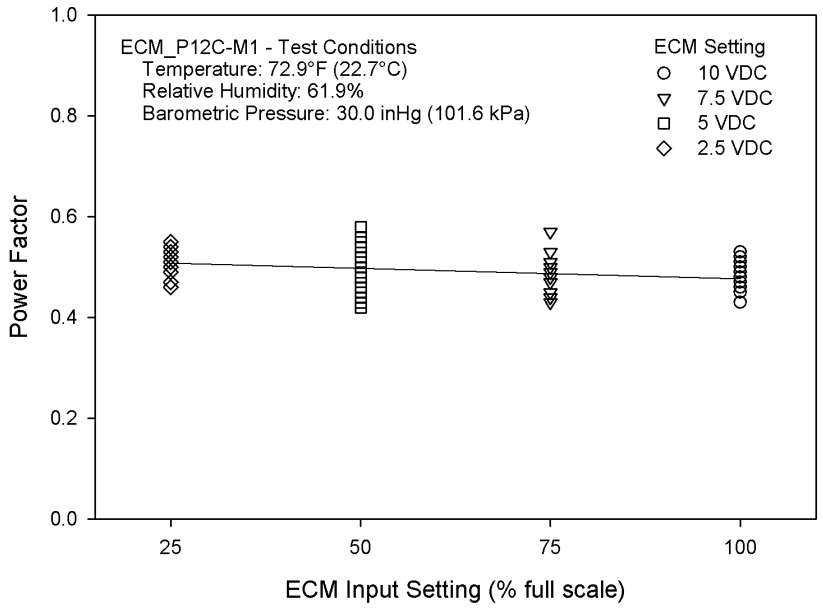

Figure B-55: Power Factor vs. ECM Input Setting for ECM_P12C-M1

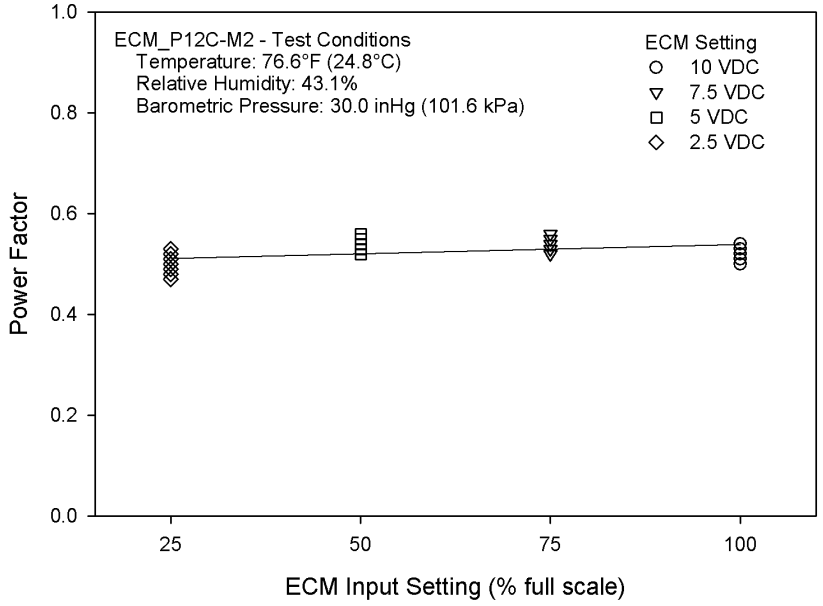

Figure B-56: Power Factor vs. ECM Input Setting for ECM_P12C-M2

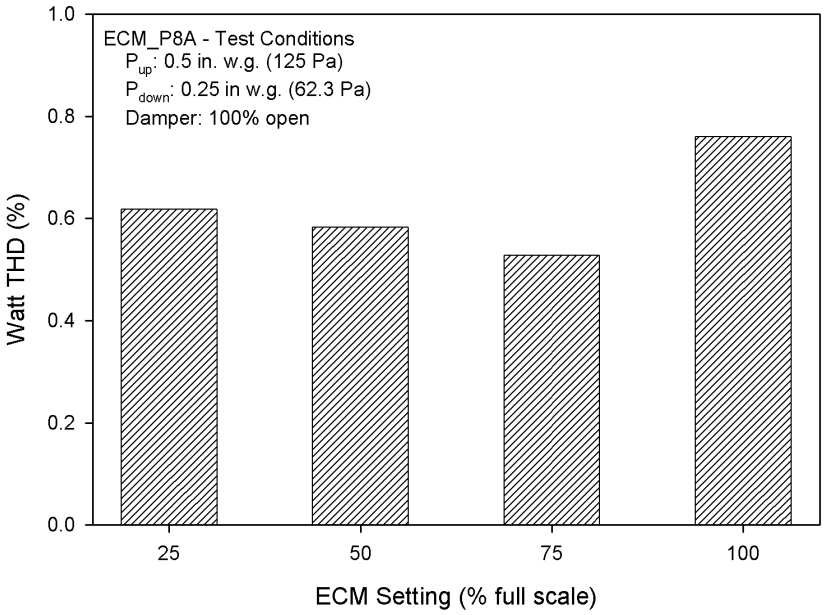

Figure B-57: Real Power THD (%) vs. ECM Input Setting for ECM_P8A

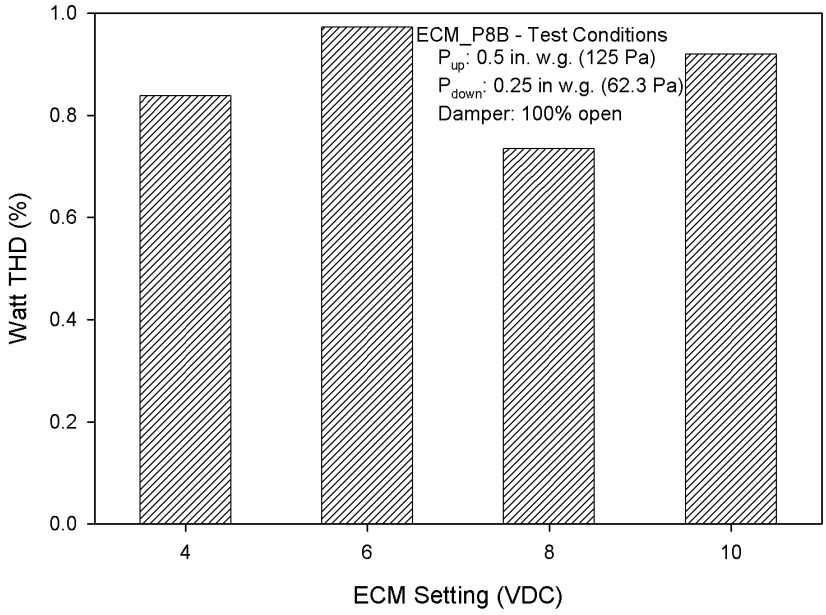

Figure B-58: Real Power THD (%) vs. ECM Input Setting for ECM_P8B

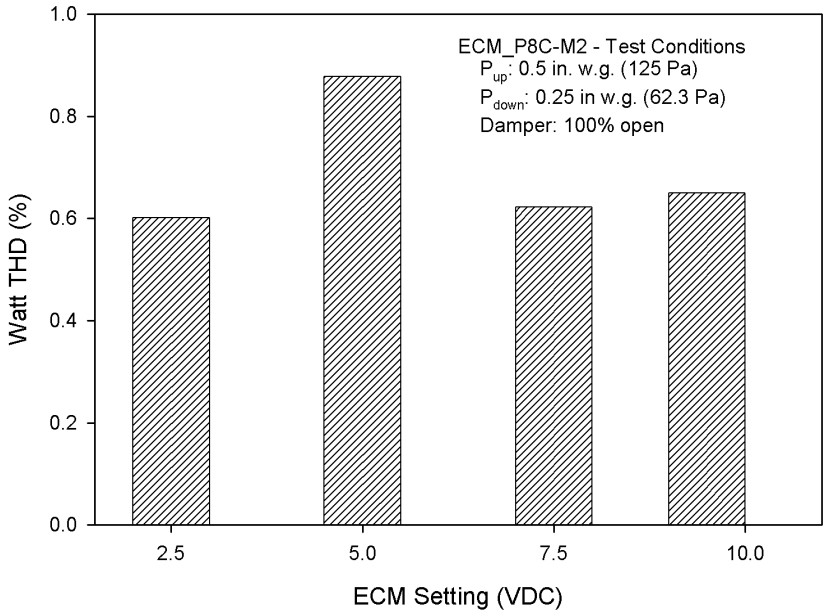

Figure B-59: Real Power THD (%) vs. ECM Input Setting for ECM_P8C-M2

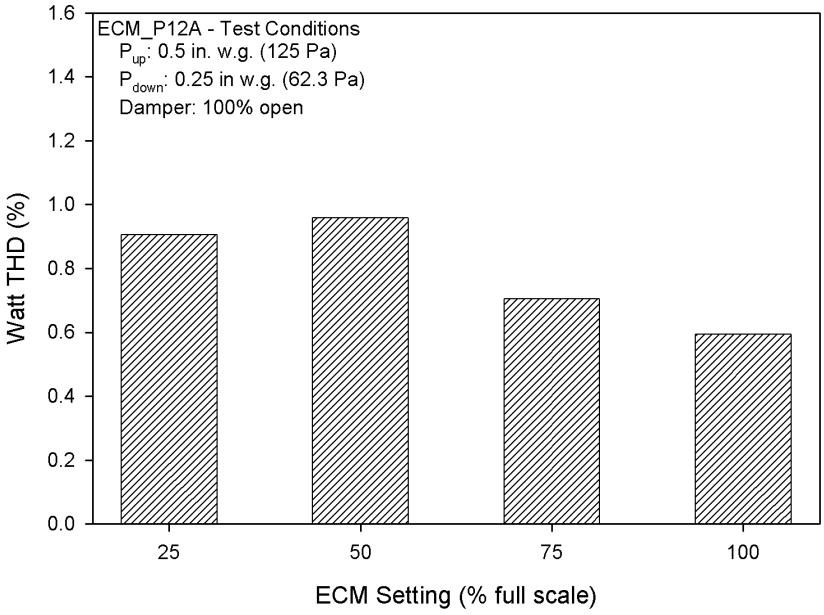

Figure B-60: Real Power THD (%) vs. ECM Input Setting for ECM_P12A

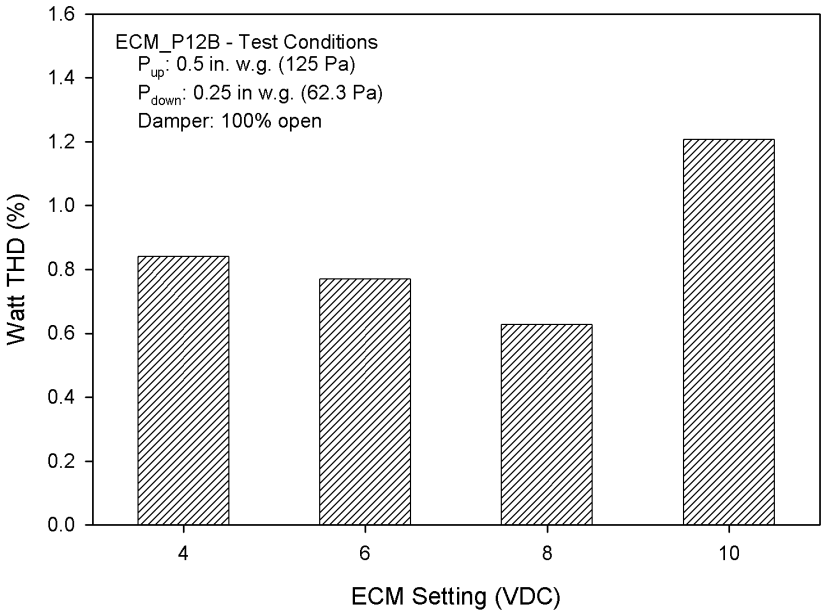

Figure B-61: Real Power THD (%) vs. ECM Input Setting for ECM_P12B

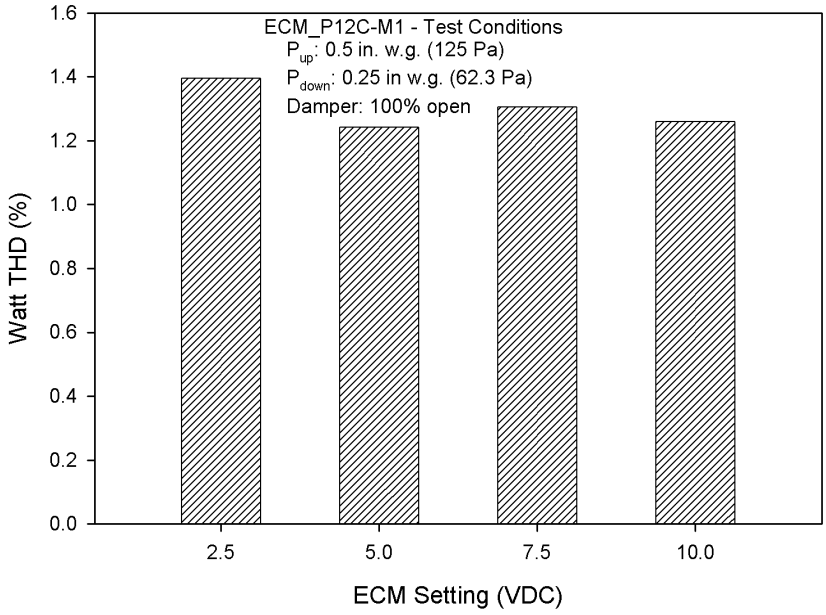

Figure B-62: Real Power THD (%) vs. ECM Input Setting for ECM_P12C-M1

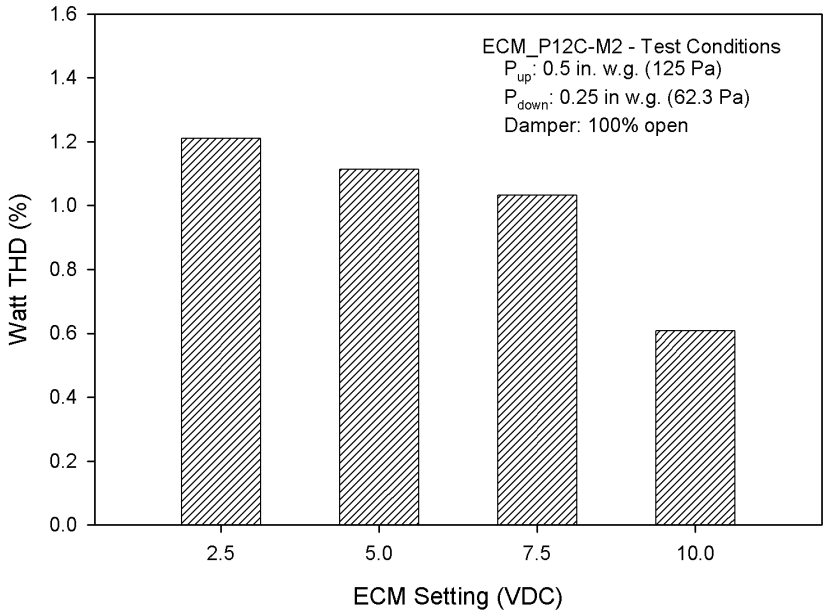

Figure B-63: Real Power THD (%) vs. ECM Input Setting for ECM_P12C-M2

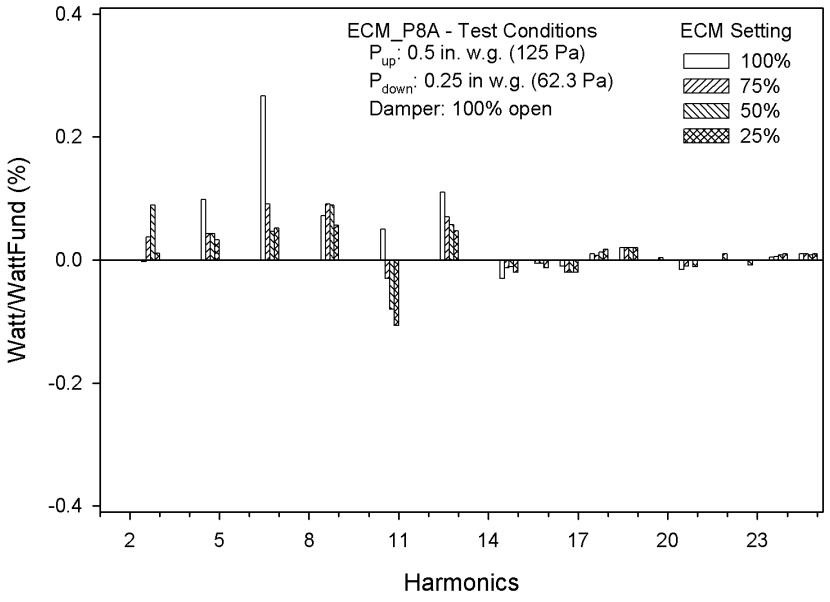

Figure B-64: Real Power Harmonics (%) for ECM_P8A

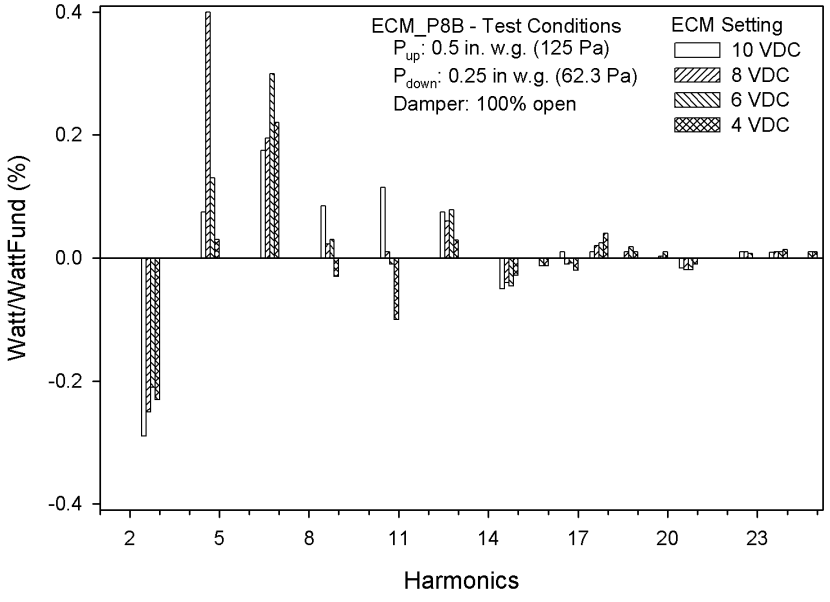

Figure B-65: Real Power Harmonics (%) for ECM_P8B

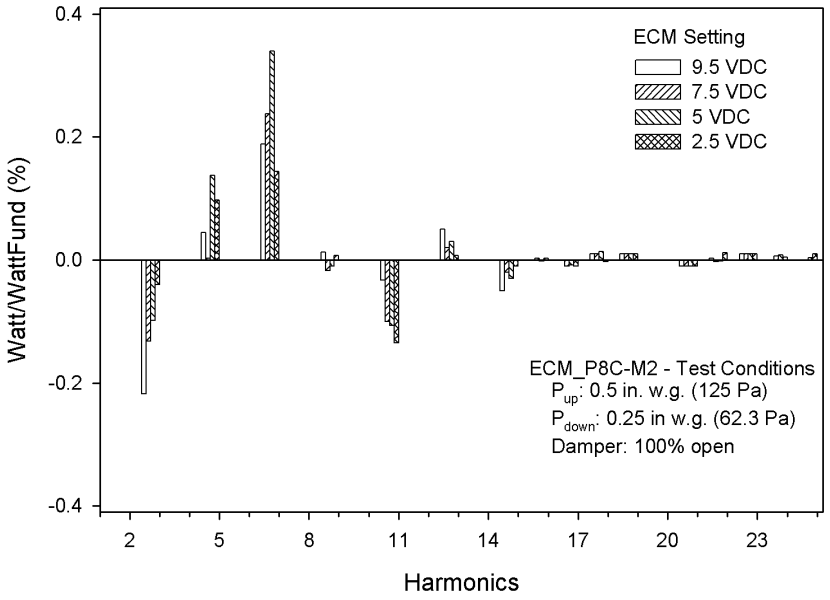

Figure B-66: Real Power Harmonics (%) for ECM_P8C-M2

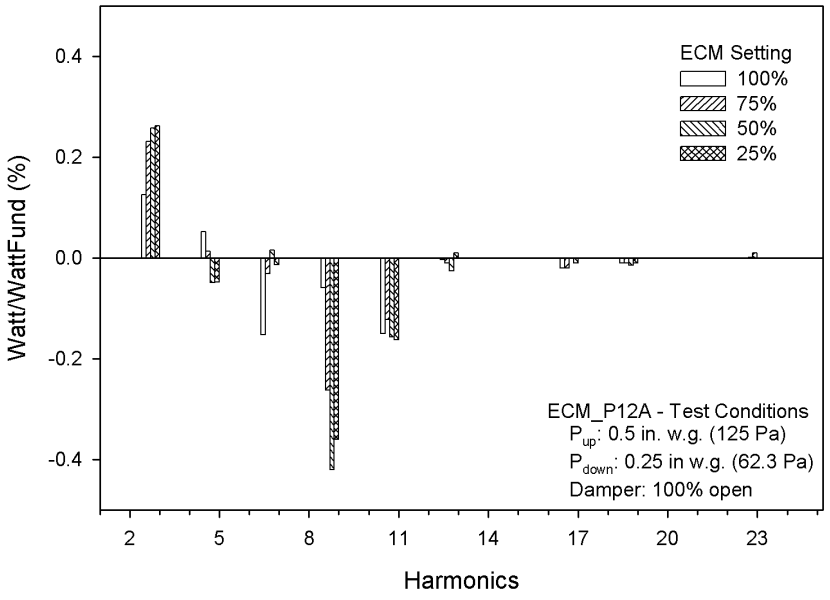

Figure B-67: Real Power Harmonics (%) for ECM_P12A

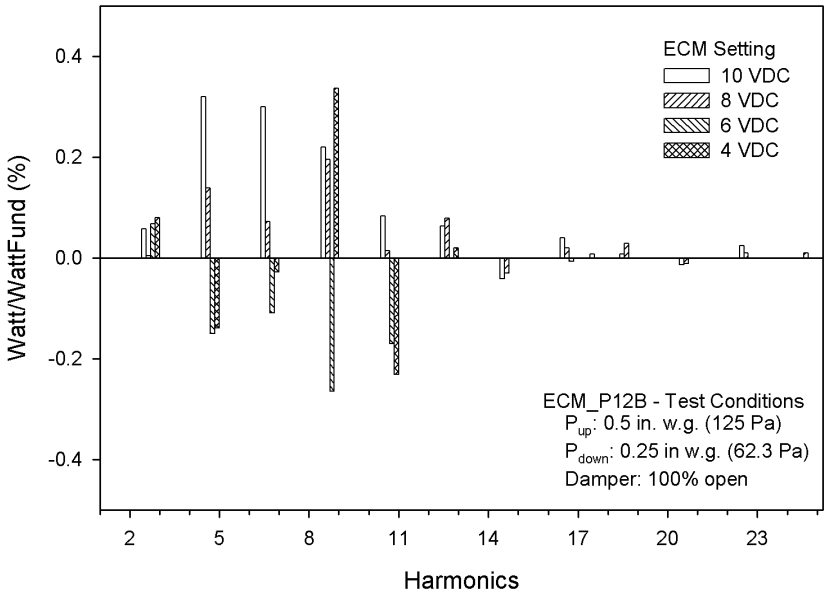

Figure B-68: Real Power Harmonics (%) for ECM_P12B

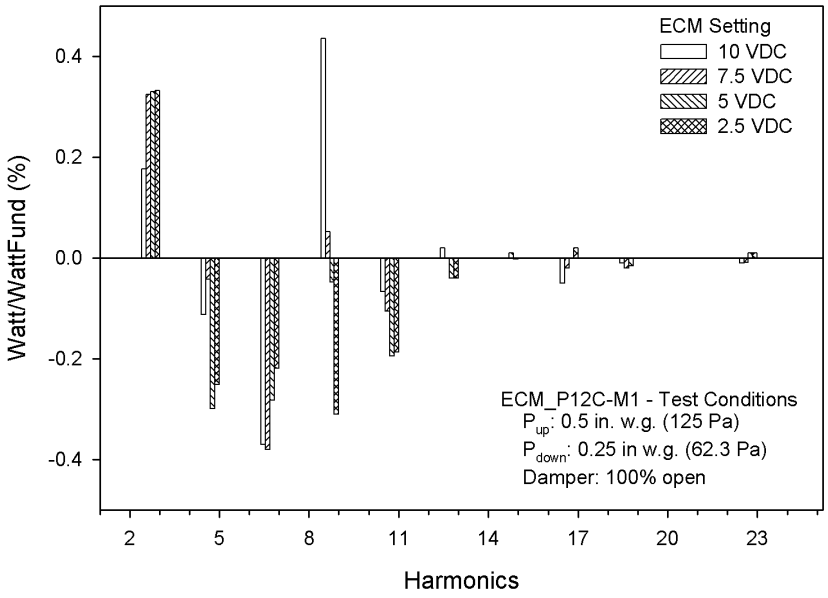

Figure B-69: Real Power Harmonics (%) for ECM_P12C-M1

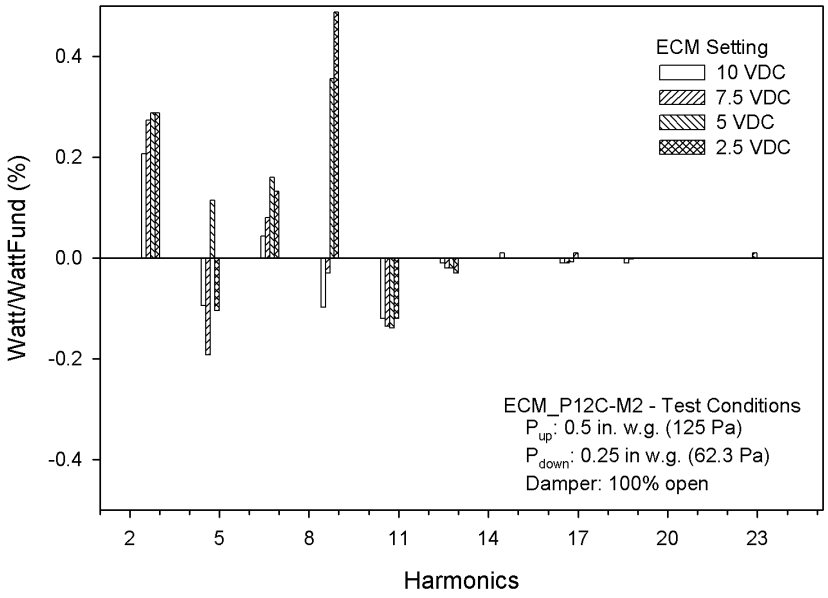

Figure B-70: Real Power Harmonics (%) for ECM_P12C-M2

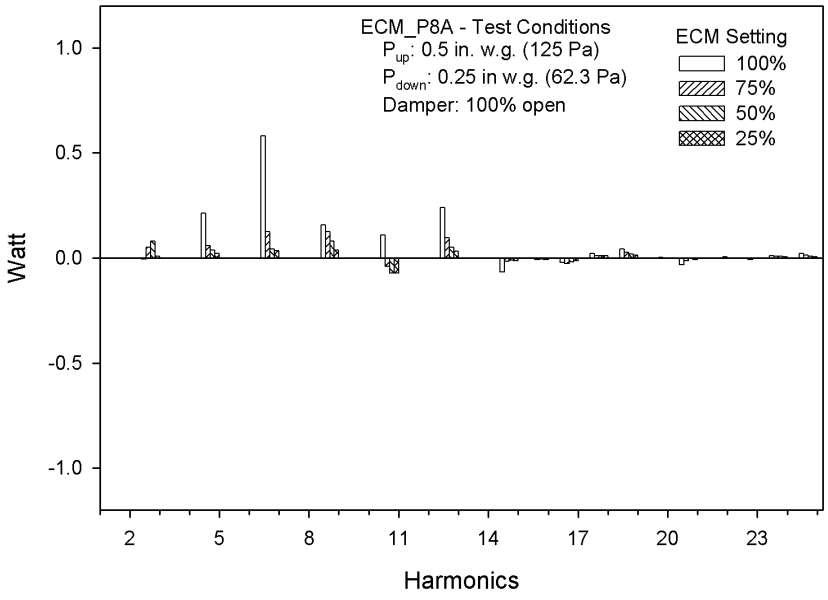

Figure B-71: Real Power Harmonics (Watts) for ECM_P8A

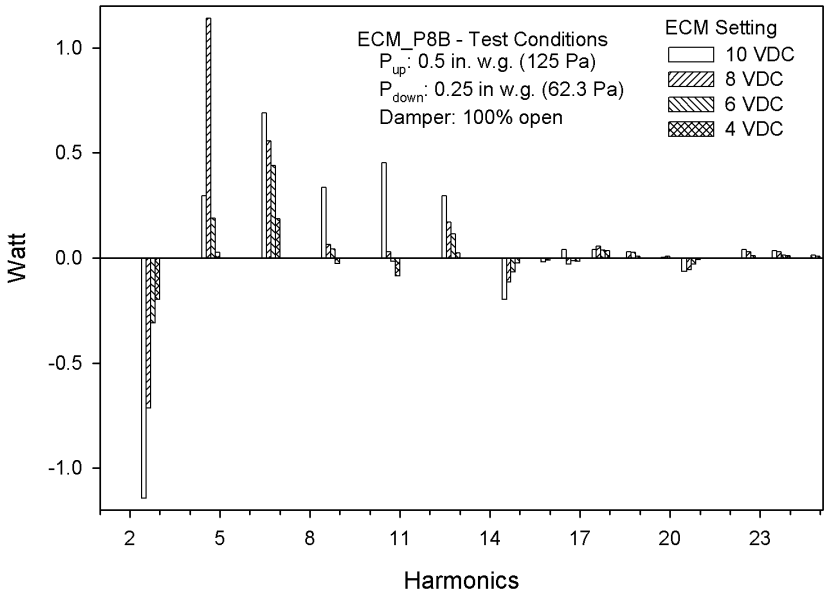

Figure B-72: Real Power Harmonics (Watts) for ECM_P8B

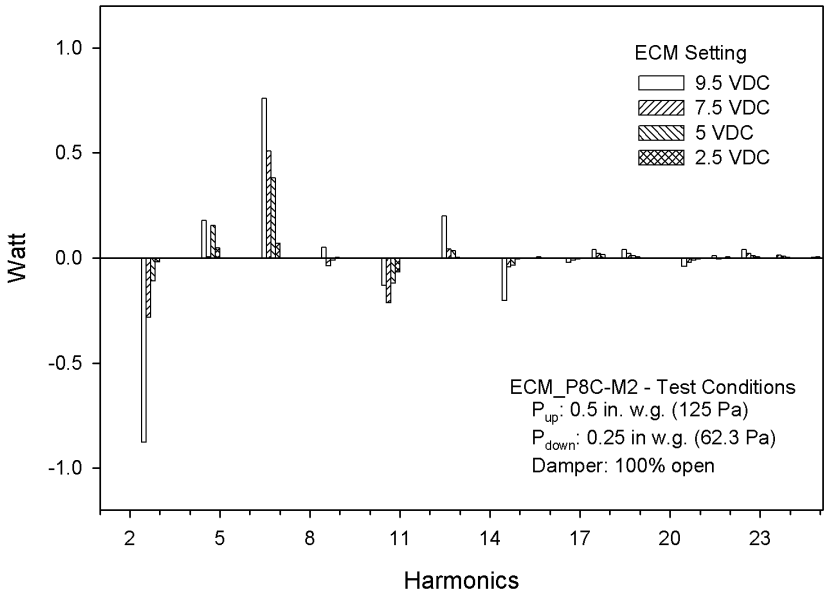

Figure B-73: Real Power Harmonics (Watts) for ECM_P8C-M2

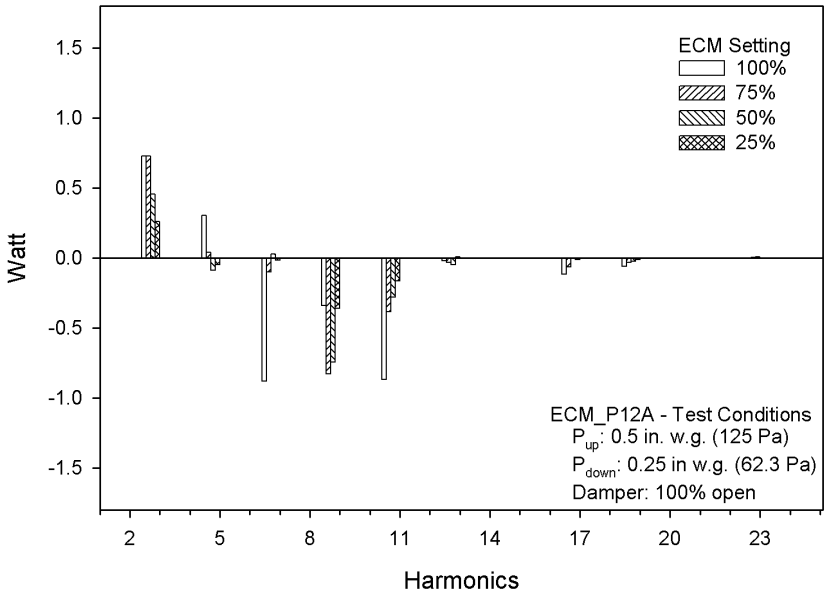

Figure B-74: Real Power Harmonics (Watts) for ECM_P12A

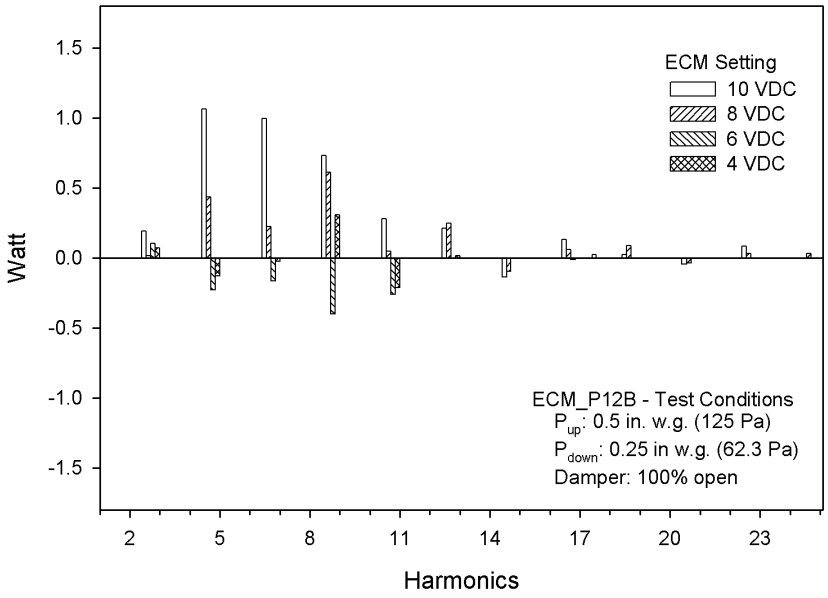

Figure B-75: Real Power Harmonics (Watts) for ECM_P12B

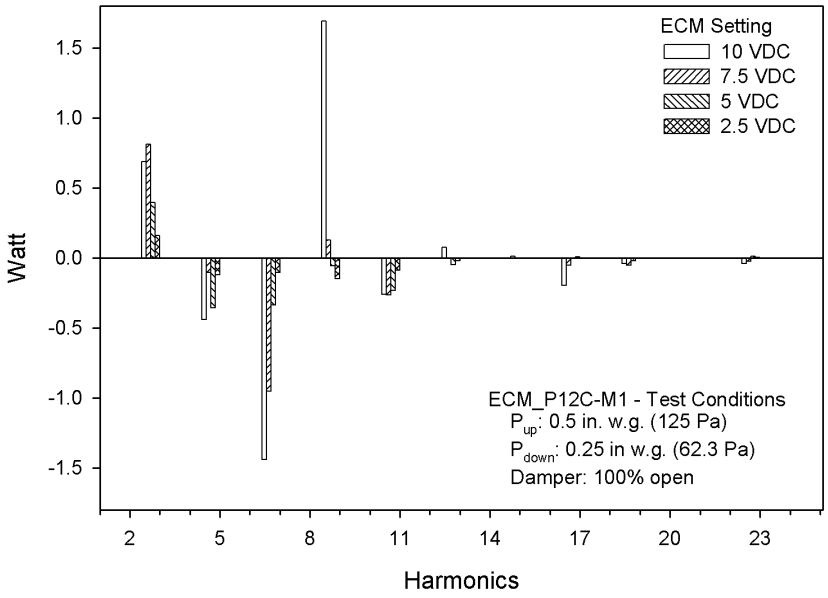

Figure B-76: Real Power Harmonics (Watts) for ECM_P12C-M1

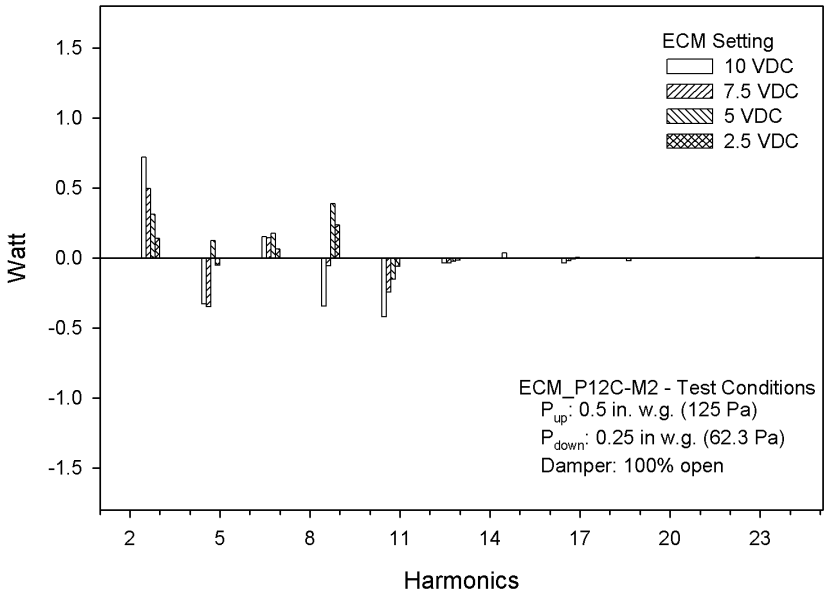

Figure B-77: Real Power Harmonics (Watts) for ECM_P12C-M2

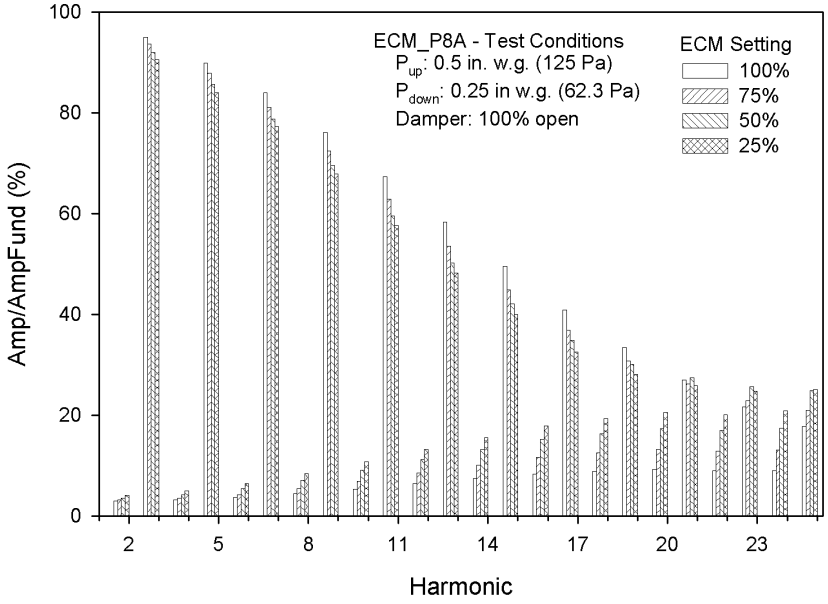

Figure B-78: Current Harmonics (%) for ECM_P8A

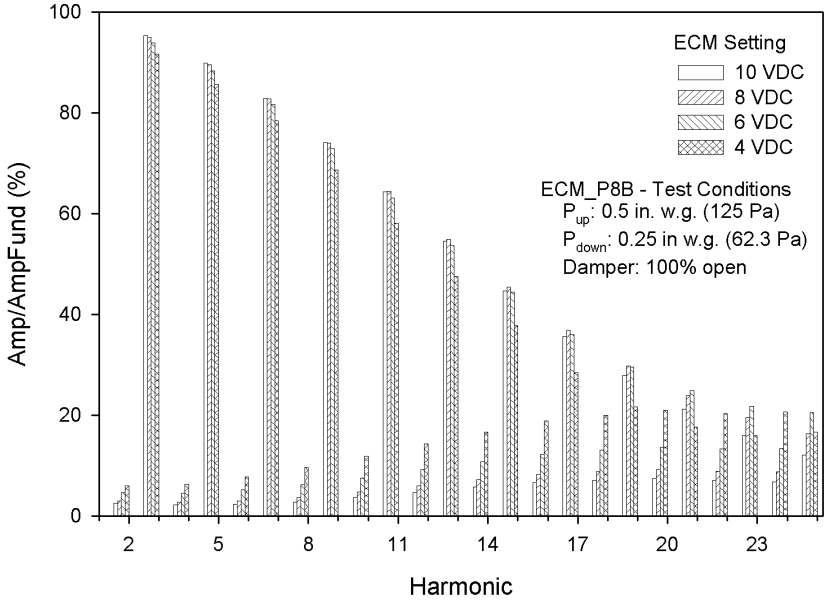

Figure B-79: Current Harmonics (%) for ECM_P8B

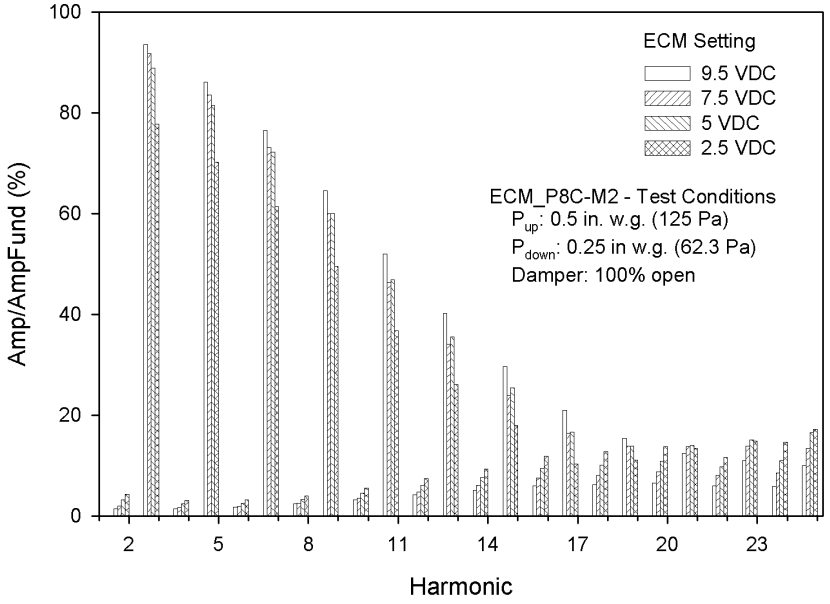

Figure B-80: Current Harmonics (%) for ECM_P8C-M2

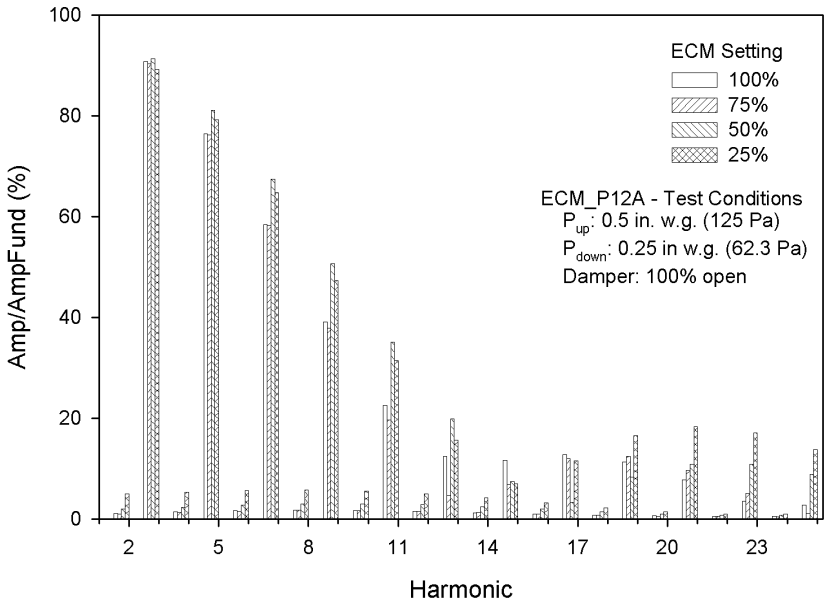

Figure B-81: Current Harmonics (%) for ECM_P12A

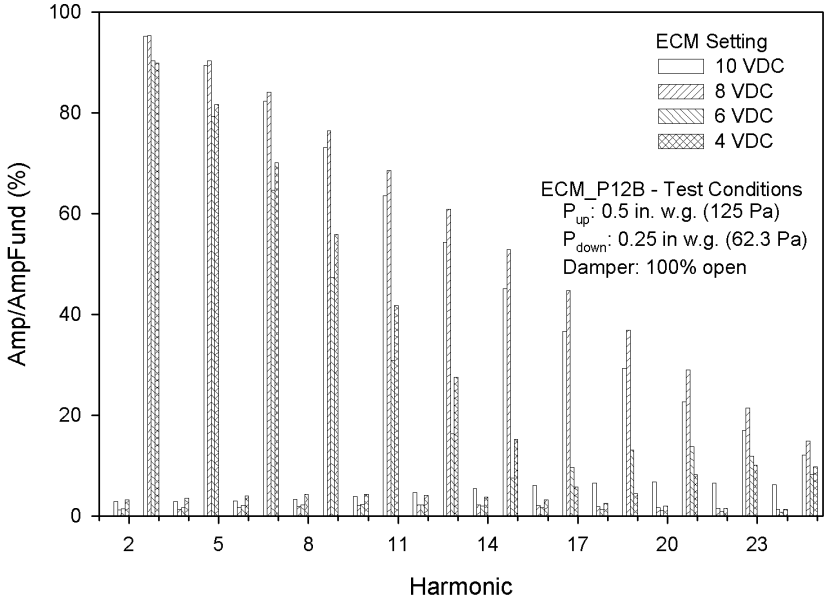

Figure B-82: Current Harmonics (%) for ECM_P12B

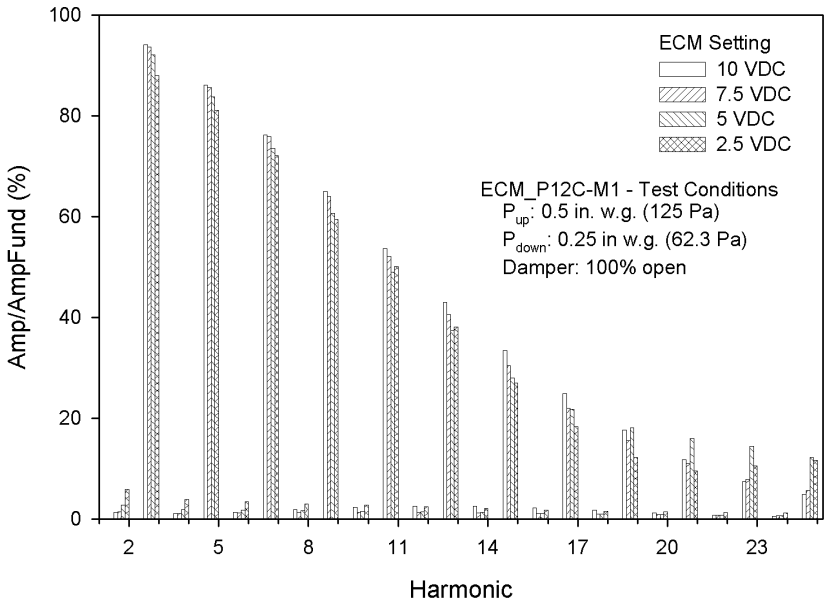

Figure B-83: Current Harmonics (%) for ECM_P12C-M1

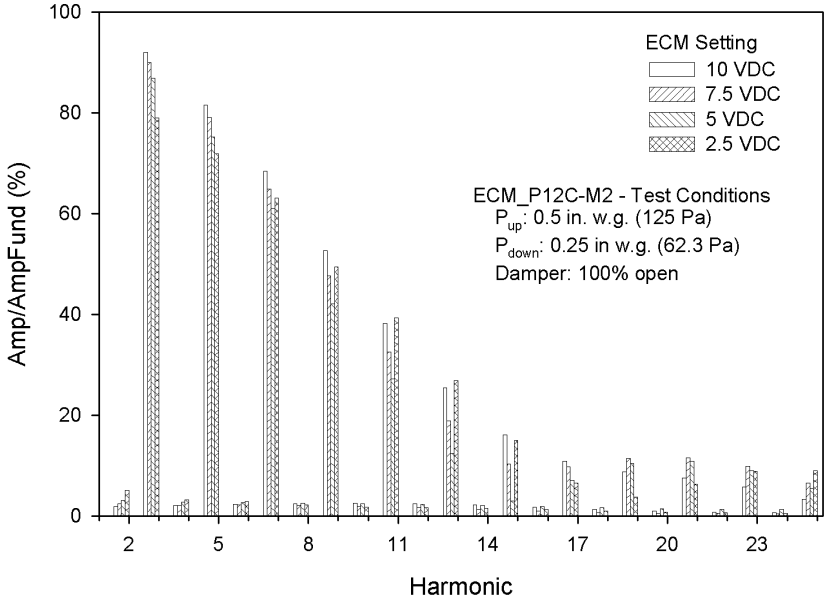

Figure B-84: Current Harmonics (%) for ECM_P12C-M2

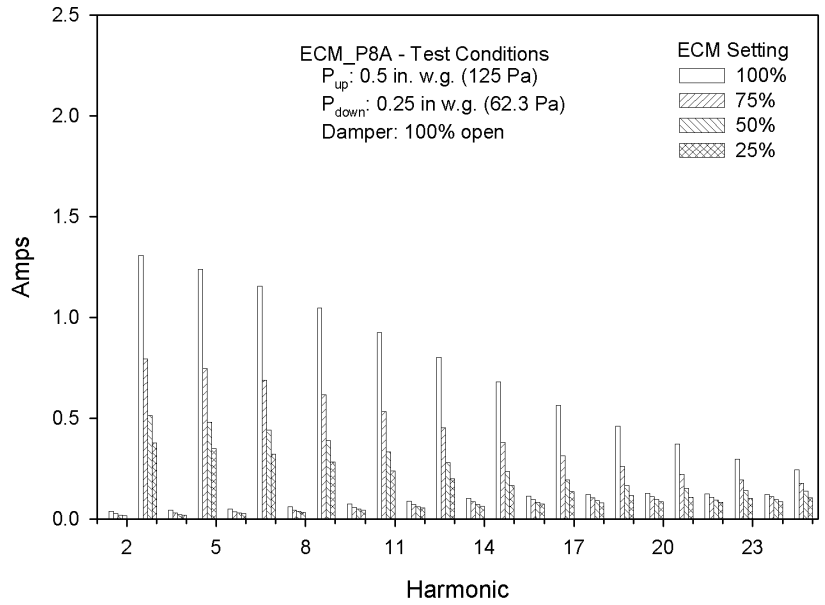

Figure B-85: Current Harmonics (Amps) for ECM_P8A

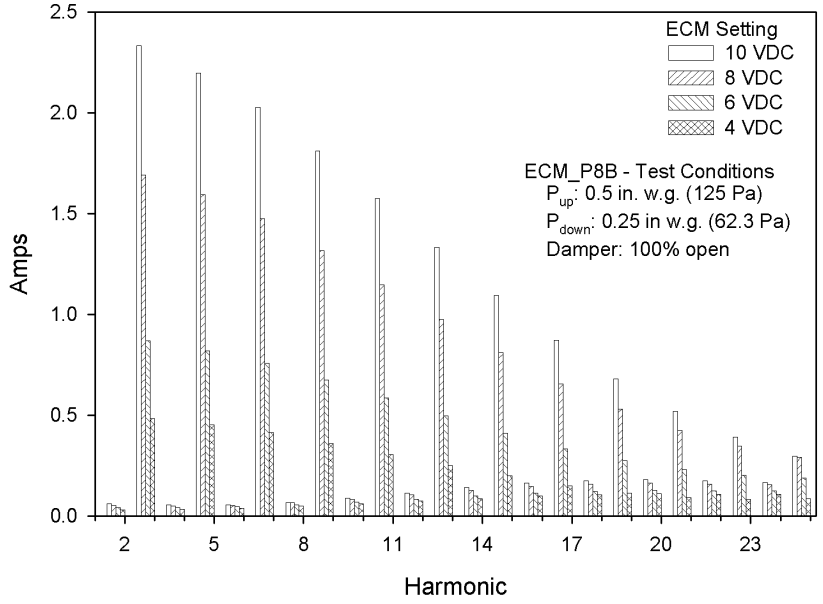

Figure B-86: Current Harmonics (Amps) for ECM_P8B

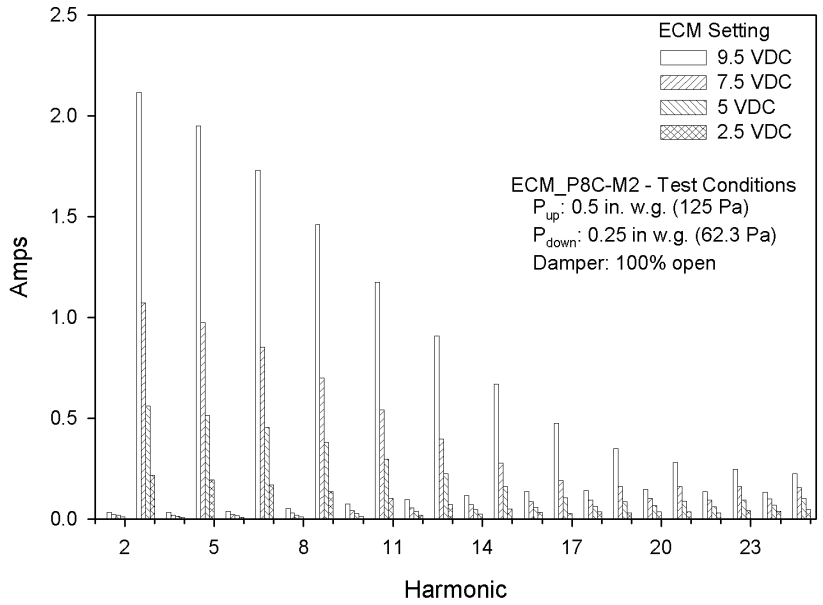

Figure B-87: Current Harmonics (Amps) for ECM_P8C-M2

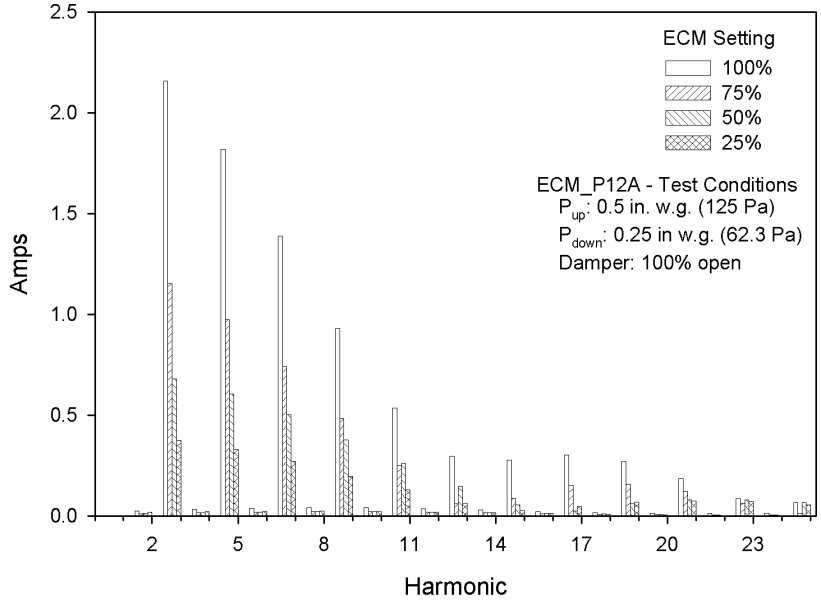

Figure B-88: Current Harmonics (Amps) for ECM_P12A

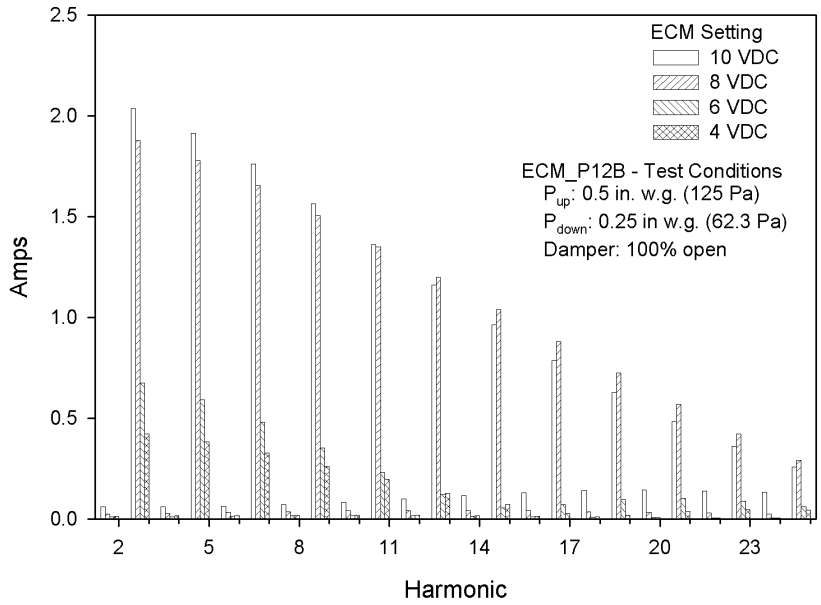

Figure B-89: Current Harmonics (Amps) for ECM_P12B

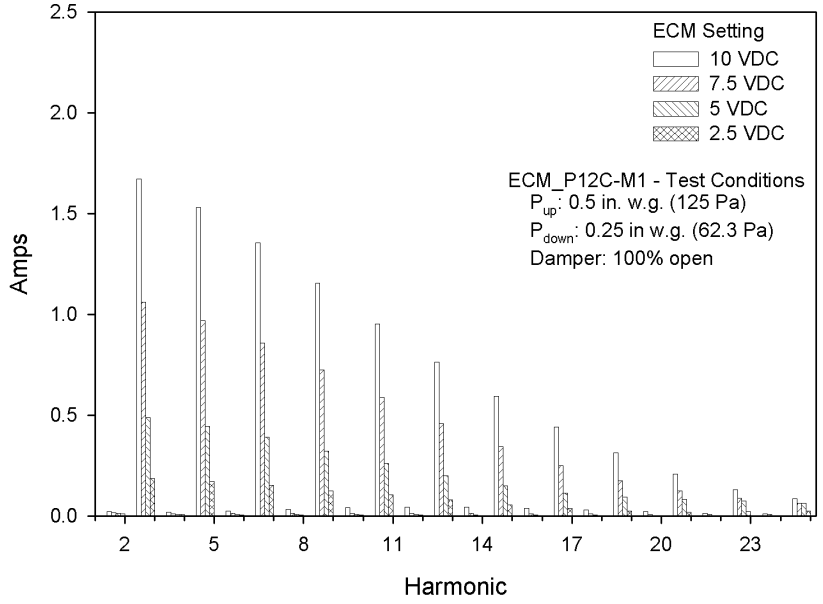

Figure B-90: Current Harmonics (Amps) for ECM_P12C-M1

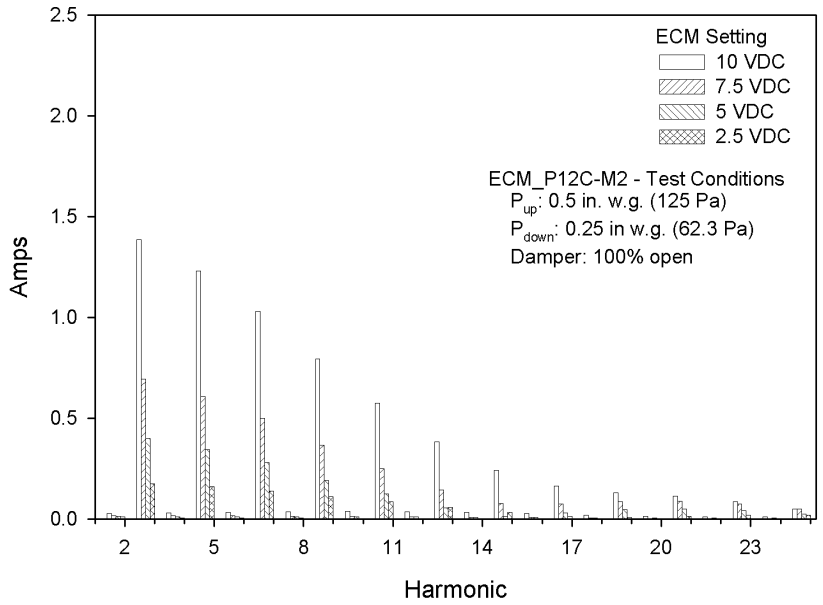

Figure B-91: Current Harmonics (Amps) for ECM_P12C-M2

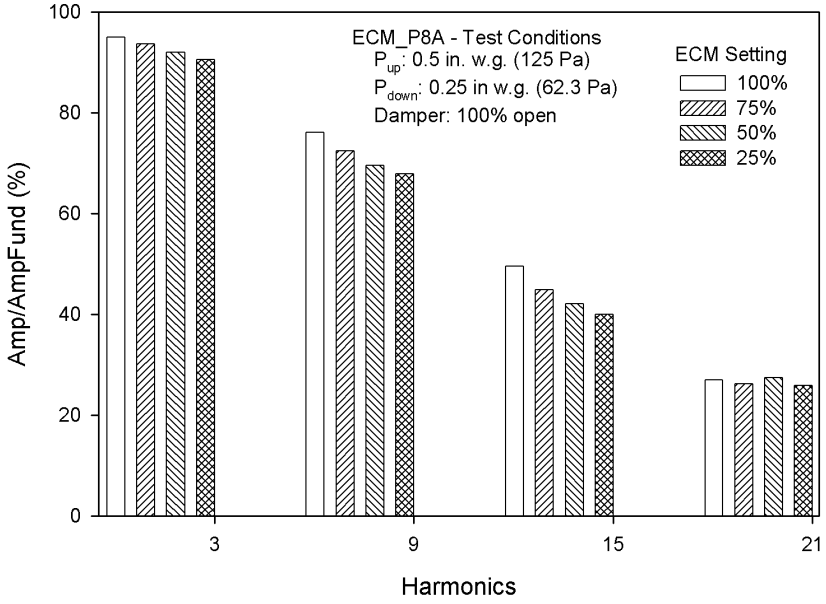

Figure B-92: Current Triplen Harmonics (%) for ECM_P8A

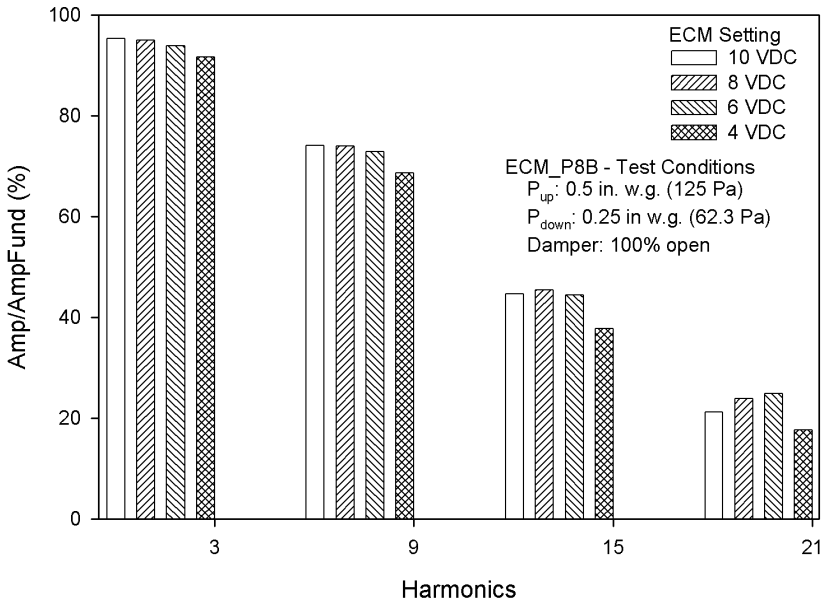

Figure B-93: Current Triplen Harmonics (%) for ECM_P8B

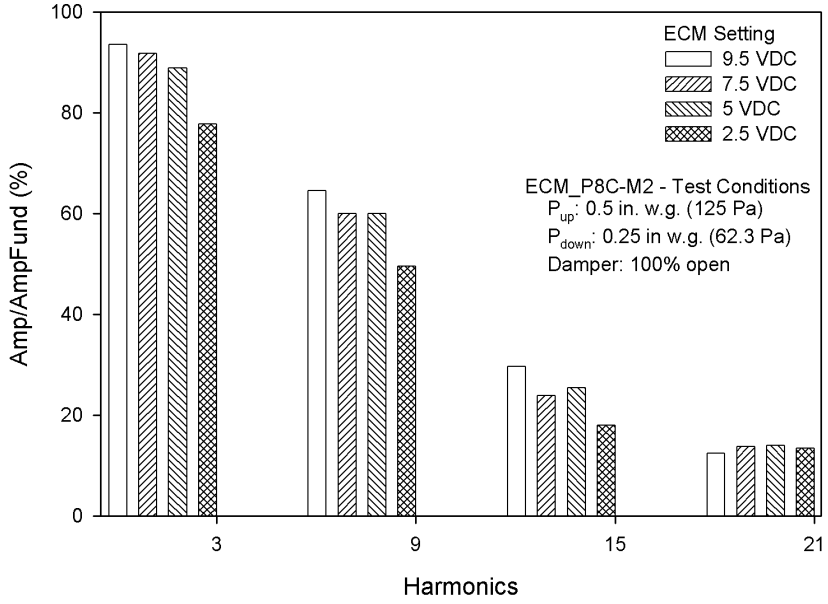

Figure B-94: Current Triplen Harmonics (%) for ECM_P8C-M2

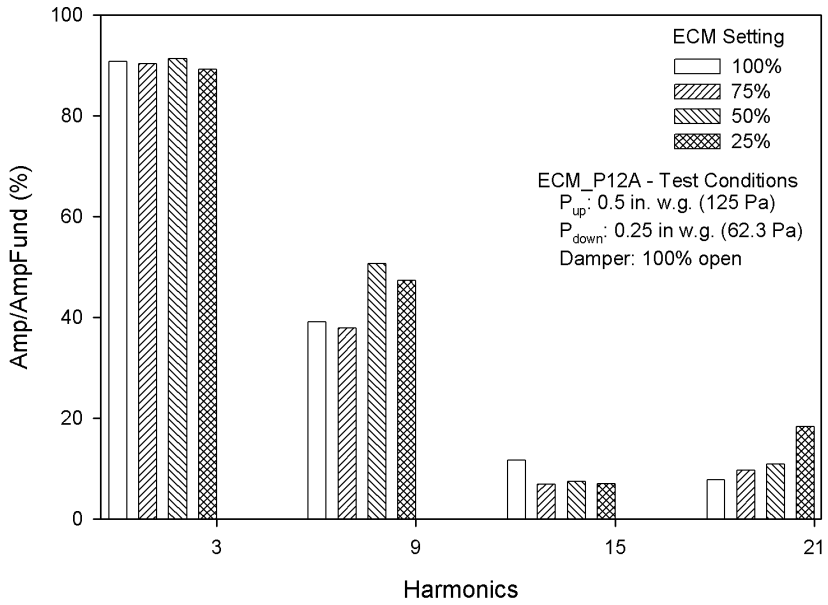

Figure B-95: Current Triplen Harmonics (%) for ECM_P12A

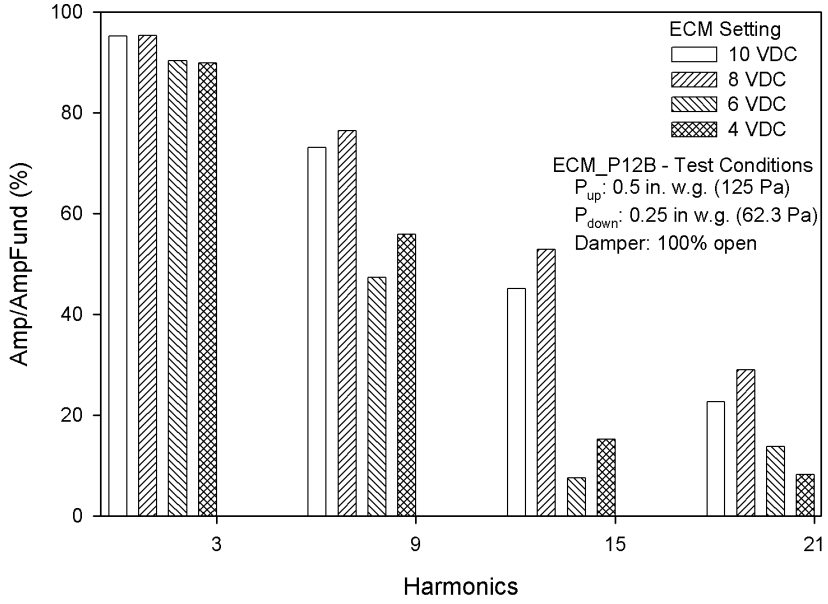

Figure B-96: Current Triplen Harmonics (%) for ECM_P12B

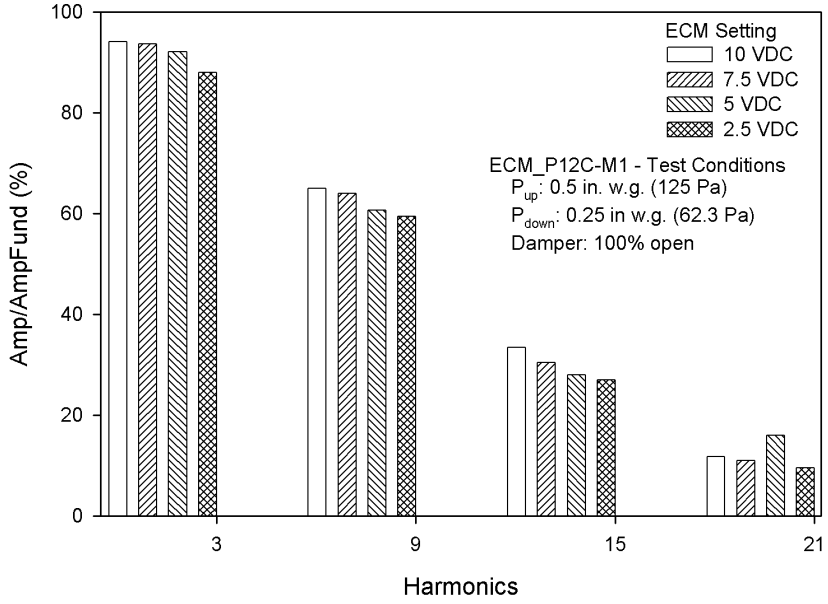

Figure B-97: Current Triplen Harmonics (%) for ECM_P12C-M1

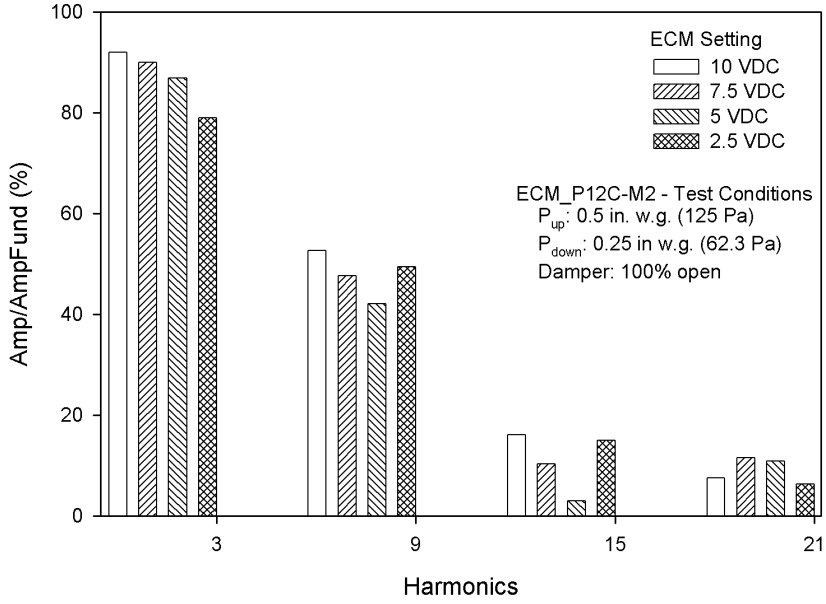

Figure B-98: Current Triplen Harmonics (%) for ECM_P12C-M2

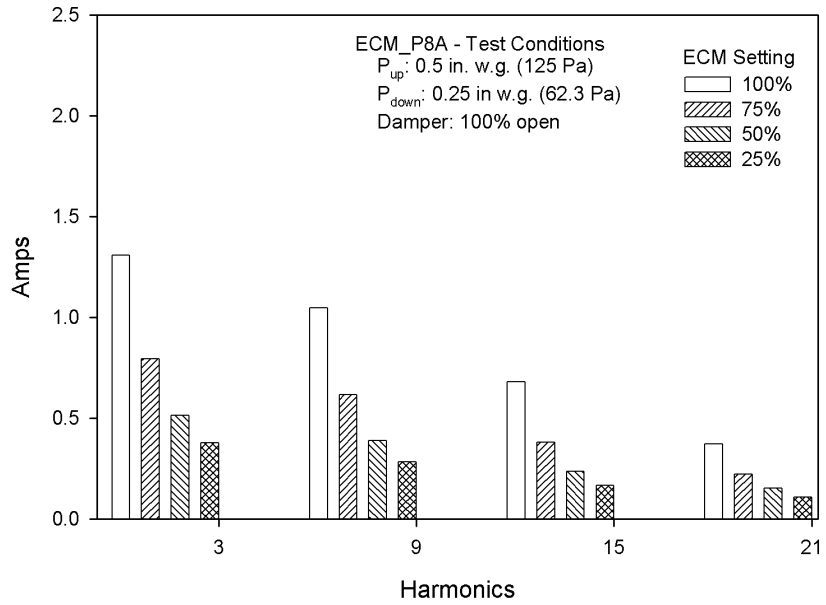

Figure B-99: Current Triplen Harmonics (Amps) for ECM_P8A

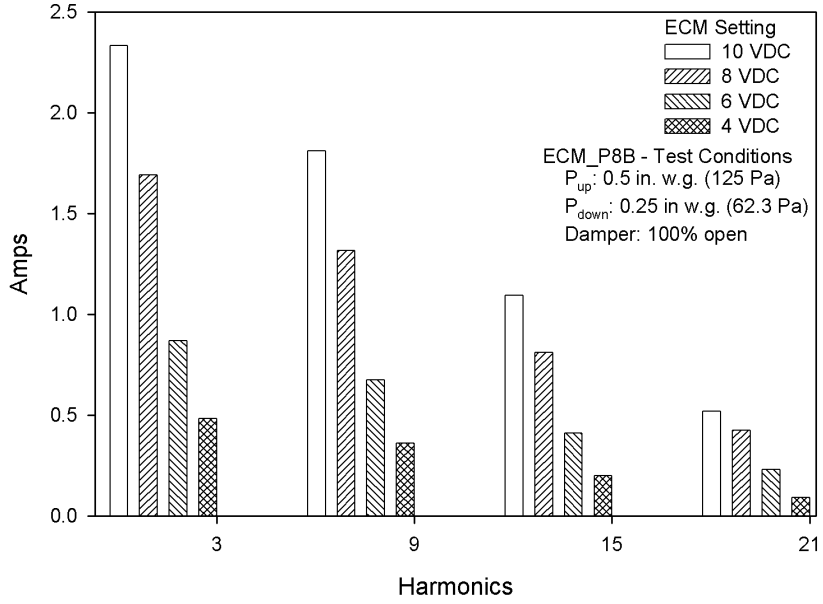

Figure B-100: Current Triplen Harmonics (Amps) for ECM_P8B

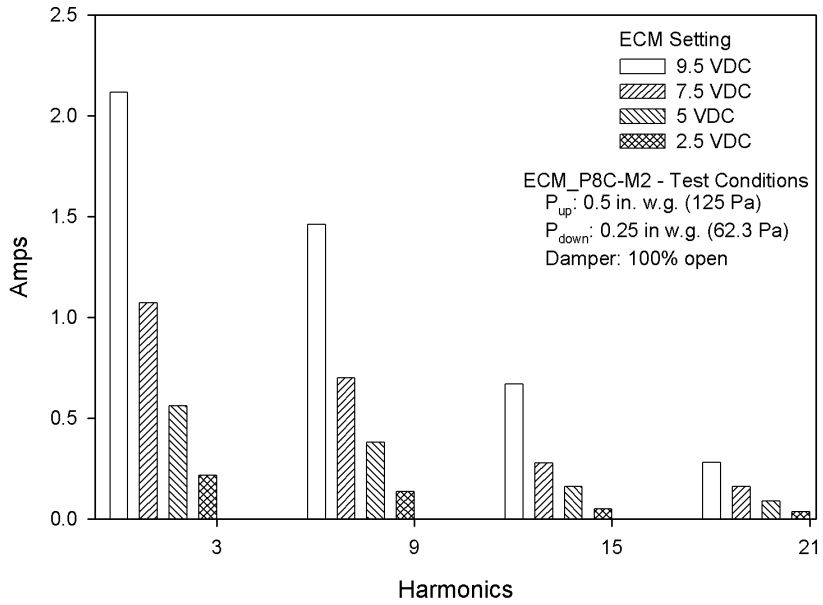

Figure B-101: Current Triplen Harmonics (Amps) for ECM_P8C-M2

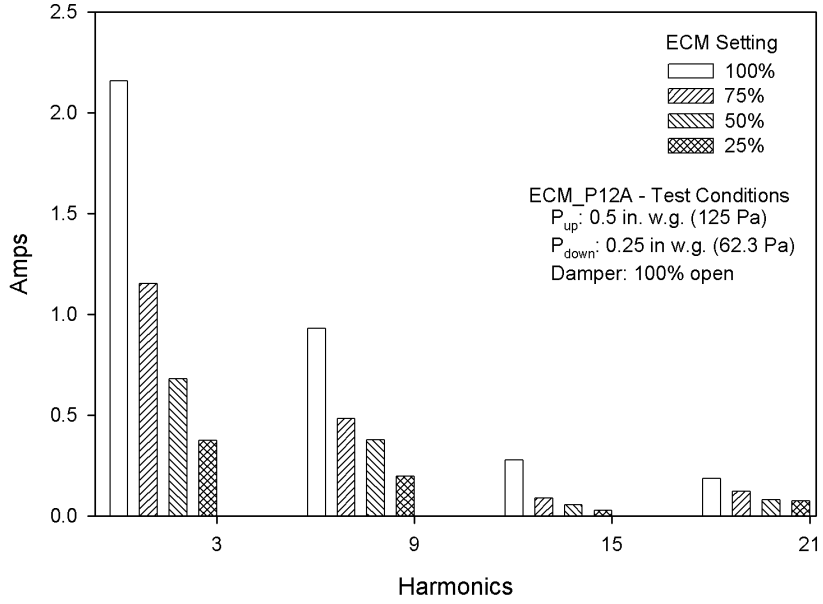

Figure B-102: Current Triplen Harmonics (Amps) for ECM_P12A

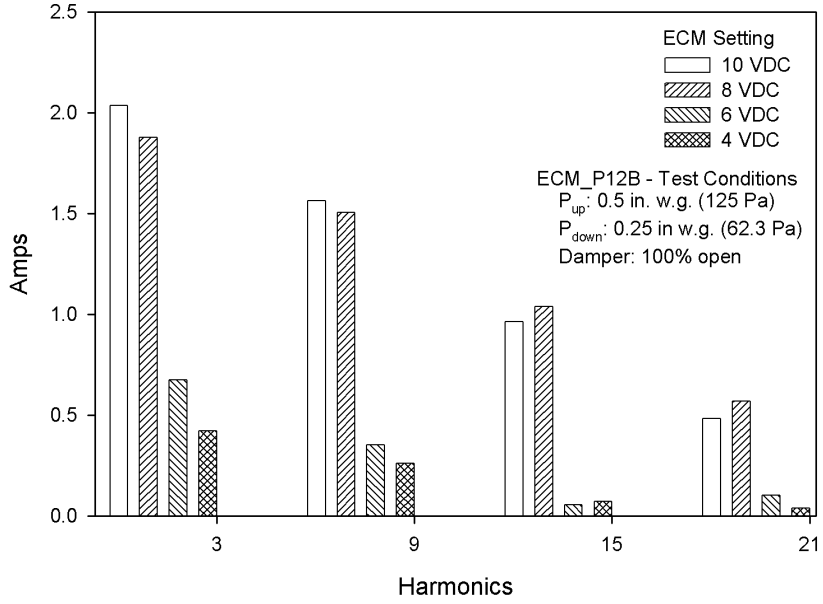

Figure B-103: Current Triplen Harmonics (Amps) for ECM_P12B

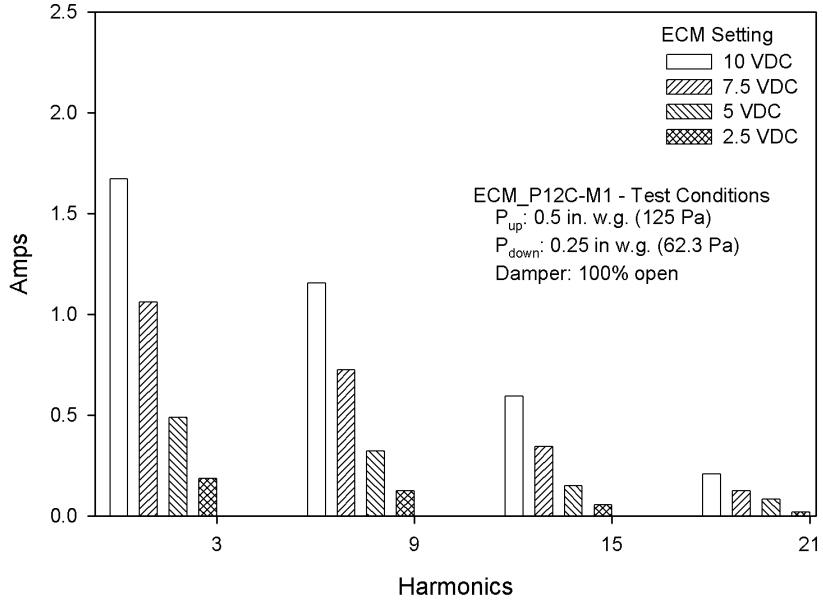

Figure B-104: Current Triplen Harmonics (Amps) for ECM_P12C-M1

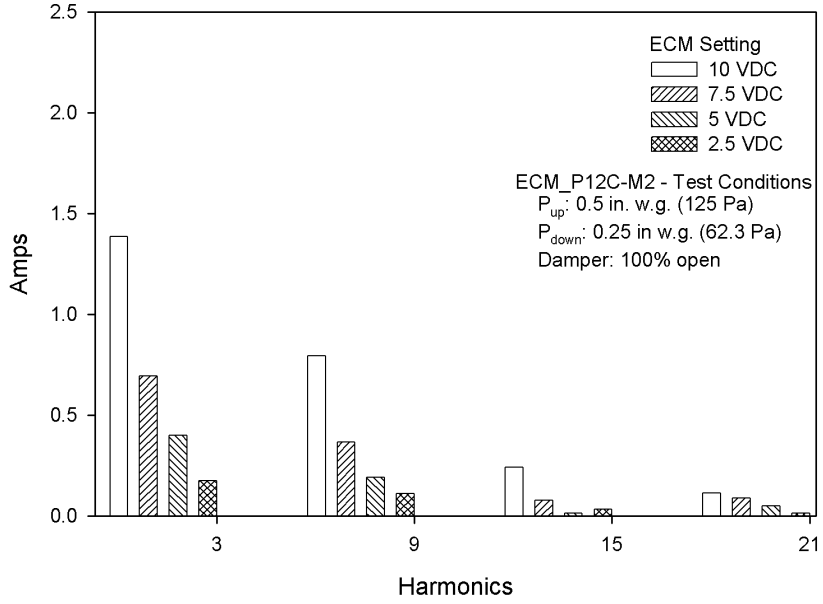

Figure B-105: Current Triplen Harmonics (Amps) for ECM_P12C-M2

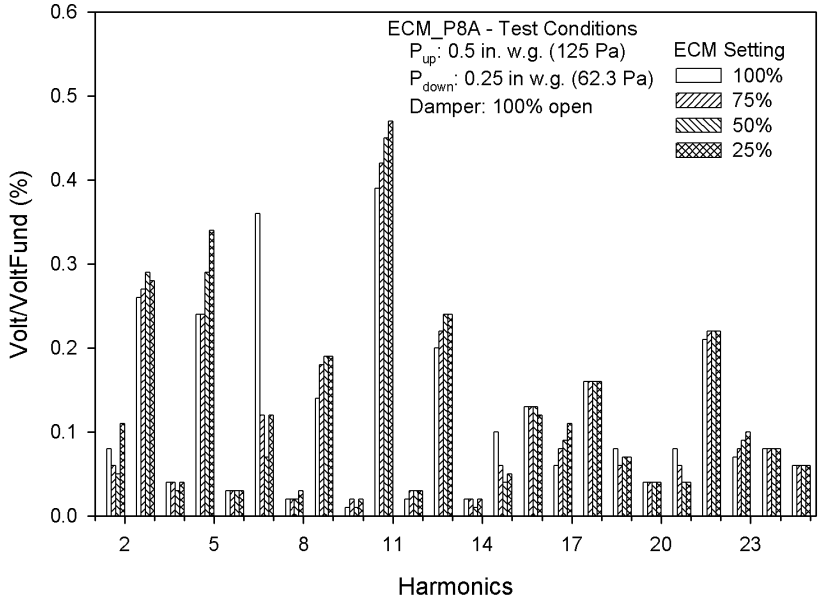

Figure B-106: Voltage Harmonics (%) for ECM_P8A

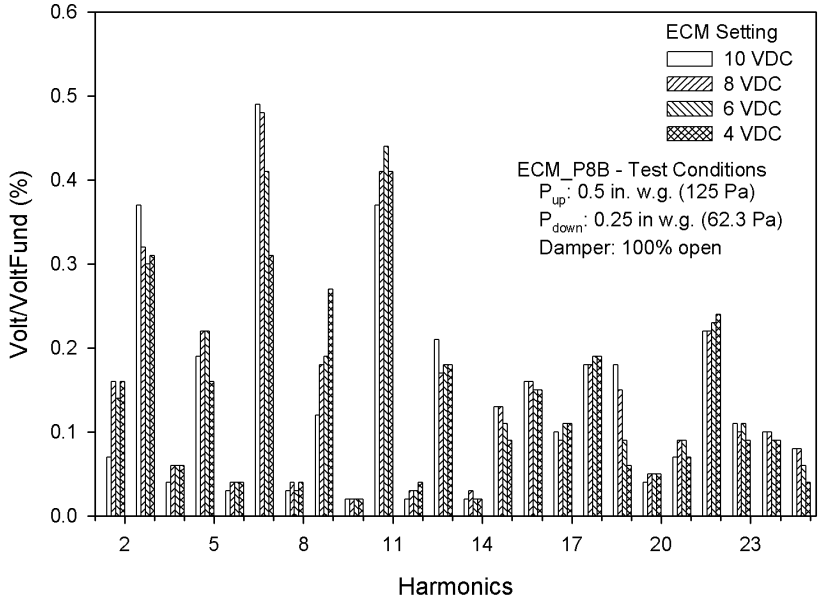

Figure B-107: Voltage Harmonics (%) for ECM_P8B

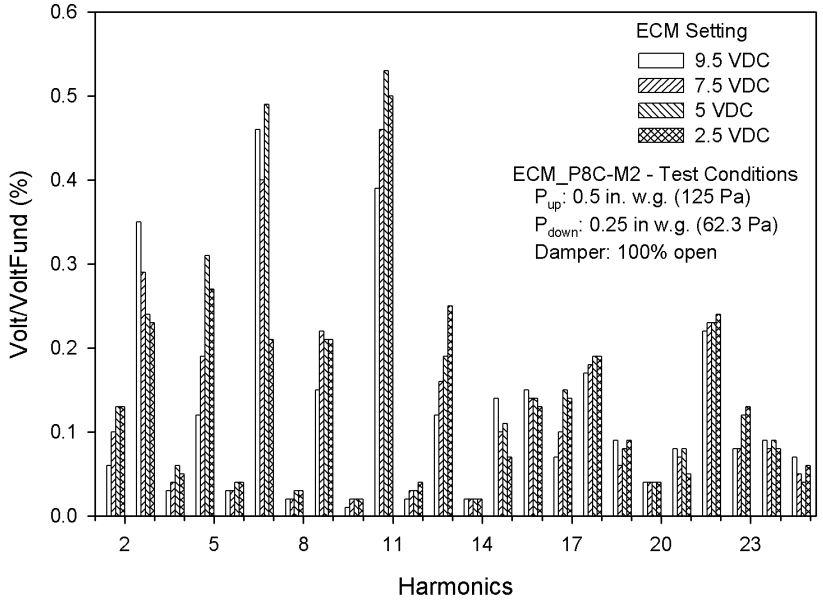

Figure B-108: Voltage Harmonics (%) for ECM_P8C-M2

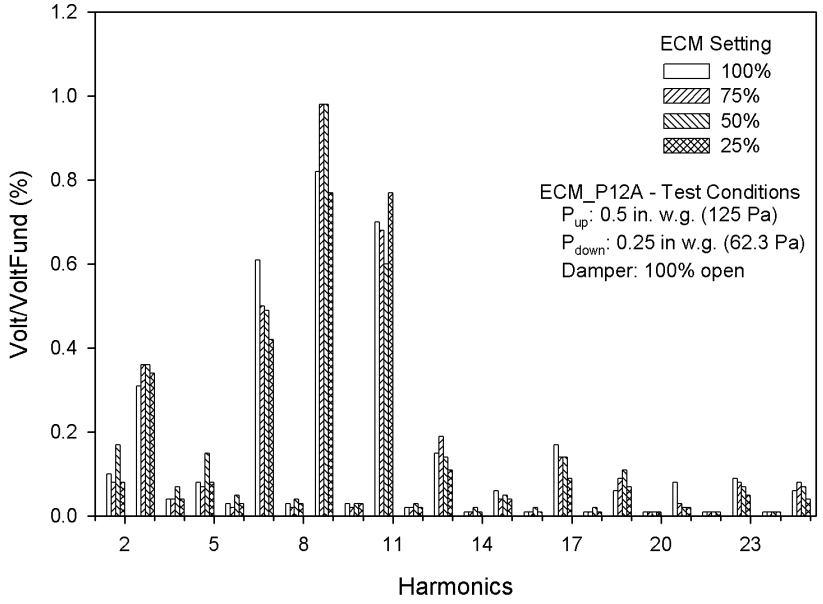

Figure B-109: Voltage Harmonics (%) for ECM_P12A

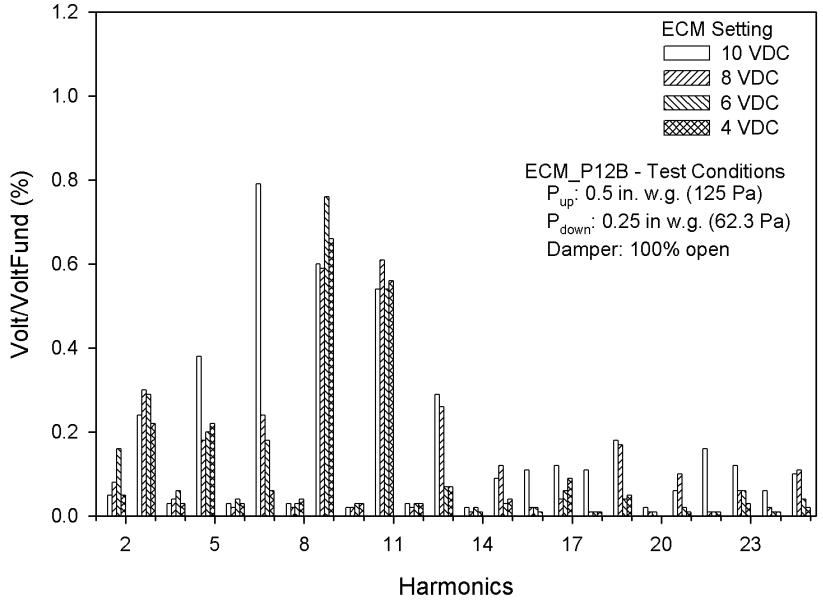

Figure B-110: Voltage Harmonics (%) for ECM_P12B

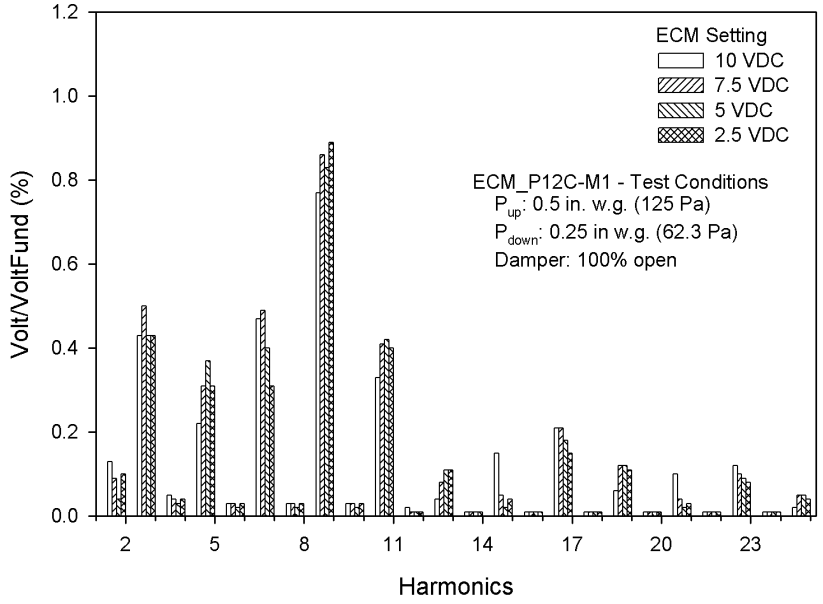

Figure B-111: Voltage Harmonics (%) for ECM_P12C-M1

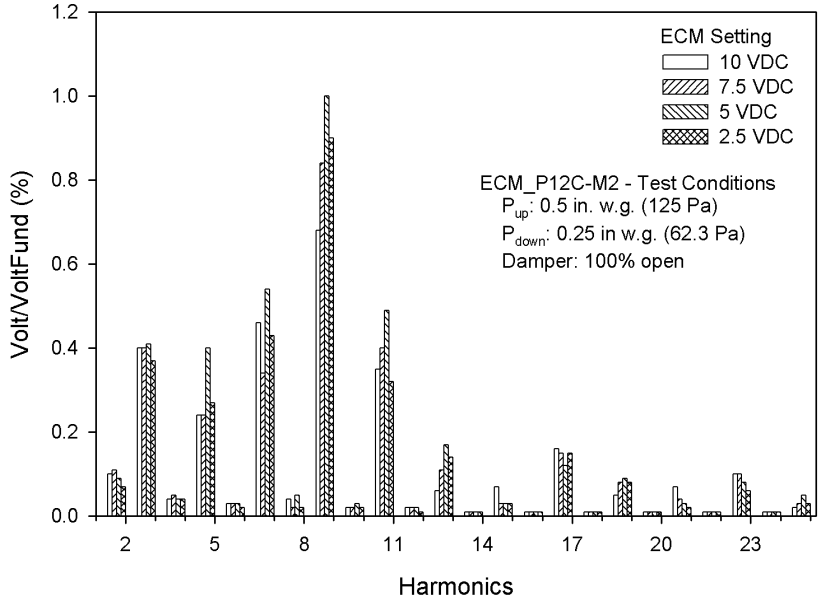

Figure B-112: Voltage Harmonics (%) for ECM_P12C-M2

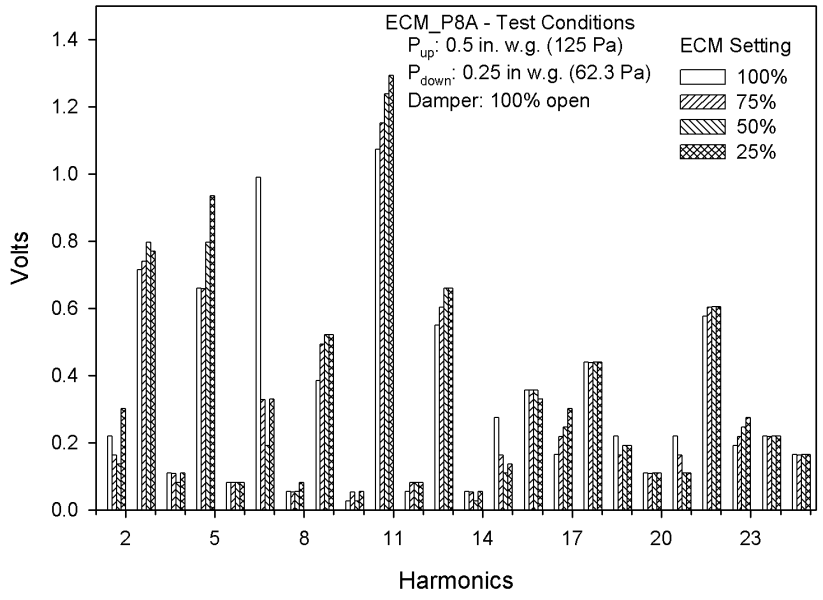

Figure B-113: Voltage Harmonics (Volts) for ECM_P8A

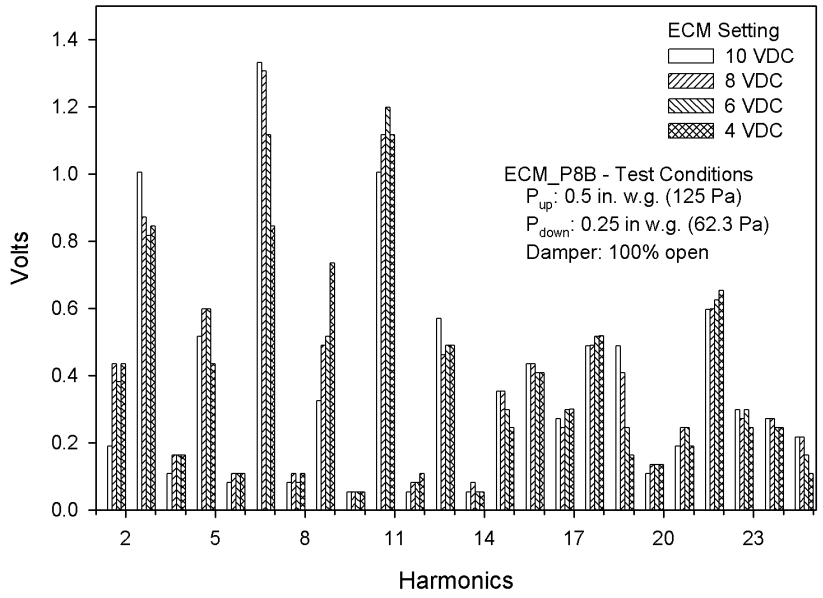

Figure B-114: Voltage Harmonics (Volts) for ECM_P8B

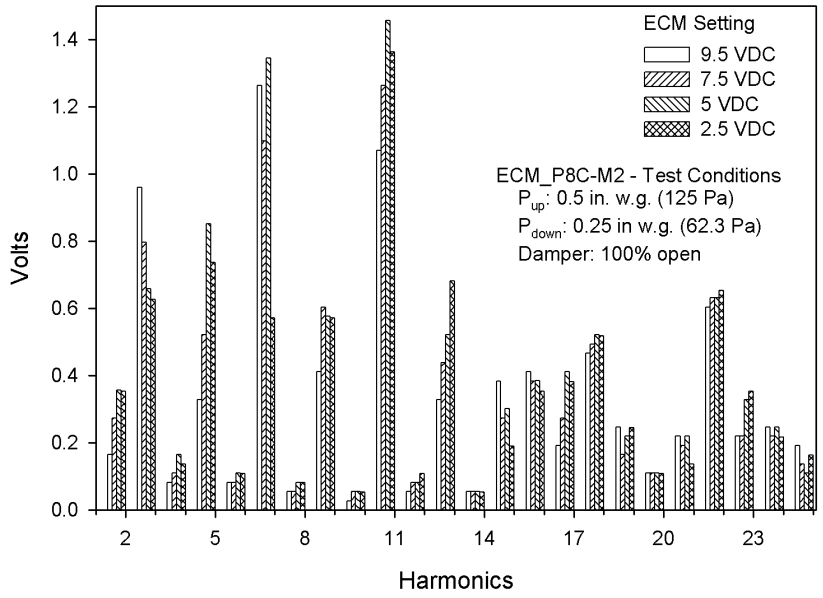

Figure B-115: Voltage Harmonics (Volts) for ECM_P8C-M2

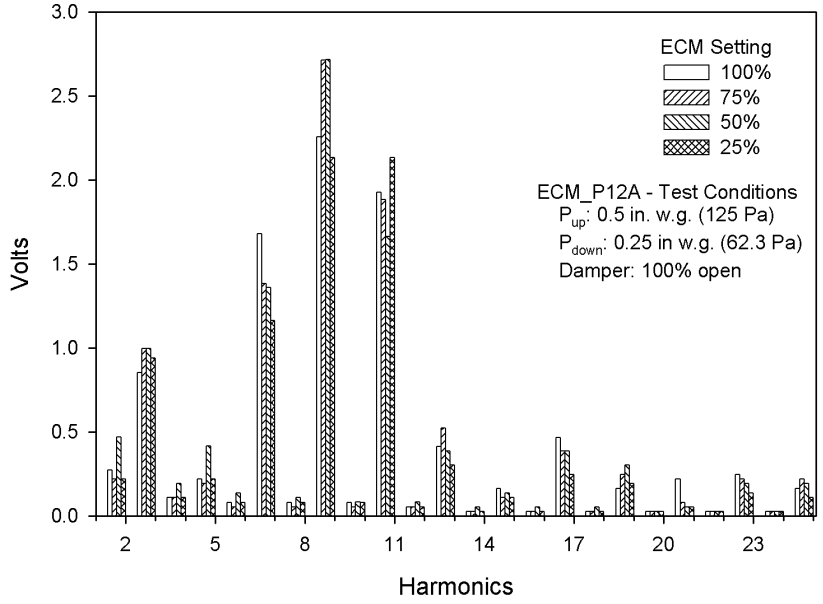

Figure B-116: Voltage Harmonics (Volts) for ECM_P12A

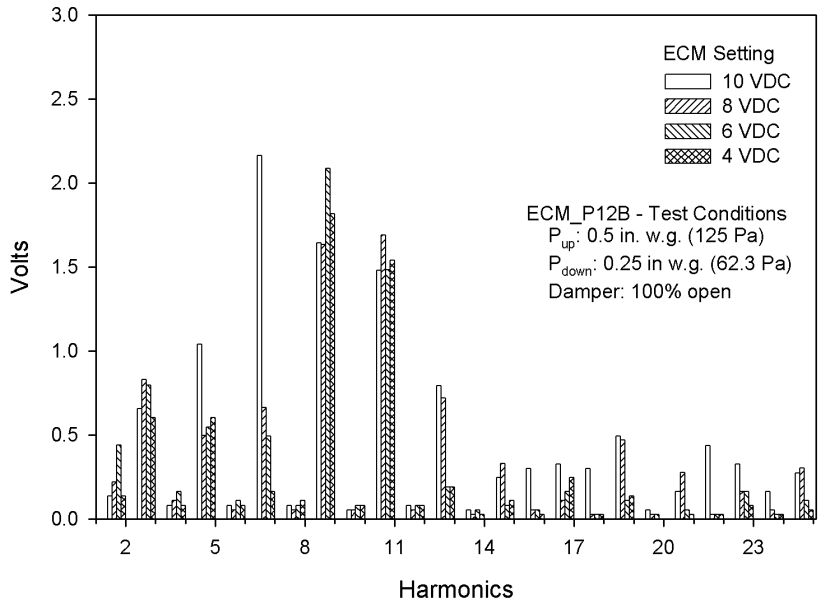

Figurea B-117: Voltage Harmonics (Volts) for ECM_P12B

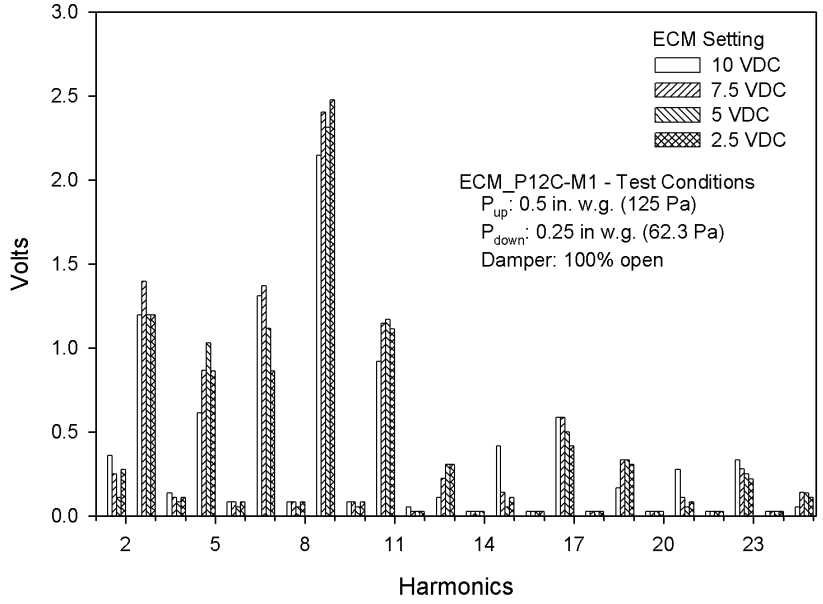

Figurea B-118: Voltage Harmonics (Volts) for ECM_P12C-M1

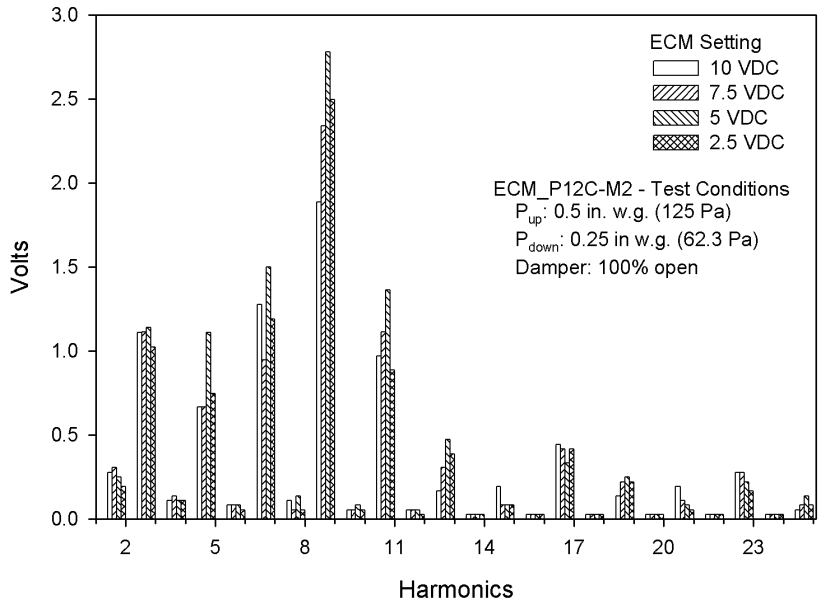

Figure B-119: Voltage Harmonics (Volts) for ECM_P12C-M2

APPENDIX C

AIRFLOW CHAMBER CHARACTERISTICS

To verify the accuracy of the upstream and downstream air flow rates against each other, the "AMCA Figure 15" and "AMCA Figure 12" airflow chambers were connected directly together without the terminal unit. The airflow rates through both chambers were then measured over the range of expected flow rates. The results are presented in Table C-1. The chamber airflow and power characteristics are presented in Tables C-2 and C-3 respectively.

Table C-1: Chamber Calibration Results

Test Point	AMCA Figure 15 CFM (m^3/s)	AMCA Figure 12 CFM (m^3/s)	Difference CFM (m^3s)	Percent Difference (%)
1	214.3 (0.101)	211.8 (0.100)	-2.5 (0.001)	-1.18036
2	520.5 (0.246)	511.8 (0.242)	-8.7 (0.004)	-1.69988
3	852.5 (0.402)	841.5 (0.397)	-11 (0.005)	-1.30719
4	1193 (0.563)	1178.2 (0.556)	-14.8 (0.007)	-1.25615
5	1532.9 (0.723)	1516.9 (0.716)	-16 (0.008)	-1.05478
6	1875.8 (0.885)	1858.4 (0.877)	-17.4 (0.008)	-0.93629
7	2217.5 (1.047)	2200 (1.038)	-17.5 (0.008)	-0.79545
8	2554.9 (1.206)	2538.3 (1.198)	-16.6 (0.008)	-0.65398
9	2892.8 (1.365)	2879.9 (1.359)	-12.9 (0.006)	-0.44793
10	3000.4 (1.416)	2983.3 (1.408)	-17.1(0.008)	-0.57319

Table C-1: Chamber Airflow Characteristics

AMCA Chamber	**Maximum Flow** CFM (m^3/s)	**Available Nozzles' Diameters** Inches (cm)					
Figure 15	4000 (1.89)	1.5 (3.8)	3 (7.6)	5 (12.7)	5 (12.7)	5 (12.7)	5 (12.7)
Figure 12	5000 (2.36	1.5 (3.8)	5 (12.7)	5 (12.7)	8 (20.3)		

Table C-2: Chamber Power Characteristics

AMCA Chamber	**Fan Power** Hp (kW)	Controller	Motor
Figure 15	10 (7.5)	VSD	AC Induction
Figure 12	7.5 (5.8)	VSD	AC Induction

VITA

Name:	Jacob Lee Edmondson
Address:	Texas A&M University Department of Mechanical Engineering 3123 TAMU College Station, TX 77843-3123
Email Address:	jake.edmondson@gmail.com
Education:	B.S., Mechanical Engineering, Brigham Young University, 2007 M.S., Mechanical Engineering, Texas A&M University, 2009